

# Nanoantennas: New Prospects in Light-Matter-Interactions

Dissertation  
zur Erlangung des akademischen Grades  
doctor rerum naturalium (Dr. rer. nat.)

vorgelegt dem Rat der Physikalisch-Astronomischen Fakultät  
der Friedrich-Schiller-Universität Jena

von Diplom-Physiker Robert Filter  
geboren am 10.08.1982 in Grevesmühlen

**Gutachter:**

1. Prof. Dr. Falk Lederer, Friedrich-Schiller-Universität Jena
2. Prof. Dr. Bert Hecht, Julius-Maximilians-Universität Würzburg
3. Prof. Dr. Javier Aizpurua, Materials Physics Center und Donostia International Physics Center in Donostia-San Sebastián, Spanien

**Tag der Disputation: 17. März 2015**

# Contents

<b>1</b>	<b>Introduction</b>	<b>1</b>
1.1	What is a Nanoantenna? . . . . .	1
1.2	Aim and Structure of this Thesis . . . . .	4
<b>2</b>	<b>Basics of Nanoantenna Theory</b>	<b>6</b>
2.1	Aspects of Classical Electrodynamics . . . . .	7
2.2	Radiation Efficiency . . . . .	8
2.3	Scaling . . . . .	13
2.4	Interaction with Quantum Systems: Semiclassical Description . . . . .	20
<b>3</b>	<b>Nanoantenna Quantization</b>	<b>22</b>
3.1	Quantized Cavity Field . . . . .	22
3.2	Quantization in Dissipative Media . . . . .	24
3.3	Quasinormal Modes . . . . .	28
3.4	Quasinormal Mode Quantization Scheme . . . . .	29
3.5	Verification of the quantization Scheme . . . . .	32
<b>4</b>	<b>Enhancing Dipole-Forbidden Transitions in Quantum Systems</b>	<b>35</b>
4.1	Plane-Wave-Excitation of Forbidden Transitions . . . . .	36
4.2	Semiclassical Multipole Coupling . . . . .	37
4.3	Enhancing Quadrupole Transition Rates . . . . .	39
4.4	Quadrupole-Driven Dynamics of a Three-Level System . . . . .	41
<b>5</b>	<b>Ultra-Bright Single-Photon Sources</b>	<b>48</b>
5.1	Investigated Quantum System, Pumping Scheme, and Two-Level Approximation . . . . .	49
5.2	Emission Rate Determination . . . . .	50
5.3	Nanoantenna Design and Determination of Parameters . . . . .	52
5.4	Density Matrix Calculations: Emission Rate Verification and Single Photon Characterization . . . . .	54
<b>6</b>	<b>Reaching the Strong Coupling Regime</b>	<b>59</b>
6.1	The Mathematical Model . . . . .	59
6.2	Nanoantenna Designs . . . . .	60
6.3	Effects of Strong Coupling . . . . .	64
<b>7</b>	<b>Conclusions and Outlook</b>	<b>68</b>
	<b>Appendices</b>	<b>72</b>
<b>A</b>	<b>Classical Considerations</b>	<b>72</b>
A.1	Poynting's Theorem . . . . .	72
A.2	Analytical Reflection Coefficients at Nanoantenna Terminations . . . . .	72
A.3	Explicit Plasmonic Modes for Layered Structures . . . . .	82
A.4	The Influence of the Purcell Effect on the Emitter Efficiency . . . . .	85
A.5	Notes on Non-Frequency Dependencies of $\varepsilon(\omega)$ . . . . .	85

<b>B</b>	<b>Quantum Considerations</b>	<b>87</b>
B.1	Notes on Fermi's Golden Rule . . . . .	87
B.2	Discriminating Electric and Magnetic Coupling . . . . .	91
B.3	Semiclassical Electric Multipole Coupling in the Quasistatic Regime . . . . .	92
B.4	Steady-State Analysis of a Three-Level System . . . . .	93
B.5	Spontaneous Emission revisited . . . . .	94
B.6	Spectral Density, Local Density of States, and the Purcell Factor . . . . .	98
B.7	The Modified Interaction Picture . . . . .	99
B.8	Emission Rates of a Two-Level System coupled to multiple Harmonic Oscillators .	100
B.9	Second-Order Correlation: Classical and Nonclassical Light States . . . . .	103
B.10	Nanoantennas for Squeezed Light and Entangled Light Generation . . . . .	106
B.11	Two Quantum Systems coupled to a Nanoantenna: Eigenstates of the Hamiltonian	108
<b>C</b>	<b>Miscellaneous</b>	<b>110</b>
C.1	Acknowledgements . . . . .	110
C.2	Publications . . . . .	111
C.3	Short Curriculum Vitae . . . . .	114
C.4	Ehrenwörtliche Erklärung . . . . .	115
C.5	Zusammenfassung . . . . .	116
	<b>References</b>	<b>118</b>
	<b>Notation</b>	<b>132</b>
	<b>Index</b>	<b>133</b>

# 1 Introduction

## 1.1 What is a Nanoantenna?

At radio frequencies, metals may be regarded as perfect conductors. The resonance lengths of metallic antennas operating in that frequency regime can be calculated using simplified standing-wave approaches. At optical frequencies, this is not possible: Metals are not perfect such that the physical properties of nanoscale antennas have to be understood in terms of their electromagnetic eigenmodes. The eigenmodes of these nanoantennas (NAs) are surface plasmon polaritons (SPPs). These quasi-particles arise from the interaction of coherent oscillations of the charge density inside the metal, so-called plasmons, with the electromagnetic field

The study of SPPs, nowadays termed plasmonics, goes back to independent works of Thomson and Sommerfeld at the end of the 19<sup>th</sup> century. They considered the propagation of SPPs along metallic wires [1,2]. Of course, neither of them actually mentioned SPPs. But that the concept of SPPs was introduced over 100 years ago got evident in Sommerfeld's "Über die Ausbreitung der Wellen in der drahtlosen Telegraphie" [3]. In this paper, Sommerfeld discusses two contributions to the propagation of radio waves. He asked<sup>1</sup> "What kind of waves are those in wireless telegraphy? Are they comparable to Hertzian waves in air or to electrodynamic waves of a wire?". Clearly, "Hertzian waves" refers to freely propagating solutions of Maxwell's equations, but earlier Sommerfeld explains "electrodynamic waves of a wire" as surface waves, *i.e.* SPPs. He further provides their well-known dispersion relation in the case of a flat surface.

Given more than a century of research on plasmonics, one might ask: What is new, what makes plasmonics such a vivid field of research? As a matter of fact, Thomson and Sommerfeld were mainly interested in a theoretical understanding of radio frequency broadcasting and telecommunication devices. Their era saw the dawn of wireless telecommunication; investigations of antenna-mediated light-matter-interactions at optical frequencies were still far away.

Whereas waves at radio frequencies exhibit energies up to the  $\mu\text{eV}$  regime, visible radiation requires several eV per photon with wavelengths roughly ranging from 400 nm to 800 nm. This spectral range is interesting for two main reasons: First of all, chemical bonds realized by outer electrons usually have energies in the eV region. Hence a lot of interesting light-matter-interactions happen at this energy scale. Second, the energy of visible light is higher than that of thermal radiation and lower than typical binding energies of inner electrons. Thus, detectors for visible light generally enable better signal-to-noise ratio than in the infrared band and suffer from much less attenuation in matter than ultraviolet radiation.

In 1959 Feynman gave a remarkable talk entitled "There's plenty of room at the bottom" in which he outlined new possibilities if we could "arrange the atoms the way we want" [4]. Arguably, this talk was the beginning of nanotechnology, which enabled to fabricate sophisticated devices on the micro- and nanoscale using different techniques. Advanced procedures are *e.g.* electron or Helium ion beam lithography, nanoimprinting, atomic layer deposition, surface functionalization, self-assembly, or epitaxial growth [5]. It was not before the early 1990s that these techniques became available on a large scale, and there is still much more to come. Because of their size, plasmonic devices may accomplish what Sommerfeld's generation could have only dreamt of: to mediate an interaction of light with matter in the visible spectrum, which is one of the driving ideas behind the investigation of NAs.

In principle, the interaction strength between plasmonic and quantum systems (QSS) such as

---

<sup>1</sup>Original excerpt: "Ferner sind die elektrodynamischen Drahtwellen typische Oberflächenwellen. [...] Welchem Typus sind nun die Wellen der drahtlosen Telegraphie zuzuzählen? Sind sie den Hertzschen Wellen in Luft zu vergleichen oder den elektrodynamischen Drahtwellen?"

atoms, molecules, or quantum dots (QDs) can be orders of magnitude stronger when compared to the free-space interaction. The reason is that plasmonic excitations are surface modes with evanescent electromagnetic fields at metal-dielectric interfaces. The strong interaction has two direct consequences, namely a strong action of a plasmonic excitation on the QS, but also a strong action of an excitation of the QS on the plasmonic system. Hence, the interaction can be used to enhance the energy absorption of the QS, to enhance an energy transfer from QS to the plasmonic system, and a combination of both, that is, a continuous energy exchange among the subsystems.

In addition to the enhanced light-matter-interaction it is desirable that the particular plasmonic mode used for the interaction can efficiently couple to free-space radiation. Only then the enhanced interaction can be used for detection or application in the farfield and the plasmonic structure acts as an antenna on the nanoscale. This requirement leads us to the definition of plasmonic NAs, inspired by the definition of optical antennas given in Ref. [6]:

A **plasmonic nanoantenna** is a device designed to efficiently convert freely propagating radiation to localized energy using plasmonic excitations, and vice versa.

The latter definition deals with the kind of devices that are the main subject of this work and we shall elaborate a little further on what it describes, and what not:

1. NAs without plasmonic materials, often termed dielectric NAs [7–11], have been explicitly excluded. Therefore, throughout this work, we shall call *plasmonic nanoantennas* simply NAs for conciseness. This seems also justified as most of the developed concepts can also be extrapolated to dielectric NAs.
2. We are not restricted to NAs made of noble metals. Depending on the frequency, various materials possess metallic properties and thus support plasmonic modes, for example graphene NAs at THz frequencies [12]. Hence, our definition constitutes no restriction to a certain *frequency* band.
3. There is also no restriction to the study of a *coupling* of NAs to QDs. For instance the coupling of plasmonic waveguides to NAs is included [13, 14].
4. NAs exhibit a great variety of *sizes*, but we require a certain *energy localization*. Questions about NA scaling will be further detailed in Sec. 2.3.

Hence, NAs are still a pretty generic class of plasmonic structures that are able to harvest light on the nanoscale. But what is the state of the art, what are the usual approaches to fabricate such devices, and how did we get there? In the following, we will try to answer these questions, specifically for the case of NAs working at optical frequencies.

The history of NAs as we understand them today started already in 1928. In a letter to Einstein, Synge proposed to use small metallic particles to convert free-space radiation to localized fields close to a sample surface to break Abbe’s diffraction limit [15]. But Einstein rejected the idea of the then-unknown scientist. The interest in light-matter-interactions close to metallic nanoparticles increased remarkably with the discovery of the so-called surface-enhanced Raman scattering (SERS) in 1974 [16]. These experiments allowed to investigate the chemical properties of molecules on an entirely new level. They also inspired a large number of theoretical and experimental works to understand the interaction of metallic surfaces to QDs [17–21].

Also, the properties of SPPs were intensively investigated during the 1980’s by Raether [22, 23] and others [24, 25]. This period saw the emergence of nanoplasmonics, *i.e.* plasmonics for nanoscale structures such as NAs [26]. Synge’s idea was suggested by researchers in several forms and culminated in the development of scanning near field optical microscopes (SNOM) by Pohl in

1982 [27]. The concept of NAs started to emerge explicitly. In 1985, Wessel mentioned the use of small particles as antennas for an incoming optical field [28]. In 1997, Grober suggested to use optical antennas as optical near-field probes [29]. But possibly due to limitations in the available fabrication techniques, Grober *et al.* were only able to perform an experiment using a bow-tie antenna working at 2.2 GHz, *i.e.* in the microwave frequency region.

Nevertheless, fabrication techniques advanced and the realization of NAs came into reach soon after [30,31]. In 2000 and 2002, Sqalli *et al.* used spherical and elliptical gold NAs with dimensions  $\approx 50$  nm as a probe for SNOM imaging [32,33]. These studies were arguably the first experimental demonstrations of NAs. Soon after, bow-tie NAs with elements in the same dimension were investigated by the groups of Moerner and Kino in 2004 [34,35]. They followed similar but much larger single-element infrared antenna designs [36]. In 2005, Mühlischlegel *et al.* were able to successfully fabricate NAs made of two gold elements with a minimum total length of approximately 190 nm [37].

The experimental breakthroughs starting with Sqalli's works immediately caused a huge response in the scientific community. New possibilities were offered by the latest NAs, especially for enhanced light-matter-interactions [38–40]. One of the consequences of an enhanced light-matter-interaction between NAs and Qs is the change of the Qs's spontaneous emission rate. This effect was first described by Purcell in the context of cavity quantum electrodynamics [41,42].

In 2005 and 2006, several groups were able to demonstrate the Purcell effect of Qs close to different kinds of NAs by varying the distance between NAs and Qs [43–45]. Further insight into this effect was provided by theoretical investigations. They underlined the importance of a suitable placement of the Qs and a thoughtful design of the NA, which was necessary because of the losses in plasmonic materials [46,47]. The prospects to design emission direction [48–51] and improvements in photovoltaics [52–54] have also contributed fruitful impetus and possible directions for NA applications.

More recently, NA fabrication reached an entirely new level. It became possible to produce NA gaps with sub-nm precision [55] and to implement sophisticated NA designs with embedded Qs [56]. All these efforts have not only brought NA research closer to large-scale industrial production techniques [57–59]. They also gave rise to many related questions on nanoscale light-matter-interactions: Which theoretical approaches are needed to describe material properties on the nanoscale and what models can be used to describe the interaction of Qs and SPPs in a simplified manner?

Some specific questions are: How to explain the spectral resonances of very small NAs that are strongly shifted with respect to calculations assuming a classical local material response [60–62]? Are density functional theory calculations needed [63–66] or is an approach using a nonlocal response of the metal better suited [67–70]? Can efficient models account for the electron spill-out at NA terminations and their interaction close to Qs [71,72]? What is the role of magnetic dipole [73–75] or electric quadrupole [76–78] “forbidden transitions” in NA light-matter interactions? Will one observe NA-enabled quantum effects such as a strong coupling to Qs [79,80] or efficient generation of entangled photons [81]? Thus, a better understanding of NA physics is of major importance.

On the other hand mankind acquired an enormous amount of knowledge, new perspectives and fabrication techniques over the last decades. We have reached a point that the generations of Sommerfeld and Feynman could only have dreamt of. Yet, the surface of what is possible has just been scratched. In the next couple of years, NA research will allow to understand light-matter-interactions on an entirely new level. Hopefully, this knowledge can be transferred into astonishing real-world applications.

## 1.2 Aim and Structure of this Thesis

I became interested in the field of NA research during my attendance of the physics school “Nanoantennas and Hybrid Quantum Systems” held by the German Physical Society in 2011. The presented concepts and outlined prospects strongly influenced my scientific work. In 2011, NA-driven light-matter-interactions were mostly understood within classical electrodynamics approaches. A number of studies detailed the modified emission characteristics such as the spontaneous emission rate and directivity of QS in the weak coupling regime [46, 82].

Very few publications considered either the quantum nature of the QS or of the NA itself, see *e.g.* Refs. [83–86]. However, most of these studies used a simplified electrostatic description of NAs which is suitable only for sufficiently small NAs. Spherical NAs were often considered for the sake of exact analytical considerations but such NAs generally exhibit a very poor performance for the investigated effects [85, 86]. In fact, such metallic particles may not be called NAs, as they are not able to efficiently convert free-space radiation to localized energy and vice versa.

So, although electrostatic quantization schemes for simplified geometries are quite appealing, their actual applicability in experiments and applications is questionable. Fully electrodynamic calculations are therefore needed to predict observables in realistic experimentally accessible systems. In turn, such calculations are also necessary to explain interesting quantum effects in plasmonics.

The newly emerging field of quantum plasmonics can open new pathways in fundamental science and applications [87, 88]. The study of light-matter-interactions enabled by NAs constitutes a major part of quantum plasmonics. The present thesis aims to contribute to this field.

The first goal of the thesis is to introduce a reasonable theoretical description for the interaction of NAs with Qs that form a hybrid system. This interaction can be understood in different approximations to account for the properties of the NA and the QS. Different degrees of approximation lead to the possibility to put emphasis on the description of different physical effects. For simplicity we may group these possibilities by the employed description of the NA, since a QS is suitably described within the laws of quantum mechanics. Three possibilities exist to describe the hybrid system: a semiclassical approach, a quantum optics approach, and a multimode quantum approach.

The semiclassical approach refers to a classical description of the NA. It allows to calculate emission rates in the weak-coupling regime and can be used to analyze sophisticated NA designs using state-of-the-art computational tools. But it does not allow a calculation of the quantum state of an external excitation field or of the emitted light of the combined system. This information is only accessible in a fully quantum description for both NA and QS. The quantum optics approach offers such a self-consistent approach by a quantization of the electromagnetic field in terms of infinitely many harmonic oscillators. This quantization scheme always works, irrespective of dominating modes of the NA, but has the disadvantage that one has to deal with an infinite-dimensional Hilbert space. Within the quantum optics quantization approach, some processes such as the spontaneous emission of an excited QS can be analyzed by tracing out the state of the light field. But the quantum state of the light field is then unknown. To calculate it, the field should not be traced and a reduction of the Hilbert space is needed. We achieve this reduction within the mentioned multimode NA quantization approach. Up to now, the quantization scheme was used in a number of publications [80, 89–91]. The description of the QS itself will be done within the framework of nonrelativistic quantum mechanics or in a simplified rate equation approximation [92]. With the help of a proper description of NA and QS their mutual interaction can then be understood in terms of well-defined coupling terms.

After reaching the first goal, we are able to use a versatile framework to describe the interaction of NAs with QS in different approximations. The second goal of the thesis is to use this frame-



work to investigate interesting hybrid systems made of NAs and Qs. We have put emphasis on questioning widely believed assumptions that may lead to false predictions and misinterpretations of experimental results. Our findings contribute to the understanding of light-matter-interactions on the nanoscale. Already in the strongest approximation, *i.e.* using a classical field description and a rate equation model, we are able to predict that so-called dipole-forbidden transitions in the vicinity of NAs might be drastically enhanced [78]. We demonstrate that an understanding of the dynamics of the QS sustaining such transitions is crucial to understand experimental observables.

Hence new insights are gained already in the simplest description of plasmonic light-matter-interactions. But there is much more. Using the multimode quantization approach for NAs, we have access to the quantum state of the emitted light. Within this description it is possible to discuss nonclassical light emitted by a hybrid system. By investigating the emission of single photons [89], we detail that not only the enhancement of the spontaneous emission rate of the QS is important. Also the nonclassical nature of the emitted light has to be considered. We shall see that the NA quantization scheme is required to self-consistently describe nonclassical light emission and the strong coupling of NAs to Qs to form truly quantum hybrid systems [80].

The thesis is structured to accomplish the aforementioned goals. In Sec. 2, the basics of classical NA theory are reviewed up to the point to describe their semiclassical interaction with Qs. Afterwards, we introduce a scheme to quantize the eigenmodes of NAs to describe truly quantum interactions (Sec. 3). In Sec. 4 we discuss how NAs can be used to change transition rates of dipole-forbidden transitions of Qs [78]. Section 5 is devoted to the use of NA-QS hybrid systems as sources for ultra-bright single-photon generation [89]. Thereafter, we investigate (Sec. 6) the possibility to reach the strong coupling regime of hybrid systems [80].

Finally, an outlook on future works using the introduced theoretical concepts in the current or a more generalized form is provided. A lot of the derivations and background information that are needed to verify and understand the outlined results are rather technical or already well documented in the literature. They are presented as additional material in a comprehensive Appendix right after the main part of the thesis.

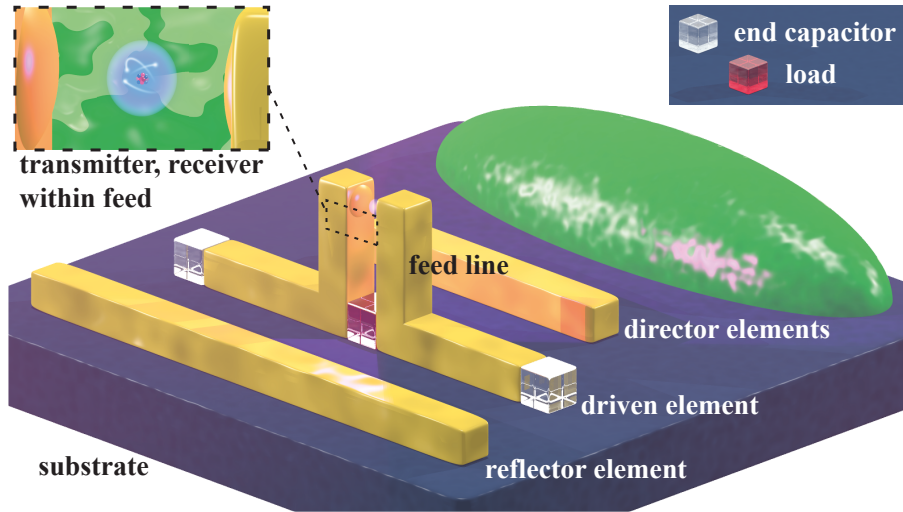


Figure 1: The structural elements of a fictive NA hosted on a substrate very similar to a Yagi-Uda NA. All elements are known from radio frequency electrical engineering and offer different possibilities in NA design.

## 2 Basics of Nanoantenna Theory

New and improved fabrication techniques made it possible to investigate the interesting properties of NAs. In fact, NA theory is not a new topic in research and engineering as most of the concepts are known within the context of antenna theory for long time.

In the following, we shall review some important aspects of classical antenna theory and put them into relation to NA theory. Introductions to classical antenna theory are given by Balanis [93] or Stutzmann & Thiele [94]. Antenna theory has also been applied as simplistic models for NAs [95,96]. In addition, a number of well-written and detailed introductions to NA theory have been provided [6, 10, 97–99]. As we are mostly concerned with light-matter-interactions, the NA designs studied here are rather simplistic compared to state-of-the-art radio frequency antennas, but still sophisticated enough to show an interesting behavior.

We are mostly interested in the new theoretical aspects that NA research provides in addition to classical antenna theory. Therefore some of the used terminology will be introduced this section. Afterwards, we will outline our description of NAs within classical electrodynamics (Sec. 2.1). In Sec. 2.2 we introduce one of the most important NA parameters, the efficiency  $\eta$ . Afterwards, we shall investigate how the resonant scaling of NAs can be calculated (Sec. 2.3). We conclude this Section with a description of the action of a time-varying electromagnetic field on a QS.

### Nanoantenna Terminology

Standard definitions for antennas are well established for radio frequencies. These definitions are essential because they serve as a common ground between different fields, especially electrical engineering and physics. Thus we shall relate vocabulary and concepts to the widely accepted “IEEE Draft Standard Definitions of Terms for Antennas” [100].

As illustrated in Fig. 1, a NA consists of several radiating elements that are themselves capable of receiving and emitting electromagnetic radiation. Three canonical radiating elements are depicted: a reflector element, a driven element and two director elements. These elements serve different purposes. The reflector and director elements are designed such that the energy flux of the emitted radiation is dominantly directed in a specified direction. They have been used

for optical Yagi-Uda NAs [49–51, 101, 102] and for other geometries involving metallic discs or spheres [103–105]. Spherical dielectric directors were investigated as well [106, 107].

Between reflector and director element is the so-called driven element, which is characterized by its connection to the transmitter and/or receiver placed inside of the feed of the NA. The connection of transmitter/receiver to the driven element may be realized by a feed line to acquire an efficient coupling of the NA [13, 108]. End capacitors placed at the termination of a radiating element are used to modify their properties *i.e.* by increasing their apparent length and thus their resonance characteristics [109, 110]. A similar function is attributed to the load which is generally placed in-between parts of radiating elements. By changing the electromagnetic properties of the load *i.e.* by short intense laser pulses, NA resonances can be actively modified on very short time scales [111–114]. Generally we can state that a lot of the concepts of electrical engineering outlined in the “IEEE Draft Standard Definitions of Terms for Antennas” have found their way into NA research.

## 2.1 Aspects of Classical Electrodynamics

In frequency space, the response of linear materials to an external electric field  $\mathbf{E}(\mathbf{r}, \omega)$  can be described by the constitutive relation

$$\mathbf{D}(\mathbf{r}, \omega) = \varepsilon_0 \varepsilon(\mathbf{r}, \omega) \mathbf{E}(\mathbf{r}, \omega) \quad (1)$$

which relates the dielectric displacement  $\mathbf{D}(\mathbf{r}, \omega)$  to  $\mathbf{E}(\mathbf{r}, \omega)$ . Here,  $\varepsilon_0 \approx 8.854 \text{ F/m}$  refers to the vacuum permittivity. We further assume that the relative permittivity  $\varepsilon(\mathbf{r}, \omega)$  is isotropic, *i.e.* just a scalar function. We also implicitly assume a local response of all materials, although this property is under current investigation for plasmonic materials [64, 69]. Please note the usage of a frequency space representation in Eq. (1). A time representation is related via a Fourier transformation of the form  $f(t) = \int_{-\infty}^{\infty} f(\omega) \exp[-i\omega t] d\omega$ .

Magnetic interactions can be neglected for solid state bodies in the visible frequency range [115]. We may thus assume that the magnetic permeability is unity for all used materials [ $\mu(\mathbf{r}, \omega) = 1$ ]. The magnetic induction  $\mathbf{B}(\mathbf{r}, \omega)$  and magnetic field  $\mathbf{H}(\mathbf{r}, \omega)$  are then related by the magnetic constitutive relation  $\mathbf{B}(\mathbf{r}, \omega) = \mu_0 \mathbf{H}(\mathbf{r}, \omega)$ , where  $\mu_0 = 4\pi \cdot 10^{-7} \text{ H/m}$  is the permeability of vacuum. In this case, Eq. (1) governs the whole material response of the NA elements and surroundings. The field equations (Maxwell’s equations) read

$$\begin{aligned} \nabla \times \mathbf{E}(\mathbf{r}, \omega) &= i\omega \mathbf{B}(\mathbf{r}, \omega) & \nabla \cdot \varepsilon(\mathbf{r}, \omega) \mathbf{E}(\mathbf{r}, \omega) &= \rho_{\text{ext}}(\mathbf{r}, \omega) / \varepsilon_0 \\ \nabla \cdot \mathbf{B}(\mathbf{r}, \omega) &= 0 & \nabla \times \mathbf{B}(\mathbf{r}, \omega) &= \mu_0 \mathbf{j}_{\text{ext}}(\mathbf{r}, \omega) - i\omega \varepsilon(\mathbf{r}, \omega) \mathbf{E}(\mathbf{r}, \omega) / c^2 \end{aligned} \quad (2)$$

with the speed of light  $c = 1/\sqrt{\varepsilon_0 \mu_0} \equiv 299\,792\,458 \text{ m/s}$ . The equations on the left, Faraday’s law of induction and Gauss’s law for magnetism, can be seen as constraint equations for the fields alone. Gauss’s law and Ampère’s law on the right relate the fields to their causes, charges and currents. Here,  $\rho_{\text{ext}}(\mathbf{r}, \omega)$  and  $\mathbf{j}_{\text{ext}}(\mathbf{r}, \omega)$  refer to all charges and currents that are not governed by Eq. (1). Then,  $\varepsilon(\mathbf{r}, \omega)$  includes conductive currents in the form of Ohm’s law,  $\mathbf{j}_{\text{cond}}(\mathbf{r}, \omega) = \sigma(\mathbf{r}, \omega) \mathbf{E}(\mathbf{r}, \omega)$ . Hence we use a generalized permittivity which can be obtained from the non-conductive permittivity  $\tilde{\varepsilon}(\mathbf{r}, \omega)$  by the formal replacement  $\tilde{\varepsilon}(\mathbf{r}, \omega) \rightarrow \varepsilon(\mathbf{r}, \omega) + i\sigma(\mathbf{r}, \omega) / \varepsilon_0 \omega$  [116].

If NAs are made of distinct materials, the generally space-dependent permittivity reduces to permittivities in different regions  $\Omega_i$ , *e.g.*  $\varepsilon_i(\omega)$  for each material from which the NA is built. For example,  $\varepsilon_d(\omega)$  may denote an embedding dielectric and  $\varepsilon_s(\omega)$  a certain substrate. Since the permittivity is constant in each of these regions, Maxwell’s equations can be used to derive

inhomogeneous wave equations for electric field and magnetic induction,

$$\begin{aligned} \left( \Delta + \frac{\omega^2}{c^2} \varepsilon_i(\omega) \right) \mathbf{B}(\mathbf{r}, \omega) &= -\mu_0 \nabla \times \mathbf{j}_{\text{ext}}(\mathbf{r}, \omega) \text{ and} \\ \left( \nabla \times \nabla \times - \frac{\omega^2}{c^2} \varepsilon_i(\omega) \right) \mathbf{E}(\mathbf{r}, \omega) &= i\omega \mu_0 \mathbf{j}_{\text{ext}}(\mathbf{r}, \omega) \text{ for } \mathbf{r} \in \Omega_i. \end{aligned} \quad (3)$$

Here,  $\nabla \times \nabla \times \mathbf{F}(\mathbf{r}) = \nabla \nabla \cdot \mathbf{F}(\mathbf{r}) - \Delta \mathbf{F}(\mathbf{r})$  has been used. In the absence of external charges, the wave equation for the electric field may be written as a vectorial Helmholtz equation. Such an equation also holds for the electromagnetic potentials  $\phi(\mathbf{r}, \omega)$  and  $\mathbf{A}(\mathbf{r}, \omega)$  that are introduced as  $\mathbf{E}(\mathbf{r}, \omega) = -\nabla \phi(\mathbf{r}, \omega) + i\omega \mathbf{A}(\mathbf{r}, \omega)$  and  $\mathbf{B}(\mathbf{r}, \omega) = \nabla \times \mathbf{A}(\mathbf{r}, \omega)$ .

Most important for our argumentations is that, by virtue of Eq. (3), the fields can be found as solutions of a set of elliptical partial differential equations with given boundary conditions. At the boundary, the tangential component of  $\mathbf{H}(\mathbf{r}, \omega)$  and  $\mathbf{E}(\mathbf{r}, \omega)$  as well as the normal component of  $\mathbf{B}(\mathbf{r}, \omega)$  and  $\mathbf{D}(\mathbf{r}, \omega)$  must be continuous. This holds very general, except in the presence of surface charges and currents.

We can define the Green's function  $G(\mathbf{r}, \mathbf{r}', \omega)$  [cf. Eq. (3)] in Cartesian coordinates as

$$\left( \nabla \times \nabla \times - \frac{\omega^2}{c^2} \varepsilon(\mathbf{r}, \omega) \right) G_{ij}(\mathbf{r}, \mathbf{r}', \omega) = \delta_{ij} \delta(\mathbf{r} - \mathbf{r}') . \quad (4)$$

In the latter equation it is evident that  $G(\mathbf{r}, \mathbf{r}', \omega)$  is a tensor, *i.e.*  $G(\mathbf{r}, \mathbf{r}', \omega) \mathbf{y} \in \mathbb{C}^3 \forall \mathbf{y} \in \mathbb{C}^3$ . To be concise, the symbol  $G$  is employed exclusively for the Green's function throughout this thesis. Following Eq. (3),  $G(\mathbf{r}, \mathbf{r}', \omega)$  can be used to calculate the electromagnetic fields via

$$\begin{aligned} \mathbf{E}(\mathbf{r}, \omega) &= i\mu_0 \omega \int G(\mathbf{r}, \mathbf{r}', \omega) \mathbf{j}_{\text{ext}}(\mathbf{r}', \omega) dV' \text{ and} \\ \mathbf{B}(\mathbf{r}, \omega) &= (i\omega)^{-1} \nabla \times \mathbf{E}(\mathbf{r}, \omega) . \end{aligned} \quad (5)$$

Please note that Eq. (4) is more general than Eq. (3) as we allow any kind of spatially varying  $\varepsilon(\mathbf{r}, \omega)$ , not only piecewise constant  $\varepsilon_i(\omega)$ . Especially in Sec. 3 we will use that any information about the electrodynamic properties of a system is contained in the knowledge of the Green's function to quantize NA fields.

It must be clearly emphasized that the classical electrodynamic description of NAs sketched here excludes some effects to make certain observables easily accessible in analytical and numerical considerations. For instance, nonlinearities may add an intensity dependency [117,118] and heating of the NA may cause a memory effects [119–122].

## 2.2 Radiation Efficiency

Now everything is at hand to discuss some physical properties of NAs. More detailed information can be found in devoted references [6,98,123]. In the following we shall focus on just two quantities which are characteristic for NAs in general and of utmost importance for any investigation and application: their efficiency and their scaling (Sec. 2.3).

The radiation efficiency  $\eta$ , often simply termed efficiency, appears in any relation of far-field and near-field observables. For radio frequency antennas,  $\eta$  can be defined as “The ratio of the total power radiated by an antenna to the net power accepted by the antenna from the connected transmitter” [100]. Hence, to find a suitable equivalent to this definition, we have to consider a certain kind of receiver or emitter, *i.e.* a QS.

In most scenarios studied thus far, the QS is assumed to exhibit a dipolar radiation characteristic, but we will see in Sec. 4 that this may not be the case in general, and that interactions

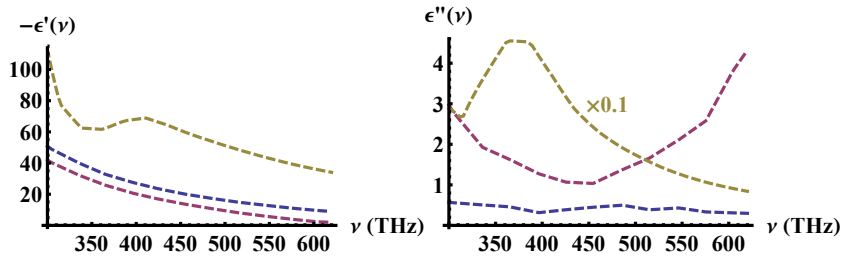


Figure 2: Permittivities of widely used plasmonic materials silver (blue dashed lines) and gold (magenta dashed lines) after Ref. [124], and aluminium (yellow dashed line) after Ref. [125] from  $\nu = 300$  THz ( $\lambda = 1 \mu\text{m}$ ) to 680 THz ( $\lambda = 480$  nm). Left:  $\varepsilon'(\nu)$  of silver and gold have a very similar dependency, whereas aluminium shows a stronger metallic character ( $\varepsilon'(\nu) \ll 0$ ) with a more complicated shape which cannot be explained by a simple Drude fit. Right:  $\varepsilon''(\nu)$  of silver shows comparably little absorption in the investigated spectral range, whereas gold obeys an absorption minimum at  $\nu \approx 450$  THz (670 nm).  $\varepsilon''(\nu)$  of aluminium is lowered by a factor of 10 to fit on the same graph.

involving higher order terms can play a significant role, too. In our discussion of the efficiency, we will restrict ourselves to a dipole emitter. A generalization to emitters with more complicated characteristics is straight forward. In the case of dipole emitters, the efficiency  $\eta$  of a NA can be defined by the fraction of the power of a radiating dipole that can escape to infinity  $P_{\text{rad}}^{\text{na}}$ , and its overall extracted power  $P_{\text{tot}}^{\text{na}}$ . With the help of Poynting's Theorem (App. A.1), these powers are given by

$$\begin{aligned}
 P_{\text{rad}}^{\text{na}}(\mathbf{r}_0, \omega_0, \mathbf{n}) &= \oint_{r \rightarrow \infty} \langle \mathbf{S}_{\text{dip}}(\mathbf{r}, t) \rangle \cdot \mathbf{e}_r d\Omega \quad \text{and} \\
 P_{\text{tot}}^{\text{na}}(\mathbf{r}_0, \omega_0, \mathbf{n}) &= \oint_{r=\delta} \langle \mathbf{S}_{\text{dip}}(\mathbf{r}, t) \rangle \cdot \mathbf{e}_r d\Omega = P_{\text{rad}}^{\text{na}} + P_{\text{nr}}^{\text{na}} \quad \text{with} \\
 P_{\text{nr}}^{\text{na}}(\mathbf{r}_0, \omega_0, \mathbf{n}) &= \int \varepsilon_0 \omega_0 \varepsilon''(\mathbf{r}, \omega_0) \langle \mathbf{E}_{\text{dip}}^2(\mathbf{r}, t) \rangle dV .
 \end{aligned} \tag{6}$$

Here,  $\delta$  is a small radius containing only the dipole,  $d\Omega$  is the differential surface element, and  $\varepsilon''(\mathbf{r}, \omega)$  is the imaginary part of the permittivity,  $\varepsilon(\mathbf{r}, \omega) = \varepsilon'(\mathbf{r}, \omega) + i\varepsilon''(\mathbf{r}, \omega)$ , and  $\langle \rangle$  denotes a sufficiently long time-average. The subscript ‘‘dip’’ shall indicate that the dipole emitter is the only source of the electromagnetic fields. It is described by its position  $\mathbf{r}_0$ , its oscillation frequency  $\omega_0$ , and its orientation  $\mathbf{n}$ . The radiation efficiency is then given as

$$\eta(\mathbf{r}_0, \omega_0, \mathbf{n}) = \frac{P_{\text{rad}}^{\text{na}}(\mathbf{r}_0, \omega_0, \mathbf{n})}{P_{\text{rad}}^{\text{na}}(\mathbf{r}_0, \omega_0, \mathbf{n}) + P_{\text{nr}}^{\text{na}}(\mathbf{r}_0, \omega_0, \mathbf{n})} . \tag{7}$$

As we can see in Eq. (7), a decreased radiation efficiency is caused by a nonvanishing dissipation in the environment of the dipole, since then  $P_{\text{nr}}^{\text{na}} \neq 0$ . Following Eq. (6),  $P_{\text{nr}}^{\text{na}}$  is caused by the imaginary part of the permittivity as well as the distribution of the electric field in the dissipative environment. Thus we shall discuss the main factors that influence the efficiency of a NA: the electrodynamic properties of the plasmonic material and the NA geometry in the following.

### 2.2.1 Dissipation in plasmonic Materials

Plasmonic excitations may only be observed if  $\varepsilon'(\omega)$  between two adjacent materials changes its sign [26]. Hence, one material must have  $\varepsilon'(\omega) < 0$ . However, as we know from Kramers-Kronig-relations, a resonant behavior inevitably leads to non-negligible values in the imaginary part of

the permittivity and thus to losses in the material. These losses are strongest if the frequency is close to an intrinsic resonance frequency of the material. Without losses, the efficiency  $\eta$  as defined by Eq. (7) would always amount to unity. This explains the interest in almost lossless dielectric NAs [8, 9, 126, 127].

A thorough discussion of the loss mechanisms, *i.e.* conduction band charges, inter- and intraband transitions can be found in Ref. [123] for plasmonics or in any introduction to solid state physics [128]. Detailed introductions to widely used plasmonic materials can be found in Refs. [129–131]. Silver, gold and aluminium are metals, which are often used in plasmonic research and application. Their respective permittivities are shown in Fig. 2. Silver has the lowest absorption, which is the reason why it is often chosen for theoretical studies.

Unfortunately, the properties of silver are much more complicated in reality. The noble metal usually exhibits a thin oxidation layer leading to an often dramatic increase of plasmonic losses. Moreover, nanoscale fabrication is often challenging and the diffusion of silver ions off nanostructures makes them toxic [129, 130]. Hence, gold is preferred in experiments as, most notably, fabrication is usually much easier with this material, in bottom-up as well as top-down approaches [132]. On the other hand, gold is usually very expensive and should only be used below  $\nu = 600$  THz (500 nm) because of strongly increased absorption due to interband transitions. Thus, other materials such as copper and tungsten have attracted considerable attention, both because of possible cost reduction and for applications in the UV spectral range [133, 134]. Aluminium is also attractive as it may also be used for short-wavelength devices, in conjunction to CMOS technology and in nonlinear processes, but it suffers from strongly increased losses compared to gold [57, 135, 136]. Hence in practice the choice of a plasmonic material follows the constraints of the experiment or application. Since we are mainly interested to show that certain effects are principally possible because of the interaction of SPPs with QDs, we shall use gold and silver in our studies.

Please note that we assume that the permittivity of the employed materials is a function of the frequency only. Further dependencies and our reasoning to neglect them are outlined in App. A.5.

### 2.2.2 Nanoantenna Geometry

We have seen that the intrinsic absorption in plasmonic materials is the reason for a decrease in the NA efficiency. So the spatial distribution of the electric field inside the NA material has a strong influence on the losses as a strong electric field inside the metal leads to a huge dissipation. Thus, the geometry of the NA, or its proper design, play a dominant role. In the following we will discuss two characteristic features of NA design: NA size and symmetry.

**Size effects** The absorption cross section  $C_{\text{abs}}$  of small metallic spheres scales with their volume, whereas the scattering cross section  $C_{\text{sca}}$  scales with the volume squared when illuminated by a plane wave [137]. As a first approximation, a similar behavior may be expected if the illumination is changed to a close-by dipole and we may take the most important result for small gold spheres as a first indication for minimum NA sizes. For these particles, absorption starts to dominate for diameters smaller than 50 nm and  $\eta$  drops considerably [137]. However, the coupling to close-by QDs strongly increases for small NAs (Sec. 3.1). Hence, pioneering experiments were performed with NAs exhibiting dimensions around 50 nm to achieve a considerable interaction strength and a reasonable efficiency [44, 45].

The assumption, that 50 nm is a characteristic dimension for efficient NAs can further be justified by basic results from electrical engineering (EE). In this field, the non-perfect overlap of an antenna mode and radiation modes is interpreted as an impedance mismatch between two systems [93]. For a one-dimensional antenna, the radiated power  $P_{\text{rad}}$  of an antenna is often

expressed in analogy to Ohm's law in terms of a radiation resistance  $R_r$  via  $P_{\text{rad}} = \frac{1}{2} |I_0|^2 R_r$ . The radiation resistance for small dipole antennas scales as  $R_r \propto (kL)^2$ , where  $k = 2\pi/\lambda$  is the wavenumber of free-space radiation and  $L$  is the length of the antenna [93]. In the near-field the integral  $\oint \mathbf{S}(\mathbf{r}, \omega) \cdot \mathbf{e}_r d\Omega$  exhibits a dominating imaginary contribution  $P_{\text{rea}} \propto 2\omega R_r / (kr)^3$ , the reactive power.  $P_{\text{rea}}$  describes a continuous energy exchange between outgoing and incoming radiation at twice the oscillation frequency  $\omega$ .

If we compare the characteristic dependencies of  $P_{\text{rad}}$  and  $P_{\text{rea}}$ , we may define a length  $L_\eta$  for which both powers are approximately even, *i.e.* a scaling roughly discriminating efficient and lossy antennas. An efficient radiation can only take place if  $L_\eta \gtrsim \lambda/2\pi$ , which gives approximately  $L_\eta = 80 \text{ nm}$  for  $\lambda = 500 \text{ nm}$ . This characteristic value is in rough agreement to the aforementioned comparison of scattering and absorption cross sections of gold spheres.

We can conclude that efficient NAs must have minimum dimensions in the order of  $L_\eta$ . This size requirement causes a general trade-off between efficiency and achievable coupling strengths of NAs to QSs. It also defines a lower characteristic size for which we may call a metallic particle a NA.

**Symmetry** For radio frequencies, the electric field is approximately normal to the surfaces of small metallic particles since metals are almost perfect conductors in this frequency range. This has severe consequences for possible antenna designs, as the Poynting vector  $\mathbf{S}$  must be always tangential to the conductor, and  $\oint \mathbf{S} \cdot d\mathbf{A}$  over the conductor surface vanishes approximately.

Hence, radio frequency antennas made of just a single small element hardly radiate - they need a gap to operate efficiently. On the other hand, single-element NAs may radiate efficiently because of their plasmonic properties. The use of single-element NAs is not generally obstructive if a plasmonic current can be formed over a somehow extended region as it is the case for ring-type NAs without classical analogue [57, 59]. But if one is interested in strong light-matter-interactions, small NAs that have at least two elements as a feed gap with large field enhancement capabilities is existing in which a QS can be placed, seem to be most desirable.

Let us assume rotational and mirror symmetry for a certain class of NAs and analyze their implications for the efficiency within a quasistatic approximation. That is, the NA elements shall consist of spheroids, wires, discs etc. with coinciding rotational  $z$ -axis of symmetry. Furthermore, for each element located at  $z_i^- < 0$  there exists a mirror symmetric element at  $z_i^+ = -z_i^-$  such that at least one gap around  $\mathbf{r} = 0$  is formed. To calculate  $\eta$ , we assume a dipole inside this gap at  $\mathbf{r} = 0$ , oriented along the  $z$ -axis, *i.e.* centered between the NA elements. The quasistatic potential  $\phi_{\text{qs}}^{\text{na}}(\mathbf{r}, \omega)$  of the NA's scattered field can then be expressed as [138, 139]

$$\phi_{\text{qs}}^{\text{na}}(\mathbf{r}, \omega) = \frac{1}{4\pi\epsilon_0} \sum_{n=0}^{\infty} \frac{M_n(\omega) P_n(\cos\theta)}{r^{n+1}}. \quad (8)$$

Here,  $P_n(\cos\theta)$  and  $M_n(\omega)$  are the usual Legendre polynomials and quasistatic multipole moments, respectively. We find that the expansion of the potential on the positive (negative) axis of symmetry for  $\theta = 0$  (or  $\theta = \pi$ ) is simply given as

$$\phi_{\text{qs}}^{\text{na}}(z, \omega) = \frac{1}{4\pi\epsilon_0} \sum_{n=0}^{\infty} \frac{M_n(\omega)}{|z|^{n+1}} \begin{cases} 1 & \text{for } z > 0 \text{ and} \\ (-1)^n & \text{for } z < 0, \end{cases}$$

since  $P_n(1) = 1$  and  $P_n(-1) = (-1)^n$ . The full information of the system is thus given by an expansion of the potential on the axis of symmetry. Note that our dipole source is a perfectly antisymmetric charge distribution. The scattered field of the NA must then also be antisymmetric

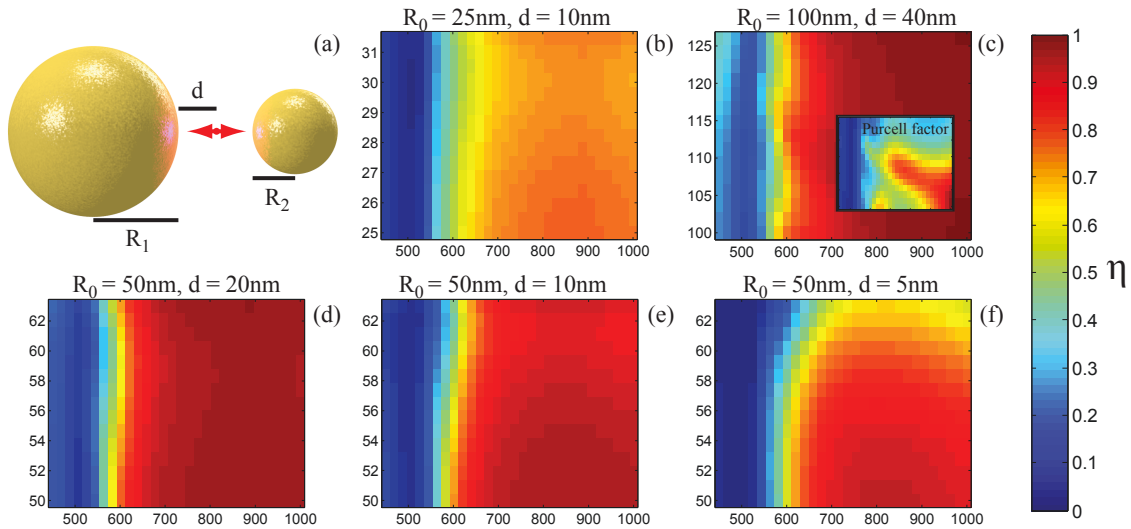


Figure 3: The effect of asymmetry on the efficiency of NAs. (a) Considered geometry: two gold spheres with radii  $R_1$  and  $R_2$ . Their surface-to-surface separation amounts to the distance  $2d$ . A dipole emits along the rotational axis of the dimer and is centered on the rotational axis inside of the gap. Hence, its distance to either sphere is  $d$ . The volume of the system is held constant at  $V \propto R_0^3$ . (b)-(f): Radiation efficiency  $\eta(\lambda, R_1)$  for fixed  $R_0$  and  $d$ .  $y$ -axis:  $R_1$  as a measure of asymmetry: the dimer is mirror symmetric if  $R_1 = R_0$  but becomes more asymmetric for increased  $R_1$ .  $x$ -axis: emission wavelength  $\lambda$  of the centered dipole. (b)-(d): For  $R_0/d = 2.5$ ,  $\eta$  remains almost constant for varying  $R_1$ , although the dipole emission rate compared to free space,  $F(\lambda, R_1)$ , reveals interesting resonance phenomena [inset in (c), scaled from 0 to  $F_{\max} \approx 35$ ], (d)-(f):  $R_0/d$  increases from 2.5 to 10. The drop in  $\eta$  for higher asymmetry becomes more and more significant.

and thus obeys  $\phi_{\text{qs}}^{\text{na}}(z, \omega) = -\phi_{\text{qs}}^{\text{na}}(-z, \omega)$ , which results in  $M_n = 0 \forall n = \{0, 2, 4, \dots\}$ .

From these symmetry considerations it follows that the octupole mode ( $n = 3$ ) is the first nonvanishing “dark mode” of the rotational and mirror symmetric NA that can be excited by the dipole emitter. This should lead to an increase of  $\eta$  compared to a) asymmetric NAs and b) asymmetric placements and orientations of the emitter. A design with the assumed symmetries is especially beneficial if the dipole resonance frequency of the NA and the oscillation frequency of the emitter coincide. Then, the octupolar mode of the NA is energetically well separated from the emitter’s oscillation frequency and the coupling to dark modes may be negligible.

We have checked the influence of the asymmetry of NAs on their efficiency with an in-house code able to calculate the electromagnetic scattering of an almost arbitrary arrangement of spheres [132]. To verify our analytical considerations via such numerical calculations, it is important to distinguish several effects, as  $\eta$  depends on many geometrical and material parameters. At the focus of our investigations shall be the influence of the NA symmetry, which results in some requirements on the NA geometry. We would like to test symmetry dependencies for the simplest systems. Consequently, we chose spherical metallic dimers with radii  $R_1$  and  $R_2$ , see Fig. 3 (a).

In a simplified picture, a dimer may be described by two radiating dipoles in addition to the dipole emitter in-between. Thus, to preserve the overall polarizability and its radiation capabilities, the total volume  $V \equiv 2 \times 4/3 \pi R_0^3 = 4/3 \pi (R_1^3 + R_2^3)$  of the dimer has to remain constant. Hence, if one radius is decreased, the other one is increased in our investigation, and the maximum (minimum) value of  $R_{1/2}$  is given by  $\sqrt[3]{2}R_0$  (0).

Furthermore, the coupling of the dipole emitter to the spheres should be kept approximately at



the same level. To achieve this, the distance  $d$  between dimer surface and dipole position is kept constant. That this volume-preserving approach is justified can be seen in Fig. 3 (b)-(d), where the efficiency  $\eta$  remains almost constant for strong changes in  $R_1$  in the case of relatively large separations of the dimer ( $R_0/d = 2.5$ ). However, if  $R_0/d$  is increased such that the mutual coupling of the dimer elements becomes stronger, the metallic spheres form a truly combined system. In that case, we find that the efficiency significantly drops with increased asymmetry, see Fig. 3 (e) and (f). Especially in Fig. 3 (f), the drop in  $\eta$  from close to 100 % at  $\lambda = 800$  nm and  $R_1 = R_2 = 50$  nm to values around 60 % for  $R_1 \rightarrow 63$  nm and  $R_2 \rightarrow 0$  nm is remarkable.

Thus the efficiency can be strongly influenced by the symmetry of the NA. The effect is most pronounced if the NA's feed gap is small such that the adjacent NA elements form a truly coupled plasmonic system. Then, symmetric NAs are considerably more efficient than asymmetric ones, since they suppress the coupling to higher-order modes of the NA. The influence on  $\eta$  is not so distinctive if the gap is large enough such that the NA elements act as independent radiators. In this case, the overall volume and material parameters of the used metal are the most important factors.

We have now discussed the main factor that influences the NA efficiency: the electrodynamic properties of the material and its geometry. The size is one of the most important quantities, which leads to the question how the scaling of NAs can be described in general.

### 2.3 Scaling

NAs exhibit sizes down to a few tens of nanometers, *i.e.* they are often much smaller than the wavelength  $\lambda$ . At first this seems contradictory as antennas in the radio frequency regime are resonant if their length is a multiple of  $\lambda/2$ . The difference in the size-to-wavelength ratio results from the different kinds of excitations of these antennas. For radio frequencies, surface currents form standing waves along the antenna. At optical frequencies and, depending on the material, down to the THz regime, the excitations must be understood in terms of SPP excitations. Those excitations may exist for very different NA sizes.

Metallic spheres much smaller than the wavelength with permittivity  $\varepsilon_m(\omega)$  embedded in a dielectric with permittivity  $\varepsilon_d(\omega)$  obey a dipolar resonance if the so-called Fröhlich condition  $\Re[\varepsilon_m(\omega) + 2\varepsilon_d(\omega)] = 0$  is fulfilled [137]. For noble metals, the Fröhlich condition is usually fulfilled at a certain frequency in the visible spectrum, but within the quasistatic approximation the resonance frequency is independent of the size of the sphere. So very small metallic spheres can be resonant at optical frequencies, too. Can those spheres be considered as NAs? The minimum size limit is given by the requirement of an efficient conversion between free-space radiation and localized energy (*cf.* page 2). This requirement loosely sets lower and upper size limits. Absorption gives a lower limit for the dimension of a NA. In Sec. 2.2 we have seen that an efficient coupling to free-space radiation modes can be achieved for NAs with dimensions larger than  $L_\eta = \lambda/2\pi$ . Hence, values of roughly 50...100 nm are characteristic lengths of NAs working in the visible spectrum.

On the other hand, NAs may be comparably large. Their maximum size can be defined via losses: an efficient energy localization is not possible if a NA is so large that an efficient energy transfer towards its feed gap is prevented. The maximum NA lengths are typically in the order of tens of  $\mu\text{m}$  for visible light, but can increase up to the mm-range for infrared radiation [26]. The use of large NAs regarding enhanced light-matter-interaction to single molecules may be very limited. However, such NAs offer different features like a high directivity [49, 50], a possible application as ultra-thin polarization filters [147]. They may also provide localized energy at different NA feed gaps for varying wavelengths [148]. In Fig. 4, experimentally investigated NAs with different

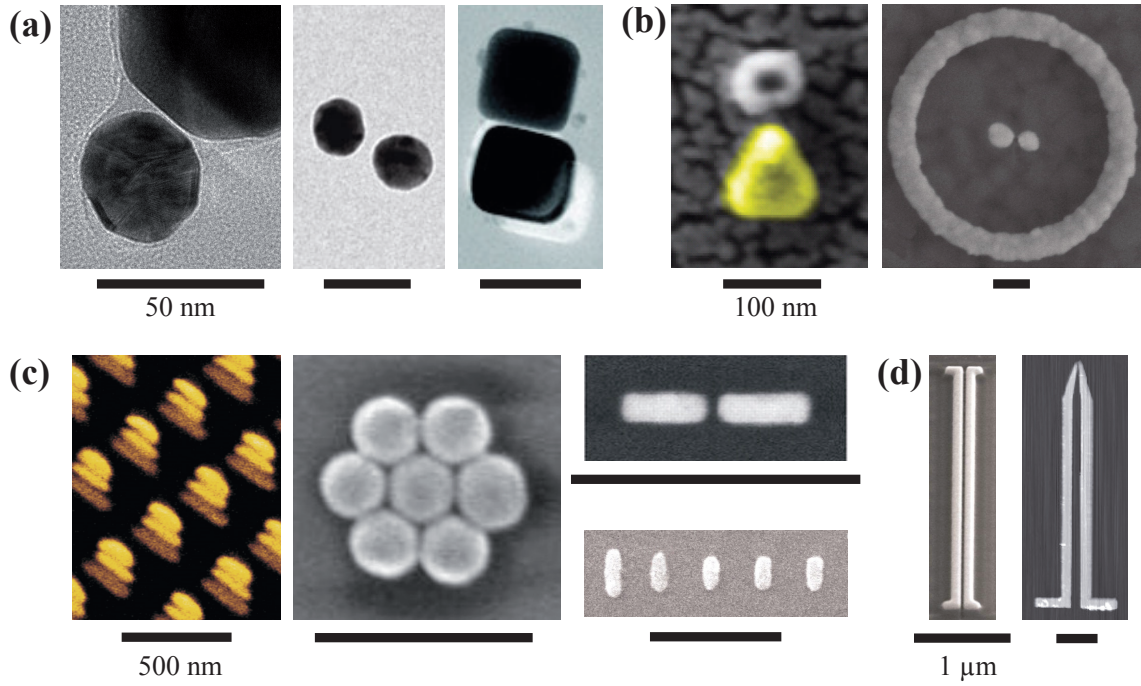


Figure 4: Experimentally investigated NAs arranged according to their characteristic sizes  $l_c$  (scale-bars) from 50 nm (a) to 1  $\mu\text{m}$  (d). The images were recorded with different techniques and published in different works. (a)  $l_c = 50$  nm: gold [140,141] and silver [142] NAs with small feed-gaps. Whereas these NAs are produced using chemical techniques, most of the following ones were fabricated by physical processes, *e.g.* electron-beam lithography. (b)  $l_c = 100$  nm: gold-palladium two-element NA [143] and a silver NA with a ring-type directional element [144]\*. The complexity of the NAs is increased in comparison to (a). This trend continues for the NAs in (c) with  $l_c = 500$  nm: an array made of Yagi-Uda NAs [51], self-assembled heptamers [145], a two-element dipole by Mühlischlegel *et al.* [37] and a single Yagi-Uda NA [49]\*. (d) Relatively large NAs with  $l_c = 1$   $\mu\text{m}$ : a two-dipole NA with an intermediate transmission line [146] and a mid-infrared NA with a tapered feed line [108]. NAs in (c) & (d) are all made of gold.

\*These images were slightly modified to enhance the visibility of the NAs.

characteristic length scales are shown.

The proper design of NAs requires insights into their scaling principles. Different approaches exist to find them, which may be grouped into three general categories depending on the employed methods:

1. Analytical approaches: scaling and resonance properties can be determined entirely and explicitly within a mathematical theory.
2. Semianalytical methods: an approximate analytical model can be found that governs the main physics and provide useful insights and reduce the mathematical complexity.
3. Numerics: physical properties may not be described by analytical models, thus numerical calculations are necessary.

These different approaches shall be briefly discussed in the following. The insights we will gain will naturally not be limited to the scaling of NAs. They will also serve us as a guideline on the use of different levels of approximations for other related questions, *i.e.* a suitable description of an interaction of Qs with NAs.

### 2.3.1 Analytical Approaches

The use of analytical solutions in terms of basic mathematical functions is generally preferable. They provide a complete understanding of the physical effects but can only be found in a few special cases. In particular, such solutions can be obtained only in coordinate systems in which the Helmholtz equation is separable [149, 150]. If the NA surface is entirely perpendicular to one of the coordinates in these coordinate systems, *e.g.* the surface of a sphere in spherical coordinates, Maxwell’s equations reduce to a finite set of algebraic equations in terms of the eigenfunctions of the Helmholtz equation. But only some of these coordinate systems are useful to describe NAs, as their volume is naturally finite. Hence, an analytical descriptions for NAs may only be achieved for certain kinds of ellipsoids. However, already the treatment of spheroids, *i.e.* ellipsoids with two axes of equal length, becomes rather involved [137] and analytical solutions usually require even simpler geometries. For this reason, most scenarios cope with single spherical NAs in the framework of Mie theory, see *e.g.* Refs. [6, 98, 123].

If the NA is much smaller than the wavelength, an approximative quasistatic description can be used. In this case, the electric field close to the NA can be determined by solving the Laplace equation for the electrostatic potential [123]. The Laplace equation is a special case of the Helmholtz equation for  $k \rightarrow 0$  ( $\lambda \rightarrow \infty$ ). It is separable in toroidal and bispherical coordinate systems [149, 150]. Hence, further analytical solutions can be anticipated. However, thus far, toroidal NAs have not been analytically investigated to the best of our knowledge, although experimental and numerical studies were performed [151, 152]. Furthermore, a description in bispherical coordinates seems rather inappropriate as Mie theory can be readily generalized to an ensemble of spheres [132, 153]. Hence we may state that quasistatic analytical solutions can be useful in coordinate systems in which the Helmholtz equation already yields analytical solutions. This is the case for spherical NAs. Here, Mie theory can be simplified from a vectorial problem involving spherical Bessel functions  $j_n(kr)$  to a scalar description in terms of polynomials in  $1/r$  [154].

But even if the accessible geometries are not very sophisticated, analytical considerations lead to results that can be used for generalizations. Furthermore, subsequent derivations may also reveal useful insights into characteristic measures of a physical process.

### 2.3.2 NAs as Fabry-Perot Resonators: a semianalytical Description

As we have seen, the number of configurations that can be investigated on purely analytical means is rather limited. Nevertheless, one does not need to apply numerical investigations directly, as approximative analytical solutions may be obtained. In particular, a Fabry-Perot resonator model has been rather successful and shall be discussed in the following, although also other semianalytical models are known [98].

**Wire NAs** The Fabry-Perot model to describe the scaling of NAs was introduced by Novotny [155]. He considered wire NAs as resonators that support propagating modes which are reflected at the terminations of the NA. This reflection is described by a complex reflection coefficient  $r = |r| \exp[i\phi_r]$ . Because of the coupling to free-space modes, the reflection at the NA terminations causes both an amplitude and phase change. This is different compared to a “perfect reflection” with  $|r| = 1$  and  $\phi_r = \{\pi \text{ or } 0\}$  for perfect metallic or magnetic conductors. The supported propagating modes of a thin wire are  $m = 0$  cylindrical Bessel modes [154]. These modes exhibit a simple phase dependency  $\phi_p \propto k'z$  in propagation direction  $z$ , where  $k'$  is the real part of the propagation constant and  $z$  the wire’s rotational axis. Then, resonant lengths  $L_n$  of the  $n^{\text{th}}$  order

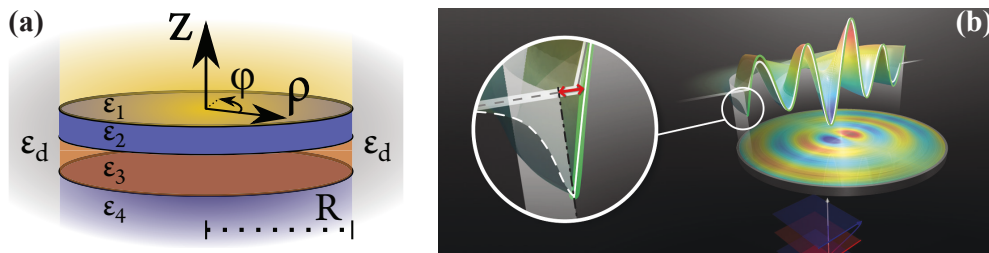


Figure 5: Circular NAs. (a) Schematic: Rotationally symmetric and piecewise homogeneous permittivity  $\varepsilon(z)$ , radial termination at  $\rho = R$ . (b) Bessel-type SPP of a specific circular NA, a metallic disc. The reflection at the termination leads to an apparent length change.

can be approximately calculated using the Fabry-Perot resonance condition

$$k' L_n + \phi_r = n\pi, \quad (9)$$

where it is assumed that the NA terminations have the same geometry on both sides [155]. Interestingly,  $\phi_r$  introduces an apparent length change as large as  $\phi_r/k'$  if Eq. (9) is compared to a perfect reflection at the termination. It should be noted that the Fabry-Perot resonance condition can be derived using the transmitted power through a one-dimensional cavity with reflections at its terminations. A resonance occurs if the transmitted power is maximal, *i.e.* if  $1 - 2|r|^2 \cos(2k'L + 2\phi_r) \exp[-2k''L] + |r|^4 \exp[-4k''L]$  is minimal for a certain length  $L$  of the resonator [116]. Hence, Eq. (9) is strictly valid only for  $k'' = 0$ , *i.e.* assuming a lossless resonator and provides a reasonable approximation for small  $k''/k'$ -ratios.

Novotny did not calculate the reflection coefficient, but rather used an ad-hoc value for  $\phi_r$ . Nevertheless, to understand the scaling of NAs in terms of their supported Fabry-Perot resonances was a very important step. Within this approach, the scaling of NAs is reduced to two calculations: 1. The dispersion relation of a certain propagating mode along the NA and 2. The reflection coefficient of that mode at the termination of the NA. For particular symmetries, both calculations can be accomplished analytically. In fact, Gordon showed that a method he earlier used to calculate the reflection of SPPs at an infinite half-space [156] could be used to calculate the scaling of wire NAs [157].

The Fabry-Perot model was later verified experimentally for wire NAs [158]. The success of the Fabry-Perot model pointed to an equivalence between localized SPPs and Fabry-Perot resonances of NAs. We were able to prove this equivalence by numerical calculations of the reflection coefficient for different NA terminations [109].

Gordon's method to derive the complex reflection coefficient can be summarized as a match of the tangential electric and magnetic fields at the termination of a NA to the adjacent space. The method can be divided into a four-step procedure that requires certain NA symmetries (App. A.2). To illustrate the mathematical approach and its limitations, a complete derivation of Gordon's result for wires can be found in App. A.2.2. We also outline why an analytical determination of the reflection coefficient for arbitrary terminations of wire NAs does not yield a true simplification.

**Circular NAs** With the help of Gordon's method, the reflection coefficient can be calculated for NAs with other geometries as well, and their resonant scaling might be described using Novotny's Fabry-Perot approach. In particular, we analyzed the scaling of circular NAs made of an arbitrary stack of materials and radius  $R$  embedded in a material with permittivity  $\varepsilon_d$  [159] [Fig. 5 (a)]. In this case, the NAs are assumed to support Bessel-type SPPs [Fig. 5 (b)] for which the  $z$ -component

of the electric field is given by

$$E_z^m(\rho, z) = J_m(k_{\text{SPP}}\rho) \cdot a(z) \text{ for } \rho \leq R. \quad (10)$$

Here,  $m$  denotes an angular index for the suppressed  $\exp[im\varphi]$ -dependency in cylindrical coordinates. The circular NAs may support different plasmonic modes, for example a symmetric and an antisymmetric mode in the case of a thin metallic disc, which is the simplest example for circular NAs. The wave vector  $k_{\text{SPP}} = k'_{\text{SPP}} + ik''_{\text{SPP}}$  and the so-called “mode profile”  $a(z)$  of the plasmonic mode can be calculated by the matrix method for layered systems [160]. To find the resonance radii  $R_{n,m}$  of the circular NAs, a resonance condition equivalent to Eq. (9) can be conjectured in which the roots of a plane wave are replaced by the  $n^{\text{th}}$  root of the Bessel function,  $x_n(J_m)$ ,

$$2 \cdot k'_{\text{SPP}} R_{n,m} + \phi_m = 2 \cdot x_n(J_m). \quad (11)$$

As for wire NAs, the phase upon reflection  $\phi_m$  causes an apparent length change. With a Fourier decomposition of the free-space fields for  $\rho \geq R$ , the reflection coefficient  $r_m = |r_m| \exp[i\phi_m]$  for a given mode characterized by  $a(z)$  and  $k_{\text{SPP}}$  can be calculated as [159]

$$r_m = \frac{2\pi\varepsilon_d k_{\text{SPP}}\sigma H_m^1(k_{\text{SPP}}R) - DH_m^1(k_{\text{SPP}}R) I_m}{-2\pi\varepsilon_d k_{\text{SPP}}\sigma H_m^2(k_{\text{SPP}}R) + DH_m^2(k_{\text{SPP}}R) I_m} \quad (12)$$

with the abbreviations

$$\begin{aligned} DH_m^{1/2}(x) &\equiv \partial_x H_m^{1/2}(x), \quad \sigma \equiv \int_{-\infty}^{\infty} \varepsilon(z) a(z)^2 dz, \\ I_m &\equiv \int_{-\infty}^{\infty} \frac{H_m^1(\sqrt{\varepsilon_d k_0^2 - k_z^2} R)}{DH_m^1(\sqrt{\varepsilon_d k_0^2 - k_z^2} R)} \cdot \sqrt{\varepsilon_d k_0^2 - k_z^2} \cdot B^-(k_z) \cdot B^+(k_z) dk_z \\ \text{and } B^\pm(k) &\equiv \int_{-\infty}^{\infty} \varepsilon(z) a(z) e^{\pm ikz} dz. \end{aligned}$$

In the latter equations,  $H_m^{1/2}(x)$  are the usual Hankel functions of the first and second kind. These functions correspond to outwards and inwards propagating cylindrical waves. These so-called Hankel-type SPPs [161] enable to define a reflection problem at the NA termination in order to derive  $r_m$  (*cf.* App. A.2.1). For strong absorption other eigenfunctions of circular NAs may be dominant such that a description in Bessel or Hankel functions is no longer valid [162, 163]. Thus, the applicability of Eq. (12) has to be verified for different kind of circular NAs. To do so, we performed finite difference time domain calculations [164, 165].

**Numerical Verification** Discs of different radii  $R = \{100 \dots 1250\}$  nm and thicknesses  $d = \{6 \dots 160\}$  nm were considered. A plane wave propagating along the  $z$ -axis of symmetry with the fixed frequency  $\nu = 625$  THz ( $\lambda = 480$  nm) was used to excite dipolar ( $m = 1$ ) modes of the NAs. Because of this illumination,  $k_{\text{SPP}}$  is constant for a given  $d$  and the scaling in terms of Eq. (12) can be verified without the need to account for the dispersion of  $k_{\text{SPP}}$ . For these discs we assumed a relative permittivity of  $\varepsilon_m \approx -8.8 + 0.03i$ , which corresponds to silver at  $\nu = 625$  THz [124] with the exception that  $\varepsilon''$  has been reduced in order to simplify the identification of resonances. However, for all other NAs the values were directly taken from the literature.

The resonance radii  $R_n \equiv R_{n,1}$  were determined by a computation of the electric field strengths below and above the structure while changing the radius of discs at a constant thickness. Using the resonance condition Eq. (11) and the phases upon reflection Eq. (12), we find a remarkable agreement of analytically predicted resonance radii with their numerically determined counterparts

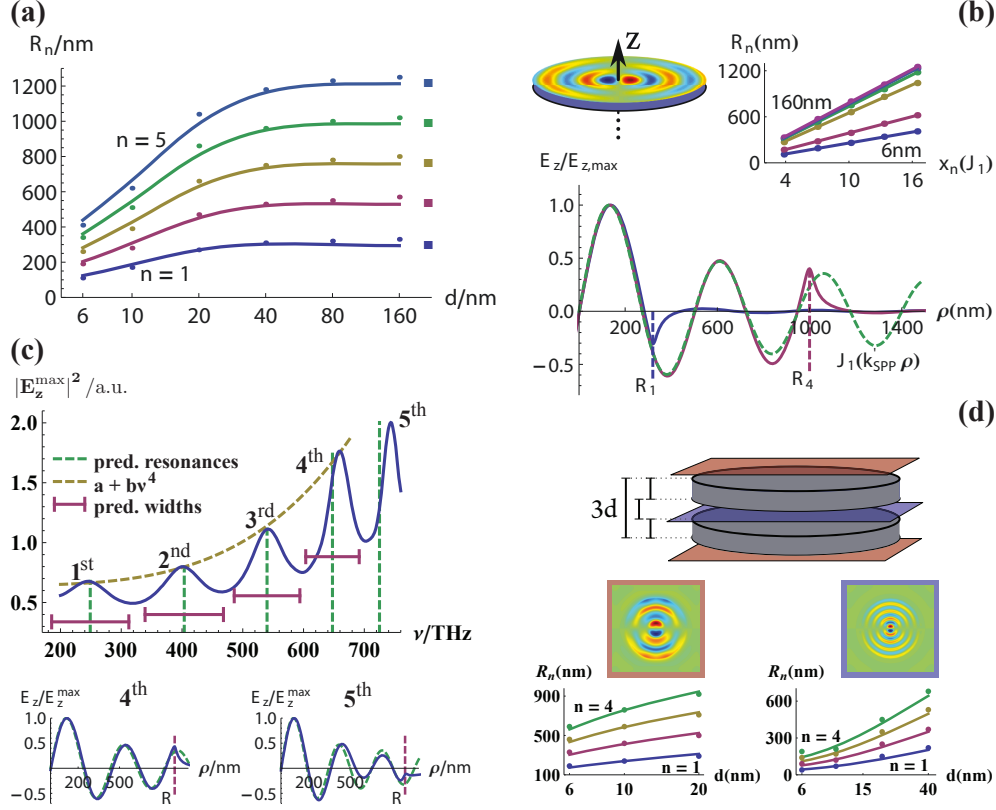


Figure 6: The scaling of circular NAs: comparison of analytical predictions [Eq. (11) and Eq. (12)] to numerical results ( $\varepsilon_d = 1$ ). (a) Analytically calculated resonance radii  $R_n$  (full lines) for silver discs with different thicknesses  $d_i$  vs. numerical results (dots). Large squares: predicted  $R_n$  for a semi-infinite disc. (b) Top left: Bessel-type  $E_z$  above a silver disc ( $d_5 = 80$  nm). Lower part: Normalized  $E_z$  for the first (blue line) and fourth (magenta line) resonant radius. For  $\rho < R$  the agreement with the expected form  $\propto J_1(k_{\text{SPP}}\rho)$  (green dashed line) is perfect except a minor deviation at the termination.  $k_{\text{SPP}}$  was calculated from the dispersion relation of a metallic layer (App. A.3). The  $R_n$  are linearly related to the roots of  $J_1$  for all  $d_i$ . (c) Resonances of a silver disc with  $R = 900$  nm and  $d = 20$  nm. Top: The maximum value of  $|E_z(\nu)|^2$  from simulations (blue line). Resonances (dashed green lines) and line widths (magenta solid lines) as predicted. The phenomenological  $\nu^4$ -scaling does not hold anymore for the fifth resonance due to high damping. Bottom:  $E_z$  for the fourth and fifth order resonances (blue lines) compared to Bessel functions (green dashed line). (d) Stacked NA. Field plots: numerically determined  $E_z$  for  $R = 810$  nm and  $d = 20$  nm. Symmetric mode on the left (orange frame) as computed 20 nm above the structure, antisymmetric one (blue frame) directly in the middle. Bottom: predictions (full lines) against simulation results (dots).

[Fig. 6 (a)]. Furthermore, the shape of the electric field corresponds to Bessel-type SPPs [*cf.* Eq. (10)] and the  $R_n$  scale linearly with the roots of  $J_1$ , which is a direct verification of Eq. (11), see Fig. 6 (b).

The model can also be applied to find the spectral resonances of a definite circular NA. To verify this, silver discs with experimental material data [124], a radius of  $R = 900$  nm and a thickness of  $d = 20$  nm were illuminated by plane waves at different frequencies  $\nu$ . An excellent agreement of the predicted resonance frequencies for nearly all orders was observed [Fig. 6 (c)]. For higher order resonances, however, the propagation length  $d_{\text{SPP}} = 1/k''_{\text{SPP}}$  can be in the order of the disc's diameter and the model must not be applied. This is also reflected by the field profiles for the 5<sup>th</sup> resonance. Here, a clear deviation from Bessel-type SPPs can be observed [Fig. 6 (c), lower part]. Furthermore, using the quality factor  $Q$  defined by

$$\frac{1}{Q} = \frac{1}{Q_{\text{prop}}} + \frac{1}{Q_{\text{r}}} = (2k''_{\text{SPP}}R)^2 + |1 - r|^2 = \frac{\Delta\nu}{\nu}, \quad (13)$$

the width of the resonances can be explained [Fig. 6 (c), upper part].

Up to now, we applied the Fabry-Perot model only to circular NAs made of a single metallic disc. But it can be used for stacked circular NAs, too [Fig. 5 (a)]. Such NAs introduce a large degree of freedom to tailor light-matter interactions [56, 82, 166]. We shall restrict ourselves to a rather simple NA with only a few plasmonic modes for simplicity. The NA under consideration consists of two silver discs ( $\varepsilon \approx -8.8 + 0.3i$ ) and a separating dielectric spacer ( $\varepsilon = 1$ ), each of thickness  $d$ , see Fig. 6 (d). It supports several Bessel-type SPPs but only two of them can be excited by the illuminating plane wave ( $\nu = 625$  THz). Because of the symmetry of the NA, its modal field maxima appear in different layers. Hence, their resonance radii  $R_n$  can be determined calculating the electric field in these layers (see App. A.3.3). For both investigated modes we find an excellent agreement between analytical predictions and theory [Fig. 6 (d), lower part].

We have seen that the complex reflection coefficient can be used to understand the scaling of NAs in terms of a simple Fabry-Perot model. It can be used to study other geometries as well, for example two-dimensional layer systems [167]. The reflection coefficient can be used to determine important physical quantities of NAs like their resonant sizes and corresponding widths. But other quantities are accessible, too. For instance, the apparent length change can be used to identify the oscillating current distribution along NAs via Ohm's law,  $\mathbf{j}_n(\mathbf{r}, \omega) = \sigma(\mathbf{r}, \omega) \mathbf{E}_n(\mathbf{r}, \omega)$ , where  $\mathbf{E}_n(\mathbf{r}, \omega)$  corresponds to the plasmonic mode under investigation. Here, the current yields the radiation characteristics of the NAs [93, 168].

### 2.3.3 Numerical Methods

The determination of NA scalings based on analytical or semianalytical methods is limited to rather simple geometries. The development of modern computers makes it possible to analyze highly sophisticated electromagnetic systems via time- or frequency domain calculations [164, 165, 169–171]. NA geometries studied thus far include bow-ties [172], quadrumers [173], fractals [148], oligomers [174], and many others.

Previously we have argued that analytical considerations in terms of simplified models are always the first choice to find the scaling of NAs. This statement is true regarding other considerations as well, as analytical treatments provide all information about the physical system in a form that can be used for many purposes. For example, the interaction to close-by Qs can be investigated in terms of the nearfield of spherical NAs [85, 175, 176]. On the other hand, the semi-analytical Fabry-Perot model provides the nearfield of a class of NAs and can be used for proper interaction studies without the need to investigate the system directly on a numerical basis.

Thus far we have discussed important electrodynamic parameters of NAs. But to understand their coupling to QSS, we have to apply quantum physics.

## 2.4 Interaction with Quantum Systems: Semiclassical Description

One of the interesting potentials of NAs is the localization of the electromagnetic field at specific spots. This feature offers a wide range of possibilities for enhanced interactions with QSS. In this section, we focus on the semiclassical description of the interaction of QSS to the electromagnetic field. Hereby, the fields are incorporated as classical background potential. Such an approach is generally applicable in the sense of Bohr's correspondence principle [177], which, loosely speaking, states that quantum calculations must agree with classical calculations for large quantum numbers [178].

However, before the electromagnetic field is dealt with (Sec. 2.4.2), we shall briefly review how time dependent perturbation theory is used to calculate observables of a QS subject to an external perturbation in Sec. 2.4.1. The results of this Section are the theoretical foundations of Sec. 4.

### 2.4.1 Fermi's Golden Rule

Without any interaction with its environment, a QS would stay in a certain state for all times. This changes if a time-dependent interaction potential  $V(t)$  is present. Then, a QS may change its state with certain transition probabilities. Let us assume a QS with a discrete spectrum and eigenstates  $|n\rangle$ . The Hamiltonian is of the form

$$H(t) = H_0 + V(t) ,$$

where  $H_0$  is the Hamiltonian of the isolated QS such that  $H_0 |n\rangle = \hbar\omega_n |n\rangle$ .

For an interaction potential with slowly varying envelope,

$$V(t) = V_{\text{env}}(t) e^{-i\omega_0 t} + V_{\text{env}}^*(t) e^{i\omega_0 t} , \quad (14)$$

the transition rates are given by

$$\Gamma_{n \rightarrow m} = \frac{2\pi}{\hbar^2} |V_{\text{env},mn}(\omega_{mn} - \omega_0)|^2 [\delta(\omega_{mn} - \omega_0) + \delta(\omega_{mn} + \omega_0)] , \quad (15)$$

with  $\omega_{mn} = \omega_m - \omega_n$ . The latter equation is Fermi's Golden Rule (see App. B.1 for a derivation and further discussions). Note that the  $\delta$ -distributions should be interpreted as energy conservation requirements. Most important for our investigations is that the QS undergoes a transition only if a transition frequency is equal to the oscillation frequency  $\omega_0$  of the interaction potential and that the interaction matrix elements enter quadratically. Hence, by enhancing these matrix elements, transition rates get enhanced likewise.

### 2.4.2 Coupling to the Electromagnetic Field

Up to now, the interaction potential has been a general term to describe a semiclassical time-dependent coupling with a QS. Here we want to describe the interaction of a NA's electromagnetic field with QSS. Hence we will briefly review how this interaction can be introduced within non-relativistic quantum mechanics. Within the so-called minimal coupling, the interaction can be described by the formal prescription [179]

$$H(\mathbf{p}, \mathbf{r}) \rightarrow H(\mathbf{p} - e\mathbf{A}(\mathbf{r}, t), \mathbf{r}) + e\phi(\mathbf{r}, t) . \quad (16)$$



Minimal coupling naturally follows from the invariance of observables with respect to a  $U(1)$  phase transformation of the wave function and an application of Weyl's gauge principle. The potentials  $\mathbf{A}(\mathbf{r}, t)$  and  $\phi(\mathbf{r}, t)$  play an explicit role in the interaction as it is the case for the Aharonov-Bohm-effect [180, 181]. In a time-representation, they are related to the electromagnetic fields via

$$\mathbf{B}(\mathbf{r}, t) = \nabla \times \mathbf{A}(\mathbf{r}, t) \quad \text{and} \quad \mathbf{E}(\mathbf{r}, t) = -\partial_t \mathbf{A}(\mathbf{r}, t) - \nabla \phi(\mathbf{r}, t) . \quad (17)$$

It is well known that  $\mathbf{A}(\mathbf{r}, t)$  and  $\phi(\mathbf{r}, t)$  are not independent from each other and that they are not uniquely determined. We shall use the Coulomb gauge, which (for  $\rho_{\text{ext}}(\mathbf{r}, t) = 0$ ) reads

$$\nabla \cdot \mathbf{A}(\mathbf{r}, t) = 0 \quad \text{and} \quad \phi(\mathbf{r}, t) = 0 . \quad (18)$$

Then, the Hamiltonian of an isolated charged particle prone to an electromagnetic field is given by

$$\begin{aligned} H &= \frac{1}{2m} [\mathbf{p} - e\mathbf{A}(\mathbf{r}, t)]^2 + \underbrace{e\phi(\mathbf{r}, t)}_{=0} = \frac{1}{2m} \left[ \mathbf{p}^2 - e\mathbf{p} \cdot \mathbf{A}(\mathbf{r}, t) - e\mathbf{A}(\mathbf{r}, t) \cdot \mathbf{p} + \underbrace{e^2 \mathbf{A}^2(\mathbf{r}, t)}_{\approx 0} \right] \\ &\approx H_0 - \frac{e}{m} \mathbf{A}(\mathbf{r}, t) \cdot \mathbf{p} . \end{aligned} \quad (19)$$

with  $H_0 = \mathbf{p}^2/2m$ . In this derivation we have used that  $\mathbf{p} \cdot \mathbf{A}(\mathbf{r}, t) = -i\hbar \nabla \cdot \mathbf{A}(\mathbf{r}, t) = \mathbf{A}(\mathbf{r}, t) \cdot \mathbf{p}$  because of the Coulomb gauge and the term in  $\mathbf{A}^2(\mathbf{r}, t)$ , has been neglected. This term corresponds to the ponderomotive force but is usually negligible for sufficiently weak fields.

For a classical light field described by a vector potential  $\mathbf{A}(\mathbf{r}, t)$ , the interaction potential of an isolated charged particle is given by

$$V_{\text{em}}(\mathbf{r}, t) = -\frac{e}{m} \mathbf{A}(\mathbf{r}, t) \cdot \mathbf{p} . \quad (20)$$

This interaction describes both electric and magnetic interaction.

In App. B.2 we derive how  $V_{\text{em}}(\mathbf{r}, t)$  can be decomposed into an electric and a magnetic part as

$$V_e(\mathbf{r}, t) = -e\mathbf{E}(\mathbf{r}, t) \cdot \mathbf{r} \quad \text{and} \quad (21)$$

$$V_m(\mathbf{r}, t) = \frac{\mu_B}{\hbar} \mathbf{B}(\mathbf{r}, t) \cdot \mathbf{L} . \quad (22)$$

We use this decomposition in Sec. 4.2 to formulate the electromagnetic coupling in terms of local electric and magnetic multipole contributions.

It has to be admitted that the outlined coupling of the electromagnetic field to the QS does not include all possible effects. Most notably, a non-radiative energy transfer between QS and NA in terms of a Förster resonance energy transfer [182] or Dexter electron transfer [183] has been regarded. They may considerably influence the physical behavior of a QS only a few nanometers away from a NA.

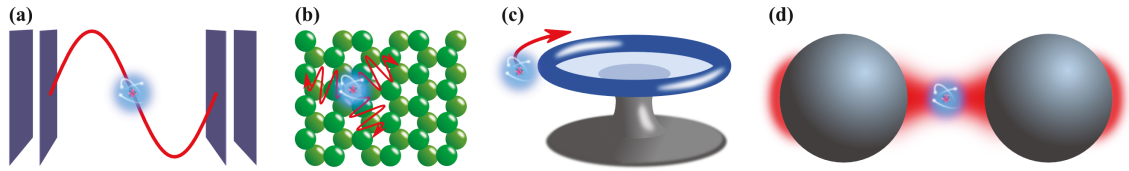


Figure 7: Examples of devices for which a cQED quantization has been applied: (a) microcavities, (b) photonic crystals, (c) microtoroids, and (d) NAs (*cf.* Sec. 3.4).

### 3 Nanoantenna Quantization

So far, the interaction of a NA to Qs has been considered on a purely semiclassical basis: the Qs were treated following the Schrödinger equation and the electromagnetic field of the NA acts on the Qs. Such an approach is not suitable to describe how the mutual interaction of NA and Qs leads to the emergence of a hybrid Qs. The physical properties of the hybrid system have to be properly described. To do so, a quantization of the electromagnetic modes of the NA is required, which we shall abbreviate “NA quantization” for conciseness. This quantization can be accomplished at different levels of approximation. One possibility is to assume a number of interacting electrons inside the NA, quantize their interaction and study the dynamics of this system for certain excitations in terms of a time-dependent density functional theory (TD-DFT) [63, 71, 184]. In this approach, the internal electron dynamics as well as the behaviour of the electromagnetic fields a few Bohr radii away from the surface of the NAs may be studied. However, this method is computationally extremely involved such that it may only be applicable for very small systems and rather simple NA geometries.

Another possibility to study the interaction of NAs and Qs in a fully quantized manner is to apply a canonical quantization of the electromagnetic field modes within the aforementioned quantum optics approach [185, 186]. However, this quantization scheme causes practical difficulties as the fields of a NA have to be represented by infinitely many modes to describe all radiative and nonradiative loss channels. Lossy system quantization is still a field of active research [187–189] and has become en vogue in plasmonics. It is used to understand the Purcell effect in terms of the classical quantities mode volume and quality factor. Especially interpretations and generalizations of the mode volume attracted appreciable attention [190–194].

The approach we follow provides an easy yet powerful way to understand the interaction of Qs with plasmonic structures. In particular a fully quantum description of the dynamics is concerned. We describe the NA fields in terms of quasinormal modes to understand the interaction dynamics. Since the equations are very similar to the approaches used in cavity quantum electrodynamics (cQED), we shall start with the respective field quantization (Sec. 3.1). Afterwards, we will briefly review the quantization in dispersive media (Sec. 3.2), *i.e.* the quantum optics approach. Then we shall introduce quasinormal modes in Sec. 3.3. These modes will be used in Sec. 3.4 to quantize the NA fields. This quantization scheme will be justified in Sec. 3.5.

#### 3.1 Quantized Cavity Field

In the following discussion we briefly review how the electromagnetic field inside a lossless cavity can be represented by harmonic oscillator modes and how the mode volume can be naturally introduced in this context. The approach is the familiar cQED quantization, which is extensively documented in the literature [195–198]. It has been used to describe different optical devices [199], see Fig. 7 (a)-(c).

## Electromagnetic Fields: Classical Hamilton Function

Let us assume a one-dimensional vacuum cavity extended in  $z$ -direction. It supports a monochromatic electromagnetic field of the form

$$\mathbf{E}(z, t) = \mathcal{N}q(t) \sin(kz) \mathbf{e}_x \quad \text{with} \quad \mathcal{N} = \sqrt{\frac{2\omega^2}{\varepsilon_0 V_n}} \quad \text{and} \quad k = \frac{\omega}{c}. \quad (23)$$

Here,  $q(t)$  denotes the real-valued amplitude of the electric field,  $k$  is the scalar wave number and  $\mathcal{N}$  is just a normalization constant at this point. The volume of the cavity  $V_n = \Delta x \Delta y \cdot n\pi/k$  is arranged in such a way that a resonance condition is realized.  $V_n$  is often also referred to as mode volume. For simplicity we shall only discuss a single mode here, but a generalization to the multimode case is straight forward. Via Ampère's law we readily find the magnetic induction as

$$\mathbf{B}(z, t) = \frac{1}{kc^2} \mathcal{N} \dot{q}(t) \cos(kz) \mathbf{e}_y.$$

The free-space energy density of the electromagnetic field is given by  $w = (\varepsilon_0 \mathbf{E}^2 + \mathbf{B}^2/\mu_0)/2$ , which is also the Hamiltonian density. The corresponding Hamiltonian reads

$$\begin{aligned} H &= \frac{1}{2} \mathcal{N}^2 \int_V \left\{ \varepsilon_0 q^2(t) \sin^2(kz) + \frac{1}{k^2 c^4 \mu_0} \dot{q}^2(t) \cos^2(kz) \right\} dV \\ &= \frac{1}{2} \frac{2\omega^2}{\varepsilon_0 V_n} \left[ \varepsilon_0 q^2(t) + \frac{1}{k^2 c^4 \mu_0} \dot{q}^2(t) \right] \Delta x \Delta y \cdot n \frac{\pi}{2k} \\ &= \frac{1}{2} [\omega^2 q^2(t) + p^2(t)] \end{aligned} \quad (24)$$

since  $\int_0^{n\pi/k} \{\sin^2(kz), \cos^2(kz)\} dz = n\pi/2k$ . We have also used Hamilton's equations  $\dot{p} = -\partial H/\partial q$  and  $\dot{q} = \partial H/\partial p$  to identify that  $\dot{q} = p$ . Equation (24) is the Hamiltonian of a harmonic oscillator.

## Quantization

The electromagnetic field has a bosonic character and the quantization of the cavity field can be accomplished interpreting  $q$  and  $p$  as quantum mechanical operators. In this approach, the Poisson bracket  $\{q, p\} = 1$  is replaced by the commutator  $\{, \} \rightarrow [, ]/i\hbar$  for conjugate variables which results in the canonical commutation relation  $[q, p] = qp - pq = i\hbar$  [200]. Note that throughout this thesis operators are not denoted by a special notation for aesthetic preferences of the author. We believe that it should be always clear from the context if a classical or quantum variable is utilized.

To cast Eq. (24) into an algebraic form, we can introduce the annihilation and creation operators  $a$  and  $a^\dagger$  as

$$a = \frac{1}{\sqrt{2}} \left( \sqrt{\frac{\omega}{\hbar}} q + \frac{i}{\sqrt{\hbar\omega}} p \right) \quad \text{and} \quad a^\dagger = \frac{1}{\sqrt{2}} \left( \sqrt{\frac{\omega}{\hbar}} q - \frac{i}{\sqrt{\hbar\omega}} p \right). \quad (25)$$

Then, the well-known commutation relation  $[a, a^\dagger] = 1$  holds. Please note that in the Schrödinger picture, the operators have time-independent representations, whereas the wave-function is time-dependent. Hence,  $a$  and  $a^\dagger$  are now constant operators in contrast to Eq. (24). Furthermore, the Hamiltonian reads as

$$H = \hbar\omega \left( a^\dagger a + \frac{1}{2} \right). \quad (26)$$

Equation (26) is the well-known Hamiltonian of the electromagnetic field in a single-mode cavity. The eigenstates of this Hamiltonian are so-called Fock states  $|n\rangle$ , for which all quantities can be found by algebraic calculations [92]. In particular:

$$\begin{aligned} H|n\rangle &= E_n|n\rangle \quad \text{with} \quad E_n = \hbar\omega \left( n + \frac{1}{2} \right), \text{ since} \\ |n\rangle &= \frac{1}{\sqrt{n}} a^\dagger |n-1\rangle \quad \text{and} \quad a^\dagger a |n\rangle = n |n\rangle. \end{aligned} \quad (27)$$

Hence, the time-dependent expectation value  $\langle N \rangle(t) \equiv \langle \psi(t) | N | \psi(t) \rangle$  of the number operator  $N = a^\dagger a$  can be interpreted as the number of photons with energy  $\hbar\omega$  inside the cavity.

To understand the interaction of the electric and magnetic fields with QSSs in terms of the annihilation and creation operators, we just have to invert Eq. (25) to find expressions of electric and magnetic field amplitudes, namely

$$q = \sqrt{\frac{\hbar}{2\omega}} (a^\dagger + a) \quad \text{and} \quad p = i\sqrt{\frac{\hbar\omega}{2}} (a^\dagger - a) .$$

Thus the operators for the electric and magnetic field can be written as

$$\begin{aligned} \mathbf{E}(z) &= \sqrt{\frac{\hbar\omega}{\varepsilon_0 V_n}} (a^\dagger + a) \sin(kz) \mathbf{e}_x \text{ and} \\ \mathbf{B}(z) &= \frac{i}{c} \sqrt{\frac{\hbar\omega}{\varepsilon_0 V_n}} (a^\dagger - a) \cos(kz) \mathbf{e}_y . \end{aligned} \quad (28)$$

The latter expressions are those that usually appear if the quantized field is coupled to matter in some way. At this point we can see that any coupling to the electromagnetic field scales  $\propto 1/\sqrt{V_n}$  which makes it so appealing to study quantum effects in terms of the mode volume.

### 3.2 Quantization in Dissipative Media

The quantization of the electromagnetic field inside a lossless vacuum cavity was outlined in the last subsection. Now we will see how this approach can be generalized to dissipative media. To achieve this, let us summarize how the quantization of a cavity was achieved conceptually: A certain mode of the cavity has been identified and the fields are assumed to exhibit a bosonic character. The canonical commutation relations are then applied to the field operators that appear in a Hamiltonian formulation.

Naturally, the one-mode cavity quantization approach can be generalized to the electromagnetic fields with a discrete mode spectrum. Then, the Hamiltonian is merely a summation over the cavity modes:

$$H = \sum_n \hbar\omega_n \left( a_n^\dagger a_n + \frac{1}{2} \right) . \quad (29)$$

Now we shall compare the situation with the canonical quantization procedure for the electromagnetic fields in dissipative media, *i.e.* the quantum optics approach [185]. In the case of an arbitrary superposition of modes, bosonic field operators  $\mathbf{f}(\mathbf{r}, \omega)$  and  $\mathbf{f}^\dagger(\mathbf{r}, \omega)$  are introduced, for which  $\mathbf{r}$  and  $\omega$  are now continuous variables. The generalization of the canonical commutation relations is achieved by the equal-time commutation relation  $\left[ f_k(\mathbf{r}, \omega), f_{k'}^\dagger(\mathbf{r}, \omega) \right] = \delta_{kk'} \delta(\mathbf{r} - \mathbf{r}') \delta(\omega - \omega')$  with  $\{k, k'\} \in \{x, y, z\}$ . The Hamiltonian is then given by  $H = \int \hbar\omega \mathbf{f}^\dagger(\mathbf{r}, \omega) \cdot \mathbf{f}(\mathbf{r}, \omega) d\omega dV$ .

In this approach, dissipation is introduced using a noise polarisation  $\mathbf{P}_N(\mathbf{r}, \omega)$ . This quantity gives rise to noise charge- and current densities  $\rho_N(\mathbf{r}, \omega) = -\nabla \cdot \mathbf{P}_N(\mathbf{r}, \omega)$  and  $\mathbf{j}_N(\mathbf{r}, \omega) =$

$-i\omega\mathbf{P}_N(\mathbf{r},\omega)$ , respectively. A linear relation between  $\mathbf{f}(\mathbf{r},\omega)$  and  $\mathbf{P}(\mathbf{r},\omega)$  that preserves the fundamental equal-time commutation relations is given by

$$\mathbf{P}_N(\mathbf{r},\omega) = i\sqrt{\frac{\hbar\varepsilon_0}{\pi}}\varepsilon''(\mathbf{r},\omega)\mathbf{f}(\mathbf{r},\omega) .$$

By virtue of the dyadic Greens function [cf. Eq. (4)], the noise polarisation can be used to find quantized expressions for the electromagnetic fields following Eq. (5):

$$\begin{aligned} \mathbf{E}(\mathbf{r},\omega) &= i\sqrt{\frac{\hbar}{\pi\varepsilon_0}}\frac{\omega^2}{c^2}\int\sqrt{\varepsilon''(\mathbf{r},\omega)}G(\mathbf{r},\mathbf{r}',\omega)\mathbf{f}(\mathbf{r}',\omega)dV' \text{ and} \\ \mathbf{B}(\mathbf{r},\omega) &= (i\omega)^{-1}\nabla\times\mathbf{E}(\mathbf{r},\omega) . \end{aligned} \quad (30)$$

The importance of the Green's function for this quantization scheme is obvious. The electric and magnetic field operators are further given by

$$\mathbf{E}(\mathbf{r}) = \int_0^\infty \mathbf{E}(\mathbf{r},\omega) d\omega + \text{H.c.} \text{ and } \mathbf{B}(\mathbf{r}) = \int_0^\infty \mathbf{B}(\mathbf{r},\omega) d\omega + \text{H.c.} . \quad (31)$$

To understand why we need a simplified scheme to quantize the fields of NAs, let us consider the probably simplest quantum calculation involving the above formalism: The spontaneous emission of a two-level-system in a dispersive environment. The calculations will be very helpful to verify the NA quasimode scheme in Sec. 3.5.

### The Weisskopf-Wigner Problem of Spontaneous Emission

The spontaneous emission of a two-level QS shall be studied now. If this effect is treated within the rotating wave and electric dipole approximations, it is usually termed Weisskopf-Wigner problem [201]. Its Hamiltonian is given by [185]

$$\begin{aligned} H &= H_{\text{qs}} + H_{\text{int}} + H_{\text{EM}} \text{ with} \\ H_{\text{qs}} &= \hbar\omega_{\text{qs}}\sigma_+\sigma_- , \\ H_{\text{int}} &= -\int_0^\infty \sigma_+\mathbf{d}^*\cdot\mathbf{E}(\mathbf{r}_{\text{qs}},\omega) + \text{H.c.} d\omega \text{ and} \\ H_{\text{EM}} &= \int \hbar\omega\mathbf{f}^\dagger(\mathbf{r},\omega)\cdot\mathbf{f}(\mathbf{r},\omega) d\omega dV . \end{aligned} \quad (32)$$

Within the applied rotating wave approximation (RWA), the creation operators couple only to annihilation operators, which preserves the photon number. All rapidly oscillating terms are neglected (see also App. B.7). Furthermore, the electric field is given by Eq. (30),  $\mathbf{r}_{\text{qs}}$  is the position of the QS,  $\mathbf{d}$  its dipole moment. The  $\sigma_+$  ( $\sigma_-$ ) are creation (annihilation) operators in the usual Pauli basis, *i.e.*  $\sigma_-|1\rangle = |0\rangle$  [197].

The Hilbert space is given by the states  $|n_{\text{qs}}, n_{\text{EM},\omega}\rangle$ , where  $n_{\text{qs}}$  is the quantum number of the QS,  $n_{\text{qs}} = \{0, 1\}$ , and  $n_{\text{EM},\omega} = \{0, 1, 2, \dots\}_\omega$  is the quantum number of the single frequency oscillator  $\hbar\omega\mathbf{f}^\dagger(\mathbf{r},\omega)\mathbf{f}(\mathbf{r},\omega)$  of the electromagnetic field. Following Ref. [185], we may analyze spontaneous decay, if the QS is initially in its excited state, *i.e.*  $|\psi(0)\rangle = |1, \{0\}\rangle$ . Within the RWA, the states of the system with exactly one excitation represented by the amplitude envelopes  $c_1(t)$  and  $\mathbf{c}_{0,\omega}(\mathbf{r},t)$  can be used:

$$|\psi(t)\rangle = e^{-i\tilde{\omega}t}c_1(t)|1, \{0\}_\omega\rangle + \int_0^\infty e^{-i\omega t}\mathbf{c}_{0,\omega}(\mathbf{r},t)\cdot|0, \{\mathbf{1}\}_{\mathbf{r},\omega}\rangle d\omega dV .$$

Here,  $\tilde{\omega} = \omega_{10} - \delta\omega$  is the new transition frequency of the QS for which the shift  $\delta\omega$  has yet to be

found. The notation  $|0, \{\mathbf{1}\}_{\mathbf{r}, \omega}\rangle = \mathbf{f}^\dagger(\mathbf{r}, \omega) |0, \{0\}\rangle$  has been used to denote an excitation of the free field at frequency  $\omega$ . If we insert the latter ansatz into Schrödinger's equation, we find the coupled system of equations

$$\begin{aligned}\dot{c}_1(t) &= -i\delta\omega c_1(t) - \frac{1}{\sqrt{\pi\varepsilon_0\hbar}} \int_0^\infty \frac{\omega^2}{c^2} e^{-i(\omega-\tilde{\omega})t} \int \sqrt{\varepsilon''(\mathbf{r}, \omega)} \mathbf{d}_{10} \cdot G(\mathbf{r}_{\text{qs}}, \mathbf{r}_{\text{qs}}, \omega) \cdot \mathbf{c}_{0,\omega}(t) dV d\omega \\ \dot{\mathbf{c}}_{0,\omega}(\mathbf{r}, t) &= \frac{1}{\sqrt{\pi\varepsilon_0\hbar}} \frac{\omega^2}{c^2} \int \sqrt{\varepsilon''(\mathbf{r}, \omega)} \mathbf{d}_{01} \cdot G^*(\mathbf{r}_{\text{qs}}, \mathbf{r}_{\text{qs}}, \omega) c_1(t) dV, \end{aligned} \quad (33)$$

in which  $\mathbf{d}_{10} = q\langle 1|\mathbf{r}|0\rangle$  is the transition dipole moment of the QS. Formal integration of the second equation and inserting the result into the first equation leads to the integro-differential equation

$$\begin{aligned}\dot{c}_1(t) &= -i\delta\omega c_1(t) - \int_0^t K(t-t') c_1(t') dt' \quad \text{with} \\ K(t-t') &= \frac{1}{\pi\varepsilon_0\hbar} \int_0^\infty \frac{\omega^2}{c^2} e^{-i(\omega-\tilde{\omega})(t-t')} \mathbf{d}_{10} \cdot \Im G(\mathbf{r}_{\text{qs}}, \mathbf{r}_{\text{qs}}, \omega) \cdot \mathbf{d}_{01} d\omega. \end{aligned} \quad (34)$$

The general relation  $\sum_k \int (\omega^2/c^2) \sqrt{\varepsilon''(\tilde{\mathbf{r}}, \omega)} G_{ik}(\mathbf{r}, \tilde{\mathbf{r}}, \omega) G_{jk}^*(\mathbf{r}', \tilde{\mathbf{r}}, \omega) d^3\tilde{\mathbf{r}} = \Im G_{ij}(\mathbf{r}, \mathbf{r}', \omega)$  was used (see App. A in Ref. [185] for a derivation).

Equation (34) can be exactly evaluated for special integral kernels  $K(\tau)$ . We shall restrict ourselves here to the weak coupling regime. The fluctuation of the amplitude  $c_1(t)$  is assumed to be much slower than any timescale of  $K(t)$  in this regime. Then we may replace  $c_1(t')$  by  $c_1(t)$ , *i.e.* we assume the interaction to be instantaneous. With this assumption, we can further replace  $\int_0^t K(t-t') dt' \rightarrow \int_0^\infty K(t-t') dt'$ . This approach is known as the Markov approximation. It leads to an exponential decay of  $c_1(t)$  at a rate  $\gamma_{\text{wc}}/2$ , where the subscript denotes the weak coupling regime. With  $\int_0^\infty e^{i\omega t} dt = \pi\delta(\omega) + i\mathcal{P}/\omega$  one gets

$$\begin{aligned}\int_0^\infty K(t) e^{i\delta\omega t} dt &= i\delta\omega + \frac{1}{2}\gamma_{\text{wc}} \quad \text{with} \\ \delta\omega &= \frac{1}{\pi\hbar\varepsilon_0} \mathcal{P} \int_0^\infty \frac{\omega^2}{c^2} \frac{\mathbf{d}_{10} \cdot \Im G(\mathbf{r}_{\text{qs}}, \mathbf{r}_{\text{qs}}, \omega) \cdot \mathbf{d}_{01}}{\tilde{\omega} - \omega} d\omega, \\ \gamma_{\text{wc}} &= \frac{2}{\hbar\varepsilon_0} \frac{\tilde{\omega}^2}{c^2} \mathbf{d}_{10} \cdot \Im G(\mathbf{r}_{\text{qs}}, \mathbf{r}_{\text{qs}}, \tilde{\omega}) \cdot \mathbf{d}_{01}. \end{aligned} \quad (35)$$

This result is very intuitive since  $\Im G(\mathbf{r}_{\text{qs}}, \mathbf{r}_{\text{qs}}, \tilde{\omega}) \cdot \mathbf{d}_{01}$  is proportional to the electric field caused by a dipole at its very position [*cf.* Eq. (5)]. Hence, the dipole interacts with itself and we may regard spontaneous emission as a self-induced stimulated emission process. Noteworthy the emission rate in the weak coupling regime is just the classical result for the emission rate of a classical dipole [123].

Note that we may also calculate emission rates in the so-called strong coupling regime (Sec. 6 and App. B.5). In this case, the atomic state population changes on time scales shorter than characteristic correlation time scales of the kernel  $K(\tau)$ . Then the decay of the QS changes to a dynamic situation with constant energy exchange of QS and its environment. Consequently, the results in the weak regime are no longer valid. They are also not valid if memory effects cause non-markovian dynamics. Such effects can occur *e.g.* if a QS is coupled to a photonic crystal that exhibits a band edge close to the resonance frequency of the QS [202, 203].

Some further work would be required to show that the change in transition frequency,  $\delta\omega$ , is mainly related to the real part of the Green's function [185]. This might be anticipated since the principal value integral in Eq. (35) has similarities to the integrations appearing in the Kramers-Kronig relations. Noteworthy,  $\delta\omega$  is given as an implicit expression, since  $\tilde{\omega} = \omega_{10} - \delta\omega$ . The

spectral shift is often ignored as it is orders of magnitude smaller than  $\gamma_{wc}$  and  $\omega_{10}$  in the weak coupling regime.

**The Purcell Factor** We further define

$$F_{\text{tot}}(\mathbf{r}, \omega) \equiv \frac{\mathbf{d}_{10} \cdot \Im G(\mathbf{r}, \mathbf{r}, \omega) \cdot \mathbf{d}_{01}}{\mathbf{d}_{10} \cdot \Im G_{\text{fs}}(\mathbf{r}, \mathbf{r}, \omega) \cdot \mathbf{d}_{01}}, \text{ with} \quad (36)$$

$$G_{\text{fs}}(\mathbf{r}, \mathbf{r}', \omega)_{ij} = \frac{c^2}{4\pi\omega^2} \left[ \partial_i \partial_j + \frac{\omega^2}{c^2} \delta_{ij} \right] \frac{\exp\left[\frac{i\omega}{c} |\mathbf{r} - \mathbf{r}'|\right]}{|\mathbf{r} - \mathbf{r}'|}, \quad (37)$$

which is the Green's function of free-space as a solution to Eq. (4) for the boundary conditions  $G_{\text{fs}}(\mathbf{r}, \mathbf{r}', \omega) \rightarrow 0$  for  $|\mathbf{r} - \mathbf{r}'| \rightarrow \infty$ . The ‘‘total’’ Purcell factor  $F_{\text{tot}}$  refers to the enhancement of spontaneous emission rates of the dipole emitter compared to free space in the weak coupling regime [*cf.* Eq. (35)]. However, in the literature mainly the ‘‘radiative’’ Purcell factor  $F = \eta F_{\text{tot}}$  is discussed. It refers to the emission rate enhancement, as it can be measured in the farfield, *i.e.* for  $r \rightarrow \infty$ . We may simply call  $F$  Purcell factor for this reason.

**The Spectral Density** In the Markov approximation,  $\Im G(\mathbf{r}, \mathbf{r}, \omega)$  is proportional to the spontaneous emission rate [Eq. (35)]. Furthermore, the kernel  $K(\tau)$  is also closely related to the imaginary part of the Green's function [Eq. (34)]. This relation can be somewhat simplified via the introduction of a useful quantity, the so-called spectral density  $J(\omega)$ . It is given by

$$K(t - t') = \int_0^\infty J(\omega) \exp[i(\tilde{\omega} - \omega)(t - t')] d\omega, \text{ such that}$$

$$J(\omega) = \frac{1}{\pi\epsilon_0\hbar} \frac{\omega^2}{c^2} \mathbf{d}_{10} \cdot \Im G(\mathbf{r}_{\text{qs}}, \mathbf{r}_{\text{qs}}, \omega) \cdot \mathbf{d}_{01}. \quad (38)$$

It must not be forgotten that  $J(\omega) \equiv J(\mathbf{r}_{\text{qs}}, \omega, \mathbf{d}_{10})$  implicitly depends on the position of the QS and the strength and orientation of its dipole moment. Furthermore, other  $J(\omega)$  may appear when transitions other than electric dipolar ones are involved. As we will discuss in Sec. 4, such ‘‘forbidden transitions’’ can be hugely enhanced by NAs and naturally lead to magnetic dipole spectral densities, electric quadrupole ones and so on [204]. Please note that  $J(\omega)$  is a quantity very similar to the local density of states (LDOS). The relation between these quantities is derived in App. B.5.2.

**A Practical Problem for Numerical Investigations** Solving integro-differential equations like Eq. (34) to determine the dynamics of hybrid plasmonic quantum system is not just theoretically demanding. It is in particular numerically involved if not only the state of the QS is of interest. This is the case if we want to understand the quantum statistics of the electromagnetic field. Then, the entire state of the combined system has to be evaluated and the dynamics of the electromagnetic states cannot be integrated out as we did to get rid of the  $\mathbf{c}_{0,\omega}(t)$ . In this case, one directly deals with an infinite-dimensional Hilbert space as  $H_{\text{EM}} = \int \mathbf{f}^\dagger(\mathbf{r}, \omega) \cdot \mathbf{f}(\mathbf{r}, \omega) d\omega dV$  is continuous in  $\omega$ .

But naive approximative methods are prone to fail, too: We may restrict an analysis to, say, only ten intervals of the spectrum around some  $\omega_n$  such that  $H_{\text{EM}} = \sum_{n=1}^{10} \int \mathbf{f}^\dagger(\mathbf{r}, \omega_n) \cdot \mathbf{f}(\mathbf{r}, \omega_n) dV$ . Furthermore, only a maximum of two photons in each oscillator ( $n = \{0, 1, 2\}$ ) shall be assumed. The Hilbert space then exhibits a dimension of  $\dim(\mathcal{H}) = \prod_i \dim(\mathcal{H}_i) = 2 \times 3^{10} > 10^5$ .

Hence we need to find a way to treat the full quantum dynamics within an approximative scheme that allows us to access the quantum state of the hybrid system. This will help us to go beyond simple spontaneous emission calculations and to enter a truly quantum regime with all

its fascinating effects. In the next subsection we will see that quasinormal modes are indeed this kind of approximation that allows us to understand the quantum dynamics in a rather simplistic cQED-like approach.

### 3.3 Quasinormal Modes

In Sec. 3.1 we have seen that the cQED approach used to describe the quantum dynamics of the electromagnetic field is quite appealing. It is a rather simple description since the Hamiltonian consists of a few harmonic oscillators. Furthermore, the study of light-matter-interactions within the minimal coupling framework [Eq. (16)] is fairly easy to achieve [Eq. (28)].

To apply a multimode cQED-approach to NA quantization, we have to assume that the field of a NA can in fact be approximated by a few modes only. But these modes cannot be normal modes in the strict sense of a solution to a Hermitian operator as the involved dielectric materials are lossy. The problem can be tackled in terms of well-defined so-called quasinormal modes (QNMs) [205–207]. Following Refs. [191] and [208], we may approach QNMs using the wave equation (3) for the electric field by introducing a background permittivity  $\varepsilon_B(\omega)$  as

$$\begin{aligned} \left[ \nabla \times \nabla \times - \frac{\omega^2}{c^2} \{ \varepsilon(\mathbf{r}, \omega) - \varepsilon_B(\omega) + \varepsilon_B(\omega) \} \right] \mathbf{E}(\mathbf{r}, \omega) &= i\omega\mu_0 \mathbf{j}_{\text{ext}}(\mathbf{r}, \omega) , \\ \left[ \nabla \times \nabla \times - \frac{\omega^2}{c^2} \varepsilon_B(\omega) \right] \mathbf{E}(\mathbf{r}, \omega) &= i\omega\mu_0 \mathbf{j}_{\text{ext}}(\mathbf{r}, \omega) + \frac{\omega^2}{c^2} \Delta\varepsilon(\mathbf{r}, \omega) \mathbf{E}(\mathbf{r}, \omega) \end{aligned} \quad (39)$$

with  $\Delta\varepsilon(\mathbf{r}, \omega) \equiv \varepsilon(\mathbf{r}, \omega) - \varepsilon_B(\omega)$ . The right hand side of Eq. (39) can be interpreted as a source term. An advantage is that the dyadic Green's function  $G_B(\mathbf{r}, \mathbf{r}', \omega)$  for the differential operator  $\mathcal{D} = \nabla \times \nabla \times - \frac{\omega^2}{c^2} \varepsilon_B(\omega)$  is just the free-space solution given in Eq. (37) with the formal replacement  $k = \omega/c \rightarrow k_B = \sqrt{\varepsilon_B(\omega)}\omega/c$ . Then Eq. (3) reads as

$$\mathbf{E}(\mathbf{r}, \omega) = \mathbf{E}_B(\mathbf{r}, \omega) + \frac{\omega^2}{c^2} \int G_B(\mathbf{r}, \mathbf{r}', \omega) \Delta\varepsilon(\mathbf{r}', \omega) \mathbf{E}(\mathbf{r}', \omega) dV' , \quad (40)$$

where  $\mathbf{E}_B(\mathbf{r}, \omega) = i\omega\mu_0 \int G_B(\mathbf{r}, \mathbf{r}', \omega) \mathbf{j}_{\text{ext}}(\mathbf{r}', \omega) dV'$  is the background field caused by external charges.

Equation (40) is a special form of the Lippmann-Schwinger equation that appears in scattering problems in quantum mechanics [209]. It can be seen as a basis for other scattering problems as well. Examples are the scattering of multiple spheres [153, 210] and the so-called boundary element method [169, 211, 212]. Most importantly, Eq. (40) allows to define QNMs in the following way:

Quasinormal modes  $\mathbf{E}_n(\mathbf{r})$  are normalized solutions of the excitation-free Lippmann-Schwinger equation

$$\mathbf{E}_n(\mathbf{r}) = \frac{\tilde{\omega}_n^2}{c^2} \int G_B(\mathbf{r}, \mathbf{r}', \tilde{\omega}_n) \Delta\varepsilon(\mathbf{r}', \tilde{\omega}_n) \mathbf{E}_n(\mathbf{r}') dV' . \quad (41)$$

Here,  $\mathbf{E}_n(\mathbf{r})$  is the electric field of the  $n^{\text{th}}$  quasi-mode. Its eigenfrequency  $\tilde{\omega}_n = \omega_n - i\Gamma_n$  is necessarily complex as Eq. (40) describes an open system for which the associated mathematical operators are not Hermitian [206]. Naturally,  $\Re(\tilde{\omega}_n) = \omega_n$  denotes the frequency of the QNM,  $-\Im(\tilde{\omega}_n) = \Gamma_n$  its loss-rate, and  $Q_n = \omega_n/2\Gamma_n$  its quality factor [123].

Please note that the normalization scheme was left open, as different approaches exist in the literature based on the actual purpose the QNMs are used for [194]. Furthermore, following Ref. [207], it is often possible to express the transverse of  $G(\mathbf{r}, \mathbf{r}', \omega)$  as a superposition of QNMs, but a discussion of the limitations of this approach is beyond the scope of this work.



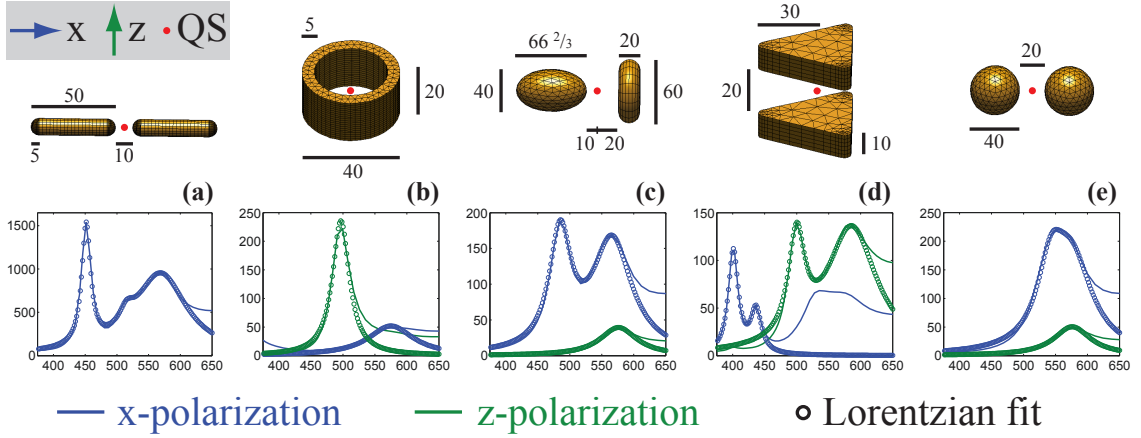


Figure 8: Lorentzian character of  $J(\omega) \propto \omega^3/\omega_0^3 F(\omega)$ . Upper part: Investigated NAs - all scales in nm. The grey inset illustrates the polarization of the dipole emitters and their position markups (red dots). Lower part:  $\omega^3/\omega_0^3 F(\omega)$  as a function of  $\nu = \omega/2\pi$  for the respective geometries in  $x$ - and  $y$ -polarization of the dipole (blue and green solid lines) and multi-Lorentzian fits (circles).

To calculate parameters for the quantization scheme based on QNMs, we assume that the time dependency of the electric field of QNMs is given by

$$\mathbf{E}_n(\mathbf{r}, t) = \frac{1}{2} [\mathbf{E}_n(\mathbf{r}) e^{-i\tilde{\omega}_n t} + \mathbf{E}_n^*(\mathbf{r}) e^{i\tilde{\omega}_n t}] . \quad (42)$$

The generalization to slowly varying amplitudes can be achieved by the replacement  $\mathbf{E}_n(\mathbf{r}) \rightarrow \mathbf{E}_{\text{env},n}(\mathbf{r}, t)$ .

### 3.4 Quasinormal Mode Quantization Scheme

We have seen how the electromagnetic field can be quantized in a cavity and in the presence of dispersive media. The advantage of the cavity quantization is that only a few modes need to be considered. In the quantum optics approach infinitely many modes are required to account for dissipation. The introduction of QNMs allows to analyze the excitations of NAs in a self-consistent manner. In the following we shall use the QNMs to quantize the field of a NA. The main step is to determine the QNMs in a way that is more practical than to solve Eq. (41).

#### Motivation and Definition

There are two main motivations for the QNM quantization we introduce.

1. The spectral density  $J(\omega)$  for QSs close to NAs can often be described by a superposition of Lorentzians. Such an approach is known to be approximative [192]. However, in Fig. 8 we show that it holds for exemplarily investigated gold NAs (Fig. 8, upper parts). Their permittivity was taken from Ref. [124] and we assume an embedding dielectric with permittivity  $\epsilon_d = 2.2$ . The electromagnetic calculations were made with a freely available simulation toolbox [169]. If we assume that the efficiency of the NAs is almost constant for the spectral range of a resonance, then  $\omega^3/\omega_0^3 F(\omega) \propto J(\omega)$  (exact relation in App. B.6,  $\omega_0 = 2\pi c/500$  nm) and we can analyze  $J(\omega)$  in terms of the familiar Purcell factor (Fig. 8, lower parts). The agreement of  $\omega^3/\omega_0^3 F(\omega)$  to multi-Lorentzian fits is remarkable for  $\nu \lesssim 600$  THz ( $\lambda \approx 500$  nm), where gold becomes rather dissipative and starts to lose its metallic character (Fig. 2).

2. It turns out that the Weisskopf-Wigner problem of spontaneous emission can be solved in full analyticity if the spectral density  $J(\omega)$  exhibits a Lorentzian shape (App. B.5). In that case, the

evolution of the QS in the quantum optics approach should be equivalent to the coupling to a lossy harmonic oscillator [213], *i.e.* equivalent to a lossy Jaynes-Cummings model [*cf.* Eq. (49)]. The equivalence to a Jaynes-Cummings model is only claimed in Ref. [213] for a spectral density  $J(\omega)$  with a single Lorentzian peak. Beyond that we may assume that this approach is also applicable for multiple independent Lorentzian contributions to  $J(\omega)$ .

Consequently the QNM quantization scheme is defined as follows:

If the spectral density  $J(\omega)$  of a NA can be approximately described by a superposition of independent Lorentzians,

$$J(\omega) = \frac{1}{\pi} \sum_{n=1}^N \alpha_n \frac{\Gamma_n/2}{(\omega - \omega_n)^2 + (\Gamma_n/2)^2}, \quad (43)$$

the interaction of that NA to a QS can be approximately calculated quantizing the NA as lossy harmonic oscillators. The parameters  $\omega_n$  and  $\Gamma_n$  of the  $n^{\text{th}}$  oscillator are given by the energies and loss rates of the QNM,  $E_n = \hbar \Re \tilde{\omega}_n = \hbar \omega_n$  and  $\Gamma_n = -\Im \tilde{\omega}_n$ . The electromagnetic fields of each QNM must be normalized in such a way that it amounts to  $E_n$ . Last but not least, the normalization constants  $\alpha_n$  fulfill  $\int_{-\infty}^{\infty} J(\omega) d\omega = \sum_n \alpha_n$ .

### Approximate Determination of Quasinormal Modes

Thus, the QNMs may be used to quantize NAs, but from a practical point of view it is not clear how to determine them. A direct solution of Eq. (41) seems to be rather involved, and the QNMs determined in this way may diverge for  $|\mathbf{r}| \rightarrow \infty$  [192]. Hence it is favourable to find a robust and simple approximative scheme to determine the QNMs. Such a scheme is provided by a rather simplistic scattering analysis and consists of four main steps (see also App. B in Ref. [80]):

1. Determine the real part of a QNM eigenfrequency,  $\omega_n$ , by a maximum in the scattering (or extinction) cross sections upon illumination with a suitable source, *i.e.* plane wave or dipole. Preferably, the illumination source should be chosen such that only the investigated QNM is excited.
2. Normalize the mode such that its energy is given by [115]

$$E_n = \frac{1}{4} \int_{\Omega} \left\{ \varepsilon_0 (\partial_{\omega} \omega \Re [\varepsilon(\mathbf{r}, \omega)]_{\omega=\omega_n}) |\mathbf{E}_n(\mathbf{r})|^2 + |\mathbf{B}_n(\mathbf{r})|^2 / \mu_0 \right\} dV \stackrel{!}{=} \hbar \omega_n. \quad (44)$$

3. Calculate the loss rates for this mode via Poynting's theorem as

$$\begin{aligned} \Gamma_n &= \Gamma_{n,\text{rad}} + \Gamma_{n,\text{diss}} \\ &= \frac{1}{2E_n} \left[ \frac{1}{\mu_0} \oint_{r \rightarrow \infty} \Re [\mathbf{E}_n(\mathbf{r}) \times \mathbf{B}_n^*(\mathbf{r})] \cdot \mathbf{n} d\Omega + \int_{\Omega} \varepsilon_0 \omega_0 \varepsilon''(\mathbf{r}, \omega_0) |\mathbf{E}_n(\mathbf{r}, t)|^2 dV \right] \end{aligned} \quad (45)$$

4. Determine the coupling constants following Eqs. 21 and 22, *i.e.* in the electric dipole approximation.

This four-step-approach to determine the QNMs of a NA is approximative for three reasons:

First, the integral to determine the mode energy  $E_n$  contains radiative contributions that in general should be subtracted [190]. But it is not clear how to do this in a self-consistent manner in practice. To study the influence of the radiative contributions in the energy normalization of Eq. (44), we performed calculations with a variation of the integration domain  $\Omega$ . We have seen almost no variation in the resulting mode parameters if  $\Omega$  contains the local near field of the NA.

Second, the scattered field is inherently excitation dependent [194]. From a mathematical point of view, this argument is certainly correct. Nevertheless, as QNMs may also be defined as the poles of the response function of a system [116], a distinctive maximum in the scattering cross section can be used to approximately identify the real part of the resonance frequency. Then, by analyzing only the scattered field of the NA, the QNM's fields  $\mathbf{E}_n(\mathbf{r})$  and  $\mathbf{B}_n(\mathbf{r})$  can be approximately determined.

Third, there is yet a completeness relation to be shown for such modes [194]. Even though this argument is also valid, only a few modes may be used to study the interaction of NAs and QNs. The main requirement is that the QNMs are orthogonal, which is naturally the case if the identification of the modes is unambiguous.

Finally, the determination of the eigenfrequencies  $\omega_n$  in the farfield by a scattering analysis incorporates a known frequency shift compared to near-field investigations [214–216]. This approximation can be avoided by a determination of the  $\omega_n$  in the near-field. A straight forward approach is to calculate the electromagnetic field at locations where the investigated QNM exhibits large field enhancements, *e.g.* in the gap of a NA.

### Incorporation of Irreversible Processes

Within the QNM quantization scheme, the Hamiltonian of the NA is given by a superposition of harmonic oscillators,

$$H_{\text{na}} = \sum_n \hbar\omega_n \left( a_n^\dagger a_n + \frac{1}{2} \right) .$$

Since the NA loss rates  $\Gamma_n$  cannot be included into a Hermitian Hamiltonian, a density matrix formulation has to be used [185]. The density matrix is given by  $\rho(t) = \sum_n p_n(t) |n\rangle \langle n|$  in the orthonormal basis  $\{|n\rangle\}$ , in which the  $p_n(t)$  are the probabilities of the  $n^{\text{th}}$  state. Note that  $\rho(t)$  contains all information about the physical system. For example, expectation values of an arbitrary operator  $A$  can be calculated as  $\langle A \rangle(t) = \sum_n p_n(t) \langle n| A |n\rangle \equiv \text{tr}[A\rho(t)]$ .

A hybrid system involving a NA and a QS can be described by the Hamiltonian  $H = H_{\text{na}} + H_0 + H_{\text{int}}$ , where  $H_0$  denotes the Hamiltonian of the QS and  $H_{\text{int}}$  an interaction between all involved subsystems. The density matrix of this system evolves according to the Lindblad-Kossakowski equation [195, 217, 218]

$$\begin{aligned} i\hbar\partial_t\rho(t) &= [H, \rho(t)] + i\hbar\mathcal{L}_{\text{decay}}[\rho(t)] + i\hbar\mathcal{L}_{\text{QS}}[\rho(t)] , \text{ with} \\ \mathcal{L}_{\text{decay}}[\rho(t)] &= \sum_n \frac{\Gamma_n}{2} \{ 2a_n\rho(t)a_n^\dagger - \rho(t)a_n^\dagger a_n - a_n^\dagger a_n\rho(t) \} . \end{aligned} \quad (46)$$

Here,  $\mathcal{L}_{\text{decay}}$  is a so-called Lindblad operator introduced to incorporate the NA radiative and nonradiative decay, and  $\mathcal{L}_{\text{QS}}$  is a Lindblad operator for the QS. The  $\mathcal{L}_{\text{QS}}$  be needed to introduce dephasing mechanism that do not affect the population distribution but the coherence of the QS [219].

Lindblad operators generally allow to introduce irreversible processes to the evolution of QNs in a self-consistent manner. They arise quite naturally in the study of coupled QNs, for which the dynamics of only a certain part is of interest and the remaining part can be “traced out” [220]. Specifically,  $\mathcal{L}_{\text{decay}}$  refers to energy relaxation. It causes an exponential decay of the expectation of the number operator for the  $n^{\text{th}}$  mode,  $a_n^\dagger a_n$ , at a rate  $\Gamma_n$  [185]. This Lindblad operator results in a Lorentzian spectral density, but other spectral densities might be approximated using different Lindblad operators [221].

**A Note on the Determination of Parameters** As mentioned already, the interaction of QS to NAs in a fully quantum description is a main motivation. To understand such interactions, additional coupling Hamiltonians  $H_{\text{int}}$  have to be introduced. Defining such interaction terms, however, one has to be careful when working in the frequency domain.

For example, within the RWA, the semiclassical interaction between a dipole and the electric field of a QNM can be formulated. According to Eqs. (21) and (42),

$$\begin{aligned} H_{\text{int}} &= (d\sigma_+ + d^*\sigma_-) \mathbf{e}_d \cdot \left( \frac{1}{2} \mathbf{E}_n(\mathbf{r}) e^{-i\omega_n t} + \frac{1}{2} \mathbf{E}_n^*(\mathbf{r}) e^{i\omega_n t} \right) \\ &\approx \mathbf{e}_d \cdot d\sigma_+ \frac{1}{2} \mathbf{E}_n(\mathbf{r}) e^{-i\omega t} + \text{H.c.} \equiv \hbar\kappa_n \sigma_+ e^{-i\omega t} + \text{H.c.} , \end{aligned}$$

with  $\sigma_+$  ( $\sigma_-$ ) as the QS's creation (annihilation) operators and dipole moment  $\mathbf{d} = d\mathbf{e}_d$ . The electric dipole coupling strength is then given by

$$\kappa_n = \frac{1}{2} \frac{d\mathbf{e}_d \cdot \mathbf{E}_n(\mathbf{r})}{\hbar} . \quad (47)$$

### 3.5 Verification of the quantization Scheme

Few-mode quantization procedures have been successfully applied already in different fields of research, see *e.g.* Refs. [185, 222, 223]. In this section we give some examples along with some intuitive arguments that such a description is applicable to NAs. We verify the equivalence of spontaneous emission of a QS in the quantum optics and QNM quantization pictures under the assumption of a Lorentzian spectral density. The equivalence of the Purcell factor calculated from QNM parameters or far-field observables is checked as well.

A good example for the applicability of few-mode quantizations was given by Laussy *et al.* [224], who investigated the coupling of the electronic states of QDs to the electromagnetic modes of semiconductor microcavities. The authors were able to explain all details of the strong coupling observed by Reithmaier *et al.* [225]. Hybrid plasmonic systems have been studied within a few-mode harmonic oscillator quantization as well [79, 86, 176, 226].

Furthermore, the widely applicable Drude model for the electron dynamics in NAs naturally leads to oscillatory motions of the electrons. In quasistatic approximations, such NAs cause a Lorentzian spectral density  $J(\omega)$  for nearby QSs [213, 227]. Moreover, it was demonstrated experimentally that certain individual NAs exhibit an oscillator-like response [228–230]. By virtue of the correspondence principle, such observations imply that the excitations of such NAs can be described as quantum harmonic oscillators. So, especially for small NAs with localized oscillating conduction electrons, the few-mode quantization seems very feasible. Thus our observations of multi-Lorentzian  $J(\omega)$  in Fig. 8 can be seen as widely applicable. Nevertheless we note that  $J(\omega)$  can be arbitrarily complicated. This can already be seen for lossy optical cavities [188, 231]. In such cases a quantum optics description is probably required.

#### Lossy Jaynes-Cummings Model vs. Lorentzian spectral Density

The equivalence of a lossy Jaynes-Cummings model and a Lorentzian spectral density shall be checked now. To do so, we numerically calculate the decay of a QS's excitation in the Jaynes-Cummings model for varying parameters. Then we compare this decay to analytical results for a QS subject to a Lorentzian spectral density with the same parameters.

In our treatment of the Weisskopf-Wigner problem of spontaneous emission in Sec. 3.2 we have seen that the excited state amplitude of the involved two-level system follows the integro-differential

equation

$$\dot{c}_1(t) = - \int_0^t K(t-t') c_1(t') dt', \quad (48)$$

if we neglect the spectral shift  $\delta\omega$  [*cf.* Eq. (34)]. As it is shown in App. B.5, this equation of motion can be solved fully analytically for a Lorentzian spectral density. Most importantly, the decay rate in the weak coupling regime,  $\gamma_{\text{wc}}$ , is correctly reproduced if

$$J(\omega) = \frac{\gamma_{\text{wc}}}{2\pi} \frac{(\Gamma/2)^2}{(\omega_{\text{na}} - \omega)^2 + (\Gamma/2)^2}.$$

The spontaneous emission rate  $\gamma_{\text{wc}}$  of the two-level system coupled to a single harmonic oscillator can be calculated under certain assumptions (*cf.* App. B.8). At resonance ( $\omega_{\text{na}} = \omega_{\text{QS}}$ ), it simply reads as  $\gamma_{\text{wc}} = 4\kappa^2/\Gamma$ . Here,  $\kappa$  is the coupling rate between QS and NA, and  $\Gamma$  the loss rate of the NA, and the Hamiltonian is given by

$$H = \hbar\omega_{\text{qs}}\sigma_+\sigma_- + \hbar\omega_{\text{na}}\left(a^\dagger a + \frac{1}{2}\right) + \hbar\kappa(\sigma_+ a + a^\dagger\sigma_-) \quad (49)$$

This Hamiltonian corresponds to the aforementioned Jaynes-Cummings model [198]. As already discussed, the losses of the NA are introduced within a density matrix formulation of the problem [Eq. (46)]. Because of the determination of  $\gamma_{\text{wc}}$  in terms of QNM parameters, it is possible to compare the evolution of the QS subject to a full Lorentzian spectral density vs. a single harmonic oscillator with the same parameters. If the quantization procedure is correct, the evolution should be equivalent.

With the help of a freely available quantum optics toolbox [232], we did calculations for different coupling rates ranging from  $\kappa = 0.1\Gamma$  (weak coupling) to  $\kappa = 2\Gamma$  (strong coupling). As expected, a perfect agreement of  $c_1(t)$  between the full quantization and single-mode quantization (Fig. 9, left part) is found. Hence we may assume that the coupling to a single harmonic oscillator is equivalent to a Lorentzian spectral density. We note that this equivalence might be obtainable in a fully analytical way tracing out the lossy harmonic oscillator [see again Eq. (46)] to obtain density matrix equations of motion for the two-level system alone. If then the equations of motion are equivalent to those of a two-level system subject to a Lorentzian spectral density, the equivalence of a coupling to a single harmonic oscillator and a Lorentzian spectral density is shown.

### Spontaneous Emission Rates

There is another way to test whether the introduced QNM quantization approach is suitable or not. In the weak coupling limit the radiative emission rate of a QS can be checked against classical dipole emission calculations. Within the classical radiation scenario, however, it is more convenient to calculate the Purcell factor  $F = \gamma_{\text{rad,wc}}/\gamma_{\text{fs}}$ , as no normalization is needed:  $F$  may be simply calculated by the ratio of the radiated power with and without NA,  $F = P_{\text{rad,na}}/P_{\text{fs}}$  [6]. Obviously, in the weak coupling regime  $F = \eta\gamma_{\text{wc}}/\gamma_{\text{fs}} = 4\eta\kappa^2/\Gamma\gamma_{\text{fs}}$ , since  $\gamma_{\text{rad,wc}} = \eta\gamma_{\text{wc}}$ . Please note that the well-known classical free-space emission rate is often defined using the real part of the refractive index of a possible homogeneous embedding medium,  $\gamma_{\text{fs}} = n_{\text{emb}}\omega_{\text{QS}}^3 |\mathbf{d}|^2 / 3\pi\epsilon_0\hbar c^3$ . We have adopted this definition for our calculations.

The coupling rate  $\kappa$  and the NA loss rate  $\Gamma = \Gamma_{\text{rad}} + \Gamma_{\text{diss}}$  are calculated within the QNM quantization scheme following Eqs. (45) and (47). The determination of the Purcell factor relies on two absolutely different schemes. An agreement would prove the applicability of the NA quantization scheme in the context of spontaneous emission. A comparison of  $F$  for both determination

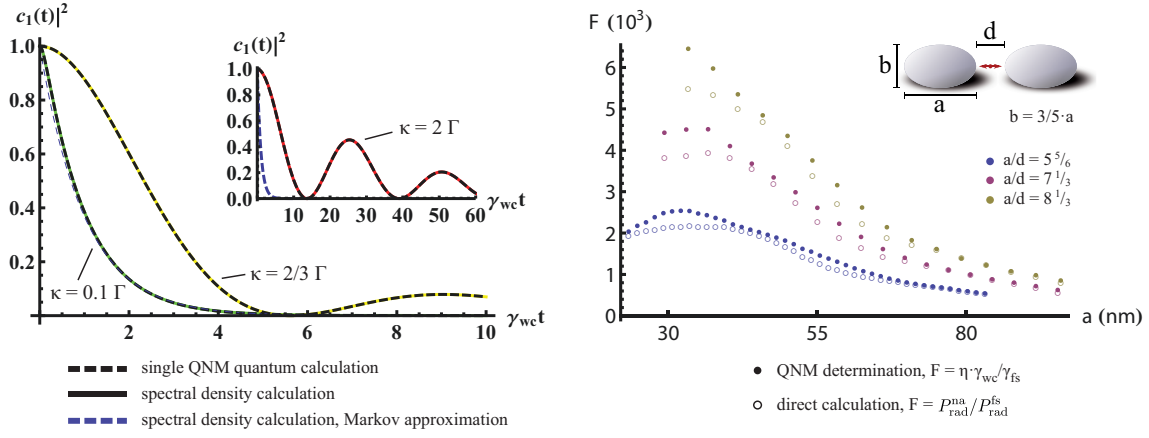


Figure 9: Verification of the NA quantization scheme. Left: Evolution of the excited state population  $|c_1(t)|^2$  of a two-level system coupled to a Lorentzian spectral density  $J(\omega)$  (solid lines) vs. single mode quantization calculations (black dashed lines).  $|c_1(t)|^2$  coincides in both weak (green line) and strong coupling regimes (red line, inset). The Markovian decay  $|c_1(t)|^2 \propto \exp[-\gamma_{wc}t]$  is only a good approximation in the weak coupling regime (blue dashed line). Right: Purcell factors for NAs with different sizes and conformal factors.  $F = \eta\gamma_\infty/\gamma_{fs}$  based on the QNM quantization scheme (solid dots) vs.  $F = P_{na}/P_{fs}$  via a direct calculation of the radiated powers [circles, Eq. (6)].

schemes is given in Fig. 9 (right). The very good agreement between the QNM determination and direct calculation of  $F$  for a wide range of NAs shows the applicability of the QNM quantization scheme.

By virtue of QNMs we have found a reliable and easy-to-implement quantization of NAs to study quantum light-matter interactions. For instance, we will investigate single photon emission by hybrid systems (Sec. 5 based on Ref. [89]) and the possibility to reach the strong coupling limit (Sec. 6 based on Ref. [80]). Furthermore, two other publications are based on this NA quantization procedure [90,91].

In Sec. 2, we described NAs in terms of classical electrodynamics. In this section we found an accessible way to quantize NA-QS-interactions. We used (and sometimes even extended) results from antenna theory, classical electrodynamics and quantum optics. Combined, these theories provide a powerful toolbox to describe and study the interactions of QNs with NAs at different levels of approximation. We will now use this toolbox to study so-called dipole-forbidden transitions in a semiclassical framework.

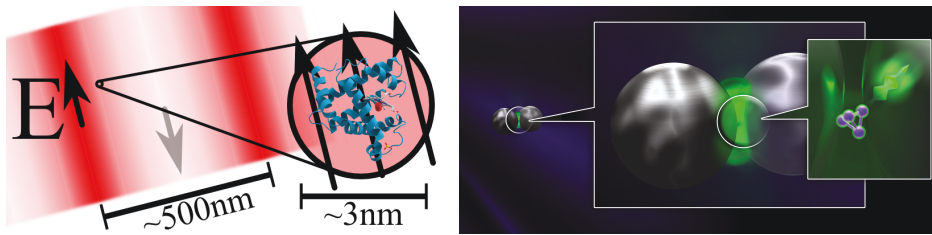


Figure 10: Schematic illustration of the enhancement of forbidden transitions via NAs. Left: The wavelength of a plane wave (red) compared to the size of a QS, myoglobin in this case. The electric field is almost constant across the QS. Right: a dimer NA illuminated by a plane wave at around 440 nm (purple) enhances the local electric field variation inside its feed gap. QSs with an electric quadrupole transition may strongly emit at lower frequencies (green region).

## 4 Enhancing Dipole-Forbidden Transitions in Quantum Systems

The interaction of light with QSs is a main subject of quantum optics. To study this interaction, QSs are frequently placed inside a cavity. The electromagnetic modes of the cavity are then used to interact with the QS. Characteristic length scales on which the electromagnetic fields vary are usually large compared to QSs. In this case it is suitable to assume the electric field as constant across the entire QS. This so-called “electric dipole approximation” is widely applied in quantum optics [195, 198, 233]. A characteristic length scale of QSs is the expectation value for the radial distance of an electron in the hydrogen atom, the Bohr radius

$$a_0 = \frac{4\pi\epsilon_0\hbar^2}{m_e e^2} \approx 5.2918 \cdot 10^{-11} \text{ m} .$$

The electric dipole approximation is usually fulfilled because  $a_0$  is much smaller than wavelengths in the visible. Transitions that are not related to an interaction within the electric dipole approximation are usually termed dipole-forbidden or just “forbidden” because their transition probabilities are extremely weak.

But in the case of near-field interactions the situation can change dramatically. In 2002, Kawazoe *et al.* [234] demonstrated that closely placed QDs (CuCl cubes) exhibit an energy transfer that cannot be understood within the electric dipole approximation. The energy transfer was attributed to the spatially strongly varying field close to the QDs - a direct observation of forbidden transitions driven by a near-field interaction. The advances in nanotechnology during the last decades have raised the interest in forbidden transitions using plasmonic structures [76, 77, 235, 236].

Especially transitions related to an electric quadrupolar interaction seem to be interesting as magnetic dipole emissions can be selectively investigated using comparably simple interference techniques [73]. Because of the strong field confinement in the feed gap of NAs, they are perfect candidates to study forbidden transitions. They may be designed to locally enhance certain multipole components. This approach has been recently investigated in the context of metamaterials [237] and optical vortices [238] as well.

Conceptually, forbidden transitions of QSs are equivalent to dark modes of plasmonic structures [239, 240]. Moreover, these dark modes may be used to couple to QSs [84, 241, 242]. It seems only a matter of time until forbidden transitions of QSs can be used as a channel to investigate light-matter-interactions without the often self-imposed electric dipole approximation. New effects might be explored and applications may benefit from novel spectroscopic schemes, nonclassical

light sources or enhanced quantum information processes.

In the following we shall first discuss forbidden transitions in the context of a plane wave excitation (Sec. 4.1). After this, we shall introduce a general scheme to understand the interaction of Qs to electromagnetic fields composed of arbitrary multipole components (Sec. 4.2). This will enable to investigate the enhancement of an electric quadrupole interaction by a NA (Sec. 4.3). A quadrupolar interaction cannot be seen as an isolated process. Thus we will consequently analyze the dynamics of a three-level system driven by a quadrupole absorption (Sec. 4.4). I will be outlined how the NA mediated enhancement of a quadrupole absorption leads to a luminescence enhancement of the QS. This section is largely based on Ref. [78].

## 4.1 Plane-Wave-Excitation of Forbidden Transitions

Let us first try to understand why higher-order transitions are usually called forbidden. To do so, we calculate the absorption rate of a hydrogen-like QS with atomic number  $Z$  subject to a plane wave illumination in a semiclassical approach. This requires an analysis of multipole expansion of the electromagnetic field of a plane wave. Fortunately, we do not have to use an expansion in vector spherical harmonics in this case. Instead, we may just perform a spatial Taylor expansion of the fields and use some characteristic numbers to find the transition rates. The electromagnetic field shall be at resonance with the transition of the QS. Then we can concisely use  $\omega \equiv \omega_{mn}$ , since transition and field oscillation frequencies coincide.

For an  $x$ -polarized plane wave, the electric and magnetic fields can be expanded in close vicinity to the quantum system at  $\mathbf{r}_{\text{qs}} = 0$  as

$$\begin{aligned} \mathbf{E}(\mathbf{r}, t) &= \frac{E_0}{2} \left[ e^{i(kz - \omega t)} + e^{-i(kz - \omega t)} \right] \mathbf{e}_x, \\ \mathbf{E}(\mathbf{r}, t) &\approx \frac{E_0}{2} \left[ (1 + ikz) e^{-i\omega t} + (1 - ikz) e^{i\omega t} \right] \mathbf{e}_x \\ &= E_0 [\cos(\omega t) + \sin(\omega t) kz] \mathbf{e}_x, \text{ and} \\ \mathbf{B}(\mathbf{r}, t) &\approx -\frac{E_0}{c} \cos(\omega t) \mathbf{e}_y. \end{aligned}$$

The electric and magnetic coupling potentials [Eq. (21) and Eq. (22)] are given by

$$\begin{aligned} V_e(\mathbf{r}, t) &= -e\mathbf{E}(\mathbf{r}, t) \cdot \mathbf{r} \approx -e [\cos(\omega t) + kz \sin(\omega t)] x \quad \text{and} \\ V_m(\mathbf{r}, t) &= \frac{\mu_B}{\hbar} \mathbf{B}(\mathbf{r}, t) \cdot \mathbf{L} \approx -\frac{\mu_B}{\hbar} \frac{E_0}{c} \cos(\omega t) L_y. \end{aligned}$$

### Comparison of Transition Rates

In  $V_e(\mathbf{r}, t)$ , the first term corresponds to an electric dipole interaction and the second one to a quadrupolar one. For the magnetic interaction  $V_m(\mathbf{r}, t)$ , only the first term needs to be taken into account, *i.e.* the magnetic dipole contribution. We can use Fermi's Golden Rule and characteristic figures for the expectation values of certain operators, *i.e.*  $\langle r \rangle = a_0/Z$  and  $\langle \mathbf{L} \rangle / \hbar \approx 1$  for the expected radius and angular momentum. The magnetic dipole contribution compared to the electric dipolar one is (see also Ref. [243] for a more elaborate approach)

$$\frac{\Gamma_{m,2}}{\Gamma_{e,1}} \approx \left| \frac{\mu_B}{\hbar} \frac{E_0}{c} \langle L_y \rangle \right|^2 / |e \langle r \rangle E_0|^2 = \frac{Z^2 \hbar^2}{4m^2 a_0^2 c^2} = \left[ \frac{Z\alpha}{2} \right]^2 \approx 1.3 \cdot 10^{-5} Z^2 \quad (50)$$



with the fine-structure constant  $\alpha \approx 1/137$ . For electric quadrupole excitations we find the simple relation

$$\frac{\Gamma_{e,2}}{\Gamma_{e,1}} \approx |k \langle r \rangle|^2 = \left( \frac{ka_0}{Z} \right)^2 \approx 4.4 \cdot 10^{-7} / Z^2 \text{ for } \lambda = 500 \text{ nm} . \quad (51)$$

Equations (50) and (51) provide a quantitative understanding of the order-of-magnitude difference of dipole-forbidden ( $\Gamma_{e,2}$  and  $\Gamma_{m,1}$ ) and dipole-allowed ( $\Gamma_{e,1}$ ) transition rates for a plane wave excitation. The result is interesting in different ways:

1. The electric quadrupole rate is always much weaker than the magnetic dipole contribution at optical frequencies. This result is rather general and is supported by explicit calculations in the trivalent lanthanide series [244]. It explains why at least magnetic dipole transitions have drawn much attention lately and electric quadrupole transitions have been less considered [73, 75, 126, 204, 245].
2. The electric quadrupole contribution gets even weaker for high atomic numbers  $Z$  as the expectation of the radial distance  $\langle r \rangle$  of electrons for a given quantum number  $n$  lowers with increasing  $Z$ . On the other hand, larger  $n$  can also be used to increase  $\langle r \rangle$  and to enhance higher order contributions, which explains the possibility to study forbidden transitions with Rydberg atoms [246–248].
3. Regarding the ratios between  $\Gamma_{e,1}$ ,  $\Gamma_{m,1}$ , and  $\Gamma_{e,2}$ , it can be stated that higher order excitations do not play any role if they are energetically close to dipole-allowed optical transitions. Hence, the electric dipole approximation can be used most of the time [195, 198, 233]. This finding is also supported by explicit calculations of the  $1s \rightarrow 2p$  transition of hydrogen atoms taking into account all multipole moments [249]. In this case, one finds that the ratio of the transition rate for the full calculation to one employing the electric dipole approximation result amounts to a factor of  $1 / \left[ 1 + \{(2/3)ka_0\}^2 \right]^2 \approx 1 - 8/9 (ka_0)^2$ .

The electric dipole approximation is therefore very well justified for plane-wave-interactions in the visible spectrum.

## 4.2 Semiclassical Multipole Coupling

Higher order transition rates are generally much lower than electric dipolar ones if a QS is excited by a plane wave. But in plasmonics, the situation may change dramatically, and the self-imposed restriction to a plane-wave excitation can be lifted. Before we show this explicitly, we need to expand the local field at the position  $\mathbf{r}_0$  of the QS. A spherical multipole expansion is a standard way to achieve this expansion in classical electrodynamics. Noteworthy, spherical and cartesian moments are often used to characterize molecular moments [250].

In a coordinate system with origin  $\mathbf{r}_0$ , the electromagnetic fields can be expanded as [78]

$$\mathbf{E}(\mathbf{r}, \omega) = \sum_{m,n} [p_{mn}(\omega; \mathbf{r}_0) \mathbf{N}_{mn}(\mathbf{r} - \mathbf{r}_0, \omega) + q_{mn}(\omega; \mathbf{r}_0) \mathbf{M}_{mn}(\mathbf{r} - \mathbf{r}_0, \omega)] \text{ and} \quad (52)$$

$$\mathbf{B}(\mathbf{r}, \omega) = \frac{\varepsilon(\omega)}{ic} \sum_{m,n} [q_{mn}(\omega; \mathbf{r}_0) \mathbf{N}_{mn}(\mathbf{r} - \mathbf{r}_0, \omega) + p_{mn}(\omega; \mathbf{r}_0) \mathbf{M}_{mn}(\mathbf{r} - \mathbf{r}_0, \omega)] . \quad (53)$$

The  $\mathbf{N}_{mn}$  and  $\mathbf{M}_{mn}$  are vector spherical harmonics and  $\varepsilon(\omega)$  is the relative permittivity of the surrounding medium (see Refs. [132, 153, 251] for further details). Since the fields are evaluated around the position  $\mathbf{r}_0$  of the QS, the  $\mathbf{N}_{mn}$  and  $\mathbf{M}_{mn}$  are evaluated around the coordinate origin, too. They have to be calculated in terms of the spherical Bessel functions  $j_n(kr)$  which are regular

at  $r = 0$  [154]. This approach is different from the usual far-field expansion in terms of outgoing spherical Hankel functions of the first kind  $h_n^1(kr)$ , which diverge for  $r \rightarrow 0$ .

The  $p_{mn}$  and  $q_{mn}$  denote the complex electric and magnetic multipole coefficients, respectively. In particular,  $n = 1$  refers to dipole contributions,  $n = 2$  to quadrupoles and so on. Please note that pre-factors of the  $p_{mn}$  and  $q_{mn}$  are often variable in the literature. Therefore we shall only discuss relative changes of the local multipole contributions for simplicity. With the help of Eqs. (52) and (53) we have found an expression for the local electric and magnetic fields in terms of their multipole coefficients  $p_{mn}$  and  $q_{mn}$ .

### Electric Multipole Coupling and Transition Rates

In the following, we are only interested in the electric coupling  $V_e(\mathbf{r}, t) = -e\mathbf{E}(\mathbf{r}, t) \cdot \mathbf{r}$ . For our analysis of transition rates, we will assume the validity of Fermi's Golden Rule [Eq. (15)] and a time-harmonic excitation field of the form  $\mathbf{E}(\mathbf{r}, t) = \mathbf{E}(\mathbf{r}) e^{-i\omega t}/2 + c.c.$ . The vector spherical harmonics can be further used to show that the electric coupling  $\propto \mathbf{E} \cdot \mathbf{r}$  depends only on the electric multipole coefficients  $p_{mn}$ , namely

$$\begin{aligned} \mathbf{N}_{mn}(\mathbf{r}) \cdot \mathbf{r} &= \frac{n(n+1)}{k} j_n(kr) P_n^m(\cos\theta) e^{im\varphi} \\ &\approx \frac{\sqrt{\pi}}{2^{n+1} (n+1/2)!} (kr)^n P_n^m(\cos\theta) e^{im\varphi} + \mathcal{O}([kr]^{n+2}) \quad \text{and} \\ \mathbf{M}_{mn}(\mathbf{r}) \cdot \mathbf{r} &= 0. \end{aligned} \quad (54)$$

The treatment of the QS via Schrödinger's equation is a non-relativistic approximation, whereas the electromagnetic field is inherently relativistic. This approximation is justified as long as the QS is small and retardation effects along the QS's wavefunction can be neglected. If this is no longer the case, one would have to use the Dirac equation. In the nonrelativistic case, however, it is possible to understand the coupling of the QS to the electromagnetic field within a quasistatic approximation which is outlined in App. B.3. Such an approach seems well-suited if one studies small NAs that can be fully described in a quasistatic approximation [85]. But as we have already outlined in Sec. 2.2, such NAs generally exhibit a very low efficiency  $\eta$  and might only be suited to study certain effects in theory.

With the help of Fermi's Golden Rule [Eq. (15)], we find that the transition rate caused by a purely electric coupling is given by [78]

$$\Gamma_{ij}^e(\mathbf{r}_0) = \frac{2\pi e^2}{\hbar^2} \left| \sum_{n,m} p_{mn}(\mathbf{r}_0, \omega) \langle i | \mathbf{N}_{mn}(\mathbf{r} - \mathbf{r}_0) \cdot (\mathbf{r} - \mathbf{r}_0) | j \rangle \right|^2 \delta(\omega_{ij} \pm \omega). \quad (55)$$

This result explicitly describes the contribution of all multipole coefficients to  $\Gamma_{ij}^e$ . However, an evaluation of Eq. (55) for a general QS is quite involved, since the amplitudes of the matrix elements,

$$\mathcal{M}_{mn}^{ij} = \langle i | \mathbf{N}_{mn}(\mathbf{r} - \mathbf{r}_0) \cdot (\mathbf{r} - \mathbf{r}_0) | j \rangle, \quad (56)$$

might be comparable for different multipole orders  $n$ . Fortunately, this is not the case for hydrogen-like atoms with (almost) spherically symmetric atomic potential. For other molecules with strong deviations from spherical symmetry, higher-order matrix elements contribute significantly [252]. This is very important since such molecules might be much more suited than hydrogen-like atoms to investigate forbidden transitions.

Re-visiting the results of Sec. 4.1, we state that  $|p_{m1}| \gg |p_{mn>1}|$  holds for a plane wave and the electric dipole approximation is very well justified. It might even hold for QNs for which the dipolar matrix elements are comparable in magnitude to higher order matrix elements, *i.e.*  $|\mathcal{M}_{m1}^{ij}| \sim |\mathcal{M}_{mn \geq 2}^{ij}|$ . Thus, a control of the local higher order multipole coefficients drastically enhances the possibilities to interact with QNs as, in principle, all  $\mathcal{M}_{mn}^{ij}$  might be used in contrast to a plane wave interaction.

Up to now, all considerations were merely theoretical. In the following we shall numerically analyze how specifically designed NAs can be used to enhance quadrupole transitions.

### 4.3 Enhancing Quadrupole Transition Rates

A characteristic length scale for the variation of the electromagnetic field is the wavelength  $\lambda$ . On the other hand, a NA can support localized plasmonic modes that may vary in the order of a few nanometers. This should result in a huge increase of higher order multipole coefficients.

A general discussion of the influence of higher-order effects for a real QN can become quite involved, since Eq. (55) predicts an influence of all multipole coefficients  $p_{mn}$  for electric transitions if the  $\mathcal{M}_{mn}^{ij}$  are not vanishing. Thus, to simplify our analysis, we shall assume that the QN we consider only exhibits electric quadrupolar transitions in the frequency range we are interested in. Then we may just ask to which extent a suitably designed NA is able to enhance the local electric quadrupole coefficients  $p_{m2}$ .

However, before we can proceed with an analysis of numerically calculated transition rate enhancements, we have to clarify the general geometry of the NA and the illumination scheme. We shall also introduce a figure of merit to describe the quadrupole enhancement quantitatively.

#### Geometry of the Nanoantenna and Illumination Scheme

To obtain a strong enhancement of the local quadrupole coefficients  $p_{m2}$ , a strongly varying field is needed. There are different means to achieve this goal. For example an extended feed line can exhibit a large effective index such that its modal wavelength is drastically reduced. However, the quadrupolar enhancement is not large enough, since effective indices are usually below ten without the use of high-index permittivities [253, 254]. For this reason, only a strong field localization in the NA feed gap gives rise to an enhancement of quadrupole coefficients by orders of magnitude: The field gets not only enhanced, but it also varies on very small length scales. A geometrical variation of the NA surface naturally leads to a variation of the fields close to it. For metallic tips it has been demonstrated that a local radius of curvature can be as small as a few nanometers [255]. Enhancements of quadrupole coefficients by several orders of magnitude close to comparable structures may be expected because of their extensive surface variations.

To also obtain a high emission efficiency at a subsequent transition, a dimer NA is preferable. A conceptionally simplified NA with a strongly curved surface could consist of two ellipsoidal particles with a small feed gap. Such a NA design results in a strong enhancement of quadrupole components due to a very high field confinement inside of the gap [80, 89]. But it is possible to further simplify the geometry and to study NAs made of two silver spheres [Fig. 11 (a)]. These NAs are potentially accessible via chemical self-assembly [132, 256].

The spherical NA elements shall have a radius of 30 nm. In this way, the NA's radius of curvature is still well below the illumination wavelength, but the NA is also large enough to circumvent a low efficiency for subsequent luminescence processes (Sec. 2.2). Furthermore, the feed gap width  $d$  shall be small enough to permit a strong field enhancement inside of it, but large enough to prevent tunneling and nonlocal effects [69, 71, 257]. We have chosen  $d = 3$  nm and  $d = 10$  nm for which the onset of these effects should be still a minor contribution.

Because of the rotational symmetry of the NA, two main illumination schemes exist: the electric field of a plane wave either parallel or normal to the rotational axis. Only for parallel illumination the largest field concentrations and thus also the largest field variations can be found inside the gap. Noteworthy, this is not the configuration with the largest far-field quadrupole response of the NA itself. To achieve this, a much bigger distance between the spheres is needed such that the induced dipoles oscillate with a  $\pi$  phaseshift. It is thus very important to once again emphasize the difference between a local expansion [spherical Bessel functions  $j_n(kr)$ ] and a scattering expansion [outgoing spherical Hankel functions of the first kind,  $h_n^1(kr)$ ] of the electromagnetic fields.

### Quantification of Quadrupole Enhancement

The local multipole coefficients are numerically determined in a spherical coordinate system. Nevertheless, the more familiar Cartesian coordinate system with electric dipole coefficients  $p_i$  and quadrupole coefficients  $Q_{ij}$ ,  $i \in \{x, y, z\}$  will be used to express the results. The  $p_i$  and  $Q_{ij}$  are given as linear combinations of the  $p_{m1}$  and  $p_{2m}$ , respectively [132,251]. To quantify the quadrupole enhancement, we compare local quadrupole components to the strongest quadrupole coefficient of the electric field of the illuminating plane wave. This is the  $xz$ -coefficient  $Q_{xz}^{\text{fs}} \propto i(p_{2-1} - p_{21})$ . We define

$$\alpha_{ij}^{\text{loc}}(\mathbf{r}, \lambda) = \left| \frac{Q_{ij}^{\text{na}}(\mathbf{r}, \lambda)}{Q_{xz}^{\text{fs}}(\lambda)} \right|^2$$

as the local quadratic enhancement of the  $ij^{\text{th}}$  quadrupole coefficient of the NA. The illumination scenario in the vicinity of a NA is denoted with the superscript “na”, without NA with the superscript “fs”, respectively. We use the quadratic enhancements because the absorption rates described by Fermi’s Golden Rule are related to the intensity of the electromagnetic field’s multipole coefficients [cf. Eq. (15)].

It may be assumed that an ensemble of Qs is present inside the feed gap or a very precise placement of a quantum system is not possible. Therefore it is preferable to define a measure of the quadrupole enhancement with respect to a certain region  $\Omega$  as

$$\alpha_{ij}(\lambda) = \int_{\Omega} \alpha_{ij}^{\text{loc}}(\mathbf{r}, \lambda) dV .$$

The quadrupole enhancement for a specific NA shall be quantified by  $\alpha_{ij}$  in relation to an integration domain  $\Omega$ . The electric field inside the feed gap is almost rotationally symmetric around the  $x$ -axis since the NA dimensions are well below optical wavelengths. It is thus sufficient to take the integration domain  $\Omega$  as a two-dimensional surface in the  $x$ - $z$ -plane to get a measure for the corresponding three-dimensional quadrupole enhancement. We chose  $\Omega$  as a fixed square with dimensions  $\Delta x = 13$  nm and  $\Delta z = 30$  nm, irrespective of the NA feed gap width  $d$  [Fig. 11 (c)]. Because of the fixed integration domain,  $\Omega$  has a large overlap with the metallic dimers for  $d = 3$  nm, where  $\alpha_{ij} = 0$ . Nevertheless, much bigger  $\alpha_{ij}$  is expected for  $d = 3$  nm since the field localization is dramatically increased compared to  $d = 10$  nm.

### Numerical Results

The numerical calculations of the local multipole coefficients are performed with Mühlig’s implementation of Xu’s approach to analyze the scattering of multiple spherical objects [132,153]. For the investigated scenario, the  $Q_{xz}$  coefficient is the dominant contribution in the NA gap and our following analysis can rely on  $\alpha_{xz}$  and its local counterpart.

Figure 11 (b) shows  $\alpha_{xz}$  for the two gap sizes. For  $d = 10$  nm  $\alpha_{xz}$  is indeed more than an

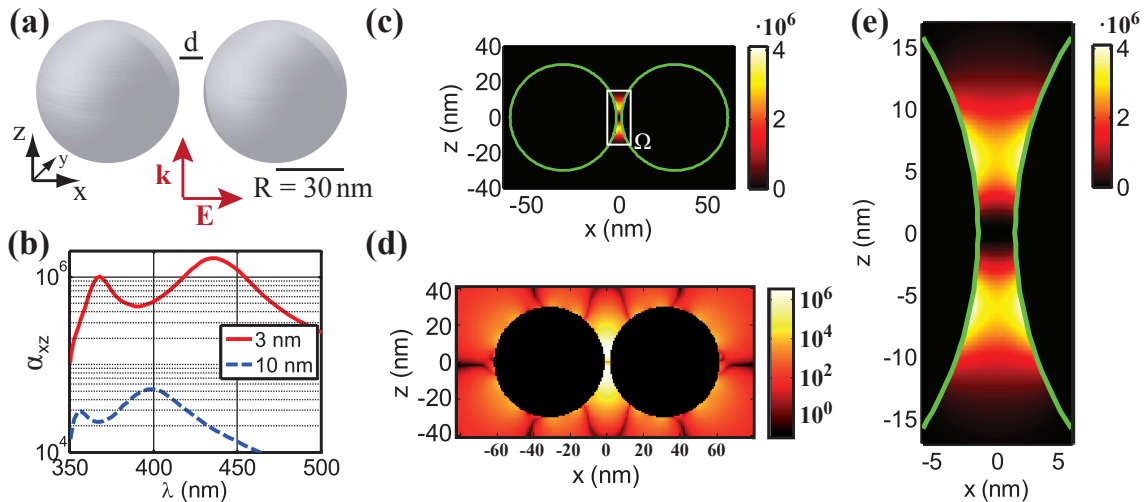


Figure 11: (a) The silver dimer configuration and the illumination scheme. In the employed coordinate system, the  $x$ -axis is the rotational axis. The incoming plane wave is polarized parallel to the rotational axis and propagates perpendicular to it along the  $z$ -axis. (b) Integrated quadrupole enhancement  $\alpha_{xz}(\lambda)$  for  $d = 3$  nm (red line) and  $d = 10$  nm (blue dashed line). (c)-(e) Local quadrupole enhancement  $\alpha_{xz}^{\text{loc}}(\mathbf{r}, \lambda)$  for  $d = 3$  nm at  $\lambda = 437$  nm for different scalings and zooms. (c) Linear scaling, (d) logarithmic scaling, (e) closeup of (c) for the integration domain  $\Omega$ .

order of magnitude smaller than for  $d = 3$  nm. Furthermore, the smaller separation leads to a general redshift of  $\alpha_{xz}$ . Two distinct peaks in both curves can be observed. These resonances can be explained by a dipole-dipole coupling of the silver spheres at larger wavelengths and a quadrupole-quadrupole coupling at smaller wavelengths, respectively. For  $d = 3$  nm, a distinct maximum at  $\lambda \approx 437$  nm of  $\alpha_{xz}(\lambda) > 10^6$  can be observed. This result is very encouraging. It is roughly in the order of magnitude of the usual difference between electric quadrupole and electric dipole transitions rates of hydrogen-like atoms subject to a plane wave.

The local distribution of quadrupole enhancement,  $\alpha_{ij}^{\text{loc}}$  at  $\lambda = 437$  nm, are outlined in Figs. 11 (c) - (e). In Fig. 11 (c) and (d),  $\alpha_{ij}^{\text{loc}}(\mathbf{r}, 437 \text{ nm})$  is displayed using a linear and a logarithmic scale. It is obvious that the strongest  $\alpha_{ij}^{\text{loc}}$  are located in the feed-gap creating two (almost) symmetric stripes with a width of approximately 5 nm each [see Fig. 11 (c) and (e)]. Because of symmetry reasons,  $\alpha_{ij}^{\text{loc}}$  is very small close to the rotational axis: the electric field is strongest here and gets weaker outwards. A saddle point of the electric field with vanishing quadrupole coefficients is formed on the rotational axis. Moreover,  $\alpha_{ij}$  indicates quadrupole enhancements by a few orders of magnitude also outside of the feed gap [Fig. 11 (d)]. This enhancement might be already sufficient to observe dipole-forbidden transitions.

#### 4.4 Quadrupole-Driven Dynamics of a Three-Level System

We have demonstrated that NAs can be used to enhance the quadrupole field components by orders of magnitude. But to exploit this interaction for interesting studies or new applications, it is extremely important to know what kind of benefits one could get using this enhancement. To discuss the limitations of these benefits, we shall analyze the simplest QS excited by a quadrupole absorption. So the first arising question is: Does a two-level-system exist that exhibits a quadrupolar transition but no competing dipole transition? If this would be the case, the analysis would significantly simplify. But unfortunately the answer is “no”, as we can see from a simple calculation.

As outlined in App. B.3.1, the matrix elements  $\mathcal{M}_{mn}^{ij}$  may be approximated in a quasistatic

manner. Then the quadrupole matrix elements  $\mathcal{M}_{m_2}^{ij}$  are related to their Cartesian counterparts  $\mathcal{M}_{x_k x_l}^{ij} \propto \langle i | \mathcal{Q}_{x_k x_l} | j \rangle$ , with  $\mathcal{Q}_{kl} = 3x_k x_l - r^2 \delta_{kl}$ . Thus, to analyze the  $\mathcal{M}_{x_k x_l}^{ij}$ , it is sufficient to analyze matrix elements of the form  $\langle 0 | x_k x_l | 1 \rangle$ . However, using the identity operator  $\mathbf{1} = |0\rangle \langle 0| + |1\rangle \langle 1|$  of the two-level system yields

$$\langle 0 | x_k x_l | 1 \rangle = \langle 0 | x_k [|0\rangle \langle 0| + |1\rangle \langle 1|] x_l | 1 \rangle = \langle 0 | x_k | 0 \rangle \langle 0 | x_l | 1 \rangle + \langle 0 | x_k | 1 \rangle \langle 1 | x_l | 1 \rangle .$$

Obviously,  $\langle 0 | x_k x_l | 1 \rangle$  is only different from zero if at least one of the dipole transitions  $\langle 0 | x_{k/l} | 1 \rangle$  is nonvanishing as well. So, an isolated quadrupole transition cannot occur in a two-level system. Hence, to analyze the dynamics of a process that is only driven by a quadrupole transition, we need to consider at least a three-level system. For such a system, the same matrix element is given by

$$\begin{aligned} \langle 0 | x_k x_l | 2 \rangle &= \langle 0 | x_k [|0\rangle \langle 0| + |1\rangle \langle 1| + |2\rangle \langle 2|] x_l | 2 \rangle \\ &= \langle 0 | x_k | 0 \rangle \langle 0 | x_l | 2 \rangle + \langle 0 | x_k | 1 \rangle \langle 1 | x_l | 2 \rangle + \langle 0 | x_k | 2 \rangle \langle 2 | x_l | 2 \rangle . \end{aligned}$$

We can assume that the dipole matrix elements  $\langle 0 | x_{k/l} | 2 \rangle$  vanish, such that  $\langle 0 | x_k x_l | 2 \rangle = \langle 0 | x_k | 1 \rangle \langle 1 | x_l | 2 \rangle$ . Then, by energy conservation, the dipole transitions  $\langle i | x_{k/l} | i+1 \rangle$  are well separated from the quadrupolar transition and all transitions may be treated independently.

The system we shall analyze is a three-level system driven by a quadrupole absorption followed by two consecutive dipole transitions [see Fig. 12 (a)].

#### 4.4.1 Rate Equation Description

To analyze the dynamics of the three-level system, we shall restrict ourselves to a rate equation approximation. In this approximation any information about coherences is lost and it is further only valid for slowly varying amplitudes of the illuminating field [198]. On the other hand, it is possible to describe the steady-state of the three-level system in a very concise form, which seems impossible for a fully quantum treatment. In this sense, we deal with the classical description of the electromagnetic field and an approximate description of the QS. In this semiclassical picture, the three-level system is governed by the equations

$$\begin{aligned} \dot{n}_0 &= \gamma_{10} \cdot n_1 - \Gamma_{02} \cdot n_0 , \\ \dot{n}_1 &= \gamma_{21} \cdot n_2 - \gamma_{10} \cdot n_1 , \text{ and} \\ \dot{n}_2 &= \Gamma_{02} \cdot n_0 - \gamma_{21} \cdot n_2 , \end{aligned} \tag{57}$$

where  $n_i$  is the occupation probability of the  $i^{\text{th}}$  level. Here, the  $\gamma_{ij}$  denote the spontaneous emission rates from the  $i^{\text{th}}$  to the  $j^{\text{th}}$  level and  $\Gamma_{02}$  denotes the excitation rate of the quadrupole transition [see again Fig. 12 (a)]. Please note that stimulated emission processes are neglected. Furthermore, Eq. (57) solely describes irreversible dynamics. It is thus valid only in the weak coupling regime. This approximation is reasonable, because the NAs under consideration are rather large such that the strong coupling limit is unlikely to be reached (*cf.* Sec. 6).

It is worthwhile to compare the emission properties of the QS with NA compared to the QS in free space. If we regard the three-level system as input-output system, the luminescence rate from  $|1\rangle \rightarrow |0\rangle$ , *i.e.*

$$\dot{n}_1^{\text{rad}} = \gamma_{10}^{\text{rad}} \cdot n_1 , \tag{58}$$

is an important quantity. The dipole transition  $|2\rangle \rightarrow |1\rangle$  is assumed to be nonradiative at rather

low energies. In that case,  $\dot{n}_1^{\text{rad}}$  may act as a benchmark of the driving process and may be used in NA enhanced spectroscopic schemes or as a light source with special characteristics [89].

In Eq. (58), the emission rate  $\gamma_{10}^{\text{rad}}$  refers to the radiative part of the relaxation rate  $\gamma_{10} = \gamma_{10}^{\text{rad}} + \gamma_{10}^{\text{nonrad}}$ . The nonradiative relaxation may be caused by different physical processes of the NA or the QS. For simplicity, we assume that the internal quantum efficiency of the luminescence is unity, *i.e.*  $\gamma_{10}^{\text{rad,fs}} \equiv \gamma_{10}^{\text{fs}}$ , but a generalization is straight forward (*cf.* App. A.4). Hence, the nonradiative part  $\gamma_{10}^{\text{nonrad}}$  is only caused by dissipation of the NA (Sec. 2.2). These losses are again characterized by the efficiency of the NA,  $\eta = \gamma_{10}^{\text{rad}}/\gamma_{10}$ .

The luminescence enhancement  $\dot{n}_1^{\text{rad,na}}/\dot{n}_1^{\text{rad,fs}}$  is a suitable figure of merit to compare the luminescence of the QS in the NA scenario to that in free space. Using this quantity, we shall analyze Eq. (57) in the steady state to encounter three different dynamical regimes of the QS. Before doing so, the transition wavelengths and transition rates in free space shall be specified.

### Transition Wavelengths and Rates

The quadrupole transition is assumed to take place at a wavelength of  $\lambda_{02} = 437$  nm, for which we achieve the maximum quadrupole enhancement of the investigated silver dimer NA. We assume that after the quadrupole absorption a successive quadrupole emission [175] is not likely. This implicitly assumes that the subsequent relaxation into the intermediate level  $|1\rangle$  at  $\lambda_{21} = 3.47$   $\mu\text{m}$  with rate  $\gamma_{21}$  is much faster than a quadrupole relaxation. The second dipole transition takes place at  $\lambda_{10} = 500$  nm because of energy conservation. The rate  $\gamma_{21}$  shall be caused by an internal relaxation process of the QS and is thus independent of the electrodynamic environment, contrary to  $\gamma_{10}$ .

The difference between  $\gamma_{ij}$  and  $\Gamma_{20}$  is that [by virtue of Eq. (55)] the quadrupole absorption rate  $\Gamma_{02}$  depends on the local quadrupole coefficients of the electric field. Thus, Eq. (57) implicitly depends on these components and we have to define ratios between these constants for a certain plane-wave intensity  $I_0$  without NA. At  $I = I_0$ , we take  $\Gamma_{02}^{\text{fs}} = 10^{-5}\gamma_{21}$ , and  $\gamma_{10}^{\text{fs}} = 10^{-2}\gamma_{21}$ , that is  $\Gamma_{02}^{\text{fs}} = 10^{-3}\gamma_{10}^{\text{fs}}$ .

The chosen energies of the three-level system correspond to hydrogen-like atomic systems, for which quadrupolar transitions are possible *e.g.* from an *s* to a *d*-orbital [258]. With an energetically intermediate *p*-orbital, the studied three-level system can be interpreted as a simplified model for hydrogen-like atoms in the notation  $|0\rangle \hat{=} |s\rangle$ ,  $|1\rangle \hat{=} |p\rangle$ , and  $|2\rangle \hat{=} |d\rangle$ . Nevertheless, the actual energy differences depend on the involved levels: potassium has a quadrupolar transition  $\lambda_{4s \rightarrow 3d} \approx 446$  nm with  $\lambda_{4s \rightarrow 4p} \approx 770$  nm and  $\lambda_{4p \rightarrow 3d} \approx 1.18$   $\mu\text{m}$ . The next alkali atom is rubidium with  $\lambda_{5s \rightarrow 4d} \approx 516$  nm,  $\lambda_{5s \rightarrow 5p} \approx 780$  nm and  $\lambda_{5p \rightarrow 4d} \approx 1.4$   $\mu\text{m}$ . For caesium, we find  $\lambda_{6s \rightarrow 5d} \approx 685$  nm,  $\lambda_{6s \rightarrow 6p} \approx 894$  nm and  $\lambda_{6p \rightarrow 5d} \approx 2.9$   $\mu\text{m}$ . However, Lithium and Sodium have quadrupolar transition energies in the near-UV with wavelengths around 300 nm.

Please note that a single photon decay from an *s*-orbital to another *s*-orbital with a lower quantum number is strictly forbidden as photons are bosons with unit spin. Such decays can only be achieved by a real two-photon emission [259], which can be described within second order perturbation theory (*cf.* App. B.1).

#### 4.4.2 Steady-State Solution

Equation (57) implicitly satisfies the conservation of probability  $n_1 + n_2 + n_3 = 1$ , since  $\sum_i \dot{n}_i = 0$  holds. The probability conservation can be used to determine the steady-state luminescence  $\dot{n}_1^{\text{rad}}$  of the QS. Setting  $\dot{n}_i = 0$ , we find

$$\dot{n}_1^{\text{rad}} = \gamma_{10}^{\text{rad}} \cdot n_1 = \gamma_{10}^{\text{rad}} \cdot \frac{\gamma_{21} \Gamma_{02}}{\gamma_{10} \gamma_{21} + \gamma_{21} \Gamma_{02} + \gamma_{10} \Gamma_{02}}, \quad (59)$$

as derived in App. B.4. Then, the luminescence enhancement can be calculated as

$$\frac{\dot{n}_1^{\text{rad,na}}}{\dot{n}_1^{\text{rad,fs}}} = \underbrace{\frac{\gamma_{10}^{\text{rad,na}}}{\gamma_{10}^{\text{rad,fs}}} \cdot \frac{\Gamma_{02}^{\text{na}}}{\Gamma_{02}^{\text{fs}}}}_{\text{Purcell effect and quadrupole enhancement}} \cdot \underbrace{\frac{\gamma_{10}^{\text{fs}} \gamma_{21} + \gamma_{21} \Gamma_{02}^{\text{fs}} + \gamma_{10}^{\text{fs}} \Gamma_{02}^{\text{fs}}}{\gamma_{10}^{\text{na}} \gamma_{21} + \gamma_{21} \Gamma_{02}^{\text{na}} + \gamma_{10}^{\text{na}} \Gamma_{02}^{\text{na}}}}_{\text{dynamics of QS}}. \quad (60)$$

Obviously, the ratio  $\dot{n}_1^{\text{rad,na}}/\dot{n}_1^{\text{rad,fs}}$  is not only influenced by an enhancement of the quadrupole absorption,  $\Gamma_{02}^{\text{na}}/\Gamma_{02}^{\text{fs}}$ . The enhancement of the spontaneous emission rate at  $\lambda_{10}$ ,  $\gamma_{10}^{\text{rad,na}}/\gamma_{10}^{\text{rad,fs}}$ , is important, too. Furthermore a term is essential that can be attributed to how fast the QS is able to transfer the energy through the different levels by its internal dynamics.

### Limiting Cases

For the present NA design, the enhancement of  $\gamma_{10}$  is strong enough such that  $\gamma_{10}^{\text{na}} \gg \gamma_{21}$  holds inside the NA feed gap. Then Eq. (60) can be evaluated with respect to different limiting cases for the intensity  $I$  to find simplified expressions for the luminescence enhancement. This is done in the following and will help to explain the results in Fig. 12 (b) and (c) in detail.

1. **Low Intensities.** For very low intensities,  $\Gamma_{02} \ll \gamma_{ij}$  holds both in free space and in the vicinity of the NA. This case is for example interesting for emission of single photons where the excitation should occur at energies different from the emission frequency as we will see in Sec. 5. In this case, Eq. (60) simplifies to

$$\begin{aligned} \frac{\dot{n}_1^{\text{rad,na}}}{\dot{n}_1^{\text{rad,fs}}} &\approx \frac{\gamma_{10}^{\text{rad,na}}}{\gamma_{10}^{\text{rad,fs}}} \cdot \frac{\Gamma_{02}^{\text{na}}}{\Gamma_{02}^{\text{fs}}} \cdot \frac{\gamma_{10}^{\text{fs}} \gamma_{21}}{\gamma_{10}^{\text{na}} \gamma_{21}} = \eta \cdot \frac{\Gamma_{02}^{\text{na}}}{\Gamma_{02}^{\text{fs}}} \\ &= \text{NA efficiency} \times \text{quadrupole enhancement} \end{aligned} \quad (61)$$

since in free space  $\gamma_{10}^{\text{fs}} = \gamma_{10}^{\text{rad,fs}}$ . Obviously the luminescence enhancement is mainly influenced by the NA efficiency  $\eta = \gamma_{10}^{\text{rad,na}}/\gamma_{10}^{\text{na}}$  and the quadrupole enhancement. The dynamics of the QS do not play a major role as the absorption rate in the low intensity limit is the actual bottleneck of the whole luminescence process.

2. **High Intensities.** For high intensities, it may be assumed that  $\Gamma_{02} \gg \gamma_{ij}$  holds both in free space and in the vicinity of the NA. In that case,

$$\begin{aligned} \frac{\dot{n}_1^{\text{rad,na}}}{\dot{n}_1^{\text{rad,fs}}} &\approx \frac{\gamma_{10}^{\text{rad,na}}}{\gamma_{10}^{\text{rad,fs}}} \cdot \frac{\Gamma_{02}^{\text{na}}}{\Gamma_{02}^{\text{fs}}} \cdot \frac{\gamma_{21} \Gamma_{02}^{\text{fs}}}{\gamma_{10}^{\text{na}} \Gamma_{02}^{\text{na}}} = \eta \cdot \frac{\gamma_{21}}{\gamma_{10}^{\text{rad,fs}}} \\ &= \text{NA efficiency} \times 10^2. \end{aligned} \quad (62)$$

This result is interesting since it does not depend on the actual quadrupole enhancement. The reason is that in the high intensity regime both relaxation processes are the bottlenecks of the luminescence enhancement. In fact, this regime may be regarded as the saturation regime which only profits from an enhancement of  $\gamma_{10}$  by the NA. According to our assumptions,  $\gamma_{10}^{\text{na}} \gg \gamma_{21}$ , whereas without NA  $\gamma_{10}^{\text{fs}} = \gamma_{10}^{\text{rad,fs}} = 10^{-2} \gamma_{21} \ll \gamma_{21}$ , and the spontaneous emission rate is the actual bottleneck.

3. **Intermediate Intensities.** There is a dramatic difference between low and high intensities. The luminescence enhancement is drastically reduced in the latter case. Now let us consider intensities comparable to  $I_0$  for which the ratios of the rates were defined in free space. At  $I \approx I_0$ ,  $\Gamma_{02}^{\text{fs}} = 10^{-5} \gamma_{21} \ll \gamma_{21}$  holds. But because of the huge enhancement of the local



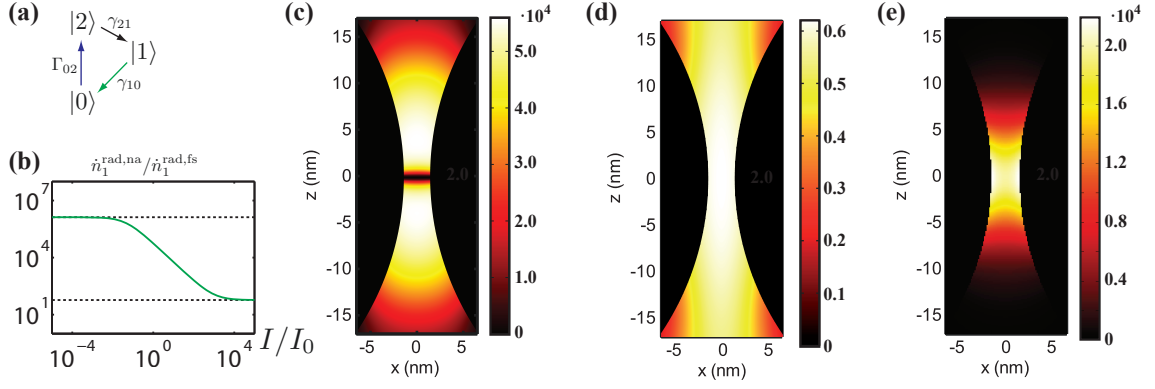


Figure 12: A three-level system driven by a quadrupole absorption for a silver dimer with  $d = 3$  nm separation (see Fig. 11). (a) Schematic of the three-level system. (b) Luminescence enhancement as a function of the intensity at the location  $x = 0$  nm,  $z = 4$  nm. Upper and lower dashed lines are predictions for low [Eq. (61)] and high intensities [Eq. (62)]. (c) Luminescence enhancement in the  $x$ - $z$ -plane at  $I = I_0$ . (d) NA efficiency  $\eta$  for a dipole emitting at  $\lambda_{10} = 500$  nm oriented parallel to the  $x$ -axis. (e) Enhancement of the local dipole components compared to a plane wave excitation without NA at  $\lambda_{02} = 437$  nm.

quadrupole components in the feed gap of the NA [Fig. 11 (b)-(e)],  $\Gamma_{02}^{\text{na}} \gg \gamma_{21}$  may be assumed, as the local quadrupole enhancement is roughly six orders of magnitude there. Thus,

$$\begin{aligned} \frac{\dot{n}_1^{\text{rad,na}}}{\dot{n}_1^{\text{rad,fs}}} &\approx \frac{\gamma_{10}^{\text{rad,na}}}{\gamma_{10}^{\text{rad,fs}}} \cdot \frac{\Gamma_{02}^{\text{na}}}{\Gamma_{02}^{\text{fs}}} \cdot \frac{\gamma_{10}^{\text{fs}} \gamma_{21}}{\gamma_{10}^{\text{na}} \Gamma_{02}^{\text{na}}} = \eta \cdot \frac{\gamma_{21}}{\Gamma_{02}^{\text{fs}}} \\ &= \text{NA efficiency} \times 10^5. \end{aligned} \quad (63)$$

The difference to the high intensity case is due to different limits with and without NA. With NA, the absorption rate is still the fastest rate in the whole process, whereas in the case of the isolated QS this rate is still the bottleneck.

Three limiting cases for different intensities have been investigated. The external driving field strength influences the overall luminescence enhancement considerably. The importance of an enhanced quadrupole absorption for a strong luminescence is mostly pronounced in the weak excitation limit, whereas for higher excitation rates other processes become a bottleneck.

### Numerical Results: Luminescence Enhancement

With the discussed limiting cases, it is able to interpret the results shown in Fig. 12 (b) and (c). Figure 12 (b) displays the intensity-dependent luminescence enhancement of the three-level system located at  $\{x, y, z\} = \{0, 0, 4\}$  nm, *i.e.* a position with very high enhancement of quadrupole absorption. The dashed lines correspond to high and low intensity limits as given by Eqs. (61) and (62). These lines indicate a perfect agreement with the numerically calculated values. Most notably, the luminescence enhancement changes by more than three orders of magnitude. These findings underline the necessity to investigate the internal dynamics of the three-level system.

Figure 12 (c) depicts the luminescence enhancement in the  $x$ - $z$  plane at the excitation intensity  $I = I_0$ . In this case the intermediate intensity result should be applicable in the regions of strong quadrupole enhancement. Using the calculated NA efficiency  $\eta \approx 0.6$  inside the feed gap at  $\lambda_{10}$  [Fig. 12 (d)], we find a perfect agreement to Eq. (63) in the regions of high quadrupole enhancement: The quadrupole enhancement is saturated at  $\approx 0.6 \times 10^5$ . Further away from the center the

enhancement of the local quadrupole absorption is not strong enough to realize  $\Gamma_{02}^{\text{na}} \gg \gamma_{21}$  and a transition to the low-intensity limit [Eq. (61)] can be observed. Hence, the quadrupole absorption rate is not the limiting process inside the regions of strong quadrupole enhancement, which leads to a luminescence saturation. Further away from the axis of symmetry, the quadrupole enhancement becomes the limiting process but is still sufficiently strong to enable a luminescence enhancement by more than four orders of magnitude for almost the whole integration region  $\Omega$  except the NA elements themselves.

The estimations provided by Eqs. (61), (62) and (63) yield a sufficient understanding of the dynamical process that leads to the luminescence enhancement of the three-level system driven by a quadrupole absorption within the employed rate equation model. Although a rather stringent approximations to calculate simplified results was used, a fairly complex luminescence behavior could be described.

Noteworthy, our results relied on the assumption that only a quadrupole transition contributes to the absorption. However, as it is shown in Fig. 12 (e), the local dipole absorption rate of the electric field is enhanced at  $\lambda_{20}$  by four orders of magnitude inside of the feed gap, too. This dipole enhancement has to be considered if dipolar transitions are competing with the investigated quadrupolar ones.

## Concluding Remarks

In Sec. 4.1 it was shown that forbidden transitions are strongly suppressed for a plane wave excitation in the optical spectrum. Afterwards, a theoretical framework was developed in Sec. 4.2 to describe the action of the electromagnetic field on a QS in terms of the field's local multipole coefficients. Based on this framework it was theoretically verified (Sec. 4.3) that NAs are very well suited to enhance higher order multipole fields. As also noted by other authors [76,77], NAs render forbidden transitions accessible.

In Sec. 4.4 it was demonstrated that a comprehensive understanding of the internal dynamics driven by a dipole-forbidden transition is necessary to understand experimentally accessible parameters such as the luminescence enhancement. This result is not only interesting and important in the context of forbidden transitions but also for any kind of experimental realization of a quantum process where internal energy conversions are involved. These findings underline that multilevel systems usually exhibit much richer dynamics than two-level systems to which they are often reduced to [260].

For simplicity, the analysis was restricted to a dimer NA with spherical elements. Nonetheless, such a NA with a feed gap of 3 nm was sufficient to achieve local quadrupole enhancements of more than six orders of magnitude. It is clear that this is not the best design for the highest quadrupole coefficients, as they are related to the local radius of curvature of a NA's surface. Dimer NAs made of recently fabricated sharp metallic nanotips [261,262] might be used to increase the feed gap while maintaining the quadrupole enhancement in a given spatial region. In this case, quadrupole-driven interactions in the visible might be easier accessible than with the investigated NA design. For instance, a placement of a single QS and also a coupling to an ensemble of Qs might be simplified.

Applications using forbidden transitions in the visible spectrum have not been realized yet. Nevertheless, the importance of magnetic dipole contributions for different light sources has been demonstrated [73, 75, 263, 264]. It has also been shown that NAs can be used to transform the dipole radiation of a QS into almost arbitrary multipole radiation [265]. This transformation can be seen as the inverse process to a NA converting free-space radiation to higher-order multipole components in the near-field. Accessing forbidden transitions in a deterministic manner with the help of NAs will open new prospects, as these new interaction channels may be used in many ways.

One could for example retrieve much more detailed information about spectroscopic samples, and quantum communication devices may hugely benefit in the future: The locally addressable Hilbert space is drastically increased, and new pathways open for the generation of nonclassical light. All these applications may be realized when fabrication techniques can be used to produce suitably designed NAs and position Qs with a high precision.

The treatment of forbidden transitions that was employed in this section has been performed using a classical description of the electromagnetic field. Their quantization was not required to understand the enhanced quadrupole interaction and the internal dynamics of the three-level system. In the following section this approximation shall be dropped. We will use a quantization of the NA's electromagnetic field to understand its utilization for the generation of nonclassical light.

## 5 Ultra-Bright Single-Photon Sources

In the near future fabrication techniques might be available to enable sophisticated NA applications that make use of enhanced couplings to QS. For a thorough theoretical understanding of the involved light-matter-interaction it is essential to go beyond a semiclassical analysis: A great deal of the interesting physics relies on the very quantum nature of the interaction. This step can be achieved by the quantization of NAs in terms of their QNMs. In this section we detail how such a fully quantum description can be used to calculate observables inaccessible by semiclassical considerations. This approach is needed to understand the generation of so-called nonclassical light, *i.e.* light that cannot be described by classical electrodynamics.

We shall specifically focus on the generation of single photons as an example for nonclassical light. Single photons are easier to realize with the investigated hybrid systems compared to other nonclassical light states<sup>2</sup>. The reason is that, in general, atomic Qs are already single-photon sources and an interaction with the environment mainly alters the rate, efficiency and directivity of the emission process [266]. The initial verification of single photons was achieved by Hanbury Brown and Twiss in the context of stellar metrology in 1956 [267]. The first single photon source in an experiment was realized by Clauser. He used the cascaded emission of two photons at different frequencies of calcium atoms in 1974 [268]. Soon afterwards, Kimble *et al.* investigated a continuous excitation of sodium atoms and studied the statistics of the emitted light in the context of resonance fluorescence [269].

Nowadays, state-of-the-art technology permits the fabrication of single photon sources using the spontaneous emission of molecules [270, 271], defect centers in solids [272, 273], and QDs [274–277]. Because of these achievements, applications of single photon sources are no longer out of reach [266]. Among them are, for example, single photon quantum cryptography [278], which was first realized by Waks *et al.* [279] using the so-called BB84 protocol [280, 281], and single photon spectroscopy of single molecules [282]. Hence, single photon sources enable secure quantum communication and offer completely new possibilities for the study of Qs.

Single photon processes are often comparably robust against losses, as a dissipated photon usually has no negative impact on subsequent processes. For instance, even the BB84 protocol works for implementations using Qs with intrinsic losses and lossy communication waveguides [283]. This is important because any NA based implementation will cause additional loss channels.

But one problem remains up to date: Single photon sources rely on the spontaneous emission of a photon. However, the emission rates of emitters oscillating at optical or telecom frequencies are usually rather low in the sub-GHz regime [86, 176]. Two main approaches exist to circumvent this problem: Cascaded photon emission to achieve more photon output per pump cycle [284] and an enhancement of the spontaneous emission rate [44]. While the first approach is based on a suitable design of the QS, the second one relies on a thoughtful design of the electrodynamic environment of the QS, a “radiative engineering” approach. As we have already seen in Fig. 3, NAs can drastically change the spectral density and cause a tremendously enhanced spontaneous emission rate. We will focus on the “radiative engineering” approach in our investigations following a number of theoretical [12, 56, 82, 97, 285, 286] and experimental investigations [141, 287–290].

The radiative engineering approach is very promising but the emission rate drops considerably in the strong coupling regime (see again Fig. 9, where the excited state population drops much slower than in the weak coupling regime due to an ongoing energy exchange between QS and NA). This puts a general limit on the maximal achievable Purcell factors. Another limitation for the single photon emission rate has been overlooked so far: The question, how the nonclassical

---

<sup>2</sup>Exemplarily, the generation of squeezed light and entangled photons is shortly discuss in App. B.10.1 and B.10.2.

character of the emitted light is influenced by the increased emission. A seminal paper by Akimov *et al.* [287] has proven that the emitted light of an incoherently pumped QS coupled to a wire NA is nonclassical. But it was not clear what happens if the emission rate is drastically altered by the mutual interaction of the hybrid system. To bridge this gap will be one of the main goals in this section which is organized as follows.

The choice of a two-level system approximation and the incoherent pumping scheme shall be discussed first. We then introduce an analytical result for the emission rate of the hybrid system consisting of QS and NA. In Sec. 5.3, the design of NAs to achieve ultrabright single photon emission shall be investigated based on numerical calculations. We will also determine the parameters needed to quantize the hybrid system. The quantization based on the introduced QNM quantization scheme (*cf.* Sec. 3.4) will then be used to study the fully quantum interaction of QS and NA (Sec. 5.4). It will also be shortly discuss why the second-order correlation function  $g^2(\tau)$  is a suitable figure of merit for the nonclassicality of the emitted light. This section is based on Ref. [89].

## 5.1 Investigated Quantum System, Pumping Scheme, and Two-Level Approximation

To keep the theoretical description as simple as possible, the QS shall exhibit as few as possible energy levels. Moreover, the geometry of the NA shall be given in terms of a few parameters. It is important to understand the physical consequences of these approximations.

### The Need for a Third Energy Level

Let us thus first discuss the theoretical description of the pertinent QS. The simplest possible model for a QS is a two-level system. Since a two-level-system can only store the energy of a single photon, it can only emit single photons. A pump of the two-level-system with a so-called  $\pi$ -pulse transfers a two-level system into its excited state [291]. The subsequent emission will then be a single photon. This direct excitation scheme, however, has severe drawbacks.

First of all, one assumes that a  $\pi$ -pulse excitation source is present. But this seems at least questionable if actual applications are envisioned. Here, the excitation of the QS shall be implemented in a very simplistic (and reasonably priced) way. Such an excitation implementation might be accomplished by electrically pumping QDs that leads to electroluminescence. This effect has been reported a long time ago [292] and was also used for single-photon emission [277]. Moreover, in the  $\pi$ -pulse pumping scheme the number of emitted photons is limited by the repetition rate of the exciting source. For laser systems, repetition rates are typically in the MHz to GHz regime, except in sophisticated ultrafast optics experiments [293].

Second, a two-level system is pumped at its emission frequency. Thus, a NA designed to enhance the emission rate of a QS will generally also interact with the pumping field. This direct excitation will also excite at least one NA mode into a certain state. The emission of the combined system will then have characteristics of the single-photon emission by the two-level system and an emission by the NA, which we may assume as coherent.

Ultimately, the emitted radiation loses its single-photon characteristics. This argument generally excludes the use of a continuous wave excitation at the emission frequency of the QS in the presence of a NA. Thus, not only from a practical but also from a fundamental point of view a direct excitation of the QS seems to be inadequate: The presence of the NA is useful for the emission of single photons at high rates but also leads to classical light emission if pumping and emission frequencies coincide.

After having ruled out the use of a simple two-level system model because of the need for a direct pump, a model system has to be chosen that is slightly more involved: a three-level system indirectly pumped at a certain frequency and emitting at another one. Such a system is conceptually similar to that discussed in Sec. 4.4. There it turned out that its behavior may strongly vary depending on the different transition rates involved (Sec. 4.4.2). Although a rate equation approach was exploited, we may rely on the main results to find a very simple effective description of the three-level system.

## Two-Level Approximation

In the rate equation model employed in Sec. 4.4, we found the steady-state occupation probability of the intermediate state as [Eq. (59)]

$$n_1 = \frac{\gamma_{21} \Gamma_{02}}{\gamma_{10} \gamma_{21} + \gamma_{21} \Gamma_{02} + \gamma_{10} \Gamma_{02}} .$$

If we assume that the nonradiative relaxation rate  $\gamma_{21}$  is much higher than any other process, it follows that

$$\lim_{\gamma_{21} \rightarrow \infty} \dot{n}_1^{\text{rad}} = \gamma_{10}^{\text{rad}} \cdot \lim_{\gamma_{21} \rightarrow \infty} n_1 = \eta \gamma_{10} \cdot \frac{\Gamma_{20}}{\gamma_{10} + \Gamma_{20}} . \quad (64)$$

This solution is simply the steady-state solution of a two-level system with excitation rate  $\Gamma_{20}$  and decay rate  $\gamma_{10}$ . Thus, in a first approximation we may regard the three-level system as a two-level system with effective pumping rate  $R = \Gamma_{20}$ .

As stated before, a thorough analysis of a three-level system dynamics can be found in Ref. [260]. It is important to keep in mind that the limit of an effective two-level system is only meaningful if the nonradiative relaxation rate  $\gamma_{21}$  is much larger than any other transition rate. In realistic QDs, such relaxation times can be ultrafast. In QDs, intraband relaxation times in the sub-ps regime can be assumed [294–296]. Thus it seems reasonable to analyze the single-photon emission of a three-level system in a two-level approximation up to several THz.

## 5.2 Emission Rate Determination

By virtue of Eq. (64), a first estimation of the emitted photon rate has been obtained based on the rate equation approximation. Although this result is useful already, we have to go a step further because any information on its single photon character is missing. To get this information, a NA quantization is inevitable. Using the QNM quantization scheme (Sec. 3.4), the interaction of the three-level system with a NA will be described in the two-level approximation. This permits the validity check of Eq. (64) and the calculation of  $\gamma_{10}$  in terms of parameters of the quantization scheme.

### Mathematical Description

Within the two-level model, the interaction of a QS to a single-mode NA can be described by the Hamiltonian

$$H = \hbar \omega_{\text{na}} \left( a^\dagger a + \frac{1}{2} \right) + \hbar \omega_{\text{qs}} \sigma_+ \sigma_- + \hbar \kappa (a^\dagger + a) (\sigma_+ + \sigma_-) . \quad (65)$$

Again,  $a$  ( $a^\dagger$ ) are the annihilation (creation) operators of the NA state and  $\sigma_-$  ( $\sigma_+$ ) the QS's annihilation (creation) operators,  $\omega_{\text{na}}$  is the eigenfrequency of the NA,  $\omega_{\text{qs}}$  that of the QS, and  $\kappa$  is the coupling strength in the dipole approximation. For simplicity and to compare different hybrid

systems, we shall assume that NA and QS are always on resonance, that is, we assume  $\omega_{\text{na}} = \omega_{\text{qs}}$  from now on.

Equation (65) does not provide any explicit information about the state of the radiated light field we are interested in. To get it, the use of a beam splitter transformation (BST) [297] is required. The BST transforms an excitation of the NA into an excitation of the radiation field with a probability equal to the NA efficiency  $\eta$ . However, the BST also involves a treatment of further dissipative channels which increases the Hilbert space and complicates a detailed analysis.

Fortunately it suffices to calculate all quantities in the hybrid system picture and to determine all observables simply replacing  $a \rightarrow \sqrt{\eta}a$ . For instance, the photon number expectation value of the free field is calculated by the replacement  $\langle a^\dagger a \rangle \rightarrow \eta \langle a^\dagger a \rangle$ . This yields the mean emitted photon rate  $\eta \langle a^\dagger a \rangle \Gamma$  by the NA, in agreement with the considerations of the luminescence rate in Sec. 4.4 [Eq. (58)]. Nevertheless, the state of the radiation field and the NA state are not exactly equivalent.

### Emission Rate of the Nanoantenna: Introducing Pump and Decay Rates

Two main ways that account for irreversible processes exist to solve the equations of motion incorporating a pump rate  $R$  of the QS and a decay rate  $\Gamma$  of the NA. In the Heisenberg picture, these parameters can be introduced phenomenologically. The equations of motion can be solved directly to find the mean emitted photon rate  $\langle \dot{n}_1^{\text{rad}} \rangle = \eta \langle a^\dagger a \rangle \Gamma$  within the cold reservoir limit (CRL). Here, a so-called adiabatic elimination of the QS operators in the RWA is performed (see App. B.8 for the complete derivation and our Ref. [89] for further details). In this limit, any reaction of the environment after dissipation by the hybrid system is neglected.

Technically, expectation values of fluctuation operators  $f_i$  are neglected. The  $f_i$  are introduced in the Heisenberg equations of motion to preserve the canonical commutation relations both of the operators describing NA and QS. For a weak interaction with the environment, *i.e.* for weak pumping and loss rates, the expectation values of the  $f_i$  are negligible compared to the operators of the NA and QS. The CRL is a good approximation in this regime [86, 195].

However, higher moments of the fluctuation operators are unknown. Consequently, higher moments of the emitted light cannot be calculated accurately within the CRL. The emitted photon rate is given by

$$\langle \dot{n}_1^{\text{rad}} \rangle = \eta \gamma_{\text{wc}} \cdot \frac{R}{\gamma_{\text{wc}} + R} \quad \text{with} \quad \gamma_{\text{wc}} = \frac{4\kappa^2}{\Gamma}. \quad (66)$$

This result is equivalent to Eq. (64) which was derived in Sec. 5.1 for a very fast nonradiative intermediate relaxation rate in a three-level system. But we have not only verified Eq. (64), we have also found an explicit expression for the spontaneous emission rate  $\gamma_{\text{wc}}$  as a function of the system parameters in the QNM quantization scheme. Similar expressions to Eq. (66) have been derived in the past [298].

Equation (66) provides a fundamental understanding for the design of hybrid systems for ultra-bright single photon emission in terms of just a few parameters: the pumping rate  $R$ , the NA efficiency  $\eta$  and the weak coupling emission rate  $\gamma_{\text{wc}}$  (or  $\kappa$  and  $\Gamma$ , respectively). Naturally,  $\gamma_{\text{wc}}$  is related to the Purcell factor by  $F = \eta \gamma_{\text{wc}} / \gamma_{\text{fs}}$ , where  $\gamma_{\text{fs}}$  is the free-space spontaneous emission rate of the investigated QS. Two interesting limiting cases for  $R$  appear.

### Emission Rate: Limiting Cases

In the weak pumping limit, where  $R \ll \gamma_{\text{wc}}$  shall hold,  $\langle \dot{n}_1^{\text{rad}} \rangle \rightarrow \eta R$ . In this limit, large Purcell factors are irrelevant for the overall process. The pumping rate constitutes the key parameter. We

have used an incoherent pump scheme, but in the weak pumping limit it seems reasonable that  $\langle \dot{n}_1^{\text{rad}} \rangle \rightarrow \eta R$  also holds for other pumping schemes, too: A low energy flux to excite the QS might always be the main parameter of the emission rate that can be achieved by the hybrid system.

On the other hand, if  $R \gg \gamma_{\text{wc}}$ , then  $\langle \dot{n}_1^{\text{rad}} \rangle \rightarrow \eta \gamma_{\text{wc}}$ . Only in this strong pumping limit, strongly enhanced emission rates can be accomplished by an appropriate NA with  $F \gg 1$ . So only for  $R \gg \gamma_{\text{wc}}$  the NA can be exploited to its full capacity. The result for the emission rate in the strong pumping limit can, however, only be considered as a tendency. The CRL may not be applicable and also the pumping rate may exceed the nonradiative rate  $\gamma_{21}$ . Furthermore, a very strong pump may also lead to an excitation of an NA mode with more than one photon. Then the single-photon character is lost (*cf.* Sec. 5.4).

Equation 66 for the determination of the photon emission rate is an important result. It puts studies that solely relied on a realization of high Purcell factors for bright single-photon sources into a more general context where also the pumping rates are taken into account. The simplicity of the formula for the emitted photon rate was achieved at the expense of some more or less crucial approximations with regard to the NA-QS-interaction, the CRL and RWA. But with the use of the introduced NA quantization scheme we have access to the parameters  $\kappa$ ,  $\Gamma$  and  $\eta$ . They are needed to investigate the quantum properties of the hybrid system and of the emitted light in terms of a density matrix formulation, which shall be discussed in the following. First we will concentrate on the design of suitable NAs based on the hybrid system's parameters which appear in Eq. (66). Afterwards we will check the validity of Eq. (66) and evaluate the statistics of the emitted light to further understand the limits of NA based ultra-bright single-photon sources.

### 5.3 Nanoantenna Design and Determination of Parameters

Theoretical studies are generally not bound to the limitations of experimental realizations. For our search of a suitable NA design, we can take advantage of this freedom to keep the design as simple as possible and to concentrate on the main aspects. Our goal is not to find the best NA design for practical ultra-bright single photon sources with all the limitations imposed by technological constraints. We aim to investigate the hybrid system's quantum properties with respect to only a few geometrical parameters that are related to the parameters  $\kappa$ ,  $\Gamma$  and  $\eta$ .

#### Design Simplifications

Based on our experiences with geometries that are needed to achieve strong coupling (Sec. 6), we restrict ourselves to a NA consisting of two identical silver spheroids with fixed aspect ratio of major vs. minor axis of  $a/b = 5/3$  [Fig. 13 (a)]. Furthermore, the ratio of NA feed to the overall dimension plays a crucial role for the field enhancement inside of the feed gap: If any other parameter is left constant, a smaller feed gap results in a higher coupling. So an investigation of the feed gap width  $d$  seems also important.

As we have already fixed the ratio  $a/b$ , there is one free parameter left so far. Since the numerical determinations of the required parameters are quite involved, a second entirely free parameter  $d$  is not feasible. Thus we shall restrict ourselves to a few selected parameter combinations. There are two options, namely a few fixed values for  $d$  or a few fixed ratios of  $a/d$ . We have chosen the latter one, which we hereafter refer to as ‘‘conformal rescaling’’ of the whole NA: When the major axis  $a$  is changed, any dimension of the NA is changed in the same manner. The reason for this approach is that the coupling strength  $\kappa$  is related to mode volume  $V_m$  as  $\kappa \sim 1/\sqrt{V_m}$  (Sec. 3.1). In the conformal rescaling scheme, an increase in  $a$  might thus be directly related to  $\kappa$ . The ratio between major axis of one of the NA elements and its feed gap width,  $a/d$ , shall be called ‘‘conformal ratio’’.



To not artificially enhance the achievable emission rates, a minimum feed gap width of  $d_{\min} = 4$  nm is used, which is in the order of the size of the smallest available QDs [299]. It should be emphasized that our analysis is not restricted to metallic NAs, but can also be applied to dielectric ones [9]. The QNM quantization scheme is likely to be applicable for them as well (see *e.g.* investigations of dielectric microspheres and spheroids [300,301]).

### Hybrid System Specifications

The hybrid system shall be embedded in a medium with relative permittivity  $\varepsilon_d = 2.2$ , comparable to fused silica. We used COMSOL [170] to perform the electromagnetic simulations. All parameters are calculated following the QNM quantization scheme described in Sec. 3.4. For the calculation of the coupling strength  $\kappa$  in the electric dipole approximation [Eq. (47)], a typical dipole moment of  $|\mathbf{d}_{\text{qs}}| = 6 \times 10^{-29}$  Cm is assumed [302]. Such a dipole moment implies free space emission rates  $\gamma_{\text{fs}}$  in the order of one GHz at optical frequencies. The dipole is further oriented parallel to the major axis of the NA and centered inside the feed gap.

As the smallest NAs we investigated have spatial dimensions comparable to the mean free path length of electrons in silver, we use a size-corrected model for the dispersive permittivity of the material [303]. In this way the NA properties include size effects without taking microscopic degrees of freedom into account that are much more involved to realize numerically [65,69]. Since the dipole is oscillating along the major axis of the NA elements, plasmonic oscillations will occur along this axis. Therefore this axis length is taken for the size corrections of the permittivity.

### Numerical Results: Achievable Emission Rates

As we have mentioned already, a large coupling strength  $\kappa$  is needed for a high rate  $\gamma_{\text{wc}}$ . This generally requires a small mode volume  $V_m$  and thus a small NA. But as seen in Fig. 3, a small NA leads to lower efficiencies  $\eta$ . This trade-off between  $\gamma_{\text{wc}}$  and  $\eta$  can again be observed in Fig. 13 (b): Whereas larger NAs provide a higher efficiency, the QS emission rate  $\gamma_{\text{wc}}$  drops considerably. Then, the emission rate in the limit of high pumping rates,  $\eta \cdot \gamma_{\text{wc}}$ , generally exhibits a maximum at a certain overall size of the NA. Regarding Eq. (66), this maximum can be considered as the optimal NA design for a given conformal ratio: For sufficiently strong pumping rates, such a design results in the highest photon emission rates.

The geometrical parameters of an optimal design can be found in Fig. 13 (c). Here,  $\eta \cdot \gamma_{\text{wc}}$  peaks for  $a/d = 5\frac{5}{6}$  at  $2a \approx 61$  nm with a feed gap of  $d_1 \approx 5$  nm. The investigated larger conformal ratios are expected to also exhibit maxima in  $\eta \cdot \gamma_{\text{wc}}$ . Those maxima, however, are not visible in Fig. 13 (c) as they occur below the minimal feed gap width  $d_{\min} = 4$  nm. Generally, an optimal NA design with a feed gap larger than  $d_{\min}$  seems experimentally favorable as parasitic effects such as electron tunneling can be avoided. For this reason we investigate NAs with the lowest conformal ratio  $a/d = 5\frac{5}{6}$  that exhibit a maximum in  $\eta \cdot \gamma_{\text{wc}}$  at  $d_1 > d_{\min}$ , even though these NAs provide a slightly lower emission rate than those with higher  $a/d$ .

So far we discussed the optimal NA design considering the relative behavior of  $\eta$ ,  $\gamma_{\text{wc}}$ , and their product with respect to the NA size. However, it is also very important to discuss the maximal achievable emission rate  $\eta \cdot \gamma_{\text{wc}}$  on its own. The considered NAs with the lowest conformal ratio have generally lower  $\eta \cdot \gamma_{\text{wc}}$ . Nevertheless, their emission rates are still in the order of 1 THz for NAs with  $a \approx 60$  nm (and thus  $d \approx 10$  nm and an overall lateral dimension of  $L = 2a + d \approx 130$  nm) with an efficiency of  $\eta \approx 0.6$  [see again Figs. 13 (b) & (c)]. These results are very promising even if realistic experimental conditions are taken into account. These conditions might reduce the emission rates by one order of magnitude because of an altered fabrication design, lower effective pumping rates, poorer NA material, or certain QS specifics. If such a decrease is included, the

Figure 13: Single photon emission by a hybrid system made of a NA and an incoherently pumped two-level system. (a) Geometry of the investigated NAs: a dimer made of two silver spheroids with major and minor axis  $a$  and  $b$  and feed gap  $d$ . The inset illustrates the incoherent pumping scheme of the centered QS (red double-arrow). (b) QS emission rate  $\gamma_{\text{wc}}$  following Eq. (66) (circles) and NA efficiency  $\eta$  (full points) for different conformal ratios  $a/d$  vs. major axis  $a$ . (c) Emission rate of the hybrid system in the limit of strong pumping rates,  $\eta \cdot \gamma_{\text{wc}}$ . (d)-(f) Different observables in function of the major axis  $a$  for  $a/d = 5\frac{5}{6}$ . (d) Emitted photon rate depending on pumping rate  $R$  based on density matrix calculations after Eq. (67) (large image) compared to predictions by Eq. (66) (inset). (e) Large image: Density-matrix calculations of  $g^2(0)$  with the full Hamiltonian [Eq. (65)]. Inset: The same, but with applied RWA. (f) Normalized fluorescence spectra at  $R = 1$  THz.

calculated  $\eta \cdot \gamma_{\text{wc}}$  suggest single photon emission rates around 100 GHz. This is still two order of magnitudes faster than emission rates by isolated Qs.

For the investigated NA designs, the ratio of  $\kappa/\Gamma$  was well below unity {Fig. 1 (b) in Ref. [89]}. This indicates that the weak coupling limit is valid and spontaneous emission processes can be simply described by an exponential decay (see again App. B.5 or Fig. 9). Furthermore, the weak coupling regime suggests that the reservoir, in this case the NA and its loss channels, merely act as a passive background system [see again the Purcell factor as defined in the weak coupling regime via the Green's function in Eq. (36)] - a totally classical result [123]. Then it is no surprise that the semiclassical rate equation approach yields the correct emission rates and an application of a complicated quantization scheme seems unnecessary. But we will see in the next section that even in the weak coupling regime effects can occur that cannot be explained using semiclassical arguments.

## 5.4 Density Matrix Calculations: Emission Rate Verification and Single Photon Characterization

To verify Eq. (66) and to calculate the statistical characteristics of the emitted light, it is suitable to use a density matrix representation of the hybrid system (Sec. 3.4). Within this formulation, NA loss and QS pumping rates  $\Gamma$  and  $R$  are introduced into the Lindblad-Kossakowski equations

in the following way:

$$\begin{aligned}
i\hbar\partial_t\rho(t) &= [H, \rho(t)] + i\hbar\mathcal{L}_{\text{decay}}[\rho(t)] + i\hbar\mathcal{L}_{\text{pump}}[\rho(t)] \text{ with} \\
\mathcal{L}_{\text{decay}}[\rho(t)] &= \frac{\Gamma}{2} \{2a\rho(t)a^\dagger - \rho(t)a^\dagger a - a^\dagger a\rho(t)\} \text{ and} \\
\mathcal{L}_{\text{pump}}[\rho(t)] &= \frac{R}{2} \{2\sigma_+\rho(t)\sigma_- - \rho(t)\sigma_-\sigma_+ - \sigma_-\sigma_+\rho(t)\} .
\end{aligned} \tag{67}$$

The Hamiltonian describing the interaction is given by Eq. (65) and the constants  $\Gamma$  and  $\kappa$  are determined as outlined in Sec. 5.3. Note that in our formulation of the QS dynamics other irreversible processes such as the emission of the QS into other modes than the dominating NA QNM as well as other dephasing mechanisms of the QS are neglected. Such processes can be easily added to the system dynamics using corresponding Lindblad operators [298].

Equation (67) describes the evolution of the hybrid system in terms of a density matrix formulation. This formulation can be used to numerically calculate all observables without further approximations. The evolution of the system was computed with the help of a quantum optics toolbox [304] and checked against an in-house code. In the following we shall focus on the steady-state solution of Eq. (67), disregarding well-known transient processes [185].

As we have discussed before, we restrict ourselves to NAs designs with a conformal ratio of  $a/d = 5\frac{5}{6}$ . Only one geometrical parameter is varied - the length of the major axis  $a$ . The calculated photon emission rates depending on the pumping rate are depicted in Fig. 13 (d). The quantum computation results are illustrated based on the density matrix formulation [Eq. (67), large image] and on the analytical predictions [Eq. (66), inset]. There is virtually no difference between both results in the investigated pumping region. This agreement underlines the applicability of our analytical result. Note that the analytically determined emission rate is based on the RWA. However, rapidly oscillating terms  $\hbar\kappa(\sigma_+a^\dagger + \sigma_-a)$  are included in the density matrix calculations. Regarding Fig. 13 (d), these terms do not play any significant role in the emission rate of the hybrid system.

### The Second-Order Correlation $g^2(\tau)$ as a Measure of Nonclassicality

One of our main motivations to employ a fully quantum approach is to verify the nonclassical character of the emitted light. We shall now briefly discuss why the second-order correlation function  $g^2$  is a suitable figure of merit to describe the nonclassicality of single-photon sources. Explicit derivations can be found in App. B.9.

For a single-mode field polarized in  $x$ -direction,  $g^2$  can be written as [197]

$$g^2(\mathbf{r}_1, \mathbf{r}_2, t, \tau) = \frac{\langle E_x^*(\mathbf{r}_1, t) E_x^*(\mathbf{r}_2, t + \tau) E_x(\mathbf{r}_1, t + \tau) E_x(\mathbf{r}_2, t) \rangle}{\langle E_x^*(\mathbf{r}_1, t) E_x(\mathbf{r}_1, t) \rangle \langle E_x^*(\mathbf{r}_2, t + \tau) E_x(\mathbf{r}_2, t + \tau) \rangle} .$$

For simplicity, we drop the spatial dependencies and concentrate only on the time difference  $\tau$ . We may assume a stationary field, *i.e.* the absolute time  $t$  is irrelevant. Then,  $g^2$  only depends on  $\tau$  and  $\tau = 0$ , *i.e.* zero delay, can be calculated for three important special states of the light field:

$$g^2(\tau = 0) = \begin{cases} 2 & \text{for thermal radiation,} \\ 1 & \text{for coherent light, and} \\ 1 - \frac{1}{n} & \text{for a Fock state with } n \text{ photons.} \end{cases} \tag{68}$$

A Fock state  $|n\rangle$  is an eigenstate of the number operator  $N = a^\dagger a$ , *i.e.*  $N|n\rangle = n|n\rangle$ . Obviously in the case of a single photon Fock state,  $g^2(0) = 0$ , which cannot be explained by classical considerations since  $g^2(0)$  is always bigger than one there (App. B.9). Hence, if  $g^2(0) < 1$ , the

light state is truly nonclassical and a single photon state may be seen as a prominent example.

Other figures of merit like the Fano factor and the Wigner function can also be used to analyze the nonclassical character of a light state [197]. The Fano factor is slightly more general than  $g^2$ , as it is also a good figure for higher  $n$  Fock states. However, an advantage of  $g^2(0)$  is its independence of the BST which we incorporate by the replacement  $a \rightarrow \sqrt{\eta}a$  (*cf.* Sec. 5.2). This independence is caused by our assumption that only the NA directly radiates. Then,  $g^2(0)$  of the radiated field is equal to  $g^2(0)$  of the NA state. Hence, as we are mainly interested in the characterization of single photon emission,  $g^2(0)$  is our main figure of merit to characterize the nonclassicality of the emitted light.

It was already mentioned that the photon emission rates determined in Sec. 5.3 correspond to a weak coupling of QS and NA. In this regime, the Markov approximation is valid and the spontaneous emission rate  $\gamma_{\text{wc}}$  can be incorporated into equations of motion for the QS. This is done to describe resonance fluorescence within the well-known Bloch equations [185]. This simplifies the calculations enormously, since the resulting description solely relies on an emission of the QS into a passive background medium. As a consequence,  $g^2$  is directly determined by the state of the QS. Hence,

$$g^2(0) = \frac{\langle \sigma_+ \sigma_+ \sigma_- \sigma_- \rangle}{\langle \sigma_+ \sigma_- \rangle^2} \equiv 0 \quad (69)$$

always holds for the Bloch equations since  $\sigma_+^2 = \sigma_-^2 = 0$ . This result is very natural as a two-level system cannot emit two photons at the same time if we disregard frequency conversions attributed to higher-order perturbation terms. From a semiclassical scenario we would thus expect that  $g^2(0)$  always vanishes.

### Numerical Results: $g^2(0)$ does not vanish

But our calculations for  $g^2(0)$  based on the QNM quantization scheme and fully quantum calculations reveal a drastically different result [Fig. 13 (e)]. We observe that, depending on the pump rate  $R$  and the major axis length  $a$ , strong deviations of  $g^2(0)$  from zero occur. For  $a > 80$  nm,  $g^2(0)$  is minimal for  $R \approx 1$  THz and reaches values around 0.01, which is practically zero when compared to state-of-the-art  $g^2(\tau)$  measurements from QDs [305, 306]. Most notably, these hybrid systems are the largest under consideration and exhibit a relatively weak coupling and thus comparably low  $\gamma_{\text{wc}}$ .

On the other hand, smaller NAs with stronger coupling (and higher  $\gamma_{\text{wc}}$ ) generally feature larger minimal  $g^2(0)$  reaching values larger than 0.1 at  $a \lesssim 35$  nm. Hence, we find a trade-off between the maximum emission rate  $\gamma_{\text{wc}}$  of the QS and the nonclassicality of the emitted light. This trade-off can be explained as follows: Because of a stronger coupling between NA and QS it becomes more likely that energy is transferred from QS to NA before the NA is able to emit a photon. A stronger coupling therefore leads to a higher probability of the NA to be in a higher excited state. This is a clear deviation from the ideal single-photon Fock state and  $g^2(0)$  becomes larger with increased coupling. On the other hand, if the coupling is comparably weak, a photon is likely to be emitted by the NA before an energy transfer from QS to NA occurs and  $g^2(0)$  is close to zero.

Furthermore, we can see in Fig. 13 (e) that  $g^2(0)$  strongly depends on the pumping rate  $R$ : for each NA there exists a local minimum in  $g^2(0)$  with respect to  $R$ . This minimum corresponds to a pumping region in which the emitted light exhibits maximal nonclassical properties by the respective NA. Higher and lower pumping rates lead to light states with less single-photon characteristics.

In the high pumping region it is clear that a stronger pumping of the QS leads to a higher

probability of the NA to be in a state with more than one photon. The increased NA excitation ultimately results in increased  $g^2(0)$ . The interpretation is more complicated for lower pumping rates. To get a better understanding, we can compare  $g^2(0)$  for calculations with the full Hamiltonian to one employing the RWA, *i.e.* neglecting the fastly oscillating terms  $\propto \sigma_+ a^\dagger + \text{H.c.}$ . These results can be seen in the inset of Fig. 13 (e). They show that there is no rise in  $g^2(0)$  for lower pumping rates, in agreement to known results obtained within the RWA [298, 307].

Hence, for low pumping rates, the fastly oscillating terms are responsible for the drop in non-classicality: These terms lead to a distribution of energy from *i.e.* a state with no excitation neither in the QS nor in the NA to a state with a photon in the QS and in the NA;  $\sigma_+ a^\dagger |0, 0\rangle = |1, 1\rangle$ . This process is very unlikely. But it has the potential to change the steady state solution for low pumping rates considerably and to cause deviations in the photon statistics that we see in a raise of  $g^2(0)$ . It has been pointed out lately by Zhang *et al.* [308] that  $g^2(0)$  can be lowered using a bimodal cavity. We may interpret this system as two-mode NA within the QNM quantization scheme. But their findings are based on the RWA and may be applicable for the investigated higher pumping regime.

Because of the different geometries of the NAs, their resonance frequencies  $\omega_{\text{na}}$  are altered. Under conformal rescaling, a larger NA generally causes a redshift of  $\omega_{\text{na}}$ . This is also reflected in the calculated power spectra  $S(\omega)$  which are illustrated in Fig. 13 (f); Please note again that we have assumed that NA and QS are at resonance ( $\omega_{\text{na}} = \omega_{\text{qs}}$ ).  $S(\omega)$  can be calculated using the Wiener–Khinchin theorem as the Fourier transform of the first-order correlation of  $a$  [185, 195],

$$S(\omega) \propto \int \langle a^\dagger(0) a(\tau) \rangle e^{i\omega\tau} d\tau .$$

For weak pumping rates for which power broadening does not occur, the linewidths of the spectra are linked to the emission rate of the combined system. They are not related to the radiative rate of the NA, as one might guess. So we find that hybrid systems with comparably low emission rates not only exhibit superior single-photon characteristics of the emitted light. They also offer a much narrower linewidth than those with stronger coupling.

## Concluding Remarks

Based on the QNM quantization scheme, we analyzed the possibility to enhance single photon emission rates using NAs. We introduced a simple approximate theory to analytically describe the emission rate. With respect to the assumed incoherent pumping scheme we could reveal that not only the spontaneous emission rate enhancement, *i.e.* the Purcell factor, plays an important role, but also the achievable pumping rate of the QS is crucial. A fundamental trade-off between high Purcell factors and NA efficiency  $\eta$  has to be accounted for the design of NAs for enhanced single photon emission rates.

We have further shown that it is necessary to understand the emission of single photons by suitable QNs taking into account the interaction with NAs. The reason is that the statistical properties of the emitted light are drastically altered by this interaction, even in the weak coupling regime. Based on density matrix quantum calculations we find a trade-off between high Purcell factors and the single photon emission characteristics of the emitted light. This was only possible because of the quantization of the NA that permits the calculation of the emitted light statistics.

Fundamental trade-offs have to be considered while designing hybrid systems. Nevertheless we were able to show that miniaturized NA-enabled single photon sources with emission rates around 1 THz sustaining good statistical properties are possible. The suggested designs further exhibit experimentally feasible parameters of the hybrid system. Our results are not only important from

a fundamental point of view, we also disclose the crucial parameters for NA-based ultra-bright single photon sources. These parameters may serve as design guidelines for future devices. We envision these nonclassical light sources to be extremely useful for quantum computation, quantum cryptography, and advanced sensing applications.

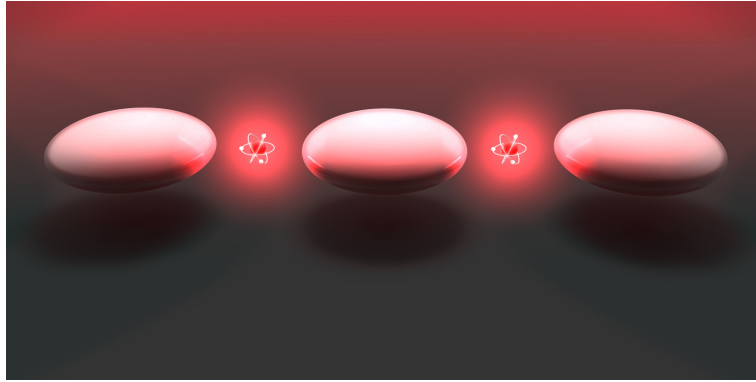


Figure 14: Schematic of the considered hybrid system. A NA made of three silver spheroids is strongly coupled to two identical QDs in its feed gaps.

## 6 Reaching the Strong Coupling Regime

In the last Section it has been shown how NAs alter the spontaneous emission characteristics of QDs. Another phenomenon that can only be understood in a fully quantum description is the strong coupling of QDs. In this section we investigate how suitably designed NAs can strongly couple to QDs.

Recent advances in nanotechnology allow the fabrication of gaps with a precision on the nm scale [55] and precise placement of QDs [309]. The possibility of substantial spatial localization of NA modes inside their feed gaps promises a strong coupling to QDs. In the strong coupling regime, NAs and QDs exhibit a continuous energy exchange which replaces the irreversible dynamics of spontaneous emission in the weak coupling regime (Fig. 9). In the infrared and visible spectral domain, strong coupling has been achieved for non-plasmonic cavities [225,310,311].

If the strong coupling regime can be reached for plasmonic systems, promising applications would come into reach. They include nanoscale signal processing at the single-photon level and quantum computation [312]. Hence it is a challenging task, but equally rewarding. It has been predicted for different kinds of plasmonic structures [79,80,313–317], see also Ref. [318] for a recent overview. The system we consider consists of two identical two-level QDs symmetrically placed close to a mirror- and rotationally symmetric NA (Fig. 14). We consider the coupling of a NA to two QD because of the arising possibilities in ultra-fast interactions between the QDs mediated by the NA. Furthermore it is easier to reach the strong coupling regime for two identical QDs, as we will see shortly.

In Sec. 6.1 we shall describe our mathematical model of the hybrid system. Afterwards, we investigate possible designs to reach the strong coupling regime (Sec. 6.2). The effects of strong coupling on the dynamics of the hybrid system (Sec. 6.3.1) and its extinction spectrum (Sec 6.3.2) will be discussed as well. This section is based on Ref. [80].

### 6.1 The Mathematical Model

As discussed before (Sec. 2.4 and Sec. 3.4), the theoretical description of hybrid systems may be performed in several approximations. In the strong coupling regime, however, a quantization of the NA and the QD is generally inevitable. This is emphasized by explicit comparisons to results within a semiclassical model [80].

The NA shall be illuminated by a monochromatic plane wave which excites the NA mode that interacts with the QDs. Then, the Hamiltonian of the hybrid system within the RWA (*cf.* Eq. 49)

can be written as

$$H = \hbar\Delta\omega_{\text{qs}} \sum_{j=1}^{N_{\text{qs}}} \sigma_+^{(j)} \sigma_-^{(j)} + \hbar\Delta\omega_{\text{na}} \left( a^\dagger a + \frac{1}{2} \right) + \hbar\kappa \sum_{j=1}^{N_{\text{qs}}} \left( \sigma_+^{(j)} a + a^\dagger \sigma_-^{(j)} \right) + \hbar\Omega (a + a^\dagger) \quad (70)$$

with  $\Delta\omega_{\text{qs}} = \omega_{\text{qs}} - \omega_{\text{dr}}$  and  $\Delta\omega_{\text{na}} = \omega_{\text{na}} - \omega_{\text{dr}}$ . Furthermore, the Rabi frequency  $\Omega$  of the NA illuminated by the external field can be calculated as  $\Omega = \mathbf{d}_{\text{na}} \cdot \mathbf{E}_{\text{dr}}(\mathbf{r} = 0) / 2\hbar$  within the electric dipole approximation. Here,  $\mathbf{d}_{\text{na}}$  is the NA's dipole moment at the illumination frequency  $\omega_{\text{dr}}$  for a single-photon excitation of the NA.

Because of the monochromatic drive, the Hamiltonian is expressed in the rotating frame of  $\omega_{\text{dr}}$  (see App. B.7 for an explanation). The scattering response of the NAs to local dipole emitters has been checked in numerical calculations to ensure that the electric dipole approximation is valid. Then, the NAs can be approximated by single-mode harmonic oscillators. This approximation simplifies our treatment considerably, but neglects the coupling to higher order modes. But since the QSs are symmetrically placed (Fig. 14), we can assume that these modes are spectrally well separated (Sec. 2.2). Hence, they constitute only a minor contribution to the investigated NAs.

The number of identical QSs is  $N_{\text{qs}} = 2$  and their transition frequency is  $\omega_{\text{qs}}$ . The operators  $\sigma_+^{(j)}$  ( $\sigma_-^{(j)}$ ) denote the creation (annihilation) operators of the  $j^{\text{th}}$  QSs and  $a^\dagger$  ( $a$ ) those of the NA. There is only a single coupling constant  $\kappa$  due to the symmetric placement of the QSs.  $\kappa$  can be calculated according to Eq. (47). Because of the intended strong coupling, we have further assumed that there is no direct interaction of the illuminating field with the QSs. This approximation is equivalent to the assumption that the interaction of the QSs to the NA is much bigger than to other free-space modes.

The dynamics of the hybrid system is described by the Lindblad-Kossakowski equation [*cf.* Eq. (46)]:

$$\begin{aligned} i\hbar\dot{\rho}(t) &= [H, \rho(t)] + i\hbar\mathcal{L}_{\text{na}}[\rho(t)] \quad \text{with} \\ \mathcal{L}_{\text{na}}[\rho(t)] &= -\frac{\Gamma}{2} (a^\dagger a \rho(t) + \rho(t) a^\dagger a - 2a\rho(t) a^\dagger) . \end{aligned} \quad (71)$$

Here,  $\rho(t)$  is the density operator of the hybrid system and  $\mathcal{L}_{\text{na}}[\rho(t)]$  is the Lindblad operator describing the losses of the NA. Again,  $\Gamma = \Gamma_{\text{r}} + \Gamma_{\text{nr}}$  refers to radiative and nonradiative losses of the NA. Typically, the radiative and nonradiative loss rates in the NA are much larger than nonradiative decay and dephasing rates of the QS and we neglect such processes. These processes can be easily incorporated with corresponding Lindblad operators.

## 6.2 Nanoantenna Designs

The aim is to design NAs to reach the strong coupling regime. The latter can be defined by

$$4\sqrt{N_{\text{qs}}}\kappa > \Gamma , \quad (72)$$

when the identical coupling of  $N_{\text{qs}}$  equivalent two-level systems to a harmonic oscillator leads to dressed states and an observable Rabi splitting occurs [79, 313, 319] (see also App. B.5). This condition implies that a mutual exchange of energy between the QSs and NA emerges.

To find NAs that are suitable to reach strong coupling we investigate coupling constants and loss rates depending on the shape and sizes of different NAs. One of our main results is that the strong coupling regime requires rather small NA dimensions. This can be anticipated since  $\kappa \sim 1/\sqrt{V_n}$  [*cf.* Eqs. (23) and (47)]. Specifically, we find that NA elements have to be in the order of a few tens of nanometers and their mutual separation must be a few nanometers only.



Figure 15: NA designs to reach the strong coupling regime. (a) Investigated NAs consisting of three identical silver spheroids with aspect ratio  $a/b$  with a mutual distance  $r_0$ . QS placement and polarization denoted by the red arrows. (b) Absolute value of  $E_x(\mathbf{r}, \omega_{\text{na}})$  normalized by the value to the illuminating field for a NA with  $a = 13.3$  nm,  $b = 8$  nm and by  $r_0 = 2$  nm. (c)  $\kappa/\Gamma$  for  $d_{\text{ge}} = 6 \times 10^{-29}$  Cm and NAs with different geometries for single- (left) and three-spheroid (right) NAs: dependence on spheroid size (red circles), a change of the minor axis  $b$  (red crosses), and distance  $r_0$  (blue squares) as given in the legend. (d) NA efficiency  $\eta$  and (e) Purcell factor  $F$ .

### Preliminaries: Figures of Merit, Numerical Setup and Considered Geometries

The NAs are analyzed with respect to their Purcell factor  $F$  and efficiency  $\eta$  [Eqs. (36) and (6)]. Such an analysis is strictly valid only in the weak coupling regime since these figures are calculated via classical electrodynamic calculations. In the strong coupling regime, however, the effective loss rate of the QSs is essentially given by the NA's dissipation rate [198]. The classical character of  $F$  and  $\eta$  have to be kept in mind when discussing the properties of the NAs in the strong coupling regime.

The electromagnetic simulations were performed with COMSOL [170]. The dispersive permittivity of the NA elements was taken from Ref. [125]. To determine the resonance frequencies  $\omega_{\text{na}}$  of the investigated NAs, their extinction cross-section under monochromatic plane-wave illumination have been calculated in a certain spectral range. The use of a plane wave ensures that only the dipolar mode of the NA is excited that is used within the single-mode approximation. An embedding with permittivity  $\varepsilon_d = 2.2$  is further assumed. Then, following Sec. 3.4, the loss rate  $\Gamma$  of each NA and coupling constant  $\kappa$  at the positions of the QS were determined assuming a realistic dipole moment of  $|\mathbf{d}_{\text{qs}}| = 6 \times 10^{-29}$  Cm [302].

Two basic NA geometries are considered: A single or three identical silver spheroids with axis lengths  $a$  and  $b$ . If  $a > b$  holds, the spheroids are prolate [Fig. 15(a)]. The distance between neighbouring spheroids along the  $x$  axis is given by  $r_0$ . Single- and multiple-spheroidal NAs are interesting from different perspectives: For single spheroids, there is no gap required and they might be easier to fabricate and investigate in experiments [320]. It has further been predicted that single-particle structures might be suitable to reach the strong coupling regime [79, 321]. On the other hand, NAs made of multiple elements potentially confine and enhance fields much stronger

inside their feed gaps when compared to isolated nanospheroids. This confinement generally leads to an increase of the Purcell factor and the mutual coupling. Furthermore, as we will see, such NAs are larger and generally exhibit higher efficiencies, which makes them appealing for applications [81, 322].

### The Final Design

An example of the field enhancement around a specific NA consisting of three spheroids with the parameters  $a = 13.3$  nm,  $b = 8$  nm, and  $r_0 = 2$  nm is provided in Fig. 15 (b). The absolute value of the scattered electric field normalized to the illuminating field in  $x$ -direction is shown at the resonance frequency of the NA,  $\omega_{\text{dr}} \approx 2\pi \cdot 535$  THz ( $\lambda_{\text{dr}} \approx 560$  nm). The illuminating field propagates along the  $y$ -axis, *i.e.* perpendicular to the rotational symmetry axis of the NA, and is polarized along the  $x$ -axis. This NA corresponds to a design with the largest calculated  $\kappa/\Gamma$  ratio, which is termed “final design” for this reason ( $\kappa \approx 116$  THz,  $\Gamma \approx 183$  THz,  $\kappa/\Gamma \approx 0.63$  and  $\eta \approx 3.1\%$ ). The absolute value of the scattered field is about two orders of magnitude larger than the illumination field. This justifies to neglect the direct interaction of the illumination field with the QS [Eq. (70)].

### Achievable $\kappa/\Gamma$ -Ratios

According to Eq. (72), the  $\kappa/\Gamma$ -ratio is the most important figure to decide if the strong coupling regime has been reached. This ratio is shown in Fig. 15 (c) for NAs with rescaled spheroids (red circles) and those for which the minor axis is changed, *i.e.* different aspect ratios (red crosses). The strong coupling regime is denoted by two dashed lines at  $\kappa/\Gamma = 1/4$  for  $N_{\text{qs}} = 1$  and at  $\kappa/\Gamma = 1/\sqrt{32}$  for  $N_{\text{qs}} = 2$ . As expected, the overall size of the NA is the most important quantity. For rescaled spheroids and rescaled minor axis  $\kappa/\Gamma$  decreases considerably for larger NAs.

For the single-spheroid case the dependency is almost equivalent for both scalings. The strong coupling regime is realized for a minor axis  $b$  below 20 nm for single-spheroid designs. For three spheroids, strong coupling can be observed for  $b < 35$  nm and fixed  $a/b$ -ratio. For fixed major axis  $a$ , the dependency on the minor axis’ scaling is less pronounced. Please note that the  $\kappa/\Gamma$  ratio in the case of a single spheroid with small minor axes is larger than for three spheroids. The reason is that  $\kappa$  and  $\Gamma$  are decreased for the single spheroid, but the drop in  $\kappa$  is slightly less pronounced. For example, the parameters of the single spheroid final design are given by  $\kappa \approx 61.8$  THz,  $\Gamma \approx 90.5$  THz,  $\kappa/\Gamma \approx 0.68$  and  $\eta \approx 3.0\%$  at  $\lambda_{\text{dr}} = 476$  nm.

In the same figure, the dependency of  $\kappa/\Gamma$  on the separation distance  $r_0$  between neighbouring spheroids with a fixed geometry is displayed (blue squares). For  $r_0 = 2$  nm, the NA design corresponds to the aforementioned final design [Fig. 15 (b)]. Because of the symmetric placement of the QSs inside of the feed gap an increase in  $r_0$  implies an increase in the distance between QSs and NA surface. For increasing  $r_0$  the field is less localized inside the gap, which explains why the coupling constant  $\kappa$  decreases. In the case of three spheroids, strong coupling can be achieved until about  $r_0 = 5$  nm. Interestingly, in the single-spheroid case, this critical distance can be in the order of  $r_0 = 7$  nm. This difference is quite important for an experimental realization. Since the smallest QDs are in the order of 4 nm [299], the three-spheroid NAs might be best suited for atomic QSs with characteristic sizes around  $a_0$ , whereas strong coupling might be achieved for single spheroids with the help of QDs.

### Trade-off between Efficiency and Coupling Strength

The results for  $\kappa/\Gamma$  are quite promising, since the strong coupling regime can be reached for different kinds of investigated NAs. However, following the definition of a NA (page 2), an “efficient

conversion of free-propagating radiation to localized energy” is required. In addition, we expect to find a fundamental trade-off between coupling strength and efficiency again (Fig. 13). We may pose the question if the strong coupling regime can be achieved with a somehow large efficiency.

In a comparison of both sub-figures of Fig. 15 (d), it can be seen that three-spheroid NAs generally exhibit larger efficiencies. This can be explained by their larger overall sizes. Furthermore, in the case of varied  $r_0$ , the  $\eta$  are well below 5% for all investigated cases. The reason is that the overall size of the NA is only marginally changed by a change of  $r_0$ . The radiation characteristics are consequently almost unchanged. A clear distinction between single- and three-spheroid NAs can be observed for changed minor axis  $b$ . Whereas in the latter case  $\eta$  rises with increased  $b$ , the efficiency drops for the single prolate spheroid NAs. This behavior might be explained by an increased coupling to dark modes of the single spheroids, which are included in the classical calculation of  $\eta$ .

The highest efficiencies can be observed for rescaled spheroids with constant ratio  $a/b$ . In this case the major axis is also increased with  $b$  such that the overall size of the NA is considerably changed. For example, a three-spheroid NA with  $b \approx 28$  nm has an efficiency of  $\eta \approx 61\%$  and enables strong coupling even for a single QS. This NA exhibits a total length of  $L = 3a + 2r_0 \approx 146$  nm, which is in the order of efficient NA sizes at the NAs resonance wavelength  $\lambda = 504$  nm (Sec. 2.2). The efficiency of the largest single-spheroid NA that enables strong coupling only for  $N_{\text{qs}} = 2$  ( $b \approx 22$  nm) is considerably lower ( $\eta \approx 45\%$ ).

In Fig. 15 (e), the classically calculated Purcell factors  $F$  for the investigated NA designs are shown. Because of the lower efficiencies, the single-spheroid NAs generally exhibit strongly decreased  $F$  compared to their three-element counterparts. Furthermore,  $F$  drops for the single-spheroid NAs for all geometrical variations albeit a local maximum for the rescaled spheroids. For these NAs, the increase in the mode volume is the most important factor.

For the three-spheroid NAs, however, the results are more diverse. For the scaling of  $r_0$ ,  $F$  drops orders of magnitudes with an increase in the gap sizes. For those NAs,  $\eta$  is almost constant and the drop in  $F$  is caused by a weaker localization of the electric field inside larger gaps. For changed minor axis, the Purcell factor remains almost constant. In this case, a decrease in the coupling constants is countered by a slight increase in the efficiency. On the other hand, NAs with rescaled spheroids show a strong increase in  $F$  up to  $b \approx 20$  nm and the Purcell factor increases until  $b \approx 30$  nm, after which a slight decrease can be observed. This behaviour is readily explained by the fundamental trade-off between coupling strength and efficiency, in agreement to our observations in Fig. 13 (c) for conformally rescaled NAs.

## Summary

In summary, a variety of different NA designs can be used to reach the strong coupling regime. Three-spheroid structures exhibit a better field localization in their feed gaps and thus have generally larger coupling constants. Because of the increased mode localization, the strong coupling regime can be reached for considerably larger NAs and their efficiency is much better than their one-spheroid counterparts. Geometries with rescaled spheroids turn out to be superior to the other investigated geometrical variations because of the much larger efficiencies associated with larger NA elements. Because of the fundamental trade-off between coupling strengths and efficiency due to their opposite size dependencies, the strongest  $\kappa/\Gamma$  ratios around 0.6...0.7 can be achieved for NAs with rather poor efficiency  $\eta \ll 10\%$ .

However, as indicated in Fig. 13 (d), more efficient NAs with  $\eta \approx 50\%$  seem feasible for lower  $\kappa/\Gamma = 0.2 \dots 0.3$ , which is still in the strong coupling regime for  $N_{\text{qs}} = 2$ . Furthermore, rather small separations are needed, which might require the use of atomic Qs in experiments. Note

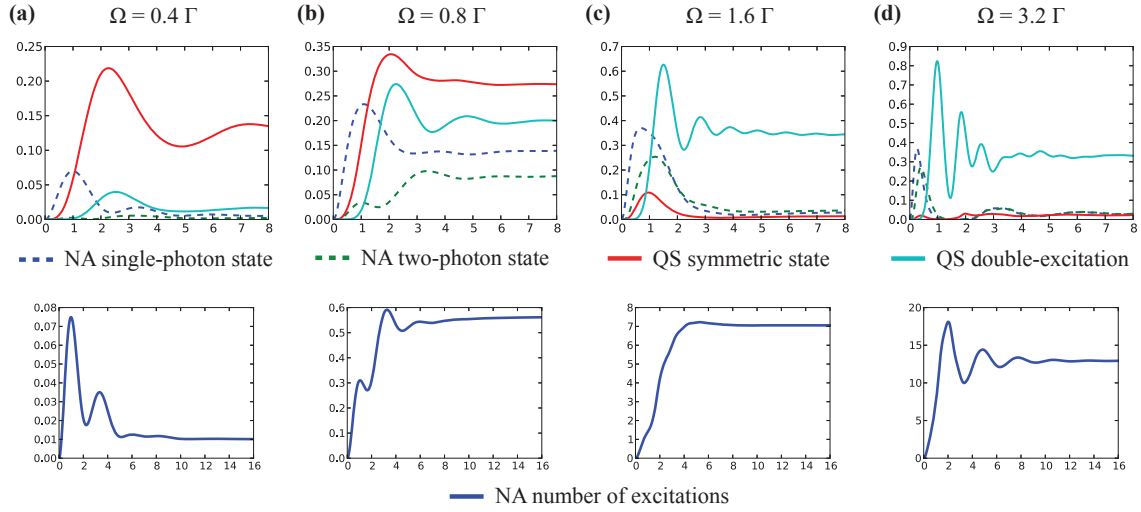


Figure 16: Probabilities of different QS and NA states (upper part) and the number of excitations  $\langle a^\dagger a \rangle$  (lower part) in the normalized timescale  $\kappa t$ . Strong coupling between NA and Qs causes a mutual exchange of excitations between NA (dashed lines) and Qs (solid lines). The dynamics strongly depend on the Rabi frequency  $\Omega$ .

that the NA-QS separation  $r_0/2$  is still larger than characteristic electron tunneling distances of a few Å [72]. But corresponding interactions might already constitute a significant contribution as we have discussed already (Sec. 2.1).

### 6.3 Effects of Strong Coupling

The effects which are caused by the strong coupling of NAs to Qs shall be investigated now. First, we investigate how the quantum dynamics change. Afterwards, we discuss the extinction spectra of such hybrid systems which are accessible in experimental setups. All outlined calculations are performed using a freely available quantum optics framework [232] for which the NA's Hilbert space is truncated but much larger than its number of excitations  $\langle a^\dagger a \rangle$ .

#### 6.3.1 Quantum Dynamics

An example for the quantum dynamics of a hybrid system is given in Fig. 16. The hybrid system is assumed to be at resonance, *i.e.* with  $\omega_{\text{na}} = \omega_{\text{qs}}$ . Its physical parameters are given by  $\kappa = 0.034\omega_{\text{qs}}$  and  $\kappa/\Gamma \approx 0.752$ , which is comparable to the final design in Sec. 6.2. The hybrid system is initially in its ground state and subject to an illumination with varying Rabi frequencies  $\Omega = 0.4\Gamma \dots 3.2\Gamma$ .

**Weak Illumination** The excitation of the NA by the external illumination quickly leads to a fast increase of the probability of a single photon excitation of the NA for all cases of  $\Omega$  (dashed blue lines). In the limit of a weak driving field with  $\Omega = 0.4\Gamma$  [Fig. 16 (a), top], the excitation of the NA is transferred to an excitation of the Qs's symmetric state  $|S\rangle = (|1, 0\rangle + |0, 1\rangle)/\sqrt{2}$  (red line). But the probability of the Qs's state with two excitations,  $|D\rangle = |1, 1\rangle$ , does not vanish (solid cyan line), too. For this illumination strength, higher-order excitations of the NA are negligible as it can be seen for the two-photon NA state probability (dashed green line).

The relaxation to a steady state takes several  $\kappa t$ , while a continuous energy exchange between the Qs's symmetric state and the NA takes place. In the steady state, dissipative and radiative losses of the NA level the energy supply by the external drive. The significant probability of a symmetric state occupation albeit a very low NA excitation [Fig. 16 (a), bottom] is a truly

nonclassical phenomenon and shows the potential of the hybrid system to generate entangled states [91, 323, 324].

**Strong Illumination** For the strongest investigated illumination [ $\Omega = 3.2\Gamma$ , Fig. 16 (d)], the dynamics are completely altered compared to weak illuminations. Here, the Qs exhibit a high probability to be in the doubly excited state  $|D\rangle$  and the symmetric state is negligible. Furthermore, the NA stores most of the energy, since its mean number of photons  $\langle a^\dagger a \rangle \approx 13$  for  $t \rightarrow \infty$ . The change of the quantum dynamics from weak to strong pumping rates [Fig. 16 (a) to (d)] indicates the huge importance of the driving field strength.

Whereas in the weak illumination case the energy of the hybrid system is mainly stored in the symmetric state of the Qs, the NA becomes the main energy reservoir for stronger illuminations. In this case we expect a transition to a classical behavior of the hybrid system. Possible applications are much different than in the case of a weak illumination for which the evolution of the system shows a strongly nonclassical behaviour. This observation underlines the interesting possibilities of single-photon spectroscopy of hybrid systems and the need to understand single-photon sources (Sec. 5).

### 6.3.2 Spectra Modifications

Before we analyze the modification of extinction spectra of certain NAs, it is worthwhile to reconsider the experimental feasibility of such devices. It was demonstrated that the strong coupling regime may be achieved for single- and three-spheroid NAs. Three-spheroid NAs may be generally superior because of their larger coupling strengths and higher efficiencies. Nevertheless, single-spheroid NAs might be much easier to fabricate, mainly because they do not require extremely precise feed gaps. For an experimental realization, an extremely accurate fabrication of the NA and a likewise precise placement of the Qs seems necessary. Fortunately, recent advances in nanotechnology meet both requirements [55, 309, 325–328].

As we have discussed already, the dissipative and radiative losses of the NA are the dominating loss channels of the hybrid system. Furthermore, since most NAs considered in Sec. 6.2 exhibit low efficiencies, the extinct power is approximately given by the absorbed power

$$P_{\text{nr}}(\omega_{\text{dr}}) = \hbar\omega_{\text{na}}\langle a^\dagger a \rangle\Gamma_{\text{nr}}. \quad (73)$$

In the last paragraph the rich dynamics of the hybrid system was discussed. In this paragraph  $P_{\text{nr}}$  shall be investigated in the steady-state.

**From Weak to Strong Coupling** The extinction spectra due to the strong coupling of a NA to two Qs are modified when compared to that of the bare NA. These modifications are mostly pronounced if the mean number of excitations of the hybrid systems is low, *i.e.* at the single-quantum level. The main influence on the extinction spectrum is due to the coupling strength  $\kappa$  between the subsystems. To outline this effect, we calculate  $\langle a^\dagger a \rangle \propto P_{\text{nr}}$  for a hybrid system with characteristic values for the NAs discussed in Sec. 6.2 but for  $\omega_{\text{qs}} \neq \omega_{\text{na}}$ , *i.e.* a detuned QS [Fig. 17 (a)]. With respect to a variation of  $\kappa$ , the parameters are  $\Gamma = 0.025\omega_{\text{na}}$  and  $\omega_{\text{qs}} = \omega_{\text{na}} - 1.2\Gamma$ , which is a small detuning. Furthermore, the Rabi frequency is constant at  $\Omega = 0.6\Gamma$ .

In the weak coupling limit ( $\kappa = 0$  and  $\kappa = 0.1\Gamma$ ), the broad resonance of the NA dominates the extinction spectrum and the modification of the spectrum is barely visible. In the case of strong coupling ( $\kappa = 0.4$  and  $\kappa = 0.8\Gamma$ ), the spectrum is strongly modified. The QS's resonance position gets shifted to lower frequencies, whereas the peak attributed to the NA can be found for higher

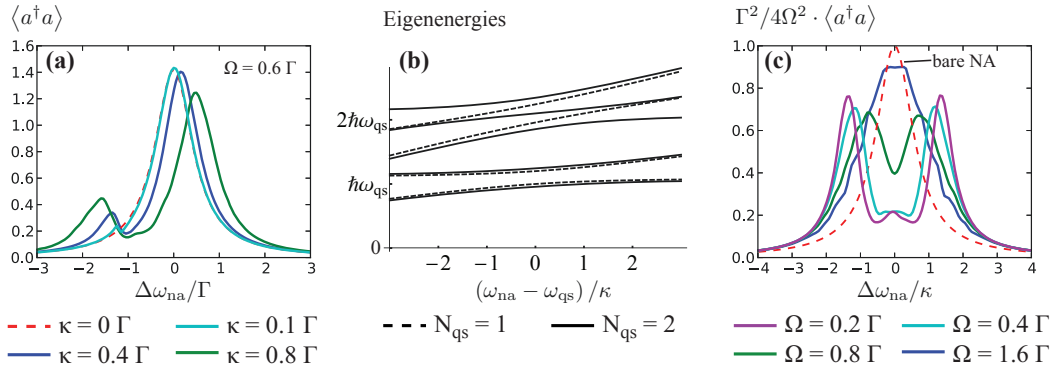


Figure 17: Mean number of excitations proportional to the extinction spectra for different hybrid systems [(a) and (c)] and their analytical eigenenergies in the lossless case (b). (a) Influence of the coupling strength  $\kappa$  for detuned systems ( $\omega_{na} = \omega_{qs} + 1.2\Gamma$ ). Steady-state mean NA excitations of the NA vs. normalized illumination frequency ( $\Delta\omega_{na} = \omega_{na} - \omega_{dr}$ ) for a weak illumination. (b) Eigenenergies of the hybrid system as function of the detuning  $\omega_{na} - \omega_{qs}$  for  $N_{tls} = 1$  (dashed lines) and  $N_{tls} = 2$  (solid lines) for a total number of  $n \leq 2$  excitations. (c) Influence of the illumination strength for a hybrid system on resonance ( $\omega_{na} = \omega_{qs}$ ). Mean number of NA excitations normalized by the dimensionless parameter  $4\Omega^2/\Gamma^2$ .

frequencies. The shift of the NA peak is in the order of the resonance width. Furthermore, the strengths of the resonances are strongly affected.

The additional deviations of the spectrum from a simple superposition of two Lorentzians indicates the importance of higher photon-number states in the response of the hybrid system. Their energies can be understood in terms of a hybridization of all involved sub-systems [39, 198]. They can be derived with the help of a lossless Jaynes-Cummings model (App. B.11). Without detuning ( $\omega_{na} = \omega_{qs}$ ), the energy splitting for the single-excitation states amounts to  $\sqrt{N_{qs}}\kappa$ , but becomes more involved for  $\omega_{na} \neq \omega_{qs}$  [Fig. 17 (b)]. In particular for  $N_{qs} = 2$  a third mode appears at an energy  $2\hbar\omega_{qs}$  for  $\omega_{na} = \omega_{qs}$ . As we will see shortly, this mode has a strong impact on the hybrid system's spectrum at  $\omega_{dr}$ .

**Varied Illumination Intensities** On the single-photon level, the influence of strong coupling is quite significant, also for detuned hybrid systems. In Fig. 17 (b) we see how the eigenenergies behave for  $n = \{1, 2\}$  excitations. However, for stronger illumination intensities, much more energy levels contribute to the interaction and we expect that the classical behavior of the NA is restored. In this case, the Qs play only a minor role in the spectrum. To check this claim, we calculate the spectrum of the NA investigated in Sec 6.3.1 ( $\kappa = 0.034\omega_{qs}$ ,  $\kappa/\Gamma \approx 0.752$ ) at resonance with the Qs.

The steady-state mean photon number has been rescaled by the dimensionless parameter  $4\Omega^2/\Gamma^2$ , which is approximately the steady-state solution for the bare NA on resonance. We find that in the weak excitation limit ( $\Omega = 0.2\Gamma$ , purple solid line) the absorption peaks appear at  $\Delta\omega_{na} = \pm\sqrt{2}\kappa$ , as predicted by the eigenenergies for a single excitation. Furthermore, a local maximum around  $\Delta\omega_{na} = 0$  can be observed which corresponds to the aforementioned excitation of the state with eigenenergy  $2\hbar\omega_{qs}$ . This peak does not appear for a single QS for which the onset of transparency has been reported [329, 330].

For stronger illumination intensities ( $\Omega = 0.4 \dots 0.8\Gamma$ ) the spectrum changes drastically. More eigenstates of the hybrid system are involved in the interaction and the extinction peaks are shifted towards the resonance of the bare NA. For strong driving fields the spectrum converges to that

of the bare NA, although the influence of the Qs is still observable for  $\Omega = 1.6\Gamma$ . In this case we find that the extinction is still lower at resonance when compared to the bare NA, but also broader. Furthermore, it exhibits oscillatory features that indicate the excitation of many states of the hybrid system again.

We may state that in the strong coupling regime the extinction spectra of the hybrid system are strongly modified. The modification is mostly pronounced for illuminations on the single-photon level.

## Concluding Remarks

Based on the QNM quantization scheme, the coupling of one and two Qs to different silver NAs designed to reach the strong coupling regime was investigated. The strongest coupling could be reached for NAs with small spheroidal elements and likewise small feed gaps. Because of the fundamental trade-off between coupling strength and efficiency, a very strong coupling with  $\kappa/\Gamma > 0.6$  can be reached for NAs with very low efficiency only.

But NAs with  $\kappa/\Gamma$  ratios around  $0.2 \dots 0.3$  can be comparably efficient if they are made of three spheroids. To reach strong coupling, the distance of the Qs to the NAs has to be in the order of just a few nanometers, which might render the use of atomic Qs necessary. Furthermore, an introduction of other interaction channels at such low distances might become inevitable for a correct theoretical description.

Reaching the strong coupling regime has a strong impact on the dynamics of the hybrid system. An ongoing energy exchange between NA and Qs leads to dynamics drastically different than the characteristic exponential decay in the weak coupling regime. These dynamics give rise to quantum properties of the hybrid system that might be used to generate nonclassical light as discussed in Sec. 5.

The coupling of the subsystems furthermore leads to a strong modification of experimentally accessible quantities such as the extinction spectra. However, to verify strong coupling, spectral measurements on the single-photon level, *i.e.* small  $\Omega/\Gamma$ -ratios have to be realized. Then, a true quantum regime is reached and Rabi splittings can be observed.

## 7 Conclusions and Outlook

Plasmonics has raised considerable interest during the past several years [331]. Because of ongoing improvements in fabrication techniques, new possibilities arised in the field that made Feynman's dream come true to arrange atoms on the nanoscale [332]. And as Feynman has foreseen [4], these new possibilities open spectacular opportunities to control light-matter-interactions on the nanoscale. But to apply these opportunities, a description of such devices within the realms of quantum mechanics is required. Then plasmonics evolves into quantum plasmonics. The results of this thesis were aimed at contributing to this newly arising field.

In Sec. 2 and Sec. 3 we have provided a theoretical framework to describe the interaction of NAs with Qs. The applicability of the outlined approximations is extremely versatile and can be used for completely different physical regimes. A classical electrodynamics description of NAs gives the possibility to freely design and tune them for specific means, but it leads to a semiclassical description of the hybrid system. On the other hand, a quantization scheme for NAs based on QNMs has been developed. A fully quantum treatment of the hybrid system is then realized.

The novelty of our treatment lies in the explicit determination of the quantized electric and magnetic fields of the NA. These fields can be used for different kinds of interactions beyond the electric dipole approximation. Within the QNM quantization, we are restricted to NAs that can effectively be described as lossy harmonic oscillators. Hence we exchange a freedom in the design of NAs for a better understanding of the truly quantum interaction between NAs and Qs based on just a few parameters. The appeal of the QNM quantization lies in a low-dimensional Hilbert space and an easy determination of the aforementioned parameters using state-of-the-art numerical tools.

In Sec. 4 we used the semiclassical description to show how the internal dynamics of a three-level system is influenced by the presence of a suitably designed NA undergoing a quadrupolar excitation. Two important aspects of NA-QS-interaction have been demonstrated: First, NAs allow to access transitions of Qs that are barely accessible by other excitation techniques. Second, the internal dynamics have a huge influence on the resulting emission enhancement when compared to free space. Although a relatively restrictive rate equation approximation was used, we encountered rich physics. A general scheme to treat multipolar couplings based on a local expansion of the fields was also outlined. It provides a clear distinction between electric and magnetic effects. In Ref. [78] we questioned not only the electric dipole approximation, but also the influence of a QS's dynamics on experimental measurables. These considerations may have influenced the way how light-matter interactions on the nanoscale are investigated.

Our studies are based on the idea to show the occuring effects with the simplest possible setup. Hence the simplest possible theoretical description and rather simplistic NA designs are used. The effects of truly quantum interactions between NA and QS require the use of a NA quantization scheme. This is especially true if the statistics of the light emitted by the hybrid system needs to be investigated. In Sec. 5 (inspired by Ref. [89]), we have discussed the potential of NAs as ultra-bright single-photon sources, an indispensable prerequisite for practical quantum communication schemes. We have shed some new light on the accepted assumption that the Purcell factor is basically the only figure of merit for such light sources. The pumping scheme and an associated pumping rate have to be accounted for. Furthermore, the actual nonclassicality of the emitted light has to be verified. Based on analytical and numerical investigations, several trade-offs between NA efficiency, Purcell factor, and nonclassicality of the emitted light could be identified. In general it seems necessary to account for the actual quantum nature of the interactions between Qs and NAs.

In the case of a strong coupling between different Qs and NAs it is clear that the hybrid



system's dynamics can only be described consistently within a fully quantum description. In Sec. 6 we have discussed the possibility to reach the strong coupling regime using the interaction of Qs and suitably designed NAs based on Ref. [80]. This goal might be achieved in principle. But the fundamental trade-off between efficiency and coupling strength may set ultimate limits for practical implementations. Furthermore, the necessary small dimensions of the involved NAs and the precise placement of the Qs are quite challenging. But if the strong coupling regime can be reached, the benefits may outweigh the efforts dramatically: Promising applications such as ultra-fast signal processing at the nanoscale and at the single-photon level would come into reach.

Overall it was shown how different descriptions of NA-QS interactions can be used to unravel prospects in fundamental research and applications. Semiclassical approaches allow in-depth investigations for sophisticated NA designs, whereas the focus of the QNM quantization scheme lies on the fully quantum description of the hybrid system. This description permits an access of quantum observables within relatively simple calculations. For both approaches there exist a plethora of possibilities for future investigations and applications that we shall briefly discuss in the following.

### **Outlook: Semiclassical Interactions**

The interaction between QS and NA can be treated semiclassically if the correspondence principle for the electromagnetic field holds and the coupling between both subsystems is sufficiently weak. Such conditions are experimentally much easier to realize than scenarios where the true quantum nature of the interaction must be taken into account. So it seems logical to discuss future prospects for the semiclassical interactions mainly in the context of practical applications in the following. Afterwards, the perspectives of the QNM quantization approach for academic studies are considered.

There may be further applications of forbidden transitions than those mentioned in Sec. 4.4.2. The deterministic access to such transitions might be used to effectively acquire so-called  $\Lambda$ - and  $V$ -configurations by a suitable coupling of NAs and Qs.  $\Lambda$ -configurations can be used to deterministically enable/disable a certain transition by the help of a control beam in another transition [185]. Such an effect might be adapted for new kinds of transistors [333] and electromagnetically induced transparency devices [334]. In a  $V$ -configuration, a QS is driven by two competing pumps at different frequencies for two different transitions. Usually, one of the transitions is long-living in free-space, *e.g.* because it is dipole-forbidden. Depending on the environment, the probability of the  $V$ -type QS to emit one or the other frequency can drastically change [335]. This dependency might be employed in spectroscopic schemes to measure occurrence and position of certain Qs. All of these approaches can be described within the semiclassical multilevel Bloch equations that can also be used to evaluate much more complicated Qs [185].

But the biggest advantage of the semiclassical approach is the absolute freedom in NA design. This freedom permits a true NA engineering for a specific purpose in conjunction with a suitable QS (see *i.e.* Ref. [98] for some NA design examples). Prominent examples of NA engineering are the combination of Qs with directional NAs [49,103] that might for example be used for directional single-photon emission, NA-enhanced efficiency enhancements for upconversion processes in solar cells [336], and for nonlinear NA elements to change NA properties on demand [337,338]. But all these design-related questions have to address the limitations of reproducible and cost-efficient NA fabrication and QS placement schemes to find their way into practical applications. A very promising attempt has been made with large-scale ring NA fabrication techniques and a new QD placement technique [57,59,309]. Since both fabrication methods are based on electron-beam lithography, a combination of them seems very likely to realize large-scale reproducible, versatile

and cost-efficient arrays of hybrid systems in the near future.

Once, the practical applicability of NA-based hybrid systems is proven, a further development might take place. We believe that it is unlikely that this trend will result in a stronger utilization of plasmonic particles, *i.e.* to combine NA-QS hybrid systems to functionalized metamaterials [339]: The main advantage of NAs is their efficient energy localization to tiny volumes. Hence, an unwritten paradigm is to use just as much metal as needed to reduce losses. Enhancing the metal filling fraction seems to be an ill-conditioned way for sophisticated light-matter-interactions unless losses may be used to provide some additional value like for absorbers [340].

A combination of NAs with photonic crystals without additional Ohmic losses seems promising: No further dissipation is introduced but one gains a large tunability of the coupling of NA-QS hybrid systems to the modes of the photonic crystal [341]. These modes may then be used to enable interactions between hybrid systems over long distances in conjunction with optical fibre technology for telecommunication applications. A photonic crystal may also be used to couple hybrid systems along relatively short distances *e.g.* for NA-enabled quantum computers. The combination of NA and photonic crystal technology will open entirely new possibilities that are not available with one of these technologies alone.

These ideas were just a few to illustrate how semiclassical approaches may lead to amazing applications which are mainly based on advancements in fabrication technology. On the other hand, QS-NA-interactions will continue to contribute significantly to our fundamental understanding of light-matter-interactions on the nanoscale. A lot of interesting physics is expected to occur when a quantum description of the NA is necessary. In the following we shall discuss how the introduced QNM quantization might yield new perspectives.

## Fully Quantum Interactions

The introduced QNM quantization scheme is a powerful tool to understand the quantum nature of QS-NA-interactions. As discussed already, a lot of interesting physical systems can be studied in this approach.

The physical model in terms of harmonic oscillators coupled to Qs is rather simplistic. Thus, an overwhelming number of questions that arose in the context of quantum optics and cavity quantum electrodynamics can be applied to NA systems. Hence we may simply refer to some standard references of these topics to give an impression of possible future directions in research and application [185, 195, 198, 342–344].

Noteworthy, the QNM quantization of NAs can be applied to a large class of plasmonic structures. It can consequently also be used to double-check and extend classically derived results. One interesting verification would be the emission of coherent light with coherence lengths of many wavelengths by heated structured media [345].

Furthermore, generalizations of the QNM quantization seem to be straight forward. One option is the construction of effective Hamiltonians for hybrid systems based on an at least partially non-Lorentzian mode expansion of the density of states  $J(\omega)$ . In this way, the interaction can again be described by a low-dimensional Hilbert space. For example, coupled harmonic oscillators can be used to mimic a Fano-type  $J(\omega)$  [346]. Such resonances will open new pathways to study strong coupling phenomena for extended structures. Such investigations may benefit from a large number  $N$  of involved Qs for which we know that an effective coupling strength scales as  $\kappa_N \propto \sqrt{N}\kappa_1$  [314].

The incorporation of quantum size effects [66] and of nonlocal responses of the NA material [65, 69, 70] seems to be easily achievable. But considerations of electron-spill-out [64, 71, 347] would at least require a new coupling term in the Hamiltonian to account for this additional interaction channel. A combination of the aforementioned generalizations might be a prime candidate to grasp

the physics of truly near-field interaction within a relatively simple framework.

Another way to extend the quantization scheme is the use of intrinsic nonlinear materials for which a canonical quantization is known [348]. A nonlinear QNM quantization might be very suited to contribute to ongoing questions about nonlinear responses of metallic NAs [118].

In conclusion we may state that the current form of the QNM quantization scheme is a powerful tool that allowed to investigate NA-QS-interactions on an entirely new level compared to semiclassical calculations. The scheme is simple yet extremely versatile in an effective description of different effects such that generalizations are easily possible.

# Appendices

## A Classical Considerations

### A.1 Poynting's Theorem

Starting from Maxwell's equations in Fourier space it is possible to determine Poynting's theorem for dispersive media for fields which slowly vary around a frequency  $\omega_0$  [115,349]. In this approach, the electric field is written as

$$\mathbf{E}(\mathbf{r}, t) = \frac{1}{2} [\mathbf{E}_{\text{env}}(\mathbf{r}, t) e^{-i\omega_0 t} + \mathbf{E}_{\text{env}}^*(\mathbf{r}, t) e^{i\omega_0 t}] , \quad (74)$$

where  $\mathbf{E}_{\text{env}}(\mathbf{r}, t)$  is the slowly varying envelope whose Fourier transform is limited to a small spectrum  $\Delta\omega \ll \omega_0$  around  $\omega = 0$ ,  $\mathbf{E}_{\text{env}}(\mathbf{r}, t) = \int_{\Delta\omega} \mathbf{E}_{\text{env}}(\mathbf{r}, \omega) \exp[-i\omega t] d\omega$ . Equation (74) shall hold likewise for other electromagnetic fields. Then, Poynting's theorem can be derived by a Taylor expansion of  $\dot{\mathbf{D}}(\mathbf{r}, t)$  using Eq. (1). The time-averaged energy density reads

$$\langle w(\mathbf{r}, t) \rangle = \frac{1}{2} \varepsilon_0 \partial_{\omega_0} [\omega_0 \varepsilon'(\mathbf{r}, \omega_0)] \langle \mathbf{E}^2(\mathbf{r}, t) \rangle + \frac{1}{2\mu_0} \langle \mathbf{B}^2(\mathbf{r}, t) \rangle \quad (75)$$

in which the notation  $\varepsilon(\mathbf{r}, \omega) = \varepsilon'(\mathbf{r}, \omega) + i\varepsilon''(\mathbf{r}, \omega)$  is employed.  $\langle \dots \rangle$  denotes a time average in which fastly varying terms  $\propto \exp[\pm 2i\omega_0 t]$  are neglected. Throughout this thesis, no dispersion in the magnetic permeability is assumed, although a generalization is straightforward.

Poynting's theorem in the time domain then reads as

$$\partial_t \langle w(\mathbf{r}, t) \rangle = -\nabla \cdot \langle \mathbf{S}(\mathbf{r}, t) \rangle - \varepsilon_0 \omega_0 \varepsilon''(\mathbf{r}, \omega_0) \langle \mathbf{E}^2(\mathbf{r}, t) \rangle , \quad (76)$$

with the Poynting vector  $\mathbf{S}(\mathbf{r}, t) = \mathbf{E}(\mathbf{r}, t) \times \mathbf{H}(\mathbf{r}, t)$ . This relation is derived using the slowly varying envelope approach. Please note that

$$\langle \mathbf{E}^2(\mathbf{r}, t) \rangle = \frac{1}{4} \langle [\mathbf{E}_{\text{env}}(\mathbf{r}, t) e^{-i\omega_0 t} + \text{c.c.}]^2 \rangle = \frac{1}{2} |\mathbf{E}_{\text{env}}(\mathbf{r}, t)|^2$$

has been used. We can also see that the factor 1/2 in Eq. (74) causes some prefactors if one compares time and frequency space representations. For example, the time-averaged Poynting vector simplifies to  $\langle \mathbf{S}(\mathbf{r}, t) \rangle \approx \Re [\mathbf{E}_{\text{env}}(\mathbf{r}, t) \times \mathbf{B}_{\text{env}}^*(\mathbf{r}, t)] / 2\mu_0$  assuming  $\Delta\omega \ll \omega_0$  for an averaging process during the time  $T_{\text{av}}$  for which  $\omega_0 \ll T_{\text{av}}/2\pi \ll \Delta\omega$  holds.

### A.2 Analytical Reflection Coefficients at Nanoantenna Terminations

A lot of the physics of NAs can be understood with the help of simple Fabry-Perot models (Sec. 2.3). At the core of this model is a determination of the reflection coefficient at the termination of the NA, which is the main subject of this section. We have used this approach to find the scaling behaviour of so-called circular NAs made of a stack of different materials [159]. A further investigation of the scaling of slab system is well documented in Ref. [167]. All of these findings are conceptionally based on a generalization of an earlier work of Gordon [156].

The general approach to calculate reflection coefficients of a certain mode at a termination of a NA can be summarized as follows:

1. Determine the electric and magnetic fields of the plasmonic mode under investigation. Express the free-space modes at the termination of the NA as a superposition of modes that offer orthogonality relations to the plasmonic mode.

2. Decompose the fields into “incoming” and “reflected” components. Rewrite the electric and magnetic field with respect to their incoming parts only. This step naturally introduces the reflection coefficient  $r$ .
3. Calculate the components of the modes in free space with respect to the unknown  $r$  via a suitable integration of the electric field tangential to the NA termination.
4. Integrate the product of continuous tangential components of the electric and magnetic fields to determine the reflection coefficient up to a one-dimensional integration.

To illustrate this scheme, we shall derive the reflection coefficient for two different classes of NAs. First, we calculate the reflection coefficient for Hankel-type SPPs of circular NAs (Ref. [159]). Afterwards, the reflection of a plasmonic  $m = 0$  mode of a wire NA is derived. The result is the same as provided by Gordon [157] who, however, did not provide an explicit derivation. The limitations of the method will be outlined as well.

### A.2.1 Circular Nanoantennas

In this section, the complex reflection coefficient for Hankel-type SPPs of circular NAs is derived. For a definition of the geometry see again Fig. 6 (a).

First, we examine radially propagating plasmonic modes supported by the NA and a suitable ansatz for the free-space fields. Afterwards, the Fourier components of the radiating field are calculated. Finally, the continuity of  $H_\varphi^m$  is used to calculate the reflection coefficient integrating  $E_z^m \cdot H_\varphi^m$  at  $\rho = R$ . The derivation corresponds to App. A in Ref. [159] with minor modifications only.

**Plasmonic Modes and Outer Fields** The studied NAs exhibit a piecewise translational symmetry in  $z$ -direction. Thus, the structure consists of several discs which may be denoted by the subscript  $i$  in the following. We assume that the NA supports plasmonic surface modes propagating in radial direction. Hence, at least one of the materials needs to be metallic.

In each layer, one may split the fields into tangential ( $\mathbf{E}_{i,t}$ ,  $\mathbf{H}_{i,t}$ ) and normal components ( $E_{i,z}$ ,  $H_{i,z}$ ) relative to the interface of the discs. Then, the entire dynamic can be calculated using only the normal components. The tangential fields in the  $i$ -th layer are given by [154]

$$\begin{aligned}\mathbf{E}_{i,t} &= \frac{i}{k_\rho^2} [k_{i,z} \nabla_t E_{i,z} - \omega \mu_0 \mu_i \mathbf{e}_z \times \nabla_t H_{i,z}] \text{ and} \\ \mathbf{H}_{i,t} &= \frac{i}{k_\rho^2} [k_{i,z} \nabla_t H_{i,z} + \omega \varepsilon_0 \varepsilon_i \mathbf{e}_z \times \nabla_t E_{i,z}] ,\end{aligned}\tag{77}$$

where  $k_{i,z}$  is the wave vector component in  $z$ -direction and  $\nabla_t$  is the transversal gradient, *i.e.*  $\nabla_t = \mathbf{e}_x \partial_x + \mathbf{e}_y \partial_y$  in Cartesian coordinates. In this formulation, all fields exhibit  $\exp(ik_{i,z}z)$  and  $\exp(-i\omega t)$  dependencies [154]. The radial wave vector

$$k_\rho^2 = \frac{\omega^2}{c^2} \mu_i \varepsilon_i - k_{i,z}^2$$

has to be independent of  $z$  since it is a conserved quantity in all layers. The various plasmonic modes of the NA are thus characterized by different  $k_\rho$  and it is convenient to define

$$\gamma_i = ik_{i,z} \text{ and } k_{\text{SPP}} \equiv k_\rho .$$

In general, the NA may support several modes. Nevertheless, for the sake of simplicity a corresponding index will be suppressed.

Furthermore, we assume transverse-magnetic (TM) modes with  $H_z = 0$  and the materials shall be non-magnetic, *i.e.*  $\mu_i = 1$ . Then

$$\mathbf{H}_{i,t} = \frac{i}{k_{\text{SPP}}^2} \omega \varepsilon_0 \varepsilon_i \mathbf{e}_z \times \nabla_t E_{i,z} = \frac{i}{k_{\text{SPP}}^2} \omega \varepsilon_0 \varepsilon_i \mathbf{e}_z \times \left[ \partial_\rho E_{i,z} \mathbf{e}_\rho + \frac{1}{\rho} (\partial_\varphi E_{i,z}) \mathbf{e}_\varphi \right]. \quad (78)$$

The only nonvanishing normal field component  $E_z$  is described by the scalar two-dimensional Helmholtz equation

$$\Delta_t E_z + k_{\text{SPP}}^2 E_z = 0.$$

Since  $k_{\text{SPP}}$  is a constant throughout the layers, this differential equation generally applies to the plasmonic modes supported by the NA. In rotational symmetry, the latter equation has solutions in terms of Bessel and Neumann functions  $J_m(k_{\text{SPP}}\rho)$  and  $N_m(k_{\text{SPP}}\rho)$  modulus an angular variation of  $\exp(im\varphi)$  which will be denoted by the index  $m$  in the following. For the calculation of the complex reflection coefficient, however, we have to use Hankel functions which describe propagating rather than standing wave fields. They read

$$H_m^{1/2}(k_{\text{SPP}}\rho) \equiv J_m(k_{\text{SPP}}\rho) \pm iN_m(k_{\text{SPP}}\rho)$$

and represent radially outgoing (1) and incoming (2) cylindrical waves in the given time-dependence. Since the fields are given in terms of  $E_z$ , it is convenient to introduce the reflection coefficient  $r_m$  as

$$\begin{aligned} E_z^{m,-}(\rho, z) &= \mathcal{A}_m(k_{\text{SPP}}\rho) \cdot a(z) \quad , \quad \text{with} \\ \mathcal{A}_m(k_{\text{SPP}}\rho) &= H_m^1(k_{\text{SPP}}\rho) + r_m \cdot H_m^2(k_{\text{SPP}}\rho) \end{aligned}$$

where the boundary conditions at the NA termination determine the “mode profile”  $a(z)$  in  $z$ -direction as well as the propagation constant  $k_{\text{SPP}}$ . Furthermore, the superscript “ $-$ ” was used to indicate fields for  $\rho \leq R$ . Likewise, “ $+$ ” will be used for the outer region.

From Eq. (78), the angular component of the magnetic field is given by

$$H_\varphi^{m,-}(\rho, z) = \frac{i\omega\varepsilon_0\varepsilon_i}{\frac{\omega^2}{c^2}\varepsilon_i + \gamma_i^2} \partial_\rho E_z^{m,-}(\rho, z) = \frac{i\omega\varepsilon_0}{k_{\text{SPP}}} \mathcal{B}_m(k_{\text{SPP}}\rho) \varepsilon(z) a(z) \quad (79)$$

with

$$\begin{aligned} \mathcal{B}_m(k_{\text{SPP}}\rho) &\equiv \frac{1}{k_{\text{SPP}}} \partial_\rho \mathcal{A}_m(k_{\text{SPP}}\rho) = DH_m^1(k_{\text{SPP}}\rho) + r_m \cdot DH_m^2(k_{\text{SPP}}\rho) \quad , \\ DH_m^{1/2}(\xi) &\equiv \partial_x H_m^{1/2}(\xi) \quad . \end{aligned}$$

With the determination of  $E_z^{m,-}$  and  $H_\varphi^{m,-}$ , a reasonable ansatz for the fields outside the NA with the same symmetry properties, *i.e.* the same angular modulus  $m$ , can be constructed. For  $\rho \geq R$ , both fields are a superposition of outgoing Hankel-type SPPs whose amplitudes are given by certain Fourier coefficients  $c_m(k_z)$ . For each of these waves, the wave vector in radial direction is given by  $k_\rho^+ = \sqrt{\varepsilon_d k_0^2 - k_z^2}$ . Here, a relative permittivity  $\varepsilon_d$  is assumed in the outer region. With this ansatz, the fields can be represented as

$$\begin{aligned} E_z^{m,+}(\rho, z) &= \int_{-\infty}^{\infty} c_m(k_z) H_m^1\left(\sqrt{\varepsilon_d k_0^2 - k_z^2}\rho\right) e^{ik_z z} dk_z \quad , \\ H_\varphi^{m,+}(\rho, z) &= i \int_{-\infty}^{\infty} c_m(k_z) \frac{\varepsilon_0 \varepsilon_d \omega}{\sqrt{\varepsilon_d k_0^2 - k_z^2}} \cdot DH_m^1\left(\sqrt{\varepsilon_d k_0^2 - k_z^2}\rho\right) e^{ik_z z} dk_z \quad (80) \end{aligned}$$

where the magnetic field follows from Eq. (78).

**Fourier Components of the Free-space Modes** Now we use the continuity of the magnetic field to determine the Fourier components  $c_m(k_z)$ . Since  $\mathcal{B}_m$ , by definition, explicitly depends on  $r_m$ , this will likewise hold for the  $c_m(k_z)$ .

A Fourier transformation for  $\rho \leq R$  yields

$$\int_{-\infty}^{\infty} H_{\varphi}^{m,-}(\rho, z) e^{-ik_z z} dz = \frac{i\omega\varepsilon_0}{k_{SPP}} \mathcal{B}_m(k_{SPP}\rho) \cdot B^-(k_z) \quad \text{with } B^{\pm}(k_z) \equiv \int_{-\infty}^{\infty} \varepsilon(z) a(z) e^{\pm ik_z z} dz.$$

The same operation for the outer region results in

$$\begin{aligned} \int_{-\infty}^{\infty} H_{\varphi}^{m,+}(\rho, z) e^{-ik_z z} dz &= i \int_{-\infty}^{\infty} c_m(k) \frac{\varepsilon_0\varepsilon_d\omega}{\sqrt{\varepsilon_d k_0^2 - k^2}} DH_m^1\left(\sqrt{\varepsilon_d k_0^2 - k^2}\rho\right) \underbrace{\int_{-\infty}^{\infty} e^{i(k-k_z)z} dz}_{2\pi\delta(k-k_z)} dk \\ &= 2\pi i \cdot c_m(k_z) \frac{\varepsilon_0\varepsilon_d\omega}{\sqrt{\varepsilon_d k_0^2 - k_z^2}} \cdot DH_m^1\left(\sqrt{\varepsilon_d k_0^2 - k_z^2}\rho\right). \end{aligned} \quad (81)$$

Matching at  $\rho = R$  gives

$$\frac{i\omega\varepsilon_0}{k_{SPP}} \mathcal{B}_m(k_{SPP}R) B^-(k_z) = 2\pi i \cdot c_m(k_z) \frac{\varepsilon_0\varepsilon_d\omega}{\sqrt{\varepsilon_d k_0^2 - k_z^2}} \cdot DH_m^1\left(\sqrt{\varepsilon_d k_0^2 - k_z^2}R\right).$$

Hence,

$$c_m(k_z) = \frac{\frac{i\omega\varepsilon_0}{k_{SPP}} \mathcal{B}_m(k_{SPP}R) \cdot B^-(k_z)}{2\pi i \cdot \frac{\varepsilon_0\varepsilon_d\omega}{\sqrt{\varepsilon_d k_0^2 - k_z^2}} DH_m^1\left(\sqrt{\varepsilon_d k_0^2 - k_z^2}R\right)} = \frac{\mathcal{B}_m(k_{SPP}R)}{2\pi \cdot \varepsilon_d \cdot k_{SPP}} \cdot \frac{\sqrt{\varepsilon_d k_0^2 - k_z^2} B^-(k_z)}{DH_m^1\left(\sqrt{\varepsilon_d k_0^2 - k_z^2}R\right)}. \quad (82)$$

Note that the Fourier components of the free-space modes are given as explicit result and no further integration is needed. The reason is that we used the same modal expansion in  $z$ -direction, *i.e.* in terms of plane waves that allowed the simplification  $\int_{-\infty}^{\infty} e^{i(k-k_z)z} dz = 2\pi\delta(k-k_z)$  in Eq. (81). This simplification is at the core of the derivation of the reflection coefficient. We will find a similar expression in App. A.2.2 and deduce limitations of the general method at that point.

**Integration over  $E_z^m \cdot H_{\varphi}^m$**  The final step to calculate the reflection coefficient is the integration of the inner and outer  $E_z^m$  using  $H_{\varphi}^{m,-}$  at  $\rho = R$ . Since  $\mathcal{B}_m(k_{SPP}R)$  is a constant, it is sufficient to use the field profile  $\varepsilon(z) \cdot a(z)$ .

First, we find

$$\int_{-\infty}^{\infty} E_z^{m,-}(R, z) \varepsilon(z) a(z) dz = \mathcal{A}_m(k_{SPP}R) \cdot \sigma \quad \text{with } \sigma = \int_{-\infty}^{\infty} a(z)^2 \cdot \varepsilon(z) dz.$$

Performing the same integration over the mode field for  $\rho \geq R$  gives

$$\begin{aligned} \int_{-\infty}^{\infty} E_z^{m,+}(R, z) \varepsilon(z) a(z) dz &= \int_{-\infty}^{\infty} c_m(k_z) H_m^1\left(\sqrt{\varepsilon_d k_0^2 - k_z^2}R\right) \cdot \left(\int_{-\infty}^{\infty} e^{ik_z z} \varepsilon(z) a(z) dz\right) dk_z \\ &= \int_{-\infty}^{\infty} c_m(k_z) H_m^1\left(\sqrt{\varepsilon_d k_0^2 - k_z^2}R\right) \cdot B^+(k_z) dk_z. \end{aligned}$$

We can now equate the last two results to obtain

$$\mathcal{A}_m(k_{SPP}R) \cdot \sigma = \int_{-\infty}^{\infty} c_m(k_z) H_m^1\left(\sqrt{\varepsilon_d k_0^2 - k_z^2}R\right) \cdot B^+(k_z) dk_z.$$

With the known  $c_m(k_z)$  [Eq. (82)], we conclude that

$$\begin{aligned} \mathcal{A}_m(k_{SPP}R) \cdot \sigma &= \frac{\mathcal{B}_m(k_{SPP}R)}{2\pi \cdot \varepsilon_d \cdot k_{SPP}} \cdot I_m \text{ with} \\ I_m &= \int_{-\infty}^{\infty} \frac{H_m^1(\sqrt{\varepsilon_d k_0^2 - k_z^2} R)}{DH_m^1(\sqrt{\varepsilon_d k_0^2 - k_z^2} R)} \cdot \sqrt{\varepsilon_d k_0^2 - k_z^2} B^-(k_z) \cdot B^+(k_z) dk_z. \end{aligned} \quad (83)$$

Using  $\mathcal{A}_m$  and  $\mathcal{B}_m$ , the reflection coefficient [cf. Eq. (12)] can be calculated as

$$r_m = \frac{2\pi \cdot \varepsilon_d \cdot k_{SPP} \sigma \cdot H_m^1(k_{SPP}R) - DH_m^1(k_{SPP}R) \cdot I_m}{-2\pi \cdot \varepsilon_d \cdot k_{SPP} \sigma \cdot H_m^2(k_{SPP}R) + DH_m^2(k_{SPP}R) \cdot I_m}.$$

Note that the result is independent of the amplitude of the mode: A linear rescaling  $a(z) \rightarrow \alpha a(z)$  does not affect the reflection coefficient.

**Reflection Coefficient for a semi-infinite Cylinder** Equation (12) constitutes a rather general result that allows the investigation of the scaling of a large class of circular NAs (Sec. 2.3). Nevertheless it is often possible to find simpler solutions for special geometries. In these cases, the reflection coefficient can be given in a rather simple form and may be compared to known results.

As an example, let us consider the reflection of cylindrical waves on top of a semi-infinite cylinder, which is a limit case in two aspects: For large radii, the reflection coefficient is converging towards that of SPPs for normal incidence at a planar interface [156]. Furthermore, it is equivalent to the reflection of Hankel-type SPPs on cylinders of large thicknesses. Specifically, the dispersion relation takes an explicit form [Eq. (98)], and it is possible to find a more explicit formula for the reflection coefficient.

As a preliminary step, we have to calculate  $B^-(k) \cdot B^+(k)$  and  $\sigma$  using the permittivity  $\varepsilon(z)$  and mode profile  $a(z)$

$$\begin{aligned} B^-(k) \cdot B^+(k) &= \varepsilon_d^2 \varepsilon_m^2 \frac{(\gamma_d + \gamma_m)^2}{(k^2 + \gamma_d^2)(k^2 + \gamma_m^2)}, \\ \sigma &= \frac{\varepsilon_d \varepsilon_m}{2\gamma_d \gamma_m} (\gamma_d \varepsilon_d + \gamma_m \varepsilon_m) = \frac{\varepsilon_d^2 \varepsilon_m^2}{2} \left[ \frac{1}{\varepsilon_m \gamma_m} + \frac{1}{\varepsilon_d \gamma_d} \right]. \end{aligned}$$

Using Eq. (83), we can further simplify

$$\begin{aligned} \mathcal{A}_m(k_{SPP}R) \cdot \frac{\varepsilon_d^2 \varepsilon_m^2}{2} \left[ \frac{1}{\varepsilon_m \gamma_m} + \frac{1}{\varepsilon_d \gamma_d} \right] &= \frac{\mathcal{B}_m(k_{SPP}R)}{2\pi \cdot \varepsilon_d \cdot k_{SPP}} \cdot \int_{-\infty}^{\infty} \frac{H_m^1(\sqrt{\varepsilon_d k_0^2 - k_z^2} R)}{DH_m^1(\sqrt{\varepsilon_d k_0^2 - k_z^2} R)} \\ &\quad \cdot \sqrt{\varepsilon_d k_0^2 - k_z^2} \varepsilon_d^2 \varepsilon_m^2 \frac{(\gamma_d + \gamma_m)^2}{(k^2 + \gamma_d^2)(k^2 + \gamma_m^2)} dk_z \end{aligned}$$

to

$$\mathcal{A}_m(k_{SPP}R) = \frac{\mathcal{B}_m(k_{SPP}R)}{\pi \cdot \varepsilon_d \cdot k_{SPP}} \cdot \frac{(\gamma_d + \gamma_m)^2}{\frac{1}{\varepsilon_m \gamma_m} + \frac{1}{\varepsilon_d \gamma_d}} \int_{-\infty}^{\infty} \frac{H_m^1(\sqrt{\varepsilon_d k_0^2 - k_z^2} R)}{DH_m^1(\sqrt{\varepsilon_d k_0^2 - k_z^2} R)} \frac{\sqrt{\varepsilon_d k_0^2 - k_z^2}}{(k^2 + \gamma_d^2)(k^2 + \gamma_m^2)} dk_z.$$

With

$$\frac{(\gamma_m + \gamma_d)^2}{\frac{1}{\varepsilon_m \gamma_m} + \frac{1}{\varepsilon_d \gamma_d}} = \sqrt{-\varepsilon_d \varepsilon_m} \cdot k_{SPP}^3 \cdot \frac{\varepsilon_m - \varepsilon_d}{\varepsilon_m + \varepsilon_d},$$



which follows directly from the definitions of the  $\gamma_i$ , we obtain

$$\begin{aligned}
\mathcal{A}_m(k_{SPP}R) &= \frac{\mathcal{B}_m(k_{SPP}R)}{\varepsilon_d\pi} \cdot \sqrt{-\varepsilon_d\varepsilon_m} \cdot k_{SPP}^2 \cdot \frac{\varepsilon_m - \varepsilon_d}{\varepsilon_m + \varepsilon_d} \int_{-\infty}^{\infty} \frac{H_m^1(\sqrt{\varepsilon_d k_0^2 - k_z^2}R)}{DH_m^1(\sqrt{\varepsilon_d k_0^2 - k_z^2}R)} \\
&\quad \frac{\sqrt{\varepsilon_d k_0^2 - k_z^2}}{(k^2 + \gamma_d^2)(k^2 + \gamma_m^2)} dk_z \\
&= \frac{\mathcal{B}_m(k_{SPP}R)}{\varepsilon_d\pi} \cdot \sqrt{-\varepsilon_d\varepsilon_m} \cdot \frac{\varepsilon_m\varepsilon_d}{\varepsilon_m + \varepsilon_d} \cdot \frac{\varepsilon_m - \varepsilon_d}{\varepsilon_m + \varepsilon_d} k_0^2 \int_{-\infty}^{\infty} \frac{H_m^1(\sqrt{\varepsilon_d k_0^2 - k_z^2}R)}{DH_m^1(\sqrt{\varepsilon_d k_0^2 - k_z^2}R)} \\
&\quad \frac{\sqrt{\varepsilon_d k_0^2 - k_z^2}}{(k^2 + \gamma_d^2)(k^2 + \gamma_m^2)} dk_z.
\end{aligned}$$

Furthermore, we can relate

$$\pi\sqrt{-\varepsilon_d\varepsilon_m}\mathcal{A}_m(k_{SPP}R) = \mathcal{B}_m(k_{SPP}R) \cdot \varepsilon_p^2 \cdot \left(1 - \frac{\varepsilon_m}{\varepsilon_d}\right) I_m^\infty$$

with the abbreviations

$$\begin{aligned}
I_m^\infty &= \int_{-\infty}^{\infty} \frac{\sqrt{\varepsilon_d - u^2}}{\left(u^2 - \frac{\varepsilon_m^2}{\varepsilon_m + \varepsilon_d}\right)\left(u^2 - \frac{\varepsilon_d^2}{\varepsilon_m + \varepsilon_d}\right)} \cdot \frac{H_0^1(\sqrt{\varepsilon_d - u^2}\frac{\omega}{c}R)}{H_1^1(\sqrt{\varepsilon_d - u^2}\frac{\omega}{c}R)} du, \\
\varepsilon_p &\equiv \frac{\varepsilon_d\varepsilon_m}{\varepsilon_d + \varepsilon_m}.
\end{aligned}$$

Then, the reflection coefficient is given by

$$r_m = \frac{\pi\sqrt{-\varepsilon_d\varepsilon_m} \cdot H_m^1(k_{SPP}R) - DH_m^1(k_{SPP}R) \varepsilon_p^2 \cdot \left(1 - \frac{\varepsilon_m}{\varepsilon_d}\right) I_m^\infty}{-\pi\sqrt{-\varepsilon_d\varepsilon_m} \cdot H_m^2(k_{SPP}R) + DH_m^2(k_{SPP}R) \cdot \varepsilon_p^2 \cdot \left(1 - \frac{\varepsilon_m}{\varepsilon_d}\right) I_m^\infty}.$$

This result has, as expected, similarities to the reflection of SPPs at a planar interface [156].

### A.2.2 Wire Nanoantennas

We have seen how the reflection coefficient can be calculated for circular NAs made of a stack of materials. The theory can be used to predict the resonance positions and widths of these NAs (Fig. 6). Now we may turn to the next educative example, the calculation of the reflection coefficient for metallic wire NAs.

**Mode determination** The first step is the determination of the plasmonic modes of the NA and the free-space modes. We have to use a modal system for both NA and free-space with mutual orthogonality relations. As we shall see later, such orthogonality relations will reduce the complexity of the reflection coefficient determination considerably.

If a physical system exhibits a translational symmetry, Maxwell's equations can be decomposed into transversal and longitudinal components [154]. We assume the  $z$ -axis to be the wire's rotational axis. Then, the longitudinal components of the electric and magnetic fields,  $\psi = E_z$  or  $\psi = H_z$ , follow the two-dimensional Helmholtz equation

$$\begin{aligned}
(\Delta_t + k^2)\psi(\rho, \varphi) &= 0 \text{ with } k^2 = \varepsilon(\omega)\frac{\omega^2}{c^2} - k_z^2 \text{ and} \\
\Delta_t &= \partial_{\rho\rho} + \frac{1}{\rho}\partial_\rho + \frac{1}{\rho^2}\partial_{\varphi\varphi}
\end{aligned} \tag{84}$$

in cylindrical coordinates for a specific frequency  $\omega$ . The solution in  $z$ -direction,  $\exp[\pm ik_z z]$  will be suppressed for visibility in the following calculations as well as the obvious  $\omega$ -dependency of the involved quantities. As we are still assuming non-magnetic media, we also set  $\mu = 1$ .

For modes propagating in positive  $z$ -direction, *i.e.* with  $\exp[ik_z z]$ -dependency, the transversal components can then be readily computed as

$$\begin{aligned} \mathbf{E}_t(\rho, \varphi) &= \frac{i}{k^2} [k_z \nabla_t E_z(\rho, \varphi) - \omega \mu_0 \mathbf{e}_z \times \nabla_t H_z(\rho, \varphi)] \text{ and} \\ \mathbf{H}_t(\rho, \varphi) &= \frac{i}{k^2} [k_z \nabla_t H_z(\rho, \varphi) + \omega \varepsilon_0 \varepsilon \mathbf{e}_z \times \nabla_t E_z(\rho, \varphi)] . \end{aligned} \quad (85)$$

For simplicity, we denote the plasmonic mode in the half-space  $z \leq 0$  with the superscript “-” and all free-space modes with “+”. Parts of the field that are propagating in positive  $z$  direction will be denoted with “i” for incoming and those propagating in the opposite direction with “r” for reflected. Furthermore, we denote the embedding dielectric with a subscript “d” and the domain of the metallic wire with “m”. Since the plasmonic mode under investigation has no  $\varphi$ -dependency ( $m = 0$ ) we may in addition suppress the  $\varphi$  coordinate completely.

We are interested in the plasmonic field of a wire that does only exhibit a longitudinal contribution from the electric field consequently termed transverse-magnetic modes (TM). Those are the most common plasmonic modes [30] but also TE modes can generally occur for thin metallic structures [160]. Equations 84 and 85 are only valid in domains with constant permittivity  $\varepsilon(\omega)$ . So we need to find solutions for  $\psi = E_z$  in each of the domains of interest while respecting the appropriate boundary conditions.

**The  $m = 0$  Plasmonic Mode of a Metallic Wire,  $z \leq 0$**  We now determine the mode profile of a plasmonic mode propagating in positive  $z$  direction that is directly governed by Eq. (85). The mode we are searching for is evanescent inside the metal but also in the dielectric. It is natural to define damping constants  $\gamma_i$  as

$$\gamma_i^2 = k_z^2 - \varepsilon_i \frac{\omega^2}{c^2} = -k_i^2$$

and the solution of  $E_z^{-,i}(\rho)$  is given in terms of the Bessel Functions  $\propto I_0(\gamma_m \rho)$  inside of the metal and  $\propto K_0(\gamma_d \rho)$  in the dielectric. Using

$$H_\varphi^{-,i}(\rho) = \frac{i}{k_i^2} \omega \varepsilon(\rho) \partial_\rho E_z^{-,i}(\rho) \quad (86)$$

for  $\rho > R$  and for  $\rho < R$ , we find the dispersion relation of the  $m = 0$  mode of a wire using the continuity of both fields at  $\rho = R$ . It is an implicit definition using the  $\gamma_i$ 's and called Characteristic Equation

$$\frac{K_1(\gamma_d \cdot R)}{K_0(\gamma_d \cdot R)} \cdot \frac{I_0(\gamma_m \cdot R)}{I_1(\gamma_m \cdot R)} = -\frac{\gamma_d \varepsilon_m}{\gamma_m \varepsilon_d} . \quad (87)$$

This approach also yields explicit formulas for the electric and magnetic fields, namely

$$E_z^{-,i}(\rho) = H_0 \cdot \begin{cases} i \cdot \frac{\gamma_m \cdot I_0(\gamma_m \cdot \rho)}{\omega \varepsilon_m \cdot I_1(\gamma_m \cdot R)} & \rho < R \\ -i \cdot \frac{\gamma_d \cdot K_0(\gamma_d \cdot \rho)}{\omega \varepsilon_d \cdot K_1(\gamma_d \cdot R)} & \rho > R \end{cases} \quad (88)$$

and

$$H_{\varphi}^{-,i}(\rho) = H_0 \cdot \begin{cases} \frac{I_1(\gamma_m \cdot \rho)}{I_1(\gamma_m \cdot R)} & \rho < R \\ \frac{K_1(\gamma_a \cdot \rho)}{K_1(\gamma_a \cdot R)} & \rho > R \end{cases} . \quad (89)$$

Here,  $H_0$  merely acts as a constant to describe the field strength.

For the calculation of the actual wire mode it was rather useful to employ the field component that are continuous at the boundary  $\rho = R$ . When considering the termination to free space, however, it is more convenient to use  $E_{\rho}^{-,i}$  as this field component is continuous at  $z = 0$ . It is given by

$$E_{\rho}^{-,i}(\rho) = \frac{k_z}{\omega \varepsilon(\rho)} \cdot H_{\varphi}^{-,i}(\rho) . \quad (90)$$

**Modes in Free Space,  $z \geq 0$**  Now we are interested in free-field solutions of the two-dimensional Helmholtz equation for  $m = 0$  and find the modal solution

$$\psi_k(\rho) = J_0(k \cdot \rho) \text{ with } k = \sqrt{k_o^2 - k_z^2} \text{ and } k_o^2 = \varepsilon_o \frac{\omega^2}{c^2} .$$

It has to be marked here that  $k$  refers to a continuous modal index. Note that we use the subscript ‘‘o’’ for the dielectric  $\varepsilon_o$  for  $z > 0$ . As the plasmonic modes of the wire are transverse magnetic, we only need to investigate such free-space modes as well. So,  $H_z^+ \equiv 0$  and  $E_{z,k_z}^+(\rho, \varphi, z) = J_0(k \cdot \rho) \exp[ik_z z]$ . This is a solution for a given  $k_z$  (or  $k$ ); any  $m = 0$  solution will be superposition of such modes with certain amplitudes. We may write this superposition as

$$\begin{aligned} E_z^+(\rho, z, \varphi) &= \int_0^{\infty} c(k_z) J_0\left(\sqrt{k_o^2 - k_z^2} \cdot \rho\right) e^{ik_z z} dk_z \text{ or} \\ &= \int_0^{\infty} a(k) J_0(k \cdot \rho) e^{i\sqrt{k_o^2 - k^2} \cdot z} dk , \end{aligned}$$

depending on a description using  $k_z$  or  $k$ . These modes naturally also include evanescent field components for  $k_z > k_o$ . It is obvious that the choice of the boundary at  $z = 0$  simplifies the calculation of the reflection coefficient and we can express  $E_z^+$  at the termination of the wire as

$$E_z^+(\rho) = \int_0^{\infty} a(k) J_0(k \cdot \rho) dk ,$$

suppressing the coordinates  $z$  and  $\varphi$  again. Thus, using Eqs. (86) and (90), we find

$$\begin{aligned} H_{\varphi}^+(\rho) &= \int a(k) \frac{i}{k^2} \varepsilon_o \omega \partial_{\rho} J_0(k \cdot \rho) dk \\ &= -i \int a(k) \frac{\varepsilon_o \omega}{k} J_1(k \cdot \rho) dk \text{ and} \\ E_{\rho}^+(\rho) &= -i \int a(k) \frac{k_z = \sqrt{k_o^2 - k^2}}{k} J_1(k \cdot \rho) dk . \end{aligned}$$

To have some preliminary results comparable to those of Gordon, we may introduce rescaled Fourier components of the free-space field via

$$t(k) = -ia(k) \frac{\varepsilon_o \omega}{k}$$

to arrive at

$$H_{\varphi}^{+}(\rho) = \int_0^{\infty} t(k) J_1(k \cdot \rho) dk \quad \text{and} \quad E_{\rho}^{+}(\rho) = \int_0^{\infty} t(k) \frac{\sqrt{\omega^2 \varepsilon_o - k^2}}{\omega \varepsilon_o} J_1(k \cdot \rho) dk .$$

Now the modes of the wire and in free space are determined in a way that the continuity relations can be employed. To find the relation to the reflection coefficient, the wire field is separated into incoming and reflected components to introduce the reflection coefficient.

**Decomposition of the Incoming and Reflected Fields** We assume that the reflection of the plasmonic mode does not excite other modes of the wire. Then,  $E_z^{-}$  is a superposition of the incident and reflected parts

$$E_z^{-} = E_z^{-,i} + E_z^{-,r} . \quad (91)$$

With the help of this superposition, we can use

$$\begin{aligned} E_z^{-,r} &= -r \cdot E_z^{-,i} \quad \text{to find} \\ E_z^{-,i} \pm E_z^{-,r} &= (1 \mp r) \cdot E_z^{-,i} , \end{aligned} \quad (92)$$

which defines the reflection coefficient of this mode.

For the calculated fields of the plasmonic mode we assumed a propagation in positive  $z$  direction. But of course the reflected mode propagates in negative  $z$  direction which we have to take into account. To do so, we may simply change  $k_z \rightarrow -k_z$  going from incoming to reflected fields.

Using these considerations, we will now express  $E_z^{-}$  and  $H_{\varphi}^{-}$  in terms of the incoming fields. This step introduces the reflection coefficient in a suitable manner. First, regarding  $H_{\varphi}^{-}$ , we find with Eq. 92

$$\begin{aligned} H_{\varphi}^{-,i/r}(\rho) &= \frac{i}{k^2} \omega \varepsilon(\rho) \partial_{\rho} E_z^{-,i/r}(\rho) , \quad \text{so} \\ H_{\varphi}^{-}(\rho) &= H_{\varphi}^{-,i}(\rho) + H_{\varphi}^{-,r}(\rho) = \frac{i}{k^2} \omega \varepsilon(\rho) \partial_{\rho} [E_z^{-,i}(\rho) + E_z^{-,r}(\rho)] \\ &= \frac{i}{k^2} \omega \varepsilon(\rho) \cdot (1 - r) \cdot \partial_{\rho} E_z^{-,i}(\rho) , \quad \text{hence} \\ H_{\varphi}^{-}(\rho) &= (1 - r) \cdot H_{\varphi}^{-,i}(\rho) . \end{aligned}$$

Second, for  $E_{\rho}^{-}$  we deduce

$$\begin{aligned} E_{\rho}^{-,i/r}(\rho) &= \pm \frac{k_z}{\varepsilon(\rho) \omega} H_{\varphi}^{-,i/r}(\rho) , \quad \text{so} \\ E_{\rho}^{-}(\rho) &= \frac{k_z}{\varepsilon(\rho) \omega} [H_{\varphi}^{-,i}(\rho) - H_{\varphi}^{-,r}(\rho)] = \frac{k_z}{\varepsilon(\rho) \omega} \cdot \frac{i}{k^2} \varepsilon(\rho) \omega \partial_{\rho} [E_z^{-,i}(\rho) - E_z^{-,r}(\rho)] \\ &= \frac{ik_z}{k^2} \cdot (1 + r) \cdot \partial_{\rho} E_z^{-,i}(\rho) , \quad \text{which leads to} \\ E_{\rho}^{-}(\rho) &= \frac{k_z}{\varepsilon(\rho) \omega} \cdot (1 + r) \cdot H_{\varphi}^{-,i}(\rho) . \end{aligned}$$

Now we have successfully introduced the reflection coefficient in the expression of the fields for  $z \leq 0$ . The only step that is left to do is to use the continuity of tangential electric and magnetic fields to finally determine the reflection coefficient.

**Free-space Mode Component Determination - Electric Field Continuity** As a first step, the continuity of  $E_{\rho}^{\pm}$  at the wire termination is used. This will provide the unknown Fourier

components  $t(k)$  of the field in free space.

The continuity of  $E_\rho^\pm$  at  $z = 0$  results in

$$(1+r) \cdot \frac{k_z}{\omega \varepsilon(\rho)} \cdot H_\varphi^{-,i}(\rho) = \int_0^\infty t(k) \frac{\sqrt{\omega^2 \varepsilon_o - k^2}}{\omega \varepsilon_o} J_1(k \cdot \rho) dk. \quad (93)$$

An integration of the latter equation using  $J_1(k' \rho) \rho$  yields

$$\begin{aligned} (1+r) \cdot \int_0^\infty \frac{k_z}{\omega \varepsilon(\rho)} \cdot H_\varphi^i(\rho, \varphi) J_1(k' \rho) \rho d\rho &= \\ (1+r) H_0 \frac{k_z}{\omega} \left[ \frac{1}{\varepsilon_m} \int_0^R \frac{I_1(\gamma_m \rho)}{I_1(\gamma_m r_s)} J_1(k' \rho) \rho d\rho \right. & \\ \left. + \frac{1}{\varepsilon_m} \int_R^\infty \frac{K_1(\gamma_d \rho)}{K_1(\gamma_d r_s)} J_1(k' \rho) \rho d\rho \right] &= \int_0^\infty t(k) \frac{\sqrt{\omega^2 \varepsilon_o - k^2}}{\omega \varepsilon_o} J_1(k \rho) J_1(k' \rho) \rho d\rho dk \\ &= t(k) \frac{\sqrt{\omega^2 \varepsilon_o - k^2}}{k \cdot \omega \varepsilon_o}, \end{aligned} \quad (94)$$

where in the last step the so-called closure equation

$$\int_0^\infty J_m(k_1 \cdot \rho) J_m(k_2 \cdot \rho) \rho d\rho = \frac{1}{k_1} \delta(k_1 - k_2) \quad (95)$$

was used.

The remaining parts on the left hand side are

$$\begin{aligned} \int_0^R I_1(\gamma_m \rho) J_1(k \rho) \rho d\rho &= \frac{R}{\gamma_m^2 + k^2} [\gamma_m \cdot I_2(\gamma_m R) J_1(kR) + k \cdot I_1(\gamma_m R) J_2(kR)] \\ \int_R^\infty K_1(\gamma_d \rho) J_1(k \rho) \rho d\rho &= \frac{R}{\gamma_d^2 + k^2} [\gamma_d \cdot J_1(kR) K_2(\gamma_d R) - k \cdot J_2(kR) K_1(\gamma_d R)] \end{aligned}$$

which were calculated using Mathematica [350].

Note that the latter two integrations are the main steps that lead to a one-dimensional integration. Only because the field of the plasmonic mode and the field in free-space were expressed using modes that obey mutual orthogonality relations, we could find a rather explicit expression for the free-space Fourier components  $t(k)$  [Eq. (94)]. If this integration step cannot be accomplished, the final result can only be determined with respect to higher dimensional integrals. In this case, this approach is not very useful and numerical considerations seem more appropriate [109]. Here we find

$$\begin{aligned} t(k) &= (1+r) H_0 \frac{k_z k \cdot \varepsilon_o}{\sqrt{\omega^2 \varepsilon_o - k^2}} \cdot R [A_1(k) + A_2(k)] \text{ with} \\ A_1(k) &= \frac{\gamma_m \cdot I_2(\gamma_m R) J_1(kR) + k \cdot I_1(\gamma_m R) J_2(kR)}{\varepsilon_m \cdot (\gamma_m^2 + k^2) \cdot I_1(\gamma_m R)} \text{ and} \\ A_2(k) &= \frac{\gamma_d \cdot J_1(kR) K_2(\gamma_d R) - k \cdot J_2(kR) K_1(\gamma_d R)}{\varepsilon_d \cdot (\gamma_d^2 + k^2) \cdot K_1(\gamma_d R)}. \end{aligned} \quad (96)$$

The Fourier components  $t(k)$  of the free field are now completely determined with respect to the still unknown reflection coefficient.

**Reflection Coefficient Determination and Magnetic Field Continuity** The closure equation provided a decent simplification of the  $t(k)$  using the continuity of  $E_\rho$ . Now we employ an integration of  $\int E_\rho \cdot H_\varphi \rho d\rho \propto \int H_\varphi^2 / \varepsilon(\rho) \rho d\rho$  to reduce the complexity of the problem as much as

possible. Multiplying  $H_\varphi^\pm$  with  $H_\varphi^{-,i}\rho/\varepsilon(\rho)$  and integrating over  $\rho$ , we have to solve

$$(1-r) \int_0^\infty \frac{1}{\varepsilon(\rho)} H_\varphi^{-,i}(\rho)^2 \rho d\rho = \int_0^\infty t(k) \int_0^\infty J_1(k\rho) \frac{1}{\varepsilon(\rho)} H_\varphi^{-,i}(\rho) \rho d\rho dk.$$

Due to the form of  $H_\varphi^-$  given in Eq. (89), the integral of the left-hand side evaluates to

$$\begin{aligned} \int_0^\infty \frac{1}{\varepsilon(\rho)} H_\varphi^{-,i}(\rho)^2 \rho d\rho &= H_0^2 \cdot \left[ \frac{1}{\varepsilon_m} \int_0^R \left[ \frac{I_1(\gamma_m \rho)}{I_1(\gamma_m R)} \right]^2 \rho d\rho + \frac{1}{\varepsilon_d} \int_R^\infty \left[ \frac{K_1(\gamma_d \rho)}{K_1(\gamma_d R)} \right]^2 \rho d\rho \right] \\ &\equiv \frac{1}{2} \cdot H_0^2 \cdot R^2 [B_1 - B_2] \quad , \text{ with} \end{aligned}$$

$$B_1 = \frac{1}{\varepsilon_m} \frac{I_1(\gamma_m R)^2 - I_0(\gamma_m R) I_2(\gamma_m R)}{I_1(\gamma_m R)^2} \quad \text{and} \quad B_2 = \frac{1}{\varepsilon_d} \frac{K_1(\gamma_d R)^2 - K_0(\gamma_d R) K_2(\gamma_d R)}{K_1(\gamma_d R)^2}.$$

Using Eqs. (96) and (93), we can further identify

$$(1-r) \cdot \frac{1}{2} \cdot H_0^2 \cdot R^2 [B_1 - B_2] = (1+r) \cdot H_0^2 \int_0^\infty \frac{k_z k \cdot \varepsilon_o \cdot R^2}{\sqrt{\omega^2 \varepsilon_o - k^2}} \cdot [A_1(k) + A_2(k)]^2 dk.$$

The latter equation can now be solved for  $r$  to finally yield

$$\begin{aligned} r &= \frac{1-G}{1+G} \quad \text{with} \\ G &= \frac{1}{B_1 - B_2} \int_0^\infty \frac{2 \cdot k_z k \cdot \varepsilon_o}{\sqrt{\omega^2 \varepsilon_o - k^2}} \cdot [A_1(k) + A_2(k)]^2 dk. \end{aligned} \tag{97}$$

The given result is the same as outlined in [157].

Most of the steps that were performed in this section were rather technical. But only the explicit calculation reveals the main steps that enabled to calculate  $r$  in terms of a one-dimensional integration. Namely, a direct the determination of the Fourier components of the free-space modes seems to be the most important part. This is also the reason why an analytical determination of the reflection coefficient for arbitrary terminations of wire NAs would not reduce to a one-dimensional integral.

For instance, if the termination of a wire NA was half-spherical, an expansion of eigenmodes must be done in spherical Bessel functions, whereas the eigenmode of the wire is a cylindrical Bessel function. There is no orthogonality relation between these functions. Hence, the determination of the reflection coefficients for different wire terminations as outlined in our Ref. [109] had to be performed using sophisticated numerical methods. This conclusion also holds for general NA terminations in other geometries. Only if the NA- and free-space-modes can be expressed in eigenfunctions that allow orthogonality relations to the free-space modes, the reflection coefficient can be given due to a one-dimensional integration.

### A.3 Explicit Plasmonic Modes for Layered Structures

Hankel-type plasmonic modes as the ones considered for circular NAs (Sec. 2.3) have the same dispersion relation as those for plane-wave plasmonic modes [161] with the same layer structure. In the following we shall provide the analytic expressions for plasmonic modes used in the main text: for semi-infinite layers, layers with finite thicknesses and structure consisting of two metallic layers separated by a dielectric spacer. We closely follow App. C of Ref. [159].

### A.3.1 Semi-Infinite Layer

The relative permittivity of the semi-infinite layer is described by

$$\varepsilon(z) = \begin{cases} \varepsilon_d & z > 0 \\ \varepsilon_m & z < 0 \end{cases}, \text{ with } \varepsilon'_d \geq 0 \text{ and } \varepsilon'_m < -\varepsilon'_d.$$

In this case, a plasmonic mode exists with the mode profile

$$a(z) = \begin{cases} \varepsilon_m e^{-\gamma_d z} & z \geq 0 \\ \varepsilon_d e^{\gamma_m z} & z \leq 0 \end{cases}, \quad \varepsilon(z) a(z) = \varepsilon_d \varepsilon_m \begin{cases} e^{-\gamma_d z} & z \geq 0 \\ e^{\gamma_m z} & z \leq 0 \end{cases}$$

and the well-known dispersion relation [26, 160]

$$k_{SPP}^2 = \frac{\varepsilon_m \varepsilon_d}{\varepsilon_m + \varepsilon_d} k_0^2 \text{ and } \gamma_i^2 = k_{SPP}^2 - \varepsilon_i k_0^2 = -\frac{\varepsilon_i^2}{\varepsilon_d + \varepsilon_m} k_0^2. \quad (98)$$

By definition, the  $\gamma_{d/m}$  are related to penetration depths of the plasmonic fields  $d_{p,m/d} = (\gamma'_{m/d})^{-1}$ .

### A.3.2 Finite Thickness

For a metallic layer with finite thickness and equivalent embedding above and below, the permittivity is given by

$$\varepsilon(z) = \begin{cases} \varepsilon_d & z > d/2 \\ \varepsilon_m & |z| \leq d/2 \\ \varepsilon_d & z < -d/2 \end{cases}.$$

In this case, there are two transverse magnetic plasmonic modes supported by the structure. They can be described by

$$a_{\pm}(z) = \begin{cases} \varepsilon_m \exp[-\gamma_d(z - \frac{d}{2})] & z > \frac{d}{2} \\ \mp \varepsilon_m \exp[\gamma_d(z + \frac{d}{2})] & z < \frac{d}{2} \\ \varepsilon_d \frac{\text{hyp}_{\mp}(\gamma_m z)}{\text{hyp}_{\mp}(\gamma_m \frac{d}{2})} & |z| \leq \frac{d}{2} \end{cases},$$

where  $\text{hyp}_{\mp}$  refers to the hyperbolic functions  $\sinh$  and  $\cosh$ . The dispersion relation is given by

$$\tanh\left(\gamma_m \frac{d}{2}\right) = -\left[\frac{\gamma_m \varepsilon_d}{\gamma_d \varepsilon_m}\right]^{\pm 1} \text{ with } \gamma_i^2 = k_{SPP}^2 - \varepsilon_i k_0^2.$$

Modes which are odd in  $E_z$ , thus odd in  $a(z)$  may be called even according to the symmetry of the tangential electric field component [26]. The even mode here is denoted by  $a_+(z)$  and corresponds to  $\text{hyp}_-(x) \equiv \sinh(x)$ . An illustration of this mode can be found in Fig. 18 a). For the odd mode, the corresponding conventions hold along with  $\text{hyp}_+(x) \equiv \cosh(x)$ .

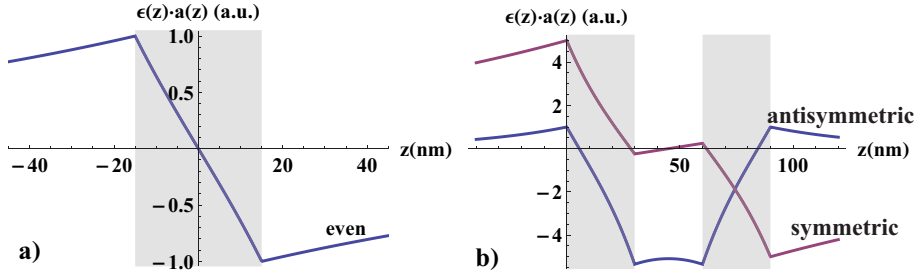


Figure 18: Plasmonic modes of a single metallic layer embedded in air and two metallic layers. The material of the metals is taken to be silver with  $\varepsilon_m \approx -8.8 + 0.3i$  at  $\nu = 625$  THz. In a), one can see  $\varepsilon(z)a(z)$  for the even mode of a metallic layer with 30 nm thickness. The same quantity is outlined in b) for the symmetric and antisymmetric modes of a structure consisting of two silver layers with 30 nm thickness and a 30 nm air cavity in between. These modes can be understood as symmetric and antisymmetric coupling between even single layer modes. The antisymmetric mode is strongly confined inside the cavity. On the contrary,  $E_z$  of the symmetric mode is mostly located outside the metal layers.

### A.3.3 Two metallic Layers

We assume two metallic layers of thickness  $d_m$ , which are separated by some dielectric with thickness  $d_d$ . Furthermore, this simple system is surrounded by the same dielectric, hence

$$\varepsilon(z) = \begin{cases} \varepsilon_d & \text{for } z < 0, d_m < z < d_m + d_d \text{ and } 2d_m + d_d < z \\ \varepsilon_m & \text{for } 0 \leq z \leq d_m \text{ and } d_m + d_d \leq z \leq 2d_m + d_d \end{cases}.$$

The structure supports several plasmonic modes that can be characterized by the mode profile

$$a_i(z) = \begin{cases} \varepsilon_m C_{1+,i} e^{\gamma_{d,i} z} & z < 0 \\ \varepsilon_d C_{2+,i} e^{\gamma_{m,i}(z-d_m)} + \varepsilon_d C_{2-,i} e^{-\gamma_{m,i} z} & 0 \leq z \leq d_m \\ \varepsilon_m C_{3+,i} e^{\gamma_{d,i}(z-d_m-d_d)} + \varepsilon_m C_{3-,i} e^{-\gamma_{d,i}(z-d_m)} & d_m < z < d_m + d_d \\ \varepsilon_d C_{4+,i} e^{\gamma_{m,i}(z-2d_m-d_d)} + \varepsilon_d C_{4-,i} e^{-\gamma_{m,i}(z-d_m-d_d)} & d_m + d_d \leq z \leq 2d_m + d_d \\ \varepsilon_m C_{5-,i} e^{-\gamma_{d,i}(z-2d_m-d_d)} & 2d_m + d_d < z \end{cases},$$

with  $\gamma_{m/d,i}^2 = k_{SPP,i}^2 - \varepsilon_{m/d,i} k_0^2$ . The dispersion relation and the coefficients  $C_{l\pm,i}$  can be found by applying the transfer matrix method [160], which can also be used for more complex stack compositions.

For  $d_d = d_m$ , only two dominating modes have to be considered. The first one is characterized by

$$C_{1+,1} = C_{5-,1}, C_{3+,1} = C_{3-,1}, C_{2-,1} = C_{4+,1} \text{ and } C_{2+,1} = C_{4-,1}.$$

With the conventions used in the previous subsection, it is natural to call this mode antisymmetric, since it is symmetric in  $E_z \propto a(z)$ . The second mode is given due to the relations

$$C_{1+,2} = -C_{5-,2}, C_{3+,2} = -C_{3-,2}, C_{2-,2} = -C_{4+,2} \text{ and } C_{2+,2} = -C_{4-,2}$$

and consequently termed symmetric. The modes are illustrated in Fig. 18 b). However, the explicit coefficients  $C_{l\pm,i}$  and corresponding dispersion relations for  $k_{SPP,i}$  turn out to be too complicated to be presented here.



## A.4 The Influence of the Purcell Effect on the Emitter Efficiency

In the vicinity of a QS it can also be useful to define an efficiency  $\tilde{\eta}$  of the overall emission process if the efficiency of the QS  $\eta_{\text{qs}}$  is smaller than unity:

$$\tilde{\eta} = \frac{P_{\text{rad}}^{\text{na}}}{P_{\text{rad}}^{\text{na}} + P_{\text{nr}}^{\text{na}} + P_{\text{nr}}^{\text{fs}}} . \quad (99)$$

With the intrinsic quantum efficiency of the QS

$$\eta_{\text{qs}} = \frac{P_{\text{rad}}^{\text{fs}}}{P_{\text{rad}}^{\text{fs}} + P_{\text{nr}}^{\text{fs}}} , \quad (100)$$

we may re-formulate Eq. (99) as

$$\tilde{\eta} = \frac{P_{\text{rad}}^{\text{na}}/P_{\text{rad}}^{\text{fs}}}{(P_{\text{rad}}^{\text{na}} + P_{\text{nonrad}}^{\text{na}})/P_{\text{rad}}^{\text{fs}} + (1 - \eta_{\text{qs}})/\eta_{\text{qs}}} \equiv \eta \frac{\eta_{\text{qs}}F}{\eta_{\text{qs}}F + \eta(1 - \eta_{\text{qs}})}$$

Where  $F$  is the Purcell factor [Eq. (36)].

The overall emission efficiency  $\tilde{\eta}$  exhibits two interesting regimes. If the quantum emitter has a high quantum efficiency, *i.e.*  $\eta_{\text{qs}} \approx 1$ , we find that  $\tilde{\eta} \rightarrow \eta$ . But if the QS has a low quantum efficiency ( $\eta_{\text{qs}} \ll 1$ ), then  $\tilde{\eta} \approx \eta\eta_{\text{qs}}F/(\eta_{\text{qs}}F + \eta)$ . In the limit of a strong Purcell effect for which  $\eta_{\text{qs}}F \gg 1$  holds, the efficiency of the QS approaches that of the NA,  $\tilde{\eta} \rightarrow \eta$ . Hence, if one is interested in a highly efficient conversion process, for example in solar cells, the NA efficiency is one of the main quantities of interest. But also the Purcell factor can be beneficial if the QS exhibits a low quantum efficiency.

## A.5 Notes on Non-Frequency Dependencies of $\varepsilon(\omega)$

In most of the outlined studies we assumed that the permittivity of the plasmonic material depends on the frequency only. But in general, there may be further dependencies and we will now briefly discuss why we do not consider them.

We have neglected all thermodynamical aspects, *e.g.* dependencies on the temperature  $T$ , pressure  $p$  and so on. In particular the  $T$ -dependency of metals can be observed in experiments [128]. However, it has been reported that the temperature dependency of  $\varepsilon(\omega)$  for gold at room temperature is rather small [351] and that the permittivity of small silver particles does not change significantly from room temperature  $T_0 \approx 300$  K down to a few K [352].

Characteristic transition processes depending on  $T$  are energetically well separated to the room temperature energy equivalent  $E_0 = k_B \cdot 300 \text{ K} \approx 26 \text{ meV}$ . The Fermi energy for the investigated materials is in the eV regime and much bigger than  $E_0$ . Specifically, we have  $E_F = \{5.51, 5.48 \text{ and } 11.63\} \text{ eV}$  for gold, silver and aluminium, respectively [128]. This implies that at room temperature the density of conduction-band electrons is not significantly altered.

Other low-energy transitions are also energetically separated but the argumentation is a bit more involved. At low temperatures, strong electron-phonon coupling (superconductivity) [128] and electron-electron scattering becomes more important [353]. The Debye temperature  $\Theta$  is not only a characteristic temperature for thermal properties of metals, but also for  $\varepsilon(\omega)$  [354].  $\Theta$  is given by  $\{165, 225 \text{ and } 428\} \text{ K}$  for gold, silver and aluminium [128]. Thus,  $k_B\Theta$  is energetically well separated from  $E_0$  for gold and silver.

For aluminium, however,  $\Theta > T_0$  and another characteristic temperature below  $T_0$  has to be found. Aluminium undergoes a drastic change in the material properties at the so-called critical temperature  $T_c \approx 1.2 \text{ K} \ll T_0$  for which a phase transition to a superconducting state is achieved

[355]. Aluminium-epoxy composites show a very small temperature dependence around 300 K for frequencies  $\nu \gg 1$  MHz [356]. Hence we may assume that pure aluminium also has a very small dependency on  $T$ . With all these experimental results and theoretical considerations, we can assume that the permittivity of metals depends only weakly on their temperature for  $T \approx T_0$  and we can safely ignore this effect.

The structure of the material and impurities have an influence on the material, too [128]. A comparison of permittivity measurements by different research groups has shown a small variation of  $\varepsilon(\omega)$  for gold, which suggests that the structure, *i.e.* crystalline or amorphous, is not a crucial factor [357]. On the other hand, impurities have to be accounted for. They often depend on the actual fabrication process and can be incorporated into theoretical considerations by effective permittivity models [57].

Furthermore, if characteristic sizes of nanoparticles are below or comparable the mean free path length of the material's conduction electrons, its optical properties can be drastically altered [358, 359]. In this case, finite-size effects have to be accounted for, *i.e.* by a phenomenological increase of the imaginary part of  $\varepsilon(\omega)$ , which may increase the particle's absorption considerably [360]. Hence, finite-size effects may also alter the efficiencies  $\eta$  of NAs. Since  $\eta$  is an important quantity for single-photon sources, we phenomenologically incorporate finite-size effects in Sec. 5.

## B Quantum Considerations

In 1885, Balmer found that the visible hydrogen spectrum lines are governed by a very simple formula, namely

$$\frac{1}{\lambda_n} = R_\infty \left( \frac{1}{2^2} - \frac{1}{n^2} \right) \text{ where } R_\infty = \frac{m_e e^4}{8\varepsilon_0^2 h^3 c} \approx 1.097 \cdot 10^7 m^{-1}$$

is the Rydberg constant, which was at that time only known as numerical value and is now the most precisely determined physical constant [361]. According to Bohr's model, these lines could be interpreted as transitions between discrete energy levels of the atom. Along with the explanations of the black-body radiation by Planck in 1900 [362] and of the photoelectric effect by Einstein in 1905 [363], all these findings lead to the development of quantum mechanics.

Although Feynman is probably correct stating "I think I can safely say that nobody understands quantum mechanics." [364], quantum physics largely contributed to our understanding of nature. The list of contributors reads like the who-is-who of physics of the early 20<sup>th</sup> century including such illustre people as Heisenberg, de Boglie, Schrödinger, Born, Dirac and Pauli just to name a few aside from those already mentioned. In this section we shall outline some quantum calculations that are needed to understand the results of the main text.

### B.1 Notes on Fermi's Golden Rule

In this section we shall calculate the transition rates of a QS in first order perturbation theory following Ref. [92]. The result is at the core of our semiclassical calculations and formally known as Fermi's Golden Rule.

If a QS is prone to the action of a time-varying potential  $V(t)$ , perturbative approaches are the first choice if the evolution of the QS can be suitably formulated in terms of a perturbative expansion. In the following we review this ansatz that we used to calculate the action of an external electromagnetic field on the QS (Sec. 2.4.1).

#### The Interaction Picture

A convenient way to treat time-dependent perturbations is the so-called interaction picture in which a unitary transformation is used to calculate all observables depending on the transformed potential  $V(t)$ . We may start with a time-dependent Hamiltonian given by a part  $H_0$  responsible for the isolated QS evolution and the aforementioned time-varying interaction potential  $V(t)$  as

$$H(t) = H_0 + V(t) .$$

In the Schrödinger picture, Schrödinger's equation

$$i\hbar\partial_t |\psi(t)\rangle = H(t) |\psi(t)\rangle \tag{101}$$

describes the evolution of the QS, where  $|\psi(t)\rangle$  is the wave function in the usual Dirac notation. The transformation to the interaction picture is then performed by the following unitary transformation:

$$\begin{aligned} |\psi_I(t)\rangle &= e^{itH_0/\hbar} |\psi(0)\rangle \text{ and} \\ V_I(t) &= e^{itH_0/\hbar} V(t) e^{-itH_0/\hbar} , \end{aligned}$$

where the subscript “I” denoted interaction picture. The rule applied to  $V(t)$  holds for any operator. In the interaction picture, Schrödinger’s equation reads as

$$i\hbar\partial_t|\psi_I\rangle = i\hbar\partial_t e^{itH_0/\hbar}|\psi\rangle = e^{itH_0/\hbar}\underbrace{\{i\hbar\partial_t|\psi\rangle - H_0|\psi\rangle\}}_{V(t)|\psi} = V_I(t)|\psi_I\rangle, \quad (102)$$

the so-called Tomonaga-Schwinger equation. To calculate the transition probabilities at certain times, it is necessary to solve Eq. (102). Formally, one finds

$$|\psi_I(t)\rangle = S(t)|\psi_I(0)\rangle \text{ with} \quad (103)$$

$$S(t) = T \exp\left\{\frac{1}{i\hbar}\int_0^t V_I(t') dt'\right\} \quad (104)$$

where  $T$  denotes the time ordering operator and the propagator that realizes the time-evolution of the QS is a version of the famous  $S$ -matrix. With the help of Eq. (102), we obtained a reformulation of the interaction problem that we can solve perturbatively by an expansion of  $S$ .

### First-Order Perturbation Theory

Expanding the exponential in  $S$  up to the first order, we find that

$$S(t) \approx 1 + \frac{1}{i\hbar}\int_0^t V_I(t') dt'. \quad (105)$$

If a QS is initially in the state  $|\psi_I(0)\rangle = |n\rangle$ , we can calculate the transition amplitudes to another state  $|m\rangle$  using Eq. (105) as

$$\begin{aligned} A_{n\rightarrow m}(t) &= \langle m|\psi_I(t)\rangle = \langle m|S(t)|n\rangle \approx \underbrace{\langle m|n\rangle}_{=0} + \frac{1}{i\hbar}\int_0^t \langle m|V_I(t')|n\rangle dt' \\ &= \frac{1}{i\hbar}\int_0^t \langle m|e^{it'H_0/\hbar}V(t')e^{-it'H_0/\hbar}|n\rangle dt' = \frac{1}{i\hbar}\int_0^t e^{i\omega_{mn}t'}V_{mn}(t') dt', \end{aligned} \quad (106)$$

where

$$\hbar\omega_{mn} \equiv E_m - E_n, \text{ and } V_{mn}(t) = \langle m|V(t)|n\rangle.$$

The  $V_{mn}(t)$  are often called time-dependent matrix elements. The interaction potential  $V(\mathbf{r}, t)$  can often be written in the form of a slowly varying envelope and an oscillation at a frequency  $\omega_0$ ,

$$V(t) = V_{\text{env}}(t)e^{-i\omega_0 t} + V_{\text{env}}^*(t)e^{i\omega_0 t}. \quad (107)$$

In that case the time-dependent transition amplitudes read

$$A_{n\rightarrow m}(t) = \frac{1}{i\hbar}\int_0^t e^{i\omega_{mn}t'} \left[ V_{\text{env},mn}(t')e^{-i\omega_0 t'} + V_{\text{env},nm}^*(t')e^{i\omega_0 t'} \right] dt' \quad (108)$$

where  $V_{\text{env},mn}(t) = \langle m|V_{\text{env}}(t)|n\rangle$ . If we assume that  $V_{\text{env}}(t)$  vanishes for  $t < 0$ , we can extend the integral from 0 to  $-\infty$  and the integral is basically a truncated Fourier transform of  $V_{\text{env},mn}(t)$  at  $\omega = \omega_{mn} - \omega_0$  plus its conjugate. So, depending on  $V_{\text{env}}(t)$ , only a small part of the spectrum  $V_{\text{env},mn}(\omega)$  around  $\omega = 0$  contributes to the integral, since characteristic frequencies of  $V_{\text{env}}(t)$  are assumed to be much smaller than  $\omega_0$ .

For example, if a slow turning-on of the potential via

$$V_{\text{env}}(t) = \mathcal{V}_{\text{env}}e^{\eta t/2} \text{ with } \eta \ll \omega_0$$

is realized, the integration in Eq. (108) can again be considered from  $t = -\infty$  because of exponentially damped values for  $t < 0$ . We find

$$A_{n \rightarrow m}(t) \approx -\frac{1}{\hbar} \left[ \frac{\mathcal{V}_{\text{env},mn} e^{-i\omega_0 t}}{\omega_{mn} - \omega_0 + i\eta/2} + \frac{\mathcal{V}_{\text{env},nm}^* e^{i\omega_0 t}}{\omega_{mn} + \omega_0 + i\eta/2} \right] e^{i\omega_{mn} t + \eta t/2}.$$

The time-dependent rate at which the QS is transferred from  $|n\rangle$  to  $|m\rangle$  is then just given as the time derivative of the transition probability  $|A_{n \rightarrow m}|^2$ . In our particular case, where  $\omega_0$  merely enters as a parameter, we find

$$\begin{aligned} \Gamma_{n \rightarrow m}(t) &= \partial_t |A_{n \rightarrow m}(t)|^2 \\ &\approx \frac{1}{\hbar^2} |\mathcal{V}_{\text{env},mn}|^2 e^{\eta t} \left( \frac{\eta}{(\omega_{mn} - \omega_0)^2 + (\eta/2)^2} + \frac{\eta}{(\omega_{mn} + \omega_0)^2 + (\eta/2)^2} \right). \end{aligned} \quad (109)$$

Note that we have neglected terms oscillating at  $\pm 2i\omega_0 t$  and used  $|\mathcal{V}_{\text{env},mn}| = |\mathcal{V}_{\text{env},mn}^*|$ . Similar expressions to Eq. (109) can be found using different time dependencies of  $V_{\text{env}}(t)$ . The results are always comparable and we find important insights to understand the transition rates of QSS subject to a time-varying interaction in first-order perturbation theory, namely

1.  $\Gamma_{n \rightarrow m} \propto |\mathcal{V}_{\text{env},mn}|^2$ : A transition from  $|n\rangle$  to state  $|m\rangle$  can only be caused by the corresponding squared absolute of the matrix element  $\mathcal{V}_{\text{env},mn} = \langle m | \mathcal{V}_{\text{env}} | n \rangle$ .

2. The slowly varying part of the interaction potential enters quadratically into the corresponding transition rate. This behavior may be interpreted as the slowly varying intensity of an external field.

3. If the switching process is much slower than the oscillation of the interaction, a first-order transition may only take place if the interaction oscillates at a transition frequency of the quantum system. In the studied case we can see this directly for  $\eta \ll \omega_0$ . In particular,

$$\frac{\eta}{(\omega_{mn} \pm \omega_0)^2 + (\eta/2)^2} \rightarrow 2\pi \delta(\omega_{mn} \pm \omega_0). \quad (110)$$

4. Equation (109) describes relaxation and absorption caused by the interaction since both signs in the term  $\omega_{mn} \pm \omega_0$  are present.

Consequentially, in the limit of  $\eta \rightarrow 0$ , *i.e.* a slow switching on, the transitions rates can be written as

$$\Gamma_{n \rightarrow m}(t) \rightarrow \frac{2\pi}{\hbar^2} |\mathcal{V}_{\text{env},mn}|^2 [\delta(\omega_{mn} + \omega_0) + \delta(\omega_{mn} - \omega_0)]. \quad (111)$$

This result holds if the interaction potential is given by the assumed  $V(t) = \mathcal{V}_{\text{env}} \exp[\eta t/2 + i\omega_0 t] + H.c.$  in the limit  $\eta \rightarrow 0$ . However, Eq. (111) is rather general since the limiting process of Eq. (110) is not specific to the particular example studied here and often already called Fermi's Golden Rule after Dirac and Wentzel.

For an interaction potential with slowly varying amplitude [Eq. (107)], the transition rates depend on the Fourier spectrum of the amplitude  $V_{\text{env}}(\mathbf{r}, \omega)$  which we shall calculate now. Following Eq. (108), the absorption amplitude from state  $|n\rangle$  to state  $|m\rangle$  is given by

$$A_{n \rightarrow m}^+(t) = \frac{1}{i\hbar} \int_0^t e^{i\omega_{mn} t'} V_{\text{env},mn}(t') e^{-i\omega_0 t'} dt'. \quad (112)$$

For simplicity, we only consider the positive frequency of the transition amplitude denoted by a superscript “+”. This part of  $A_{n \rightarrow m}$  is related to absorption processes by the QS. The Fourier

transform of  $V_{\text{env},mn}(t')$  may be used to reformulate Eq. (112) as

$$A_{n \rightarrow m}^+(t) = \frac{1}{i\hbar} \int_0^t \int_{-\infty}^{\infty} e^{-i\omega t'} e^{i\omega_{mn} t'} V_{\text{env},mn}(\omega) e^{-i\omega_0 t'} d\omega dt' .$$

It may be assumed that  $V(\mathbf{r}, t) = 0$  for  $t < 0$ , such that the time integration can be extended to  $-\infty$ . Then, by interchanging the order of integrations, we find

$$\begin{aligned} A_{n \rightarrow m}^+(t) &= \frac{1}{i\hbar} \int_{-\infty}^{\infty} V_{\text{env},mn}(\omega) \int_{-\infty}^t e^{-i(\omega_0 + \omega - \omega_{mn})t'} dt' d\omega \\ &= \frac{1}{\hbar} \int_{-\infty}^{\infty} V_{\text{env},mn}(\omega) \frac{e^{-i(\omega_0 + \omega - \omega_{mn})t}}{\omega_0 + \omega - \omega_{mn}} d\omega \text{ or} \\ &= \frac{t}{\hbar} \int_{-\infty}^{\infty} V_{\text{env},mn}(\omega + \omega_{mn} - \omega_0) \frac{e^{-i\omega t}}{\omega t} d\omega . \end{aligned} \quad (113)$$

Equation (113) establishes a direct link between the Fourier transform of the slowly varying envelope and the absorption amplitude. Since the absorption rate is given by  $\Gamma_{n \rightarrow m}^+ = \partial_t |A_{n \rightarrow m}^+(t)|^2$ , a direct evaluation of the integral in Eq. (113) for general  $V_{\text{env},mn}(t)$  is not sensible because of the need to derive an absolute value. But we may still interpret our result for certain limits. In the limit of  $t \rightarrow \infty$ , the time integration in Eq. (113) yields  $2\pi\delta(\omega_0 + \omega - \omega_{mn})$  and the result will be  $A_{n \rightarrow m}^+(t \rightarrow \infty) = 2\pi/\hbar V(\omega_{mn} - \omega_0)$ .

On the other hand, the function  $\exp[-i\omega t]/\omega t$  in Eq. (113) is strongly peaked around  $\omega = 0$ . Thus, for  $t \gg 2\pi/\omega_0$ , only a small part of the spectrum of  $V_{\text{env},mn}(t)$  will contribute. These considerations lead to the final form of Fermi's Golden Rule [Eq. (15)]. However, a further discussion of the limitations and implications of Fermi's Golden Rule is beyond the scope of this work. For thorough interpretations see *e.g.* Refs. [365,366].

## Second Order Perturbation Theory

The expansion of  $S(t)$  is not limited to a linear term in the interaction potential. If first order transitions are not allowed or the perturbations are strong, one has to consider the second term as well:

$$S(t) \approx 1 + \frac{1}{i\hbar} \int_0^t V_I(t') dt' + \left(\frac{1}{i\hbar}\right)^2 \int_0^t \int_0^\tau V_I(t') V_I(\tau) d\tau dt' .$$

The transition amplitude in second order perturbation theory is given by

$$\begin{aligned} A_{n \rightarrow m}^{(2)} &\approx \left(\frac{1}{i\hbar}\right)^2 \int_0^t \int_0^\tau \langle m | V_I(t') V_I(\tau) | n \rangle d\tau dt' \\ &= \left(\frac{1}{i\hbar}\right)^2 \sum_k \int_0^t \int_0^\tau e^{it'\omega_{mk}} V_{mk}(t') e^{i\tau\omega_{kn}} V_{kn}(\tau) d\tau dt' . \end{aligned}$$

One can interpret this result as an excitation of  $|m\rangle$  using all other eigenstates of the system. Second-order interactions may be generally attributed to two-photon processes and such processes might also occur close to NAs. Multiphoton processes are usually studied in the context of nonlinear optics and describe effects such as optical bistability, higher-harmonic generation and frequency mixing [185,367].

## B.2 Discriminating Electric and Magnetic Coupling

In Sec. 2.4.2 we determined the potential that governs the interaction of a charged particle and the electromagnetic field as

$$V_{\text{em}}(\mathbf{r}, t) = -\frac{e}{m} \mathbf{A}(\mathbf{r}, t) \cdot \mathbf{p} .$$

We shall now derive the decomposition of  $V_{\text{em}}(\mathbf{r}, t)$  into electric and magnetic contributions.

The Coulomb gauge is most convenient in a non-relativistic description of electromagnetic fields. If no charges are present, one can always assume the “electrostatic” potential to vanish. Then, the electromagnetic fields are determined by

$$\mathbf{E}(\mathbf{r}, t) = -\partial_t \mathbf{A}(\mathbf{r}, t) \quad \text{and} \quad \mathbf{B}(\mathbf{r}, t) = \nabla \times \mathbf{A}(\mathbf{r}, t) .$$

To differ between electric and magnetic interaction, we split  $\mathbf{A}(\mathbf{r}, t) \cdot \mathbf{p}$  into two parts:

$$\begin{aligned} \mathbf{A}(\mathbf{r}, t) \cdot \mathbf{p} &= \frac{im}{\hbar} \mathbf{A}(\mathbf{r}, t) \cdot [H_0, \mathbf{r}] \\ &= \frac{im}{\hbar} \{ \mathbf{A}(\mathbf{r}, t) \cdot H_0 \mathbf{r} - \mathbf{A}(\mathbf{r}, t) \cdot \mathbf{r} H_0 + H_0 \mathbf{A}(\mathbf{r}, t) \cdot \mathbf{r} - H_0 \mathbf{A}(\mathbf{r}, t) \cdot \mathbf{r} \} \\ &= \frac{im}{\hbar} \{ [H_0, \mathbf{A}(\mathbf{r}, t) \cdot \mathbf{r}] + [\mathbf{A}(\mathbf{r}, t), H_0] \cdot \mathbf{r} \} . \end{aligned}$$

The first term is then given by

$$V_e(\mathbf{r}, t) = -e \frac{i}{\hbar} [H_0, \mathbf{A}(\mathbf{r}, t) \cdot \mathbf{r}] , \quad (114)$$

and we shall make a small calculation to prove that it is the electric part of the interaction. To do so, let us go back to Eq. (106), where the transition amplitudes  $A_{n \rightarrow m}$  are given for an external potential  $V(t)$  in first order perturbation.

Using  $V_e(t)$  from Eq. (114), a small calculation for a time-harmonic field shows

$$\begin{aligned} A_{n \rightarrow m}(t) &= -\frac{e}{\hbar^2} \int_0^t \langle m | e^{it'H_0/\hbar} [H_0, \mathbf{A}(\mathbf{r}, t') \cdot \mathbf{r}] e^{-it'H_0/\hbar} | n \rangle dt' \\ &= \frac{e}{i\hbar} \int_0^t \langle m | (-i\omega_{mn}) \{ \mathbf{A}(\mathbf{r}) e^{-i\omega_0 t'} + c.c. \} \cdot \mathbf{r} | n \rangle e^{i\omega_{mn} t'} dt' . \end{aligned} \quad (115)$$

Here,  $H_0 | n \rangle = \hbar\omega_n | n \rangle$  and  $\omega_{mn} = \omega_m - \omega_n$  have been used again. Because of Fermi’s Golden Rule, we may replace  $\omega_{mn}$  with  $\pm\omega_0$ . Then it is obvious that the electric coupling yields a Fourier transform of  $-i\omega \mathbf{A}(\mathbf{r}, \omega) \cdot \mathbf{r} = \mathbf{E}(\mathbf{r}, \omega) \cdot \mathbf{r}$ , so

$$V_e(\mathbf{r}, t) = -e \mathbf{E}(\mathbf{r}, t) \cdot \mathbf{r} . \quad (116)$$

Let us now consider the second term, which presumably is attributed to the magnetic coupling. It is easy to see that

$$\begin{aligned} [\mathbf{A}(\mathbf{r}, t), H_0] &= \frac{1}{2m} \{ \mathbf{A}(\mathbf{r}, t) \mathbf{p}^2 - \mathbf{p}^2 \mathbf{A}(\mathbf{r}, t) \} = -\frac{\hbar^2}{2m} \Delta \mathbf{A}(\mathbf{r}, t) \\ &= -\frac{\hbar^2}{2m} [\nabla \nabla \cdot \mathbf{A}(\mathbf{r}, t) - \nabla \times \nabla \times \mathbf{A}(\mathbf{r}, t)] = \frac{\hbar^2}{2m} \nabla \times \mathbf{B}(\mathbf{r}, t) , \quad \text{so} \\ [\mathbf{A}(\mathbf{r}, t), H_0] \cdot \mathbf{r} &= \frac{\hbar^2}{2m} \nabla \times \mathbf{B}(\mathbf{r}, t) \cdot \mathbf{r} = \frac{\hbar^2}{2m} \mathbf{B}(\mathbf{r}, t) \cdot (\mathbf{r} \times \nabla) \\ &= \frac{\hbar}{-i2m} \mathbf{B}(\mathbf{r}, t) \cdot \mathbf{L} = i \frac{\mu_B}{e} \mathbf{B}(\mathbf{r}, t) \cdot \mathbf{L} \end{aligned}$$

where  $\mu_B = e\hbar/2m$ ,  $\mathbf{p} = -i\hbar\nabla$  and  $\mathbf{L} = \mathbf{r} \times \mathbf{p}$  was used. So, it is natural to define

$$V_m(\mathbf{r}, t) = \frac{\mu_B}{\hbar} \mathbf{B}(\mathbf{r}, t) \cdot \mathbf{L} \quad (117)$$

as the magnetic coupling.

Note that Eqs. (114) and (22) include the coupling of all multipole moments of the electromagnetic field to the QS [78].

### B.3 Semiclassical Electric Multipole Coupling in the Quasistatic Regime

Starting from Eq. (21) ( $V_e(\mathbf{r}, t) = -e\mathbf{E}(\mathbf{r}, t) \cdot \mathbf{r}$ ) we outlined a theory to describe the interaction of a semiclassical electric field with a QS based on the local multipole coefficients of the electric field (Sec. 4). Unfortunately, a multipole decomposition is often quite involved because vectorial character of the electromagnetic fields. It is worth to ask whether a description in terms of a scalar quasistatic theory can be formulated.

This approach might be justified from a fundamental point of view: If a classical picture of a hydrogen's atom electron is considered within Bohr's model, one may attribute it an angular momentum of  $L \stackrel{!}{=} n\hbar = mvr$ . This angular momentum implies a characteristic velocity  $v_c = \hbar/ma_0$  and likewise a characteristic time scale  $t_c = ma_0^2/\hbar = a_0/\alpha c \approx 2.4 \cdot 10^{-17} s$ . On the other hand, for visible light the smallest typical timescale is that for  $\lambda_{\text{violet}} \approx 425 \text{ nm}$  which corresponds to a typical time of  $t_{\text{light}} \approx 1.25 \cdot 10^{-15} s$ , *i.e.*  $t_c \ll t_{\text{light}}$ .

Hence, the electron will an almost static field compared to its characteristic time scales. This is also the reason why short laser pulses are needed to study the dynamics of QSs. Furthermore, since  $\langle r \rangle \approx a_0 \ll \lambda_{\text{violet}}$ , retardation effects along the QS do not play any significant role. Overall it seems justified to use quasistatic solutions to describe the coupling of the electromagnetic field to QSs. Note that the quasistatic potential  $\phi(\mathbf{r}, t)$  might vary on length scales much smaller than  $\lambda_{\text{violet}}$  such that dipole-forbidden transitions as discussed in Sec. 4 are included within the quasistatic description.

In the quasistatic limit a quasistatic potential  $\phi(\mathbf{r}, t)$  interacts with the QS. This potential obeys Laplace's equation  $\Delta\phi(\mathbf{r}, t) = 0$ . In the vicinity of  $r = 0$ ,  $\phi(\mathbf{r}, t)$  can be expanded according to

$$\phi(\mathbf{r}, t) = T(t) \sum_{l=0}^{\infty} \sum_{m=-l}^l \tilde{p}_{lm} \sqrt{\frac{(l-m)!}{(l+m)!}} r^l P_l^m(\cos\theta) \exp(im\varphi) + c.c. \quad (118)$$

The coefficients  $\tilde{p}_{lm} \in \mathbb{C}$  denote multipole coefficients and characterize the classical electric field. Because of the complex nature of the  $\tilde{p}_{lm}$  and of  $T(t)$  a complex conjugate of  $\phi(\mathbf{r}, t)$  had to be introduced. The semiclassical quasistatic interaction of a QS with the electric field is then governed by

$$H = H_0 + V_e^{\text{static}}(\mathbf{r}, t) = H_0 + e\phi(\mathbf{r}, t) \quad .$$

Within this framework of a semiclassical quasistatic interaction we can derive the relation of the coefficients  $\tilde{p}_{lm}$  to their fully relativistic counterparts  $p_{ml}$  which were introduced in Sec. 4.2.



### B.3.1 Scale Coefficients between Mie-Theory and Quasistatic Approximation

Within the quasistatic theory, the radial component of the electric field is given as

$$\begin{aligned} E_r(\mathbf{r}, t) &= -[\nabla\phi(\mathbf{r}, t)] \mathbf{e}_r \\ &= -T(t) \sum_{l=0}^{\infty} \sum_{m=-l}^l \tilde{p}_{lm} \sqrt{\frac{(l-m)!}{(l+m)!}} l r^{l-1} P_l^m(\cos\theta) e^{im\varphi} + c.c. \end{aligned}$$

In comparison, the radial component of the field incident on a sphere in Mie-Theory reads as [153]

$$E_r(\mathbf{r}, t) = -T(t) \sum_{l=1}^{\infty} \sum_{m=-l}^l p_{lm} i^{l+1} l(2l+1)(l+1) \frac{(l-m)!}{(l+m)!} \frac{j_l(kr)}{kr} P_l^m(\cos\theta) \exp(im\varphi) + c.c..$$

Using the asymptotic behaviour of the spherical Bessel function  $j_l(kr)$  for  $kr \rightarrow 0$ ,

$$j_l(kr) \rightarrow \frac{(kr)^l}{1 \cdot 3 \cdot \dots \cdot (2l+1)},$$

one may deduce

$$E_r(\mathbf{r}, t) \approx -T(t) \sum_{l=1}^{\infty} \sum_{m=-l}^l p_{lm} i^{l+1} \frac{l(l+1)}{1 \cdot 3 \cdot \dots \cdot (2l-1)} \frac{(l-m)!}{(l+m)!} (kr)^{l-1} P_l^m(\cos\theta) e^{im\varphi} + c.c..$$

The latter equation is a quasistatic approximation to the fully relativistic case in terms of the coefficients  $p_{lm}$ . Comparing the radial parts of the electric field,

$$\tilde{p}_{lm} = i^{l+1} \frac{l+1}{1 \cdot 3 \cdot \dots \cdot (2l-1)} \sqrt{\frac{(l-m)!}{(l+m)!}} k^{l-1} p_{lm}.$$

The latter equation provides the connection between the electrodynamic coupling  $V_e(\mathbf{r}, t) = -e\mathbf{E}(\mathbf{r}, t) \cdot \mathbf{r}$  and its quasistatic counterpart  $V_e^{\text{static}}(\mathbf{r}, t) = e\phi(\mathbf{r}, t)$  in regards to their respective multipole coefficients.

## B.4 Steady-State Analysis of a Three-Level System

In Sec. 4.4 we used

$$\begin{aligned} \dot{n}_0 &= \gamma_{10} \cdot n_1 - \Gamma_{02} \cdot n_0, \\ \dot{n}_1 &= \gamma_{21} \cdot n_2 - \gamma_{10} \cdot n_1, \text{ and} \\ \dot{n}_2 &= \Gamma_{02} \cdot n_0 - \gamma_{21} \cdot n_2, \end{aligned} \tag{119}$$

as rate equations of a three-level system.

Assuming a steady state with  $\dot{n}_i = 0$ , one may eliminate  $n_0$  and  $n_2$  in favour of  $n_1$ :

$$n_0 = \frac{\gamma_{10}}{\Gamma_{02}} \cdot n_1, \text{ hence } n_2 = \frac{\Gamma_{02}}{\gamma_{21}} \cdot n_0 = \frac{\Gamma_{02}}{\gamma_{21}} \cdot \frac{\gamma_{10}}{\Gamma_{02}} \cdot n_1.$$

Due to probability conservation,  $n_0 + n_1 + n_2 = 1$  holds and we find

$$\begin{aligned} 1 = n_0 + n_1 + n_2 &= \left( \frac{\gamma_{10}}{\Gamma_{02}} + 1 + \frac{\Gamma_{02}}{\gamma_{21}} \cdot \frac{\gamma_{10}}{\Gamma_{02}} \right) n_1, \text{ and thus} \\ n_1 &= \frac{\gamma_{21} \Gamma_{02}}{\gamma_{10} \gamma_{21} + \gamma_{21} \Gamma_{02} + \gamma_{10} \Gamma_{02}}. \end{aligned}$$

We may further simplify this equation if we take the limit  $\gamma_{21} \rightarrow \infty$ , *i.e.* when the nonradiative relaxation rate from the highest to the intermediate state is by far the fastest process:

$$\lim_{\gamma_{21} \rightarrow \infty} n_1 = \frac{\Gamma_{02}}{\gamma_{10} + \Gamma_{02}} .$$

This is a special case of the steady state dynamics of the investigated three-level system. Nevertheless, it is also the exact solution of a two-level system incoherently pumped to the excited state with probability  $n_1$  at the rate  $\Gamma_{02}$  and with spontaneous emission rate  $\gamma_{10}$  from excited to ground state. Thus, assuming that  $\gamma_{21} \gg \{\Gamma_{01}, \gamma_{10}\}$ , we can describe the dynamics of a three-level system approximately by that of a two-level system (Sec. 5.1).

## B.5 Spontaneous Emission revisited

In Sec. 3.2 we have seen how spontaneous emission can be derived in the context of a field quantization in dispersive media. In this section we will repeat the derivation. A more condensed scalar approach will lead us to an effective interaction of the radiating two-level-system with its environment in form of a damped Jaynes-Cummings model. Furthermore, we shall give explicit results for the case of a coupling to a Lorentzian spectral density, *i.e.* a blueprint for the spontaneous emission dynamics of a QS in the vicinity of a single-mode NA. We have used this correspondance to check the validity of the QNM quantization approach in Sec. 3.5. The derivations are closely based on chapter 10 in Ref. [220].

### B.5.1 Determination of time-dependent non-Markovian Loss Rate

In Sec. 3.2 we used the wave function approach

$$|\psi(t)\rangle = e^{-i\tilde{\omega}t} c_1(t) |1, \{0\}_\omega\rangle + \int_0^\infty e^{-i\omega t} \mathbf{c}_{0,\omega}(\mathbf{r}, t) |0, \{\mathbf{1}\}_\omega\rangle d\omega dV , \quad (120)$$

with new transition frequency  $\tilde{\omega} = \omega_{10} - \delta\omega$  and yet to be found spectral shift  $\delta\omega$  to derive

$$\begin{aligned} \dot{c}_1(t) &= -i\delta\omega c_1(t) - \int_0^t K(t-t') c_1(t') dt' \text{ with the kernel} \\ K(t-t') &= \frac{1}{\pi\epsilon_0\hbar} \int_0^\infty \frac{\omega^2}{c^2} e^{-i(\omega-\tilde{\omega})(t-t')} \mathbf{d}_{10} \cdot \Im G(\mathbf{r}_{\text{qs}}, \mathbf{r}_{\text{qs}}, \omega) \cdot \mathbf{d}_{01} d\omega , \end{aligned} \quad (121)$$

which we then solved within the Markov approximation  $\int_0^t K(t-t') c_1(t') dt' \rightarrow c_1(t) \int_0^\infty K(t-t') dt'$ . We also related the spectral shift to the real part of the Greens function. Let us tackle this problem now in a more abstract form where the kernel  $K(t-t')$  is also responsible for the shift in the equation of motion. We shall consider only a sum over harmonic oscillators and treat the coupling in a scalar way, which we may always do, since  $\mathbf{d}_{10} \cdot \Im G(\mathbf{r}_{\text{qs}}, \mathbf{r}_{\text{qs}}, \omega) \cdot \mathbf{d}_{01}$  is a scalar quantity. Hence, we do not lose any generality, but we may formulate the problem in a very concise way. First, we shall define the Hamiltonian similar to Eq. (32) as

$$H = \hbar\omega_{\text{qs}}\sigma_+\sigma_- + \sum_k \hbar\omega_k a_k^\dagger a_k + \sum_k \left( \hbar\kappa_k \sigma_+ a_k + \hbar\kappa_k^* a_k^\dagger \sigma_- \right) . \quad (122)$$

Again,  $\sigma_-$  and  $a_k$  are the annihilation operators of the QS and the  $k$ 'th harmonic oscillator, respectively. The number of photons is conserved in the system. and we may restrict ourselves to

an analysis of a wave function of the form

$$|\psi(t)\rangle = c_1(t) |1, \{0\}\rangle + \sum_k c_{0,k}(t) |0, \{\mathbf{1}\}_k\rangle, \quad (123)$$

in which  $|1, \{0\}\rangle$  is the QS in its first excited state, the field in its ground state and  $|0, \{\mathbf{1}\}_k\rangle$  denotes that the  $k$ 'th harmonic oscillator is in its excited state. Using Schrödinger's equation, we can calculate the evolution equations for the  $c_i(t)$  as

$$\begin{aligned} i\hbar \left[ \dot{c}_1(t) |1, \{0\}\rangle + \sum_k \dot{c}_{0,k}(t) |0, \{\mathbf{1}\}_k\rangle \right] &= H \left[ c_1(t) |1, \{0\}_k\rangle + \sum_k c_{0,k}(t) |0, \{\mathbf{1}\}_k\rangle \right] \\ &= \hbar\omega_{\text{qs}} c_1(t) |1, \{0\}_k\rangle + \sum_k \hbar\omega_k c_{0,k}(t) |0, \{\mathbf{1}\}_k\rangle + \\ &\quad \sum_k \hbar\kappa_k c_{0,k}(t) |1, \{0\}_k\rangle + \sum_k \hbar\kappa_k^* c_1(t) |0, \{\mathbf{1}\}_k\rangle. \end{aligned}$$

Here we have used

$$\begin{aligned} \left\{ \sum_k \hbar\kappa_k \sigma_+ a_k \right\} \sum_l c_{0,l}(t) |0, \{\mathbf{1}\}_l\rangle &= \sum_k \hbar\kappa_k c_{0,k}(t) |1, \{0\}_k\rangle \text{ and} \\ \left\{ \sum_k \hbar\kappa_k^* a_k^\dagger \sigma_- \right\} c_1(t) |1, \{0\}_k\rangle &= \sum_k \hbar\kappa_k^* c_1(t) |0, \{\mathbf{1}\}_k\rangle. \end{aligned}$$

The orthonormality of the states yields

$$i\dot{c}_1(t) = \omega_{\text{QS}} c_1(t) + \sum_k \hbar\kappa_k c_{0,k}(t) \quad \text{and} \quad i\dot{c}_{0,k}(t) = \omega_k c_{0,k}(t) + \hbar\kappa_k^* c_1(t).$$

Now it is evident that a transformation of the form  $c_{0,k}(t) \rightarrow c_{0,k}(t) \exp[-i\omega_k t]$  and  $c_1(t) \rightarrow c_1(t) \exp[-i\omega_{\text{qs}} t]$  gives rise to

$$\begin{aligned} \dot{c}_1(t) &= -i\hbar \sum_k \kappa_k c_{0,k}(t) \exp[-i(\omega_k - \omega_{\text{qs}}) t] \text{ and} \\ \dot{c}_{0,k}(t) &= -i\hbar\kappa_k^* c_1(t) \exp[-i(\omega_{\text{qs}} - \omega_k) t]. \end{aligned} \quad (124)$$

The latter equation is a scalar equivalent to Eq. (33).

There are no additional photons in the system, *i.e.*  $c_{0,k}(0) = 0$ . Then Eq. (124) can be integrated to yield

$$\begin{aligned} c_{0,k}(t) &= -\int_0^t i\hbar\kappa_k^* e^{-i(\omega_{\text{qs}} - \omega_k)t'} c_1(t') dt', \text{ so} \\ \dot{c}_1(t) &= -\int_0^t \sum_k |\hbar\kappa_k|^2 e^{-i(\omega_k - \omega_{\text{qs}})(t-t')} c_1(t') dt' \\ &\equiv -\int_0^t K_s(t-t') c_1(t') dt' \end{aligned} \quad (125)$$

Equation (125) is formally equivalent to Eq. (121) without the distinction of emission rate and shift of the resonance frequency  $\delta\omega$ . We have also introduced the Kernel  $K_s(t-t')$ , which is again related to the spectral density via

$$K_s(t-t') = \int_{-\infty}^{\infty} J_s(\omega) e^{-i(\omega - \omega_{\text{qs}})(t-t')} d\omega.$$

The subscript “s” shall denote the difference to the former defined  $K$  and  $J$  as the new formulation corresponds to a scalar formulation and also incorporates  $\delta\omega$ .

It is now possible to show the formal equivalence to a model in which the QS evolves dissipatively. To that end we introduce the reduced density matrix of the QS according to

$$\rho_{\text{qs}}(t) = \text{tr}_{\text{EM}} [|\psi(t)\rangle\langle\psi(t)|] = \begin{pmatrix} |c_1(t)|^2 & c_0^* c_1(t) \\ c_0 c_1^*(t) & 1 - |c_1(t)|^2 \end{pmatrix}.$$

Given a Hilbert space  $\mathcal{H}_A \otimes \mathcal{H}_B$ , the partial trace to find the reduced density matrix may be defined as  $\rho_A = \text{tr}_B [\rho]$  with  $\text{tr}_B [A] = \sum_n \langle\psi_n| A |\psi_n\rangle_B$ . The  $|\psi_n\rangle_B$  are the eigenstates of the subsystem  $\mathcal{H}_B$  [195]. For the latter result one had to extend  $|\psi(t)\rangle$  in Eq. (123) by the term  $c_0 |0, \{0\}_k\rangle$  to perform the partial trace. Note that for our problem  $c_0$  is constant and may very well be set to zero. Since the density matrix evolves as  $i\hbar\partial_t\rho(t) = [H, \rho(t)]$ , the equations of motion for  $\rho_{\text{qs}}(t)$  can be derived:

$$i\hbar\partial_t\rho_{\text{qs}}(t) = i\hbar \begin{pmatrix} \partial_t |c_1(t)|^2 & c_0^* \dot{c}_1(t) \\ c_0 \dot{c}_1^*(t) & -\partial_t |c_1(t)|^2 \end{pmatrix} = [H_{\text{eff}}, \rho_{\text{qs}}(t)] + i\hbar\mathcal{L}_{\text{eff}}[\rho_{\text{qs}}(t)]. \quad (126)$$

Here, effective Hamiltonian  $H_{\text{eff}}$  and Lindblad  $\mathcal{L}_{\text{eff}}$  operator have been introduced. They are to be determined to interpret the equations of motion accordingly. To do so, it is important to remember that the evolution of a two-level system prone to dissipation is given by

$$\begin{aligned} i\hbar\partial_t\rho(t) &= [H_{\text{TLS}}, \rho(t)] + i\hbar\mathcal{L}_{\text{decay}}[\rho] \\ &= [\hbar\omega\sigma_+\sigma_-, \rho(t)] + i\hbar\frac{\gamma}{2} \{2\sigma_-\rho(t)\sigma_+ - \rho(t)\sigma_+\sigma_- - \sigma_+\sigma_-\rho(t)\}. \end{aligned} \quad (127)$$

One may now check if Eq. (126) can be written in the form of a lossy two-level system with some loss rate  $\gamma$ .

Using some matrix algebra one may deduce that the Lindblad operator  $\mathcal{L}_{\text{eff}}$  is equivalent to  $\mathcal{L}_{\text{decay}}$  if the decay rate is time varying and given by

$$\gamma(t) = -2\Re\left(\frac{\dot{c}_1(t)}{c_1(t)}\right)$$

and further if  $\omega_{\text{qs}} \rightarrow \omega_{\text{qs}} + \delta\omega(t)$  with

$$\delta\omega(t) = -2\Im\left(\frac{\dot{c}_1(t)}{c_1(t)}\right).$$

Thus, also a time-dependent frequency shift is included in the theory. These results are still valid within the RWA, no further approximation has been made. Most importantly, the bath of harmonic oscillators act as a dissipation channel for the QS even though no dissipation is given in the original Hamiltonian (Eq. 122).

### B.5.2 Coupling to a Lorentzian spectral Density: Exact Evolution

In Sec. 3.4 we claimed that, if the spectral density can be written as a superposition of oscillators, we can use the Jaynes-Cummings model to understand NA-QS interactions. In this subsection we shall investigate the spontaneous emission of a two-level system interacting with a Lorentzian spectral density. These results were used in Sec. 3.5 to compare the evolution of a such a QS in the vicinity of a single lossy harmonic oscillator to the case at hand.

A Lorentzian spectral density of the form

$$J_s(\omega) = \frac{\gamma_{wc}}{2\pi} \frac{\Gamma^2}{(\omega_{na} - \omega)^2 + \Gamma^2} \quad (128)$$

shall be assumed. Here,  $\omega_{na}$  is the resonance frequency of the NA and  $\Gamma$  its loss rate. At this point,  $\gamma_{wc}$  is just a constant that accounts for the coupling strength between QS and NA.  $J_s(\omega)$  was chosen to be Lorentzian as such a spectral density is found by González-Tudela [213] for a dipole spontaneously emitting very close to a metallic surface. Such a spectral density is used by Vogel and Welsch to discuss spontaneous emission [185] [Eq. (10.45)] and also Breuer and Petruccione [220] utilize it as an “effective spectral density” [Eq. (10.43)]. Hence to be comparable to the literature and since a treatment of a full complex  $J_{ho}(\omega) = \Re J_{ho}(\omega) + iJ_s(\omega)$  yields very similar results we neglect the spectral shift  $\delta\omega$  at this point.

By integration we find the kernel

$$\begin{aligned} K_s(t-t') &= \frac{\gamma_{wc}}{2\pi} \int_{-\infty}^{\infty} \frac{\Gamma^2}{(\omega_{na} - \omega)^2 + \Gamma^2} e^{-i(\omega - \omega_{qs})(t-t')} d\omega \\ &= \frac{1}{2} \gamma_{wc} \Gamma e^{-\Gamma|t-t'| - i(\omega_{na} - \omega_{qs})t} . \end{aligned}$$

We may briefly relate this result to a fully complex spectral density caused by a harmonic oscillator. In this case

$$J_{ho}(\omega) = \frac{\gamma_{wc}}{2\pi} \Im \left( \frac{A}{\omega_{na}^2 - \omega^2 - i\Gamma_{na}\omega/2} \right) ,$$

with some constant  $A$  that we can find by comparing  $J_{ho}(\omega)$  to  $J_s(\omega)$ . A quick calculation shows that  $J_s(\omega) \approx \Im J_{ho}(\omega)$  for  $\omega > 0$  if  $A = \Gamma_{na}\omega_{na}$  and  $\Gamma_{na} = 2\Gamma$ .

Because of the relative simplicity of  $K_s$ , we can find the solution to Eq. (125) with the help of Mathematica [350]:

```
Ks[τ_] = 1/2 γwc Γ exp[-Γτ - I(ωna - ωqs)τ];
LaplaceTransform[c'[t] == -Integrate[c[t1] Ks[t - t1], {t1, 0, t}], t, s];
Solve[%, LaplaceTransform[c[t], t, s]];
Solution = InverseLaplaceTransform[%, s, t];
```

For  $\omega_{na} = \omega_{qs}$ , the exact evolution of the excited state amplitude simplifies to

$$c_1(t) = c_1(0) e^{-\Gamma t/2} \left\{ \cosh\left(\frac{dt}{2}\right) + \frac{\Gamma}{d} \sinh\left(\frac{dt}{2}\right) \right\} \quad (129)$$

with  $d = \sqrt{\Gamma^2 - 2\gamma_{wc}\Gamma}$ .

With the help of Eq. (129), the time dependent loss rate reads

$$\gamma(t) = \gamma_{wc} \cdot \Re \left( \frac{\Gamma \sinh(dt/2)}{d \cosh(dt/2) + \Gamma \sinh(dt/2)} \right) , \quad (130)$$

and no Lamb shift is present if  $d \in \mathbb{R}$ , *i.e.* if  $4\gamma_{wc} < 2\Gamma = \Gamma_{na}$ . This condition characterizes the weak-coupling regime, equivalent to Eq. (72) for  $N_{qs} = 1$ .

Both  $\sinh(\xi)$  and  $\cosh(\xi)$  have the same behavior for large arguments. Since in the weak coupling regime  $d \approx \Gamma$ ,  $\gamma(t) \rightarrow \gamma_{wc}$  for  $t \rightarrow \infty$ . Thus we have identified  $\gamma_{wc}$  as the spontaneous emission rate of the weak coupling regime, where  $c_1(t) = c_1(0) \exp(-\gamma_{wc}t/2)$  [Eq. (35)].

Interestingly, the exact expression for the  $\alpha_n$  [Eq. (128)], which were introduced as normalization constants in Eq. (43) has been implicitly determined. Comparing these two equations,

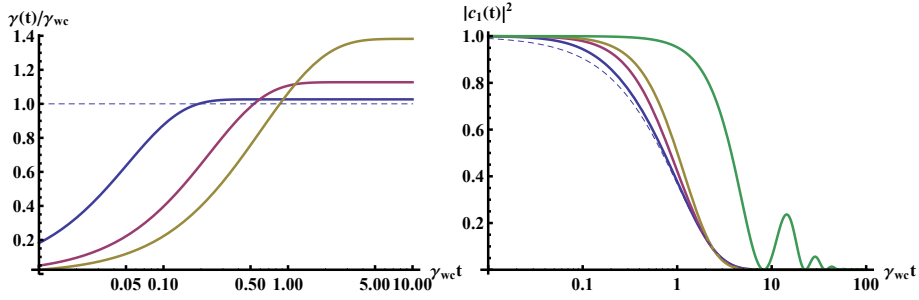


Figure 19: Difference between Markov approximation result for the spontaneous emission of a two-level system coupled to a Lorentzian spectral density as given in Sec. 3.2 compared to the exact solution outlined in App. B.5; both within the RWA. Left: time-dependent emission rate  $\gamma(t)$  in units of  $\gamma_{wc}$  (blue dashed line). Blue, magenta and yellow thick lines indicate an increased coupling ( $\gamma_{wc}/\Gamma = 0.05, 0.2$ , and  $0.4$ ). The deviation to the Markovian solution is always clearly visible for  $\gamma_{wc}t < 1$  but gets less pronounced for  $\gamma_{wc}t > 1$  and lower coupling. Right: probability of the excited state of the two-level system  $|c_1(t)|^2$ . The same legend as in the left plot with an additional plot of  $\gamma_{wc}/\Gamma = 10$  (green line).

we find that,  $\alpha_n = \gamma_{n,wc}\Gamma_{n,na}/4$ , which is equivalent to the coupling  $\kappa_n^2$ , since  $\gamma_{n,wc} = 4\kappa_n^2/\Gamma_{n,na}$  at resonance (see App. B.8). In Fig. 19 we compare the exact result for the Weisskopf-Wigner problem for a Lorentzian spectral density to the simple Markovian solution for different ratios of  $\gamma_{wc}/\Gamma$ . The deviations are pronounced for increased coupling.

## B.6 Spectral Density, Local Density of States, and the Purcell Factor

With regard to our result for the emission rate in the weak-coupling regime [Eq. (35)], it is worth to define the local density of states (LDOS). It is often used in the literature and directly related it to the spectral density  $J(\omega)$ .

In free-space, emission rate of a dipole with dipole moment  $\mathbf{d}_{10}$  oscillating at  $\omega_{qs}$  is given by [123]

$$\begin{aligned} \gamma_{fs} &= \frac{\omega_{qs}^3 |\mathbf{d}_{10}|^2}{3\pi\epsilon_0\hbar c^3} = \frac{\pi\omega_{qs} |\mathbf{d}_{10}|^2}{3\epsilon_0\hbar} \cdot \rho_{fs}(\mathbf{r}, \omega) \quad \text{with} \\ \rho_{fs}(\mathbf{r}, \omega) &= \frac{6\omega}{\pi c^2} \cdot \frac{1}{3} \text{tr} [\Im G_{fs}(\mathbf{r}, \mathbf{r}, \omega)] = \frac{\omega^2}{\pi^2 c^3}. \end{aligned} \quad (131)$$

Here,  $\rho_{fs}(\mathbf{r}, \omega)$  denotes the LDOS of free space where trace of the Green's function is taken to average over the different orientations of the QS. Comparing  $\gamma_{wc}$  and  $\gamma_{fs}$ , the partial local density of states, pLDOS, is introduced as [cf. Eqs. (38) and (35)]

$$\begin{aligned} \rho(\mathbf{r}, \omega, \mathbf{e}_d) &= \frac{6\omega}{\pi c^2} \mathbf{e}_d \cdot \Im G(\mathbf{r}, \mathbf{r}, \omega) \cdot \mathbf{e}_d \equiv \frac{6\epsilon_0\hbar}{\omega |\mathbf{d}_{10}|^2} J(\omega) \quad , \quad \text{using} \\ \gamma_{wc} &\stackrel{!}{=} \frac{\pi\omega |\mathbf{d}_{10}|^2}{3\epsilon_0\hbar} \cdot \rho(\mathbf{r}, \omega, \mathbf{e}_d) = \frac{1}{\pi\epsilon_0\hbar} \frac{\omega^2}{c^2} \mathbf{d}_{10} \cdot \Im G(\mathbf{r}, \mathbf{r}, \omega) \cdot \mathbf{d}_{01} = 2\pi J(\omega) \quad . \end{aligned} \quad (132)$$

Here,  $\mathbf{e}_d = \mathbf{d}_{10}/|\mathbf{d}_{10}|$  is the unit vector in the direction of the QS's dipole moment.

Regarding Eq. 132,  $\rho(\mathbf{r}, \omega)$  is just a rescaled version of the spectral density  $J(\omega)$ . An averaging procedure in  $\rho$  is usually not sensible in the vicinity of NAs as they generally impose strongly varying interactions to different polarizations of a QS.

We can further relate the Purcell factor  $F(\omega)$  to  $\rho(\omega)$  and  $J(\omega)$ . With Eq. (132) we get

$$F(\omega) = \eta \frac{\gamma_{\text{wc}}}{\gamma_{\text{fs}}} = \eta \frac{6\pi^2 \varepsilon_0 \hbar c^3}{\omega^3 |\mathbf{d}_{10}|^2} J(\omega) .$$

If the efficiency  $\eta$  is only weakly depending on  $\omega$ , the Purcell factor  $F(\omega)$  is approximately proportion to  $J(\omega)/\omega^3$ . Then  $F(\omega)$  can be used to show the Lorentzian character of  $J(\omega)$  close to NAs (Sec. 3.4).

## B.7 The Modified Interaction Picture

A problem in quantum mechanics is the coupling of systems with different eigenfrequencies. In this situation it is often convenient to calculate quantities in a picture that is applied to the frequency of one of the systems or for example at the frequency of an external illumination. This leads to a Hamiltonian in the so-called modified interaction picture. In the following we shall calculate the Hamiltonian for two harmonic oscillators coupled to a two-level system in this picture. It will be obvious that this approach dramatically reduces the complexity of the problem. Furthermore, the meaning of the rotating-wave approximation (RWA) can be discussed.

For time-dependent interactions (*cf.* Sec. B.1), the Hamiltonian  $H = H_0 + V$  may be given as the free evolution of the involved systems,  $H_0$ , and a term corresponding to interactions,  $V$ . As an example, a two-level system with creation (annihilation) operator  $\sigma_+$  ( $\sigma_-$ ) and eigenfrequency  $\omega_{\text{qs}}$  is coupled to a harmonic oscillator. The latter is modeled by creation (annihilation) operators  $a^\dagger$  ( $a$ ) and eigenfrequency  $\omega_{\text{na}}$ :

$$H_0 = \hbar\omega_{\text{na}} \left( a^\dagger a + \frac{1}{2} \right) + \hbar\omega_{\text{qs}} \sigma_+ \sigma_- \quad \text{and} \quad V = \hbar\kappa (\sigma_+ + \sigma_-) (a + a^\dagger) .$$

A generalization to more complicated interactions is straightforward.

A transformation to the eigenfrequency of the two-level system is suitable if this QS is pumped incoherently [*cf.* Eq. (67)]. The “transformation Hamiltonian”  $\tilde{H}$  is then given by

$$\tilde{H} \equiv \hbar\omega_{\text{qs}} (a^\dagger a + 1/2) + \hbar\omega_{\text{qs}} \sigma_+ \sigma_- . \quad (133)$$

Note that in comparison to  $H$ , all frequencies are replaced by the eigenfrequency of the two-level system.

The unitary operator  $U(t) = \exp [it\tilde{H}/\hbar]$  is further used to transform into the modified interaction picture. The state of the system in this picture is related to the Schrödinger picture via  $|\psi\rangle_{\text{mI}} = U(t) |\psi\rangle$  and operators are transformed according to  $\mathcal{O}_{\text{mI}}(t) = U(t) \mathcal{O} U^\dagger(t)$ . Naturally, the Hamiltonian  $H$  commutes with  $\tilde{H}$  and thus  $[H, U] = 0$  holds.

As in the derivation of the Tomonaga-Schwinger equation in Sec. 2.4.1, it can be concluded which operators may be attributed to the time evolution of  $|\psi\rangle_{\text{mI}}$ . Explicitly,

$$\begin{aligned} i\hbar\partial_t |\psi\rangle_{\text{mI}} &= i\hbar\partial_t e^{it\tilde{H}/\hbar} |\psi\rangle = e^{it\tilde{H}/\hbar} \left\{ i\hbar\partial_t |\psi\rangle - \tilde{H} |\psi\rangle \right\} \\ &= e^{it\tilde{H}/\hbar} \left\{ H_0 - \tilde{H} + V \right\} |\psi\rangle = e^{it\tilde{H}/\hbar} \left\{ H_0 - \tilde{H} + V \right\} e^{-it\tilde{H}/\hbar} |\psi\rangle_{\text{mI}} \\ &= \{ H_{0,\text{mI}} + V_{\text{mI}} \} |\psi\rangle_{\text{mI}} . \end{aligned}$$

Here,

$$H_{0,\text{mI}} = \hbar(\omega_{\text{na}} - \omega_{\text{qs}}) \left( a^\dagger a + \frac{1}{2} \right) , \quad V_{\text{mI}} = e^{it\tilde{H}/\hbar} V e^{-it\tilde{H}/\hbar} .$$

This form of the Hamiltonian is often convenient. Deviations from a free oscillation frequency are

expressed in terms of the detuning  $\Delta\omega = \omega_{\text{na}} - \omega_{\text{qs}}$ . Without detuning,  $H_{0,\text{mI}}$  simply vanishes.

To transform the interaction potential  $V_{\text{mI}}$  into a suitable form, the Baker-Campbell-Hausdorff formula may be used:

$$e^X Y e^{-X} = \sum_{m=0}^{\infty} \frac{1}{m!} [X, Y]_m \quad \text{with} \quad [X, Y]_m = [X, [X, Y]_{m-1}] \quad \text{and} \quad [X, Y]_0 = Y .$$

First, for an arbitrary  $\omega$ ,

$$\begin{aligned} e^{i\omega t(a^\dagger a)} a e^{-i\omega t(a^\dagger a)} &= a + i\omega t [a^\dagger a, a] + \frac{(i\omega t)^2}{2} [a^\dagger a, [a^\dagger a, a]] + \dots \\ &= a + i\omega t (-a) + \frac{(-i\omega t)^2}{2} a + \dots = e^{-i\omega t} a , \end{aligned}$$

since  $[a^\dagger a, a] = -a$ . Analogously,

$$e^{i\omega t(a^\dagger a)} a^\dagger e^{-i\omega t(a^\dagger a)} = e^{i\omega t} a^\dagger \quad \text{and} \quad e^{i\omega t \sigma_+ \sigma_-} \sigma_\pm e^{-i\omega t \sigma_+ \sigma_-} = e^{\pm i\omega t} \sigma_\pm .$$

Then, the modified interaction potential can be determined as

$$\begin{aligned} V_{\text{mI}}(t) &= \hbar\kappa e^{it\{\omega_{\text{qs}}(a^\dagger a + \frac{1}{2}) + \omega_{\text{qs}}\sigma_+ \sigma_-\}} (\sigma_+ + \sigma_-) \\ &\quad \cdot (a + a^\dagger) e^{-it\{\omega_{\text{qs}}(a^\dagger a + \frac{1}{2}) + \omega_{\text{qs}}\sigma_+ \sigma_-\}} \\ &= \hbar\kappa e^{it\omega_{\text{qs}}\sigma_+ \sigma_-} (\sigma_+ + \sigma_-) e^{-it\omega_{\text{qs}}\sigma_+ \sigma_-} \\ &\quad \cdot e^{it\omega_{\text{qs}}a^\dagger a} (a + a^\dagger) e^{-it\omega_{\text{qs}}a^\dagger a} \\ &= \hbar\kappa (e^{i\omega_{\text{qs}}t} \sigma_+ + e^{-i\omega_{\text{qs}}t} \sigma_-) (e^{-i\omega_{\text{qs}}t} a + e^{i\omega_{\text{qs}}t} a^\dagger) . \end{aligned}$$

In the latter formulation we can directly see how the transformation introduces oscillatory terms in the interaction potential. Most importantly, terms with two creation (annihilation) operators are highly oscillatory. The RWA is then introduced neglecting these rapidly oscillating terms. In this approximation, the interaction potential simply reads

$$V_{\text{mI}} = \hbar\kappa (\sigma_+ a + a^\dagger \sigma_-) .$$

Such an interaction has the advantage that the total excitation number operator  $N_{\text{all}} = a^\dagger a + \sigma_+ \sigma_-$  is a conserved quantity.

Note that the eigenfrequency of the QS,  $\omega_{\text{qs}}$ , was used to define  $\tilde{H}$  [Eq. (133)]. Likewise, one may chose any other frequency for this transformation. For example, if a driving field oscillating at  $\omega_{\text{dr}}$  is present,  $\tilde{H} = \hbar\omega_{\text{dr}}(a^\dagger a + \frac{1}{2}) + \hbar\omega_{\text{dr}}\sigma_+ \sigma_-$  can be employed. This would yield  $H_{0,\text{mI}} = \hbar(\omega_{\text{na}} - \omega_{\text{dr}})(a^\dagger a + \frac{1}{2}) + \hbar(\omega_{\text{qs}} - \omega_{\text{dr}})\sigma_+ \sigma_-$ . In this case, the Hamiltonian is said to be ‘‘in the rotating frame’’. We have used this picture in Sec. 6 to describe the strong coupling of NAs to Qs subject to an external monochromatic field.

## B.8 Emission Rates of a Two-Level System coupled to multiple Harmonic Oscillators

In this section we calculate the emission rate of a two-level system coupled to a sum of dissipative harmonic oscillators. Although in the main text only single-mode harmonic oscillators are used for calculations, a generalization to more harmonic oscillators is straightforward. This formulation may be used to specifically incorporate a coupling to dark modes.

In the Schrödinger picture, the corresponding Hamiltonian  $H = H_0 + V$  is given by



$$\begin{aligned}
H_0 &= \sum_l \hbar \omega_l \left( a_l^\dagger a_l + \frac{1}{2} \right) + \hbar \omega_{\text{qs}} \sigma_+ \sigma_- \text{ and} \\
V &= \hbar (\sigma_+ + \sigma_-) \sum_l \kappa_l \left( a_l + a_l^\dagger \right) .
\end{aligned}$$

As throughout the thesis,  $a_l$  ( $a_l^\dagger$ ) are the annihilation (creation) operators of the  $l$ 'th harmonic oscillator, *i.e.* the  $l$ 'th NA mode and  $\sigma_-$  ( $\sigma_+$ ) are the annihilation (creation) operators of the two-level system;  $\omega_l$  and  $\omega_{\text{qd}}$  are the oscillators and two-level systems resonance frequencies, respectively. Furthermore, the  $\kappa_l$  denote coupling constants. Using the unitary transformation

$$|\psi\rangle_H = e^{iHt/\hbar} |\psi\rangle_S$$

we transform into the Heisenberg picture (see also App. B.7). As the transformation is unitary and obviously commutes with  $H$ , the Hamiltonian is unchanged in the new picture.

As it is discussed in the main text and in Refs. [89,279], we disregard fluctuation terms within the so-called cold reservoir limit (CRL), which excludes any reaction of the environment that is responsible for all irreversible processes. Then, phenomenologically introducing the harmonic oscillator loss rates  $\Gamma_l$  and the incoherent pumping rate  $R$ , the equations of motion for the operators of interest are given by

$$\begin{aligned}
\dot{a}_l &= -\frac{i}{\hbar} [a_l, H] - \frac{\Gamma_l}{2} a_l = -i \left[ a_l, \omega_l a_l^\dagger a_l + \kappa_l a_l^\dagger (\sigma_+ + \sigma_-) \right] - \frac{\Gamma_l}{2} a_l \\
&= -i \omega_l a_l - i \kappa_l (\sigma_+ + \sigma_-) - \frac{\Gamma_l}{2} a_l ,
\end{aligned}$$

$$\begin{aligned}
\dot{\sigma}_- &= -\frac{i}{\hbar} [\sigma_-, H] - \frac{R}{2} \sigma_- = -i \left[ \sigma_-, (\sigma_+ + \sigma_-) \sum_l \kappa_l (a_l + a_l^\dagger) + \omega_{\text{qs}} \sigma_+ \sigma_- \right] - \frac{R}{2} \sigma_- \\
&= -i \left[ \sum_l \kappa_l (a_l + a_l^\dagger) \right] (-\sigma_z) - i \omega_{\text{qs}} \sigma_- - \frac{R}{2} \sigma_- \text{ and}
\end{aligned}$$

$$\begin{aligned}
\dot{\sigma}_z &= -\frac{i}{\hbar} [\sigma_z, H] + R(1 - \sigma_z) = -i \left[ \sigma_z, \left\{ \sum_l \kappa_l (a_l + a_l^\dagger) \right\} (\sigma_+ + \sigma_-) \right] + R(1 - \sigma_z) \\
&= -i(2\sigma_+ - 2\sigma_-) \sum_l \kappa_l (a_l + a_l^\dagger) + R(1 - \sigma_z) .
\end{aligned}$$

From these equations it can be seen that we assume an incoherent pump of the QS only. On the contrary, the NA state may decay due to radiation or dissipation;  $\Gamma_l = \Gamma_l^{\text{rad}} + \Gamma_l^{\text{pr}}$ . Because of the energy flow to the QS, it is worth to consider slowly varying amplitudes of the operators oscillating at the QS's transition frequency, *i.e.* in the rotating frame:

$$\sigma_\pm \equiv \tilde{\sigma}_\pm e^{\pm i \omega_{\text{qs}} t} \text{ and } a_l^\dagger \equiv \tilde{a}_l^\dagger e^{i \omega_{\text{qs}} t} .$$

For the operators in the rotating frame, the equations of motion are given by

$$\begin{aligned}
\dot{\tilde{a}}_l - i \omega_{\text{qs}} \tilde{a}_l &= -i \omega_l \tilde{a}_l - i \kappa_l \tilde{\sigma}_- - \frac{\Gamma_l}{2} \tilde{a}_l , \\
\dot{\tilde{a}}_l &= -i \Delta \omega_l \tilde{a}_l - i \kappa_l \tilde{\sigma}_- - \frac{\Gamma_l}{2} \tilde{a}_l \text{ with } \Delta \omega_l = \omega_l - \omega_{\text{qs}} ,
\end{aligned}$$

$$\begin{aligned}
\dot{\tilde{\sigma}}_- - i\omega_{\text{qs}}\tilde{\sigma}_- &= i \left\{ \sum_l \kappa_l \tilde{a}_l \right\} \sigma_z - i\omega_{\text{qs}}\tilde{\sigma}_- - \frac{R}{2}\tilde{\sigma}_- \\
\dot{\tilde{\sigma}}_- &= i \left\{ \sum_l \kappa_l \tilde{a}_l \right\} \sigma_z - \frac{R}{2}\tilde{\sigma}_-, \text{ and} \\
\dot{\sigma}_z &= -2i \sum_l \kappa_l \left( \tilde{\sigma}_+ \tilde{a}_l - \tilde{a}_l^\dagger \tilde{\sigma}_- \right) + R(1 - \sigma_z) .
\end{aligned}$$

As an important physical quantity, the detuning of the  $l$ 'th oscillator mode to the excitation,  $\Delta\omega_l$ , appears in the equations for the oscillator annihilation operators  $\tilde{a}_l$ . Furthermore, the RWA is applied. Hence, fastly oscillating terms of the form  $\hbar\kappa_l\sigma_+a_l^\dagger$  are neglected to find a closed-form analytical result.

### Steady State Solution

It may be assumed that a steady state exists for which all time-derivatives of the operators vanish. In this case, the  $\langle \dot{n}_l \rangle$  can be determined to yield the emitted photon rate of the  $l^{\text{th}}$  mode.

The operators' equations of motion in the steady state take the form

$$\begin{aligned}
\tilde{a}_l &= -\frac{i\kappa_l}{i\Delta\omega_l + \Gamma_l/2}\tilde{\sigma}_-, \\
\tilde{\sigma}_- &= i\frac{\sum_l \kappa_l \tilde{a}_l}{R/2}\sigma_z \text{ and} \\
\sigma_z &= 1 - i\frac{2}{R}\sum_l \kappa_l \left( \tilde{\sigma}_+ \tilde{a}_l - \tilde{a}_l^\dagger \tilde{\sigma}_- \right) .
\end{aligned} \tag{134}$$

Up to now the RWA and CRL approximations were used to obtain rather simple equations of motion. In the next step the mutual dependencies of the operators in Eq. (134) are adopted. At first,  $\tilde{\sigma}_-$  is eliminated to find an expression for  $\tilde{a}_l$ :

$$\tilde{a}_l = \frac{\kappa_l}{i\Delta\omega_l + \Gamma_l/2} \frac{\sum_l \kappa_l \tilde{a}_l}{R/2} \sigma_z .$$

Such an approach is termed adiabatic elimination and has to be handled with care in conjunction to other approximations [368]. In the present case we have already dropped the fluctuation operators and fastly oscillating terms. Hence, the intermediate results are approximative already. Therefore we may take a pragmatic point of view and check if the end results are reasonable. In fact it turns out that they agree in the case of a single mode oscillator [279] and to fully quantum calculations (see Figs. 9 and 13). Consequently, our findings can be used with confidence.

Performing an adiabatic elimination of  $\tilde{a}_l$  we conclude

$$\begin{aligned}
\sigma_z &= 1 - i\frac{2}{R}\sum_l \kappa_l \left( \tilde{\sigma}_+ \tilde{a}_l - \tilde{a}_l^\dagger \tilde{\sigma}_- \right) = 1 - i\frac{2}{R}\sum_l \kappa_l \left( -\frac{i\kappa_l}{i\Delta\omega_l + \Gamma_l/2} + \frac{i\kappa_l}{-i\Delta\omega_l + \Gamma_l/2} \right) \tilde{\sigma}_+ \tilde{\sigma}_- \\
&\equiv 1 - 2\beta\tilde{\sigma}_+ \tilde{\sigma}_- = 1 - \beta(1 + \sigma_z) , \text{ so} \\
\sigma_z &= \frac{1 - \beta}{1 + \beta} .
\end{aligned}$$

with

$$\beta = \frac{1}{R}\sum_l \kappa_l^2 \left( +\frac{1}{i\Delta\omega_l + \Gamma_l/2} - \frac{1}{-i\Delta\omega_l + \Gamma_l/2} \right) = \frac{1}{R}\sum_l \kappa_l^2 \frac{\Gamma_l}{\Delta\omega_l^2 + \Gamma_l^2/4} \equiv \frac{1}{R}\sum_l \gamma_{\text{wc},l} .$$

Here we have defined the  $l$ 'th mode weak coupling emission rate

$$\gamma_{\text{wc},l} \equiv \kappa_l^2 \frac{\Gamma_l}{\Delta\omega_l^2 + \Gamma_l^2/4} .$$

We are specifically interested in the expected photon number in each mode and its related radiative emission rate. With our result for  $\sigma_z$ , we find

$$\tilde{a}_l^\dagger \tilde{a}_l = \frac{\kappa_l^2}{\Delta\omega_l^2 + \Gamma_l^2/4} \tilde{\sigma}_+ \tilde{\sigma}_- = \frac{\gamma_{\text{wc},l}}{\Gamma_l} \frac{1 + \sigma_z}{2} = \frac{\gamma_{\text{wc},l}}{\Gamma_l} \frac{1 + \frac{1-\beta}{1+\beta}}{2} = \frac{1}{1+\beta} \frac{\gamma_{\text{wc},l}}{\Gamma_l} .$$

Then, the radiative emission rate by mode  $l$  amounts to

$$\langle \dot{n}_l \rangle = \eta_l \langle \tilde{a}_l^\dagger \tilde{a}_l \rangle \Gamma_l = \eta_l \frac{\gamma_{\text{wc},l} R}{R + \sum_l \gamma_{\text{wc},l}} .$$

For a single-mode oscillator on resonance with the QS, the latter result simplifies to (used in Sec. 3.5 and 5.2)

$$\langle \dot{n} \rangle = \eta \frac{\gamma_{\text{wc}} R}{R + \gamma_{\text{wc}}} \text{ with } \gamma_{\text{wc}} = \frac{4\kappa^2}{\Gamma} .$$

## B.9 Second-Order Correlation: Classical and Nonclassical Light States

We shall briefly review the meaning of the second order correlation function  $g^2(\tau)$  and why it is a useful observable to quantify the nonclassicality of a certain light state. Throughout our argumentation, we will loosely follow Loudon [233], but also Refs. [369,370] can be taken as instructive reviews.

Specifically, we will analyze the second-order correlation  $g^2(\tau)$  of a single-mode field where we may suppress the spatial dependency for simplicity. In that case we can concisely write

$$g^2(\tau) = \frac{\langle E^*(t) E^*(t+\tau) E(t+\tau) E(t) \rangle}{\langle E^*(t) E(t) \rangle \langle E^*(t+\tau) E(t+\tau) \rangle} .$$

If we assume stationary statistical properties,  $g^2$  is symmetric [ $g^2(\tau) = g^2(-\tau)$ ]. Thus it is sufficient to consider  $g^2$  for positive  $\tau$  only.

### B.9.1 The Classical Picture

In the case of classical fields, denoted by the subscript ‘‘c’’, the order of  $E$  in  $g_c^2$  is irrelevant. In that case we find

$$g_c^2(\tau) = \frac{\langle E^*(t) E(t) E^*(t+\tau) E(t+\tau) \rangle}{\langle E^*(t) E(t) \rangle \langle E^*(t+\tau) E(t+\tau) \rangle} = \frac{\langle I(t) I(t+\tau) \rangle}{\langle I(t) \rangle \langle I(t+\tau) \rangle} .$$

A very interesting case occurs at  $\tau = 0$ :

$$g_c^2(0) = \frac{\langle I^2(t) \rangle}{\langle I(t) \rangle^2} .$$

Note that  $I(t)$  is a classical statistical variable with a positive definite variance,

$$\text{Var}[I(t)] \equiv \langle (I(t) - \langle I(t) \rangle)^2 \rangle = \langle I^2(t) \rangle - \langle I(t) \rangle^2 \geq 0 .$$

This implies

$$g_c^2(0) \geq 1, \quad (135)$$

*i.e.* a fundamental limit of the second order correlation for classical light.

We may further deduce a very important property of  $g_c^2(\tau)$  from the Cauchy-Schwarz inequality  $|\langle a^*b \rangle|^2 \leq \langle |a|^2 \rangle \langle |b|^2 \rangle$ , namely

$$\langle I(t)I(t+\tau) \rangle^2 \leq \langle I(t) \rangle^2 \langle I(t+\tau) \rangle^2 \quad (136)$$

for real-valued intensities. If we assume stationarity, we further see that  $\langle I(t) \rangle^2 \langle I(t+\tau) \rangle^2 = \langle I(t) \rangle^4$ . Then, by taking the root of Eq. (136),

$$\begin{aligned} \langle I(t)I(t+\tau) \rangle &= \langle I(t) \rangle^2 \leq \langle I(t) \rangle^2, \text{ so} \\ g_c^2(\tau) &= \frac{\langle I(t)I(t+\tau) \rangle}{\langle I(t) \rangle \langle I(t+\tau) \rangle} \leq \frac{\langle I^2(t) \rangle}{\langle I(t) \rangle^2} = g_c^2(0). \end{aligned}$$

Hence, for positive  $\tau$ ,  $g_c(\tau)$  is a monotonously decreasing function. Using Eq. (135), the classical second order correlation functions peaks at  $\tau = 0$  and decrease to 1 as  $\tau \rightarrow \infty$ . Noteworthy, the magnitude of the maximum and the time-scales at which  $g_c(\tau)$  decreases depend on the actual light source.

## B.9.2 The Quantum Picture

For a quantized bosonic field,  $g^2(\tau)$  is given by

$$g^2(\tau) = \frac{\langle a^\dagger(t)a^\dagger(t+\tau)a(t+\tau)a(t) \rangle}{\langle a^\dagger(t)a(t) \rangle \langle a^\dagger(t+\tau)a(t+\tau) \rangle}.$$

The fundamental difference to the classical case is that one may not interchange the order of operators. In the classical picture we observed a fundamental limit for  $g^2(0)$  [Eq. (135)]. In the quantum picture, we find in the stationary case

$$g^2(0) = \frac{\langle a^\dagger a^\dagger a a \rangle}{\langle a^\dagger a \rangle^2} = \frac{\langle a^\dagger a a^\dagger a \rangle - \langle a^\dagger [a, a^\dagger] a \rangle}{\langle a^\dagger a \rangle^2} = \frac{\langle (a^\dagger a)^2 \rangle - \langle a^\dagger a \rangle}{\langle a^\dagger a \rangle^2}. \quad (137)$$

Compared to the classical analysis, an  $\langle a^\dagger a \rangle$ -term appears in the denominator. It can be anticipated that  $g^2(0) < 1$  might be possible. But before such light states are discussed, thermal and coherent radiatio shall be discussed.

## Thermal Radiation

Revisiting Eq. (137), it becomes evident that it is sufficient to determine the expectation values of the number operator  $N = a^\dagger a$  and of  $N^2$  to calculate  $g^2(0)$ . We shall follow this approach to find  $g^2(0)$  for thermal and coherent radiation.

With respect to the inverse temperature  $\beta = \hbar/k_B T$  (in time units), the probability for  $n$  photons in a thermal light field is given by the Boltzmann distribution

$$P(n) = \frac{e^{-\beta\omega n}}{\sum_{n=0}^{\infty} e^{-\beta\omega n}} = e^{-\beta\omega n} \{1 - e^{-\beta\omega}\}.$$

The well-known expectation value for the number of photons is then

$$\begin{aligned}\langle N \rangle &= \sum_{n=0}^{\infty} n P(n) = \frac{1}{e^{\beta\omega} - 1} \text{ and} \\ \langle N^2 \rangle &= \sum_{n=0}^{\infty} n^2 P(n) = \frac{1 + e^{\beta\omega}}{(e^{\beta\omega} - 1)^2} = \langle N \rangle^2 \frac{2\langle N \rangle + 1}{\langle N \rangle} = \langle N \rangle (2\langle N \rangle + 1) .\end{aligned}$$

With the help of  $\exp[-\beta\omega] = \langle N \rangle / (1 + \langle N \rangle)$ ,  $P(n)$  may be expressed as

$$P(n) = \frac{1}{1 + \langle N \rangle} \left( \frac{\langle N \rangle}{1 + \langle N \rangle} \right)^n .$$

Then it is

$$g^2(0) = \frac{\langle N^2 \rangle - \langle N \rangle}{\langle N \rangle^2} = \frac{\langle N \rangle (2\langle N \rangle + 1) - \langle N \rangle}{\langle N \rangle^2} = 2 . \quad (138)$$

Equation (138) is a rather simple but astonishing result. It implies that photons from strictly thermal sources have a high probability to exist in bunches.

### Coherent Radiation

Now to the case of coherent radiation. Coherent states obey a Poissonian distribution of the form

$$P(n) = \frac{\langle N \rangle^n}{n!} e^{-\langle N \rangle} .$$

Mean and variance are equal for the Poisson distribution,

$$\langle N \rangle = \text{Var}(N) = \langle N^2 \rangle - \langle N \rangle^2 , \text{ so } \langle N^2 \rangle = \langle N \rangle + \langle N \rangle^2 .$$

Hence,

$$g^2(0) = \frac{\langle N^2 \rangle - \langle N \rangle}{\langle N \rangle^2} = \frac{\langle N \rangle + \langle N \rangle^2 - \langle N \rangle}{\langle N \rangle^2} \equiv 1 .$$

One can further derive that  $g^2(\tau) = 1 \forall \tau$ , which even holds for a single-atom laser [371]. This second order coherence can be interpreted such that the individual photons in a coherent light state are completely unrelated to each other. The probability to find some photons in a given time frame is given by a Poisson distribution. Even for very small times there exist a non-vanishing probability of more than one photon.

### Fock states

Photons are bosons. Hence, the electromagnetic field state may be excited with an arbitrary number of them. The situation changes dramatically if a two-level system is considered. This QS may exhibit a single excitation only. It is a physical entity with fermionic properties that can in general emit only a single photon at once.

Fock states  $|n\rangle$  [cf. Eq. (27)] are often used to describe the state of a harmonic oscillator. If the light field is in a Fock state, we can easily conclude that

$$\begin{aligned}\langle N \rangle &= n \text{ and } \langle N^2 \rangle = n^2 . \\ \text{Hence } g^2(0) &= \frac{\langle N^2 \rangle - \langle N \rangle}{\langle N \rangle^2} = 1 - \frac{1}{n} \text{ for } n \geq 1 .\end{aligned}$$

It is obvious that  $g^2(0) < 1 \forall n \geq 1$ . Especially for  $n = 1$ , the case of a single photon,  $g^2(0) \equiv 0$ , which is drastically different from classical expectations.

### B.9.3 Conclusion

In the classical picture  $g^2(\tau)$  is always bigger or equal to one, which simply results from the Cauchy-Schwarz inequality. However, the quantization of the electromagnetic field is taken into account, the field operators do not commute and an additional term arises. Whereas thermal and coherent radiation exhibit light properties that can be understood within the classical picture, the same does not hold for Fock states. In the special case of a single photon state, the second order correlation vanishes at  $\tau = 0$ . Hence, to understand nonclassical light emission, a quantization of the electromagnetic field is inevitable and  $g^2(\tau)$  is a suitable figure of merit to quantify its nonclassicality.

## B.10 Nanoantennas for Squeezed Light and Entangled Light Generation

In the last subsection the second-order correlation function as a measure for the nonclassicality of single photon sources has been discussed. In this subsection we shall briefly discuss the generation of two other nonclassical light states: squeezed and entangled light.

### B.10.1 Squeezed Light

One of the basic results of quantum mechanics is Heisenberg's uncertainty principle

$$\Delta A \Delta B \geq \frac{1}{2} |\langle [A, B] \rangle|. \quad (139)$$

Here  $A$  and  $B$  are two operators and  $\Delta A \equiv \sqrt{\langle (A - \langle A \rangle)^2 \rangle} \equiv \sqrt{\text{Var}(A)}$ . The uncertainty principle prohibits a simultaneous measurement of two non-commuting variables to an arbitrary accuracy. However, the accuracy of a measurement of one variable may as well be increased at the cost of higher uncertainties in the other. For instance, one may measure the position of a particle with high precision, but loses an increasing amount of information about its momentum.

The same concept applied to the phase and amplitude of light states leads to so-called squeezed states [185,372]. Squeezed state applications arise for example in the context of quantum metrology, where phase uncertainty reduction can lead to drastically increased accuracies of interferometers [373]. The reduction of the fundamental shot noise may lead to an accurate measurement of gravitational waves as well [374]. But these nonclassical light states also play an increasing role in the realization of continuous variable quantum communication [375,376].

Squeezed states are usually analyzed with respect to the so-called quadrature operators  $X_+ = a + a^\dagger$  and  $X_- = -i(a - a^\dagger)$  [377]. These operators correspond to the real and imaginary parts of the electric field, respectively. Their variance is proportional to the variance in amplitude ( $\Delta X_1 \propto \Delta n$ ) and phase ( $\Delta X_2 \propto \Delta \phi$ ). Their commutation relation is given by  $[X_+, X_-] = 2i$ . According to Heisenberg, the uncertainty product of the quadrature operators is at least unity, which is reached for coherent radiation. A squeezed state is found if the variance for one of the quadrature operators is below unity, *i.e.*  $\text{Var}(X_\pm) < 1$ .

Squeezed light can be mathematically described by the so-called squeeze operator  $S(\xi) = \exp\left\{\frac{1}{2}(\xi^* a^2 - \xi a^{\dagger 2})\right\}$  that acts on a coherent state ( $\xi = r \exp[i\theta] \in \mathbb{C}$ ). In particular, the squeezed

vacuum state  $|\xi\rangle = S(\xi)|0\rangle$  exhibits the following variances of the quadrature operators:

$$\begin{aligned}\text{Var}(X_+) &= \cosh^2 r + \sinh^2 r - 2 \sinh r \cosh r \cos \theta \\ \text{Var}(X_-) &= \cosh^2 r + \sinh^2 r + 2 \sinh r \cosh r \cos \theta .\end{aligned}$$

For  $\theta = 0$ , we have  $\text{Var}(X_+) = \exp\{-2r\}$  and  $\text{Var}(X_-) = \exp\{2r\}$  and we have squeezing in  $X_+$ , whereas for  $\theta = \pi$  it is present in  $X_-$ .

Physically, squeezed states can be produced by different processes. In fact, they are predicted within the Jaynes-Cummings model [378] and for resonance fluorescence under certain conditions [379, 380]. Prominent ways to obtain squeezed light are degenerate parametric down-conversion with an effective Hamiltonian [377]

$$\begin{aligned}H &= \hbar\omega_0 a^\dagger a + 2\hbar\omega_0 b^\dagger b + i\hbar\chi_2 (a^2 b^\dagger - a^{\dagger 2} b) \text{ and} \\ H &= \hbar\omega_0 a^\dagger a + \hbar\omega_0 b^\dagger b + i\hbar\chi_3 (a^2 b^{\dagger 2} - a^{\dagger 2} b^2)\end{aligned}$$

for degenerate four-wave mixing [381], respectively. In both cases, the interaction part of the Hamiltonian can be written in a similar manner. Then it becomes obvious that an evolution of the system results in an occurrence of squeezed states: The driving field  $\mathbf{E} \propto b + b^\dagger$  may be regarded as a coherent state. Then, the operators  $b$  and  $b^\dagger$  can be replaced by classical amplitudes  $\beta(t) e^{-i\omega_b t}$  and  $\beta^*(t) e^{i\omega_b t}$ .

With these assumptions, the interaction part in both Hamiltonians simply reads

$$H_{I,i} = i\hbar (\eta_i^* a^2 - \eta_i a^{\dagger 2}) .$$

Here  $\eta_2 = \beta\chi_2$  and  $\eta_3 = \beta^2\chi_3$  are scalars that describe the interaction strength. For this interaction, the unitary evolution operator takes the form of a squeezing operator:

$$U_I(t) = \exp[-iH_I t/\hbar] = \exp[(\eta_i^* a^2 - \eta_i a^{\dagger 2}) t] = S(2\eta t) .$$

Unfortunately, the intrinsic losses of NAs generally prevent the creation of squeezed light. We have analyzed squeezed state creation for several realistic parameters of the a nonlinear NA material or nonlinear embedding materials.

For example, a  $\chi_3$  of silver in the order of  $10^{-8}$ esu [382] results in experimentally inaccessible squeezing. Preliminary estimations suggest that an enhancement in  $\chi_3$  by several orders of magnitude would be required. However, squeezing has been demonstrated in other systems with a much stronger nonlinearity, *i.e.* in semiconductor microcavities [383]. A combination of different approaches might be feasible. For example a NA may be embedded in a semiconductor microcavity at low temperatures. This seems possible in general, but also extremely challenging to realize.

Thus, at least up to now squeezed state production using NAs may not be possible. One more promising approach is the generation of entangled light.

### B.10.2 Entangled Light

If two Qs form a combined system via a certain kind of interaction, the quantum state of the combined system may not be written as a product of the single QS states. The QSs are said to be entangled [185]. An example is the interaction of two two-level systems [384] in the so-called Dicke basis [385], where entangled symmetric and antisymmetric states are formed (see App. B.11).

Most importantly, entanglement is a purely quantum phenomenon. Its discovery in 1935 during controversial discussions about the correctness of quantum mechanics involving Einstein, Podolsky

and Rosen [386], Schrödinger [387], Bohr [388] and many others lead to a much better understanding of quantum mechanics in general. Thirty years later, Bell pointed out that entanglement can be verified experimentally [389]. Ever since then it has been regarded as a powerful tool of quantum information theory [390, 391].

The concept of entangled Qs is not limited to localized Qs such as two-level systems or qubits. As we have seen in Sec. 3.2, the electromagnetic field can be quantized in terms of harmonic oscillators, which can be entangled. This is the case if the processes responsible for a multi-photon-emission are entangled, since then the radiated photons are entangled as well. This can be realized for example by two coupled emitting two-level systems, as discussed before. Radiative cascades of a single multilevel QS obeying two in principle indistinguishable relaxation paths can also be used to generate entangled photons [392–395].

The interaction of Qs is at the core of entanglement investigations. Since NAs are prime candidates for enhanced light-matter-interactions, their use for entanglement schemes is now also under consideration. First implementations to create polarization- and frequency-entangled photon states have been proposed [81, 396]. The investigated physical process, however, is often an enhancement in the emission rate of the entangled photons. The entanglement itself results from the QS coupled to the NA, which takes only a passive role. Thus, NA entangled state generation can often be seen as a sophisticated case of single-photon emission into two different channels. Hence, a thorough understanding of single photon emission helps to grasp important aspects of NA enhanced entangled photon generation. Nevertheless, the QNM quantization can be used to go beyond these Purcell factor considerations.

NAs generally enable stronger couplings, but also suffer from much higher losses compared to entanglement studies in the context of microcavities [397–399]. NAs may be considered as “bad cavities” [400]. Normally, such enhanced losses are detrimental for entanglement. But using the QNM quantization scheme, Hou *et al.* have demonstrated that the losses might be used to enhance entanglement in suitably designed hybrid systems [91] (see also Refs. [323, 324]).

## B.11 Two Quantum Systems coupled to a Nanoantenna: Eigenstates of the Hamiltonian

If a single-mode NA is coupled to two two-level systems, the energy spectrum in the lossless case can be given explicitly. This subsection is equivalent to App. C of Ref. [80] with minor adjustments.

It is often advantageous to analyze problems of coupled two-level systems in the so-called Dicke basis. In this basis, the ground and excited states,  $|0\rangle$  and  $|1\rangle$ , of both two-level systems form a combined eigenbasis [385]:  $\{|D\rangle \equiv |e\rangle \otimes |e\rangle, |S\rangle \equiv \frac{1}{\sqrt{2}}(|e\rangle \otimes |g\rangle + |g\rangle \otimes |e\rangle), |A\rangle \equiv \frac{1}{\sqrt{2}}(-|e\rangle \otimes |g\rangle + |g\rangle \otimes |e\rangle), \text{ and } |G\rangle \equiv |g\rangle \otimes |g\rangle\}$ . We shall denote  $|D\rangle$  as doubly excited state,  $|S\rangle$  and  $|A\rangle$  as symmetric and antisymmetric states, and  $|G\rangle$  as ground state.

In the Dicke basis, the Hamiltonian of the hybrid system [Eq. (70)] reads

$$H = \frac{1}{2}\hbar\omega_0 (2|D\rangle\langle D| + |S\rangle\langle S| + |A\rangle\langle A|) + \hbar\omega_{\text{na}}a^\dagger a - \hbar\sqrt{2}\kappa (\Sigma_+ a + a^\dagger \Sigma_-) .$$

Here,

$$\Sigma_+ = \frac{1}{\sqrt{2}} \left( \sigma_+^{(1)} + \sigma_+^{(2)} \right) = |D\rangle\langle S| + |S\rangle\langle G|$$

is the creation operators of an excitation in both Qs,  $\Sigma_- = \Sigma_+^\dagger$  the corresponding annihilation operator. Noteworthy, the antisymmetric state is decoupled in the isolated system and can be populated only by asymmetric decay mechanisms or illuminations. Thus, it is sufficient to consider only the effective three-level system, whose states belong to the Hilbert space spanned by



$\{|G\rangle, |S\rangle, |D\rangle\}$ .

We shall give the explicit form of the eigenstates of the Hamiltonian and the corresponding eigenenergies in the case of resonance between Qs and NA ( $\omega_{\text{na}} = \omega_{\text{qs}}$ ). The states of the hybrid system can be expressed in the Dicke basis for the Qs, and in the Fock basis  $\{|m\rangle\}_{m=0}^{\infty}$  for the NA.

Each state can be characterized by the total number of excitations  $n$  it corresponds to. For instance,  $n = 0$  stands for the total ground state of the system  $|\psi_0\rangle = |G, 0\rangle$  with eigenenergy  $E_0 = 0$ . For a single excitation ( $n = 1$ ), there are two eigenstates and eigenvalues:

$$|\psi_{1,\pm}\rangle = \pm|S, 0\rangle + |G, 1\rangle, \quad E_{1,\pm} = \hbar\omega_{\text{qs}} \mp \sqrt{2}\hbar\kappa.$$

However, if the number of excitations amounts to  $n \geq 2$ , there are three eigenstates:

$$\begin{aligned} |\psi_{n,\pm}\rangle &= \sqrt{n-1}|D, n-2\rangle \pm \sqrt{2n-1}|S, n-1\rangle + \sqrt{n}|G, n\rangle \quad \text{with} \quad E_{n,\pm} = n\hbar\omega_{\text{qs}} \mp \sqrt{2(2n-1)}\hbar\kappa, \\ |\psi_{n,0}\rangle &= \sqrt{n}|D, n-2\rangle - \sqrt{n-1}|G, n\rangle, \quad E_{n,0} = n\hbar\omega_{\text{qs}}. \end{aligned}$$

Note that the states are not normalized here. The eigenstates of the total system cannot be written as a product of states of the QS and NA subsystems. Hence, the subsystems are inherently entangled by their interaction.

The eigenstates attain a more complicated form if the two-level systems are not at resonance with the NA ( $\omega_{\text{na}} \neq \omega_{\text{qs}}$ ). Then, the eigenenergies strongly depend on the detuning [Fig. 17 (b)]. In the strongly off-resonant limit, the interaction becomes negligible and the subsystems are independent. Consequently, the eigenenergies converge towards the unperturbed values.

Furthermore, in the limit of strong field intensities, *i.e.* for large numbers of excitations, the eigenstates become approximately separable:

$$|\psi_{n,\pm}\rangle \approx (|D\rangle \pm \sqrt{2}|S\rangle + |G\rangle) \otimes |n\rangle \quad \text{and} \quad |\psi_{n,0}\rangle \approx (|D\rangle - |G\rangle) \otimes |n\rangle.$$

The interaction energies are then given by  $\Delta E_{n,\pm} = \mp 2\hbar\kappa\sqrt{n}$ ,  $\Delta E_{n,0} = 0$ . This means, that in the limit of large field intensities, even though the field has strong influence on the Qs, their effect on the NA state is negligible.

## C Miscellaneous

### C.1 Acknowledgements

A good work environment often creates a virtuous circle in which synergetic effects help the involved people to achieve much more than individually. I was very lucky to be in such a situation. In this section I would like to thank all those people that helped me during my doctoral studies to finally write this thesis.

Prof. Falk Lederer's Photonics group at the Institute of Condensed Matter Theory and Solid State Optics at the Friedrich-Schiller-University Jena is successful in highly competitive fields. To join the group was by no means self-evident after my discontinuation of a PhD thesis in Göttingen and I thank Prof. Lederer for this chance to put things right. I also thank him for encouraging words in several occasions and our inspiring discussions about physical concepts. With simple questions, he was often able to bring order into the chaos of my thoughts and writings. His trust in my abilities during a number of lectures and the whole time of my thesis have always been a solid ground to stand on.

My direct supervisor for the thesis was Prof. Carsten Rockstuhl, now at the Institute for Theoretical Solid State Physics at the Karlsruhe Institute of Technology. He has energetically supported me during all these years and still continued even when he was building up his new group. I thank Prof. Rockstuhl especially for all the freedom and resources he provided. He was always open-minded and helped me to finalize numerous projects. I also learnt a lot from him how to spot new and interesting topics but also to be critical against upcoming trends. I thank him for honest and pertinent replies to all kinds of questions.

I would also like to thank all other members of the Photonics group, too. One of the main open secrets of our joint success was the inspiring, creative and professional atmosphere that all of us created. It is a pleasure for me to thank Mohamed Farhat for all the nice moments we shared in the office, during lunch or playing football. Mohamed is such a polite guy that he never actually said that my French is just horrible. I thank Shakeeb Bin Hasan not only for his extremely kind personality, but also for our joint projects in which he provided the vast majority of all the work. Rasoul Alaee deserves special credit for his enormous effort in numerous ongoing investigations and his very positive mindset. Many thanks go to Karolina Słowik not just for her efficient work, but also our inspiring controversies. I also like to thank Samuel Wiesendanger to endure our lively debates during lunch. Furthermore, I appreciate Renwen Yu for his positive charisma and Jiamin Hou for her serious questions about physics and life in general.

Stefan Mühlig is greatly acknowledged for his ability to make things work. His outstanding professional attitude was exemplary not just for me. I like to thank Toni Eichelkraut for his smart contributions to our joint paper, our discussions about quantum optics and many other fields of science. I also enjoyed very much to work with Jing Qi. She was very diligent and I hope that she does not suffer from nightmares involving metallic discs. The same, only replacing discs with spheroids, goes for Jakob Straubel who performed countless simulations for Karolina and me. Jing and Jakob endured my supervision, which cannot be acknowledged enough.

I thank Sören Schmidt to be positive towards new ideas in research and teaching and to actually put effort in their realization. The same holds for Christoph Menzel who I also acknowledge for open and honest discussions. I want to accredit Tobias Kienzler for our conversations about physical concepts and his courage to face an unpleasant situation. Furthermore I would like to recognize the lessons I learnt from those working on topics that I am very little familiar with: Stefan Skupin, Rumén Iliev, Oleg Egorov, Christoph Etrich, Albrecht Werner, and Xuekai Ma. All of them have been very kind and helpful in a number of occasions.

Everything would fall apart without certain people in our group. I would like to thank our secretary Szilvia Mammel for her patience with me and her efficient way to solve problems I often didn't even know they existed. Lutz Leine manages all computer-related issues, the small and big ones. I thank him especially for the installation of tools I desperately needed.

I am also indebted to people at other research institutions. I exchanged a lot of interesting ideas and scientific approaches with Dennis Lehr and Kay Dietrich from the Institute of Applied Physics at the Friedrich-Schiller-University Jena. I thank both for our tight collaborations and all the detailed information about experimental realizations they provided. I also acknowledge the ongoing efforts by Mahshid Chekini from the Physical Chemistry Department at the University of Geneva who is always able to show surprising results. There is no doubt I further profited from in-depth discussions with Prof. Reuven Gordon (University of Victoria), Moshik Cohen (Bar-Ilan University), Kasey Russel (Harvard University), and Prof. Javier Aizpurua (Spanish Council for Scientific Research).

Thanks go also to Prof. Thomas Pertsch and Prof. Stephan Fritzsche for our joint teaching courses. Because of the provided freedom and efficient organization everything went very smoothly. This was also the case during several project proposals together with Christian Helgert and Prof. Alexander Szameit who spared me a lot of work. Dörte Hansen was also particularly helpful in correcting early versions of this thesis and proved very useful suggestions.

I also like to thank Karsten Verch to help me out with some spectacular illustrations that he managed to finalize under heavy workload.

The list of people that supported me cannot be complete without my family. But there are no words with which I could even remotely express my gratitude. Thank you<sup>10</sup> Julia, Ute, Susanne, Denis, Bernd, Wilma, Johannes, Birgit, Holger, Bianca, and Alex.

## C.2 Publications

In the following all publications by the author that appeared in peer-reviewed journals as of November 2014 are listed. Those publications that were directly discussed in this work are denoted by a bold title. A list of invited talks and conference contributions is provided afterwards.

### Peer reviewed Journals

1. **R. Filter**, C. Bösel, G. Toscano, F. Lederer, and C. Rockstuhl: “Nonlocal effects: relevance for the spontaneous emission rates of quantum emitters coupled to plasmonic structures”, *Opt. Lett.* **39** (21), p. 6118, 2014
2. D. Lehr, R. Alaei, **R. Filter**, K. Dietrich, T. Siefke, C. Rockstuhl, F. Lederer, E.-B. Kley, and A. Tünnermann: “Plasmonic nanoring fabrication tuned to pitch: Efficient, deterministic, and large scale realization of ultra-small gaps for next generation plasmonic devices”, *Appl. Phys. Lett.* **105** (14), p. 143110, 2014
3. **R. Filter**, K. Słowik, J. Straubel, F. Lederer, and C. Rockstuhl: “**Nanoantennas for ultra-bright single photon sources**”, *Opt. Lett.* **39** (5), p. 1246, 2014
4. K. Słowik, **R. Filter**, J. Straubel, F. Lederer, and C. Rockstuhl: “Coupling of quantum emitters and metallic nanoantennae for the generation of nonclassical light at high rates”, *Phys. Scr.* **T160**, p. 014037, 2014
5. S. B. Hasan, C. Etrich, **R. Filter**, C. Rockstuhl, and F. Lederer: “Enhancing the nonlinear response of plasmonic nanowire antennas by engineering their terminations”, *Phys. Rev. B* **88** (20), p. 205125, 2013

6. K Słowik, **R. Filter**, J Straubel, F. Lederer, and C. Rockstuhl: “**Strong coupling of optical nanoantennas and atomic systems**”, Phys. Rev. B **88** (19), p. 195414, 2013
7. **R. Filter**, M. Farhat, M. Steglich, R. Alaee, C. Rockstuhl, and F. Lederer: “Tunable graphene antennas for selective enhancement of THz-emission”, Opt. Expr. **21** (3), p. 3737, 2013
8. **R. Filter**, S. Mühlig, T. Eichelkraut, C. Rockstuhl, and F. Lederer: “**Controlling the dynamics of quantum mechanical systems sustaining dipole-forbidden transitions via optical nanoantennas**”, Phys. Rev. B **86** (3), p. 035404, 2012
9. **R. Filter**, J. Qi, C. Rockstuhl, and F. Lederer: “**Circular optical nanoantennas: an analytical theory**”, Phys. Rev. B **85** (12), p. 125429, 2012
10. S. B. Hasan, **R. Filter**, A Ahmed, R Vogelgesang, R Gordon, C. Rockstuhl, and F. Lederer: “Relating localized nanoparticle resonances to an associated antenna problem”, Phys. Rev. B **84** (19), p. 195405, 2011
11. **R. Filter**, T. Scharf, and H. P. Herzig: “High resolution displacement detection with speckles: accuracy limits in linear displacement speckle metrology”, J. Eur. Opt. Soc. **5**, p. 10035s, 2010
12. **R. Filter** and A Kleinwächter: “On the multipole moments of a rigidly rotating fluid body”, Ann. Phys. **18** (2-3), p. 102, 2009
13. R. Arlt, A. Sule, **R. Filter**: “Stability of the solar tachocline with magnetic fields”, Astron. Nachr. **328** (10), p. 1142, 2007

### Conference Proceedings

1. 1. D. Lehr, **R. Filter**, R. Alaee, K. Dietrich, C. Rockstuhl, F. Lederer, E.-B. Kley, and A. Tünnermann: “Enhancing the Efficiency of Upconversion by Double-Resonant Plasmonic Nanorings”, Optical Nanostructures and Advanced Materials for Photovoltaics 2014, Canberra, Australia
2. **R. Filter**, K. Słowik, J. Straubel, C. Rockstuhl, and F. Lederer: “Towards Strong Coupling of Nanoantennas and Quantum Systems”, DokDok 2013, Suhl, Germany
3. **R. Filter**, S. Mühlig, T. Eichelkraut, C. Rockstuhl, and F. Lederer: “Controlling Light-Matter-Interactions using Nanoantennas”, DokDok 2012, Schloss Oppurg, Germany
4. **R. Filter**, C. Rockstuhl, and F. Lederer: “Calculating resonances using the Boundary Element Method – A brief Introduction”, DokDok 2011, Naumburg, Germany

### Invited Talks

1. C. Rockstuhl, **R. Filter**, K. Słowik, J. Straubel, and G. Toscano: “Quantum optical properties of hybrid photonic nanostructures”, International Symposium on Nanophotonics 2014, Jena, Germany
2. C. Rockstuhl, J. Straubel, J. Hou, C. Bosel, K. Slowik, and **R. Filter**: “Weak and strong coupling of quantum emitters with optical nanoantennas”, META 2014, Singapore
3. C. Rockstuhl, **R. Filter**, S. Mühlig, T. Eichelkraut, S. Fischer, J. C. Goldschmidt, and F. Lederer: “Controlling the dynamics of quantum mechanical process using meta-atoms”, PIERS 2013, Taipai, Taiwan.

4. C. Rockstuhl, S. Mühlig, **R. Filter**, A. Cunningham, T. Bürgi, J. Dintinger, and T. Scharf: “Bottom-up metamaterials and plasmonic elements with metallic nanoparticles as basic building blocks”, PECS-X 2012, Santa Fe, New Mexico, USA.

### Conference Contributions

1. **R. Filter**, K. Słowik, J. Straubel, F. Lederer, and C. Rockstuhl: “Nanoantennas for ultra-bright single photon sources“, Nanolight 2014, Benasque, Spain
2. S. Bin Hasan, C. Etrich, **R. Filter**, C. Rockstuhl, and F. Lederer: “Enhancing the second harmonic generation of plasmonic nanowire antennas by tailoring their terminations“, UNO 3 2013, Bad Dürkheim, Germany
3. K. Słowik, **R. Filter**, J. Straubel, C. Rockstuhl, and F. Lederer, “A fully quantum description of hybrid nanosystems: Coupling of atoms and metallic nanoantennas“, CEWQO’ 2013, Stockholm, Sweden
4. K. Słowik, **R. Filter**, J. Straubel, C. Rockstuhl, and F. Lederer: “Optical Properties of Hybrid Atomic and Plasmonic Systems in the Weak and Strong Coupling Regime“, Metamaterials 2013, Bordeaux, France
5. S. Bin Hasan, C. Etrich, **R. Filter**, C. Rockstuhl, F. Lederer, “Tailoring the quadratic response of nanoantennas: use of a waveguide model”, OWTNM 2013, Twente, The Netherlands
6. **R. Filter**, M. Steglich, M. Farhat, R. Alaei, C. Rockstuhl, and F. Lederer, “Tunable Graphene Antennas for Selective Enhancement of THz-Emission” Nanometa 2013, Seefeld, Austria
7. C. Rockstuhl, **R. Filter**, T. Eichelkraut, S. Mühlig, S. Fischer, J. C. Goldschmidt, and F. Lederer: “Controlling the dynamics of quantum mechanical systems using meta-atoms”, Metamaterials 2012, St. Petersburg, Russia.

## C.3 Short Curriculum Vitae

### Robert Filter

Friedrich-Engels-Str. 77  
07749 Jena



Born 10. August 1982  
in Grevesmühlen, Germany  
Married, two children

### Work Experience

---

- 2009 Mar.–Apr. Scientist. Task: Investigate a method for high accuracy displacement detection  
*École polytechnique fédérale de Lausanne, Switzerland*
- 2003–2007 Various temporary work contracts as student assistant in mathematics and theoretical physics: seminar host and control of student works  
*Friedrich-Schiller-University Jena, Germany*

### Academic Record

---

- 2010–2014 PhD studies: nanoantennas and their potential in light-matter-interactions  
*Friedrich-Schiller-University Jena, Germany*
- 2009–2010 PhD studies: application of statistical physics to evolutionary genomics  
*Max-Planck-Institute for Dynamics and Self-Organization Göttingen, Germany*
- 2008 Diploma Thesis “Multipolmomente axialsymmetrisch stationärer Raumzeiten und die Quadrupol-Vermutunng”, mark 1.0  
*Friedrich-Schiller-University Jena, Germany and Max-Planck-Institute for Gravitational Physics Potsdam, Germany*
- 2003–2008 Studies of physics, mark: 1.1  
*Friedrich-Schiller-University Jena, Germany*
- 2002 High-school graduation, with honours in physics  
*Humboldt Gymnasium Potsdam, Germany*

### Language Skills

---

- FLUENT: English
- BASICS: French
- MOTHER TONGUE: German

place - date

signature

## C.4 Ehrenwörtliche Erklärung

Hiermit erkläre ich ehrenwörtlich, dass ich die vorliegende Arbeit selbstständig, ohne unzulässige Hilfe Dritter und ohne Benutzung anderer als der angegebenen Hilfsmittel und Literatur angefertigt habe. Die aus anderen Quellen direkt oder indirekt übernommenen Daten und Konzepte sind unter Angabe der Quelle gekennzeichnet.

Bei der Auswahl und Auswertung folgenden Materials haben mir die nachstehend aufgeführten Personen in der jeweils beschriebenen Weise unentgeltlich geholfen:

1. Die Illustrationen in Abb. 5 (b), Abb. 10 (b) und Abb. 14 wurden von Karsten Verch unter meiner Anleitung erstellt.
2. Die für Abb. 6 verwendet numerischen Daten wurden von Jing Qi unter meiner Anleitung berechnet.
3. Die numerischen Ergebnisse in Abb. 11 (c)-(e) und Abb. 12 (c)-(e) wurden nach gemeinsamen Überlegungen durch Dr. Stefan Mühlig erzielt. Dies gilt ebenso für die analytischen Ergebnisse in Anhang B.3.1.
4. Toni Eichelkraut hat sehr zur Herleitung von Glg. (59) und Glg. (60) beigetragen. Er hat darüberhinaus Abb. 12 (b) erstellt.
5. Jakob Straubel hat die Simulationen durchgeführt, deren Ergebnisse in Abb. 9 (b), Abb. 13 (b) und (c) sowie Abb. 15 (b)-(e) dargestellt sind. Ich habe ihn dabei gemeinsam mit Dr. Karolina Słowik angeleitet.
6. Dr. Karolina Słowik hat mit frühere Versionen von Abb. 13 (d)-(f) erstellt. Dies gilt ebenso für Abb. 17 (b). Sie war ebenso an Teilen der Herleitungen in den Anhängen B.7, B.8 und B.11 beteiligt.

Weitere Personen waren an der inhaltlich-materiellen Erstellung der vorliegenden Arbeit nicht beteiligt. Insbesondere habe ich hierfür nicht die entgeltliche Hilfe von Vermittlungs- bzw. Beratungsdiensten (Promotionsberater oder andere Personen) in Anspruch genommen. Niemand hat von mir unmittelbar oder mittelbar geldwerte Leistungen für Arbeiten erhalten, die im Zusammenhang mit dem Inhalt der vorgelegten Dissertation stehen.

Die Arbeit wurde bisher weder im In- noch im Ausland in gleicher oder ähnlicher Form einer anderen Prüfungsbehörde vorgelegt.

Die geltende Promotionsordnung der Physikalisch-Astronomischen Fakultät ist mir bekannt.

Ich versichere ehrenwörtlich, dass ich nach bestem Wissen die reine Wahrheit gesagt und nichts verschwiegen habe.

Datum, Unterschrift

## C.5 Zusammenfassung

Die vorliegende Arbeit befasst sich mit der theoretischen Beschreibung von Nanoantennen (NAs) und neuartigen Möglichkeiten der Licht-Materie-Wechselwirkung, welche sich durch NAs ergeben. Im Rahmen dieser Arbeit wurden einige Beiträge zur Weiterentwicklung dieses wissenschaftlichen Feldes dokumentiert. Diese sollen im Folgenden kurz zusammengefasst werden.

In Kap. 2 und 3 wurden theoretische Grundlagen eingeführt, um die Interaktion von NAs mit Quantensystemen (QSS) zu beschreiben. Die darin beschriebenen approximativen Interaktionsmodelle sind vielseitig und können in verschiedenen physikalischen Bereichen angewendet werden. Eine Beschreibung von NAs im Rahmen klassischer Elektrodynamik ermöglicht dabei den Entwurf komplexer NAs für bestimmte Anwendungen. Auf der anderen Seite wurde ein Schema zur Quantisierung von NAs basierend auf deren Quasinormalmoden (QNMs) entwickelt.

Die explizite Berechnung des quantisierten elektromagnetischen Feldes einer NA stellt eine Neuheit dar. Die so berechneten Felder können zur Untersuchung verschiedener Interaktionen mit QSS jenseits der elektrischen Dipolnäherung verwendet werden. Die vorgestellte Quantisierung mittels QNMs bedeutet eine Einschränkung auf NAs, die effektiv als verlustbehaftete harmonische Oszillatoren beschrieben werden können. Demzufolge wird die Freiheit, komplexe NAs zu entwerfen gegen die Möglichkeit, die Interaktion von NAs und QSS quantenmechanisch mittels weniger Parameter zu beschreiben, eingetauscht. Die QNM Quantisierung ist durch einen niedrigdimensionalen Hilbertraum und eine einfache Bestimmung der erwähnten Parameter mittels moderner numerischer Methoden vielseitig einsetzbar.

Die semiklassische Beschreibung der Wechselwirkung zwischen NA und QS wurde in Kap. 4 benutzt, um die Dynamik eines Dreiniveausystems zu untersuchen, welches durch eine Quadrupolwechselwirkung in der Nähe einer entsprechend entworfenen NA angeregt wird. Damit sind NAs in der Lage, Übergänge in QSS anzuregen, die mit anderen Techniken kaum zugänglich sind. Selbst unter Benutzung eines restriktiven Ratengleichungsmodells konnten interessante physikalische Effekte beschrieben werden. Neben der elektrischen Dipolnäherung wurde in Ref. [78] auch der Einfluss der Dynamik eines QSS auf experimentelle Messgrößen hinterfragt. Es zeigt sich etwa ein starker Einfluss der Lumineszenzerhöhung verglichen mit einer Freiraumanregung in Abhängigkeit von der internen Dynamik des QSS. Ein allgemeiner Ansatz zur Beschreibung von Multipolwechselwirkungen mit Hilfe einer lokalen Entwicklung der Felder, welche elektrische und magnetische Effekte klar voneinander trennt, wurde ebenfalls eingeführt. Diese Beiträge haben womögliche die Art, wie Light-Materie-Wechselwirkungen untersucht werden beeinflusst.

Ein Leitmotiv unserer Arbeit ist es, zu untersuchende Effekte mit dem physikalisch einfachsten möglichen System zu studieren. Dies bedeutet insbesondere eine möglichst angepasste theoretische Beschreibung und weithin vereinfachte NA Geometrien. Um Interaktionen zwischen NAs und QSS quantenmechanisch zu beschreiben, bedarf es einer Quantisierung der Felder der NAs. Dies ist insbesondere der Fall, wenn die Eigenschaften des emittierten Lichtes des gekoppelten Systems untersucht werden sollen. In Kap. 5 wurde die Möglichkeit untersucht, NAs als lichtstarke Einzelphotonenquellen zu benutzen, welche für mögliche Anwendungen in der Quantenkommunikation wichtig sein könnten. Wir haben herausgestellt, dass die Erhöhung der spontanen Emissionsrate nicht die einzige wichtige Kenngröße für lichtstarke Einzelphotonenquellen ist. Sowohl die Anregungsart als auch die -rate müssen beachtet werden. Es ist darüberhinaus nötig, die nichtklassischen Eigenschaften des emittierten Lichtes zu verifizieren. Mit Hilfe von numerischen und analytischen Untersuchungen konnten in Ref. [89] verschiedene notwendige Kompromisse zwischen Effizienz, Purcell Faktor und nichtklassischen Eigenschaften des emittierten Lichtes herausgestellt werden. Im Allgemeinen scheint es notwendig zu sein, die Interaktion zwischen NAs und QSS quantenmechanisch zu beschreiben.



Im Falle der starken Kopplung zwischen Qs und NAs kann die Dynamik des Systems nur quantenmechanisch konsistent beschrieben werden. In Kap. 6 wurde die Möglichkeit untersucht, die starke Kopplung zwischen Qs und dafür entworfenen NAs zu realisieren (Ref. [80]). Wir konnten zeigen, dass dieses Ziel im Prinzip erreicht werden könnte. Jedoch setzen verschiedene gegensätzliche Wirkungsmechanismen zwischen der NA Effizienz und den Kopplungsraten Grenzen beim Erreichen von hohen Verhältnissen von Kopplungsstärke zu Verlustrate. Zusätzlich sind die notwendigen kleinen Dimensionen der NAs und eine präzise Platzierung der Qs sehr anspruchsvoll. Wenn die starke Kopplung von Qs und NAs erreicht werden kann, ergeben sich jedoch lohnenswerte Perspektiven. Dies kann damit begründet werden, dass sich die dynamischen und spektralen Eigenschaften eines solchen hybriden Systems stark von denen der isolierten Systeme unterscheiden.

Zusammenfassend wurde gezeigt, wie verschiedene Beschreibungen der Interaktion von NAs und Qs interessante Möglichkeiten für grundlegende Forschung und Anwendungen bieten können. Semiklassische Ansätze ermöglichen detaillierte Untersuchungen anspruchsvoller NA Geometrien, wohingegen die QNM Quantisierung eine vollständig quantenmechanische Beschreibung der Interaktion erlaubt.

## References

- [1] J. J. Thomson, *Notes on recent researches in electricity and magnetism: intended as a sequel to Professor Clerk-Maxwell's Treatise on electricity and magnetism* (Clarendon Press, 1893).
- [2] A. Sommerfeld, *Annalen der Physik und Chemie* **303**, 233 (1899).
- [3] A. Sommerfeld, *Annalen der Physik* **333**, 665 (1909).
- [4] R. P. Feynman, *Engineering and Science* **23**, 22 (1960).
- [5] M. G. Stepanova and S. Dew, *Nanofabrication* (Springer, 2012).
- [6] P. Bharadwaj, B. Deutsch, and L. Novotny, *Adv. Opt. Phot.* **1**, 438 (2009).
- [7] J. A. Schuller and M. L. Brongersma, *Opt. Expr.* **17**, 24084 (2009).
- [8] K. Lee, X. Chen, H. Eghlidi, P. Kukura, R. Lettow, A. Renn, V. Sandoghdar, and S. Götzinger, *Nat. Phot.* **5**, 166 (2011).
- [9] A. E. Krasnok, A. E. Miroshnichenko, P. A. Belov, and Y. S. Kivshar, *Opt. Expr.* **20**, 20599 (2012).
- [10] A. E. Krasnok, I. S. Maksymov, A. I. Denisyuk, P. A. Belov, A. E. Miroshnichenko, C. R. Simovski, and Y. S. Kivshar, *Physics-USpekhi* **56**, 539 (2013).
- [11] M. Munsch, N. S. Malik, E. Dupuy, A. Delga, J. Bleuse, J.-M. Gérard, J. Claudon, N. Gregersen, and J. Mørk, *Phys. Rev. Lett.* **110**, 177402 (2013).
- [12] R. Filter, M. Farhat, M. Steglich, R. Alaee, C. Rockstuhl, and F. Lederer, *Opt. Expr.* **21**, 3737 (2013).
- [13] J. Wen, S. Romanov, and U. Peschel, *Opt. Expr.* **17**, 5925 (2009).
- [14] A. Alù and N. Engheta, *Phys. Rev. Lett.* **104**, 213902 (2010).
- [15] E. H. Synge, *The London, Edinburgh, and Dublin Philosophical Magazine and Journal of Science* **6**, 356 (1928).
- [16] M. Fleischmann, P. Hendra, and A. McQuillan, *Chem. Phys. Lett.* **26**, 163 (1974).
- [17] J. Gersten and A. Nitzan, *Journ. Chem. Phys.* **73**, 3023 (1980).
- [18] A. Wokaun, J. Gordon, and P. Liao, *Phys. Rev. Lett.* **48**, 957 (1982).
- [19] H. Metiu, *Progr. Surf. Science* **17**, 153 (1984).
- [20] M. Moskovits, *Rev. Mod. Phys.* **57**, 783 (1985).
- [21] A. Otto, I. Mrozek, H. Grabhorn, and W. Akemann, *J. Phys.: Cond. Matt.* **4**, 1143 (1992).
- [22] H. Raether, *Excitation of plasmons and interband transitions by electrons*, 88 (Springer, 1980).
- [23] H. Raether, *Surface plasmons on smooth surfaces* (Springer, 1988).
- [24] U. C. Fischer and D. Pohl, *Phys. Rev. Lett.* **62**, 458 (1989).
- [25] K. Selby, M. Vollmer, J. Masui, V. Kresin, W. A. de Heer, and W. Knight, *Phys. Rev. B* **40**, 5417 (1989).
- [26] S. Maier, *Plasmonics: fundamentals and applications* (Springer, 2007).
- [27] D. W. Pohl, "Optical near field scanning microscope", (1987). EP Patent 0,112,401, filed Dec. 1982.
- [28] J. Wessel, *JOSA B* **2**, 1538 (1985).
- [29] R. D. Grober, R. J. Schoelkopf, and D. E. Prober, *Appl. Phys. Lett.* **70**, 1354 (1997).

- [30] S. A. Maier, M. L. Brongersma, P. G. Kik, S. Meltzer, A. A. Requicha, and H. A. Atwater, *Adv. Mat.* **13**, 1501 (2001).
- [31] S. Kawata, *Near-field optics and surface plasmon polaritons*, vol. 81 (Springer, 2001).
- [32] O. Sqalli, M.-P. Bernal, P. Hoffmann, and F. Marquis-Weible, *Appl. Phys. Lett.* **76**, 2134 (2000).
- [33] O. Sqalli, I. Utke, P. Hoffmann, and F. Marquis-Weible, *Journ. Appl. Phys.* **92**, 1078 (2002).
- [34] D. P. Fromm, A. Sundaramurthy, P. J. Schuck, G. Kino, and W. E. Moerner, *Nano Lett.* **4**, 957 (2004).
- [35] P. J. Schuck, D. P. Fromm, A. Sundaramurthy, G. S. Kino, and W. E. Moerner, *Phys. Rev. Lett.* **94**, 017402 (2005).
- [36] K. Crozier, A. Sundaramurthy, G. Kino, and C. Quate, *Journ. Appl. Phys.* **94**, 4632 (2003).
- [37] P. Mühlischlegel, H.-J. Eisler, O. J. F. Martin, B. Hecht, and D. W. Pohl, *Science* **308**, 1607 (2005).
- [38] J.-J. Greffet, *Science* **308**, 1561 (2005).
- [39] J. Alda, J. M. Rico-García, J. M. López-Alonso, and G. Boreman, *Nanotechnology* **16**, S230 (2005).
- [40] L. Novotny and N. van Hulst, *Nat. Phot.* **5**, 83 (2011).
- [41] E. Purcell, *Phys. Rev.* **69**, 681 (1946).
- [42] E. del Valle Reboul, “Quantum electrodynamics with quantum dots in microcavities”, Ph.D. thesis, Universidad Autónoma de Madrid (2008).
- [43] J. N. Farahani, D. W. Pohl, H.-J. Eisler, and B. Hecht, *Phys. Rev. Lett.* **95**, 017402 (2005).
- [44] P. Anger, P. Bharadwaj, and L. Novotny, *Phys. Rev. Lett.* **96**, 113002 (2006).
- [45] S. Kühn, U. Håkanson, L. Rogobete, and V. Sandoghdar, *Phys. Rev. Lett.* **97**, 017402 (2006).
- [46] R. Carminati, J.-J. Greffet, C. Henkel, and J. Vigoureux, *Opt. Comm.* **261**, 368 (2006).
- [47] L. Rogobete, F. Kaminski, M. Agio, and V. Sandoghdar, *Opt. Lett.* **32**, 1623 (2007).
- [48] T. Taminiau, F. Stefani, F. Segerink, and N. Van Hulst, *Nat. Phot.* **2**, 234 (2008).
- [49] A. G. Curto, G. Volpe, T. H. Taminiau, M. P. Kreuzer, R. Quidant, and N. F. van Hulst, *Science* **329**, 930 (2010).
- [50] T. Kosako, Y. Kadoya, and H. F. Hofmann, *Nat. Phot.* **4**, 312 (2010).
- [51] D. Dregely, R. Taubert, J. Dorfmueller, R. Vogelgesang, K. Kern, and H. Giessen, *Nat. Comm.* **2**, 267 (2011).
- [52] C. Rockstuhl, S. Fahr, and F. Lederer, *Journ. Appl. Phys.* **104**, 123102 (2008).
- [53] C. Rockstuhl and F. Lederer, *Appl. Phys. Lett.* **94**, 213102 (2009).
- [54] H. A. Atwater and A. Polman, *Nat. Mat.* **9**, 205 (2010).
- [55] J. Kern, S. Großmann, N. V. Tarakina, T. Häckel, M. Emmerling, M. Kamp, J.-S. Huang, P. Biagioni, J. C. Prangasma, and B. Hecht, *Nano Lett.* **12**, 5504 (2012).
- [56] C. Belacel, B. Habert, F. Bigourdan, F. Marquier, J.-P. Hugonin, S. Michaelis de Vasconcellos, X. Lafosse, L. Coolen, C. Schwob, C. Javaux, B. Dubertret, J.-J. Greffet, P. Senellart, and A. Maitre, *Nano Lett.* **13**, 1516 (2013).
- [57] D. Lehr, K. Dietrich, C. Helgert, T. Käsebier, H.-J. Fuchs, A. Tünnermann, and E.-B. Kley, *Opt. Lett.* **37**, 157 (2012).

- [58] K. Dietrich, D. Lehr, C. Helgert, A. Tünnermann, and E.-B. Kley, *Adv. Mat.* **24**, OP321 (2012).
- [59] D. Lehr, R. Alaee, R. Filter, K. Dietrich, T. Siefke, C. Rockstuhl, F. Lederer, E.-B. Kley, and A. Tünnermann, *Appl. Phys. Lett.* **105**, 143110 (2014).
- [60] S. Peng, J. M. McMahon, G. C. Schatz, S. K. Gray, and Y. Sun, *Proc. Nat. Acad. Sci.* **107**, 14530 (2010).
- [61] J. A. Scholl, A. L. Koh, and J. A. Dionne, *Nature* **483**, 421 (2012).
- [62] S. Raza, N. Stenger, S. Kadkhodazadeh, S. V. Fischer, N. Kostesha, A.-P. Jauho, A. Burrows, M. Wubs, and N. A. Mortensen, *Nanophot.* **2**, 131 (2013).
- [63] J. Zuloaga, E. Prodan, and P. Nordlander, *ACS Nano* **4**, 5269 (2010).
- [64] D. Marinica, A. Kazansky, P. Nordlander, J. Aizpurua, and A. G. Borisov, *Nano Lett.* **12**, 1333 (2012).
- [65] T. V. Teperik, P. Nordlander, J. Aizpurua, and A. G. Borisov, *Phys. Rev. Lett.* **110**, 263901 (2013).
- [66] R. C. Monreal, T. J. Antosiewicz, and S. P. Apell, *New Journ. Phys.* **15**, 083044 (2013).
- [67] C. David and F. J. Garcia de Abajo, *Journ. Phys. Chem. C* **115**, 19470 (2011).
- [68] A. Fernández-Domínguez, A. Wiener, F. García-Vidal, S. Maier, and J. Pendry, *Phys. Rev. Lett.* **108**, 106802 (2012).
- [69] G. Toscano, S. Raza, A. Jauho, N. Mortensen, and M. Wubs, *Opt. Expr.* **20**, 4176 (2012).
- [70] R. Filter, C. Bösel, G. Toscano, F. Lederer, and C. Rockstuhl, *Opt. Lett.* **39**, 6118 (2014).
- [71] R. Esteban, A. G. Borisov, P. Nordlander, and J. Aizpurua, *Nat. Comm.* **3**, 825 (2012).
- [72] K. Andersen, K. L. Jensen, N. A. Mortensen, and K. S. Thygesen, *Phys. Rev. B* **87**, 235433 (2013).
- [73] S. Karaveli and R. Zia, *Phys. Rev. Lett.* **106**, 193004 (2011).
- [74] T. Grosjean, M. Mivelle, F. Baida, G. Burr, and U. Fischer, *Nano Lett.* **11**, 1009 (2011).
- [75] T. H. Taminiau, S. Karaveli, N. F. van Hulst, and R. Zia, *Nat. Comm.* **3**, 979 (2012).
- [76] J. R. Zurita-Sánchez and L. Novotny, *Journ. Opt. Soc. Am. B* **19**, 1355 (2002).
- [77] A. Kern and O. J. Martin, *Phys. Rev. A* **85**, 022501 (2012).
- [78] R. Filter, S. Mühlig, T. Eichelkraut, C. Rockstuhl, and F. Lederer, *Phys. Rev. B* **86**, 035404 (2012).
- [79] A. Trügler and U. Hohenester, *Phys. Rev. B* **77**, 115403 (2008).
- [80] K. Słowik, R. Filter, J. Straubel, F. Lederer, and C. Rockstuhl, *Phys. Rev. B* **88**, 195414 (2013).
- [81] I. S. Maksymov, A. E. Miroshnichenko, and Y. S. Kivshar, *Phys. Rev. A* **86**, 011801 (2012).
- [82] R. Esteban, T. V. Teperik, and J. J. Greffet, *Phys. Rev. Lett.* **104**, 026802 (2010).
- [83] R. Hawaldar, U. Mulik, K. Patil, R. Pasricha, S. Sathaye, A. Lewis, and D. Amalnerkar, *Mat. Res. Bull.* **40**, 1353 (2005).
- [84] K. Li, X. Li, M. I. Stockman, and D. J. Bergman, *Phys. Rev. B* **71**, 115409 (2005).
- [85] J.-Y. Yan, W. Zhang, S. Duan, X.-G. Zhao, and A. O. Govorov, *Physical Review B* **77**, 165301 (2008).
- [86] E. Waks and D. Sridharan, *Phys. Rev. A* **82**, 043845 (2010).

- [87] V. Giannini, A. I. Fernández-Domínguez, Y. Sonnefraud, T. Roschuk, R. Fernández-García, and S. A. Maier, *Small* **6**, 2498 (2010).
- [88] M. Tame, K. McEnery, Ş. Özdemir, J. Lee, S. Maier, and M. Kim, *Nat. Phys.* **9**, 329 (2013).
- [89] R. Filter, K. Słowik, J. Straubel, F. Lederer, and C. Rockstuhl, *Opt. Lett.* **39**, 1246 (2014).
- [90] K. Słowik, R. Filter, J. Straubel, F. Lederer, and C. Rockstuhl, *Phys. Scr.* **2014**, 014037 (2014).
- [91] J. Hou, K. Słowik, F. Lederer, and C. Rockstuhl, *Phys. Rev. B* **89**, 235413 (2014).
- [92] A. Wipf, “Quantenmechanik II”, Lecture Notes, Theoretisch-Physikalisches-Institut Friedrich-Schiller-Universität Jena (2006).
- [93] C. A. Balanis, *Antenna Theory: Analysis and Design, 3rd ed.* (John Wiley & Sons, 2005).
- [94] W. L. Stutzman and G. A. Thiele, *Antenna theory and design, 3rd ed.* (John Wiley & Sons, 2012).
- [95] J.-J. Greffet, M. Laroche, and F. Marquier, *Phys. Rev. Lett.* **105**, 117701 (2010).
- [96] R. L. Olmon and M. B. Raschke, *Nanotechn.* **23**, 444001 (2012).
- [97] V. Giannini, A. I. Fernández-Domínguez, S. C. Heck, and S. A. Maier, *Chem. Rev.* **111**, 3888 (2011).
- [98] P. Biagioni, J.-S. Huang, and B. Hecht, *Rep. Progr. Phys.* **75**, 024402 (2012).
- [99] M. Agio and A. Alù, *Optical Antennas* (Cambridge University Press, 2013).
- [100] IEEE Std. 145-1993 pp. 1 – 32 (1993).
- [101] J. Li, A. Salandrino, and N. Engheta, *Phys. Rev. B* **76**, 245403 (2007).
- [102] I. S. Maksymov, I. Staude, A. E. Miroshnichenko, and Y. S. Kivshar, *Nanophot.* **1**, 65 (2012).
- [103] T. Pakizeh and M. Kall, *Nano Lett.* **9**, 2343 (2009).
- [104] T. Shegai, S. Chen, V. D. Miljković, G. Zengin, P. Johansson, and M. Käll, *Nat. Comm.* **2**, 481 (2011).
- [105] N. Bonod, A. Devilez, B. Rolly, S. Bidault, and B. Stout, *Phys. Rev. B* **82**, 115429 (2010).
- [106] A. Devilez, B. Stout, and N. Bonod, *ACS Nano* **4**, 3390 (2010).
- [107] B. Rolly, B. Stout, and N. Bonod, *Opt. Expr.* **20**, 20376 (2012).
- [108] M. Schnell, P. Alonso-Gonzalez, L. Arzubiaga, F. Casanova, L. Hueso, A. Chuvilin, and R. Hillenbrand, *Nat. Phot.* **5**, 283 (2011).
- [109] S. B. Hasan, R. Filter, A. Ahmed, R. Vogelgesang, R. Gordon, C. Rockstuhl, and F. Lederer, *Phys. Rev. B* **84**, 195405 (2011).
- [110] S. B. Hasan, C. Etrich, R. Filter, C. Rockstuhl, and F. Lederer, *Phys. Rev. B* **88**, 205125 (2013).
- [111] A. Alu and N. Engheta, *Nat. Phot.* **2**, 307 (2008).
- [112] M. Abb, P. Albella, J. Aizpurua, and O. L. Muskens, *Nano Lett.* **11**, 2457 (2011).
- [113] M. Kauranen and A. V. Zayats, *Nat. Phot.* **6**, 737 (2012).
- [114] I. S. Maksymov, A. E. Miroshnichenko, and Y. S. Kivshar, *Opt. Expr.* **20**, 8929 (2012).
- [115] L. D. Landau, E. M. Lifšic, J. B. Sykes, J. S. Bell, M. Kearsley, and L. P. Pitaevskii, *Electrodynamics of continuous media*, vol. 364 (Pergamon press Oxford, 1960).
- [116] F. Lederer and S. Skupin, *Fundamentals of Modern Optics* (Springer Verlag, Berlin, 2015).

- [117] I. V. Shadrivov, A. B. Kozyrev, D. W. van der Weide, and Y. S. Kivshar, *Appl. Phys. Lett.* **93**, 161903 (2008).
- [118] T. Utikal, T. Zentgraf, T. Paul, C. Rockstuhl, F. Lederer, M. Lippitz, and H. Giessen, *Phys. Rev Lett.* **106**, 133901 (2011).
- [119] S. Sershen, S. Westcott, N. Halas, and J. West, *Journ. Biomed. Mat. Res.* **51**, 293 (2000).
- [120] T. Driscoll, H.-T. Kim, B.-G. Chae, B.-J. Kim, Y.-W. Lee, N. M. Jokerst, S. Palit, D. R. Smith, M. Di Ventra, and D. N. Basov, *Science* **325**, 1518 (2009).
- [121] G. Baffou, R. Quidant, and F. J. Garcia de Abajo, *ACS Nano* **4**, 709 (2010).
- [122] G. Baffou and R. Quidant, *Las. & Phot. Rev.* **7**, 171 (2013).
- [123] L. Novotny and B. Hecht, *Principles of Nano-Optics* (Cambridge university press, 2006).
- [124] P. B. Johnson and R. W. Christy, *Phys. Rev. B* **6**, 4370 (1972).
- [125] E. D. Palik, *Handbook of optical constants of solids*, vol. 3 (Academic press, 1998).
- [126] G. Boudarham, R. Abdeddaim, and N. Bonod, *Appl. Phys. Lett.* **104**, 021117 (2014).
- [127] J. Sun, E. Timurdogan, A. Yaacobi, E. S. Hosseini, and M. R. Watts, *Nature* **493**, 195 (2013).
- [128] C. Kittel and P. McEuen, *Introduction to solid state physics*, vol. 8 (Wiley New York, 1986).
- [129] P. R. West, S. Ishii, G. V. Naik, N. K. Emani, V. M. Shalaev, and A. Boltasseva, *Laser & Phot. Rev.* **4**, 795 (2010).
- [130] M. Rycenga, C. M. Cobley, J. Zeng, W. Li, C. H. Moran, Q. Zhang, D. Qin, and Y. Xia, *Chem. Rev.* **111**, 3669 (2011).
- [131] P. Tassin, T. Koschny, M. Kafesaki, and C. M. Soukoulis, *Nat. Phot.* **6**, 259 (2012).
- [132] S. Mühlig, “Towards self-assembled metamaterials”, Ph.D. thesis, Friedrich-Schiller-Universität Jena (2014).
- [133] P. Wang, D. Zhang, and R. Qiu, *Appl. Surf. Sci.* **257**, 8438 (2011).
- [134] T. Weber, T. Käsebier, M. Helgert, E.-B. Kley, and A. Tünnermann, *Appl. Opt.* **51**, 3224 (2012).
- [135] M. Castro-Lopez, D. Brinks, R. Sapienza, and N. F. van Hulst, *Nano Lett.* **11**, 4674 (2011).
- [136] M. W. Knight, L. Liu, Y. Wang, L. Brown, S. Mukherjee, N. S. King, H. O. Everitt, P. Nordlander, and N. J. Halas, *Nano Lett.* **12**, 6000 (2012).
- [137] C. F. Bohren and D. R. Huffman, *Absorption and Scattering of Light by Small Particles* (1998).
- [138] R. Filter, “Multipolmomente axialsymmetrisch stationärer Raumzeiten und die Quadrupol-Vermutung”, Diplomarbeit, Friedrich-Schiller-Universität Jena (2008).
- [139] R. Filter and A. Kleinwächter, *Ann. Phys.* **18**, 102 (2009).
- [140] C. Höppener, Z. J. Lapin, P. Bharadwaj, and L. Novotny, *Phys. Rev. Lett.* **109**, 017402 (2012).
- [141] M. P. Busson, B. Rolly, B. Stout, N. Bonod, and S. Bidault, *Nat. Comm.* **3**, 962 (2012).
- [142] N. Grillet, D. Manchon, F. Bertorelle, C. Bonnet, M. Broyer, E. Cottancin, J. Lermé, M. Hillenkamp, and M. Pellarin, *ACS Nano* **5**, 9450 (2011).
- [143] N. Liu, M. L. Tang, M. Hentschel, H. Giessen, and A. P. Alivisatos, *Nat. Mat.* **10**, 631 (2011).
- [144] D. Wang, W. Zhu, M. D. Best, J. P. Camden, and K. B. Crozier, *Nano Lett.* **13**, 2194 (2013).
- [145] J. A. Fan, K. Bao, L. Sun, J. Bao, V. N. Manoharan, P. Nordlander, and F. Capasso, *Nano Lett.* **12**, 5318 (2012).

- [146] J.-S. Huang, V. Callegari, P. Geisler, C. Brüning, J. Kern, J. C. Prangma, X. Wu, T. Feichtner, J. Ziegler, P. Weinmann *et al.*, *Nat. Comm.* **1**, 150 (2010).
- [147] K. A. Bachman, J. J. Peltzer, P. D. Flammer, T. E. Furtak, R. T. Collins, and R. E. Hollingsworth, *Opt. Expr.* **20**, 1308 (2012).
- [148] L. Rosa, K. Sun, and S. Juodkazis, *Phys. Status Solidi (RRL) - Rap. Res. Lett.* **5**, 175 (2011).
- [149] C. Boyer, E. Kalnins, and W. Miller Jr, *Nagoya Math. J* **60**, 35 (1976).
- [150] P. M. Morse and H. Feshbach, *Methods of theoretical physics* (1953).
- [151] J. Aizpurua, P. Hanarp, D. S. Sutherland, M. Käll, G. W. Bryant, and F. J. Garcia de Abajo, *Phys. Rev. Lett.* **90**, 057401 (2003).
- [152] T. V. Teperik and A. Degiron, *Phys. Rev. B* **83**, 245408 (2011).
- [153] Y.-L. Xu, *Appl. Opt.* **34**, 4573 (1995).
- [154] J. D. Jackson, *Classical Electrodynamics Third Edition* (Wiley, 1998).
- [155] L. Novotny, *Phys. Rev. Lett.* **98**, 266802 (2007).
- [156] R. Gordon, *Phys. Rev. B* **74**, 153417 (2006).
- [157] R. Gordon, *Opt. Expr.* **17**, 18621 (2009).
- [158] J. Dorfmüller, R. Vogelgesang, R. T. Weitz, C. Rockstuhl, C. Etrich, T. Pertsch, F. Lederer, and K. Kern, *Nano Lett.* **9**, 2372 (2009).
- [159] R. Filter, J. Qi, C. Rockstuhl, and F. Lederer, *Phys. Rev. B* **85**, 125429 (2012).
- [160] B. E. Sernelius, *Surface Modes in Physics* (Wiley, 2001).
- [161] S. Nerkararyan, K. Nerkararyan, N. Janunts, and T. Pertsch, *Phys. Rev. B* **82**, 245405 (2010).
- [162] A. Y. Nikitin, S. G. Rodrigo, F. García-Vidal, and L. Martín-Moreno, *New Journ. Phys.* **11**, 123020 (2009).
- [163] A. Y. Nikitin, F. J. García-Vidal, and L. Martín-Moreno, *Phys. Rev. Lett.* **105**, 073902 (2010).
- [164] A. Taflove and S. C. Hagness (2000).
- [165] A. F. Oskooi, D. Roundy, M. Ibanescu, P. Bermel, J. D. Joannopoulos, and S. G. Johnson, *Comp. Phys. Comm.* **181**, 687 (2010).
- [166] F. Bigourdan, F. Marquier, J.-P. Hugonin, and J.-J. Greffet, *Opt. Expr.* **22**, 2337 (2014).
- [167] J. Qi, “Resonance Properties of Multilayered Optical Nanoantennas”, Master’s thesis, Friedrich-Schiller-Universität Jena (2012).
- [168] T. H. Taminiau, F. D. Stefani, and N. F. van Hulst, *Nano Lett.* **11**, 1020 (2011).
- [169] U. Hohenester and A. Trügler, *Comp. Phys. Comm.* **183**, 370 (2012).
- [170] C. Multiphysics, “4.3 user’s guide”, (2012).
- [171] M. N. Sadiku, *Numerical techniques in electromagnetics* (CRC press, 2010).
- [172] J.-W. Liaw, Selected Topics in Quantum Electronics, *IEEE Journal of* **14**, 1441 (2008).
- [173] J. A. Fan, K. Bao, C. Wu, J. Bao, R. Bardhan, N. J. Halas, V. N. Manoharan, G. Shvets, P. Nordlander, and F. Capasso, *Nano letters* **10**, 4680 (2010).
- [174] A. Artar, A. A. Yanik, and H. Altug, *Nano Lett.* **11**, 3694 (2011).
- [175] V. V. Klimov and V. S. Letokhov, *Phys. Rev. A* **54**, 4408 (1996).
- [176] W. Zhang, A. O. Govorov, and G. W. Bryant, *Phys. Rev. Lett.* **97**, 146804 (2006).

- [177] N. Bohr, *Zeitschr. Phys. A Hadrons and Nuclei* **2**, 423 (1920).
- [178] J. R. Nielsen, *The correspondence principle (1918-1923)* (Elsevier, 1976).
- [179] N. A. Doughty, *Lagrangian interaction* (Addison-Wesley, 1990).
- [180] W. Ehrenberg and R. Siday, *Proc. Phys. Soc. Sec. B* **62**, 8 (1949).
- [181] Y. Aharonov and D. Bohm, *Phys. Rev.* **115**, 485 (1959).
- [182] T. Förster, *Ann. Phys.* **437**, 55 (1948).
- [183] D. L. Dexter, *Journ. Chem. Phys.* **21**, 836 (1953).
- [184] V. Kulkarni, E. Prodan, and P. Nordlander, *Nano Lett.* **13**, 5873 (2013).
- [185] W. Vogel and D.-G. Welsch, *Quantum Optics: An Introduction* (2006).
- [186] T. G. Philbin, *New J. Phys.* **12**, 123008 (2010).
- [187] S. Scheel, L. Knöll, and D.-G. Welsch, *Phys. Rev. A* **60**, 4094 (1999).
- [188] M. Khanbekyan, L. Knöll, D.-G. Welsch, A. Semenov, and W. Vogel, *Phys. Rev. A* **72**, 053813 (2005).
- [189] C. Krattenthaler, S. I. Kryuchkov, A. Mahalov, and S. K. Suslov, *Int. Journ. Theor. Phys.* **52**, 4445 (2013).
- [190] A. F. Koenderink, *Opt. Lett.* **35**, 4208 (2010).
- [191] J. R. de Lasson, J. Mørk, and P. T. Kristensen, *JOSA B* **30**, 1996 (2013).
- [192] C. Sauvan, J.-P. Hugonin, I. Maksymov, and P. Lalanne, *Phys. Rev. Lett.* **110**, 237401 (2013).
- [193] S. Hughes, *ACS Phot.* (2013).
- [194] R.-C. Ge, P. T. Kristensen, J. Young, S. Hughes *et al.*, arXiv preprint (2013).
- [195] M. O. Scully and M. S. Zubairy, *Quantum Optics* (Cambridge University Press, 1997).
- [196] S. M. Dutra, *Cavity quantum electrodynamics: the strange theory of light in a box* (John Wiley & Sons, 2005).
- [197] M. Fox, *Quantum Optics: An Introduction*, vol. 15 (Oxford Univ. Press, 2006).
- [198] P. Meystre and M. Sargent, *Elements of quantum optics* (Springer, 2007).
- [199] K. J. Vahala, *Nature* **424**, 839 (2003).
- [200] P. A. M. Dirac, "Lectures on quantum mechanics", (1964).
- [201] V. von Weiskopf and E. Wigner, *Z. Phys.* **63**, 54 (1930).
- [202] S. John and T. Quang, *Phys. Rev. A* **50**, 1764 (1994).
- [203] U. Hoeppe, C. Wolff, J. Küchenmeister, J. Niegemann, M. Drescher, H. Benner, and K. Busch, *Phys. Rev. Lett.* **108**, 043603 (2012).
- [204] S. M. Hein and H. Giessen, *Phys. Rev. Lett.* **111**, 026803 (2013).
- [205] P. Leung, S. Liu, and K. Young, *Phys. Rev. A* **49**, 3982 (1994).
- [206] E. Ching, P. Leung, A. M. van den Brink, W. Suen, S. Tong, and K. Young, *Rev. Mod. Phys.* **70**, 1545 (1998).
- [207] K. Lee, P. Leung, and K. Pang, *JOSA B* **16**, 1409 (1999).
- [208] P. T. Kristensen, C. Van Vlack, and S. Hughes, *Opt. Lett.* **37**, 1649 (2012).
- [209] B. A. Lippmann and J. Schwinger, *Phys. Rev. B* **79**, 469 (1950).



- [210] F. G. de Abajo, Phys. Rev. B **60**, 6086 (1999).
- [211] J. Wiersig, J. Opt. A: Pure and Appl. Opt. **5**, 53 (2003).
- [212] V. Myroshnychenko, E. Carbó-Argibay, I. Pastoriza-Santos, J. Pérez-Juste, L. M. Liz-Marzán, and F. J. Garcia de Abajo, Adv. Mat. **20**, 4288 (2008).
- [213] A. González-Tudela, P. Huidobro, L. Martín-Moreno, C. Tejedor, and F. García-Vidal, Phys. Rev. B **89**, 041402 (2014).
- [214] B. J. Messinger, K. U. Von Raben, R. K. Chang, and P. W. Barber, Phys. Rev. B **24**, 649 (1981).
- [215] P. Alonso-González, P. Albella, F. Neubrech, C. Huck, J. Chen, F. Golmar, F. Casanova, L. Hueso, A. Pucci, J. Aizpurua, and R. Hillenbrand, Phys. Rev. Lett. **110**, 203902 (2013).
- [216] C. Menzel, E. Hebestreit, S. Mühlig, C. Rockstuhl, S. Burger, F. Lederer, and T. Pertsch, Opt. Expr. **22**, 9971 (2014).
- [217] A. Kossakowski, Rep. Math. Phys. **3**, 247 (1972).
- [218] G. Lindblad, Comm. Math. Phys. **48**, 119 (1976).
- [219] D. Heiss, S. Schaeck, H. Huebl, M. Bichler, G. Abstreiter, J. Finley, D. Bulaev, and D. Loss, Phys. Rev. B **76**, 241306 (2007).
- [220] H.-P. Breuer and F. Petruccione, *The theory of open quantum systems* (Oxford University Press, 2002).
- [221] H.-P. Breuer, in *Theoretical Foundations of Quantum Information Processing and Communication* (Springer, 2010), pp. 125–139.
- [222] K. Sakoda, *Optical properties of photonic crystals*, vol. 80 (Springer, 2005).
- [223] B. Deveaud, *The physics of semiconductor microcavities* (John Wiley & Sons, 2007).
- [224] F. P. Laussy, E. del Valle, and C. Tejedor, Phys. Rev. Lett. **101**, 083601 (2008).
- [225] J. Reithmaier, G. Şek, A. Löffler, C. Hofmann, S. Kuhn, S. Reitzenstein, L. Keldysh, V. Kulakovskii, T. Reinecke, and A. Forchel, Nature **432**, 197 (2004).
- [226] T. Hümmer, F. García-Vidal, L. Martín-Moreno, and D. Zueco, Phys. Rev. B **87**, 115419 (2013).
- [227] P. Gay-Balmaz and O. J. Martin, Appl. Opt. **40**, 4562 (2001).
- [228] M. Husnik, M. W. Klein, N. Feth, M. König, J. Niegemann, K. Busch, S. Linden, and M. Wegener, Nat. Phot. **2**, 614 (2008).
- [229] M. Husnik, S. Linden, R. Diehl, J. Niegemann, K. Busch, and M. Wegener, Phys. Rev. Lett. **109**, 233902 (2012).
- [230] N. Accanto, L. Piatkowski, J. Renger, and N. F. van Hulst, Nano Lett. **14**, 4078 (2014).
- [231] D. O. Krimer, M. Liertzer, S. Rotter, and H. E. Türeci, Phys. Rev. A **89**, 033820 (2014).
- [232] J. Johansson, P. Nation, and F. Nori, Comp. Phys. Comm. **184**, 1234 (2013).
- [233] R. Loudon, *The quantum theory of light* (Oxford university press, 2000).
- [234] T. Kawazoe, K. Kobayashi *et al.*, Phys. Rev. Lett. **88**, 067404 (2002).
- [235] S. Tojo and M. Hasuo, Phys. Rev. A **71**, 012508 (2005).
- [236] K. Deguchi, M. Okuda, A. Iwamae, H. Nakamura, K. Sawada, and M. Hasuo, Journ. Phys. Soc. Jap. **78**, 024301 (2009).
- [237] B. le Feber, N. Rotenberg, D. Beggs, and L. Kuipers, Nat. Phot. **8**, 43 (2014).
- [238] V. Lembessis and M. Babiker, Phys. Rev. Lett. **110**, 083002 (2013).

- [239] M. I. Stockman, S. V. Faleev *et al.*, Phys. Rev. Lett. **87**, 167401 (2001).
- [240] M.-W. Chu, V. Myroshnychenko, C. H. Chen, J.-P. Deng, C.-Y. Mou, and F. J. García de Abajo, Nano Lett. **9**, 399 (2008).
- [241] J.-Y. Yan, W. Zhang *et al.*, Phys. Rev. B **77**, 165301 (2008).
- [242] M. Liu, T.-W. Lee *et al.*, Phys. Rev. Lett. **102**, 107401 (2009).
- [243] I. Hertel and C. Schulz, *Atom-, Molekül- und Optische Physik* (Springer Verlag, Berlin, 2007).
- [244] C. M. Dodson and R. Zia, Phys. Rev. B **86**, 125102 (2012).
- [245] R. Pires, M. Ascoli, E. Eyler, P. Gould, and A. Derevianko, Phys. Rev. A **80**, 062502 (2009).
- [246] T. Gallagher, R. Kachru, and N. Tran, Phys. Rev. A **26**, 2611 (1982).
- [247] T. F. Gallagher, *Rydberg atoms*, vol. 3 (Cambridge University Press, 2005).
- [248] D. Tong, S. Farooqi, E. Van Kempen, Z. Pavlovic, J. Stanojevic, R. Côté, E. Eyler, and P. Gould, Phys. Rev. A **79**, 052509 (2009).
- [249] D. P. Craig and T. Thirunamachandran, *Molecular quantum electrodynamics: an introduction to radiation-molecule interactions* (Courier Dover Publications, 1998).
- [250] D. E. Stogryn and A. P. Stogryn, Molec. Phys. **11**, 371 (1966).
- [251] S. Mühlig, C. Menzel, C. Rockstuhl, and F. Lederer, Metamat. **5**, 64 (2011).
- [252] L. D. Barron, *Molecular light scattering and optical activity*, vol. 2 (Cambridge University Press Cambridge, 2004).
- [253] S. I. Bozhevolnyi, Opt. Expr. **14**, 9467 (2006).
- [254] A. Hänsel, O. A. Egorov, S. B. Hasan, C. Rockstuhl, and F. Lederer, Phys. Rev. A **85**, 053843 (2012).
- [255] F. Huth, A. Chuvilin, M. Schnell, I. Amenabar, R. Krutokhvostov, S. Lopatin, and R. Hillenbrand, Nano Lett. **13**, 1065 (2013).
- [256] S. Mühlig, A. Cunningham, J. Dintinger, T. Scharf, T. Bürgi, F. Lederer, and C. Rockstuhl, Nanophot. **2**, 211 (2013).
- [257] K. J. Savage, M. M. Hawkeye, R. Esteban, A. G. Borisov, J. Aizpurua, and J. J. Baumberg, Nature **491**, 574 (2012).
- [258] W. Wiese and J. Fuhr, J. Phys. Chem. Ref. Data **38**, 565 (2009).
- [259] M. Lipeles, R. Novick, and N. Tolk, Phys. Rev. Lett. **15**, 690 (1965).
- [260] L. Narducci, M. Scully, G.-L. Oppo, P. Ru, and J. Tredicce, Phys. Rev. A **42**, 1630 (1990).
- [261] S. Berweger, J. M. Atkin, R. L. Olmon, and M. B. Raschke, Journ. Phys. Chem. Lett. **3**, 945 (2012).
- [262] S. Jager, A. M. Kern, M. Hentschel, R. Jager, K. Braun, D. Zhang, H. Giessen, and A. J. Meixner, Nano Lett. **13**, 3566 (2013).
- [263] N. Noginova, R. Hussain, M. Noginov, J. Vella, and A. Urbas, Opt. Expr. **21**, 23087 (2013).
- [264] S. Karaveli, S. Wang, G. Xiao, and R. Zia, ACS Nano **7**, 7165 (2013).
- [265] A. G. Curto, T. H. Taminiau, G. Volpe, M. P. Kreuzer, R. Quidant, and N. F. van Hulst, Nat. Comm. **4**, 1750 (2013).
- [266] S. Scheel, Journ. Mod. Opt. **56**, 141 (2009).
- [267] R. H. Brown and R. Twiss, Nature **178**, 1046 (1956).
- [268] J. F. Clauser, Phys. Rev. D **9**, 853 (1974).

- [269] H. J. Kimble, M. Dagenais, and L. Mandel, *Phys. Rev. Lett.* **39**, 691 (1977).
- [270] C. Brunel, B. Lounis, P. Tamarat, and M. Orrit, *Phys. Rev. Lett.* **83**, 2722 (1999).
- [271] B. Lounis and W. Moerner, *Nature* **407**, 491 (2000).
- [272] C. Kurtsiefer, S. Mayer, P. Zarda, and H. Weinfurter, *Phys. Rev. Lett.* **85**, 290 (2000).
- [273] A. Beveratos, R. Brouri, T. Gacoin, J.-P. Poizat, and P. Grangier, *Phys. Rev. A* **64**, 061802 (2001).
- [274] J. Kim, O. Benson, H. Kan, and Y. Yamamoto, *Nature* **397**, 500 (1999).
- [275] P. Michler, A. Kiraz, C. Becher, W. Schoenfeld, P. Petroff, L. Zhang, E. Hu, and A. Imamoglu, *Science* **290**, 2282 (2000).
- [276] C. Santori, M. Pelton, G. Solomon, Y. Dale, and Y. Yamamoto, *Phys. Rev. Lett.* **86**, 1502 (2001).
- [277] Z. Yuan, B. E. Kardynal, R. M. Stevenson, A. J. Shields, C. J. Lobo, K. Cooper, N. S. Beattie, D. A. Ritchie, and M. Pepper, *Science* **295**, 102 (2002).
- [278] A. Beveratos, R. Brouri, T. Gacoin, A. Villing, J.-P. Poizat, and P. Grangier, *Phys. Rev. Lett.* **89**, 187901 (2002).
- [279] E. Waks, K. Inoue, C. Santori, D. Fattal, J. Vuckovic, G. S. Solomon, and Y. Yamamoto, *Nature* **420**, 762 (2002).
- [280] C. H. Bennett and G. Brassard, in *Proceedings of IEEE International Conference on Computers, Systems and Signal Processing* (1984), pp. 175–179.
- [281] C. H. Bennett, G. Brassard, and N. D. Mermin, *Phys. Rev. Lett.* **68**, 557 (1992).
- [282] Y. Rezus, S. Walt, R. Lettow, A. Renn, G. Zumofen, S. Götzinger, and V. Sandoghdar, *Phys. Rev. Lett.* **108**, 093601 (2012).
- [283] G. Brassard, N. Lütkenhaus, T. Mor, and B. C. Sanders, *Phys. Rev. Lett.* **85**, 1330 (2000).
- [284] T. Aichele, G. Reinaudi, and O. Benson, *Phys. Rev. B* **70**, 235329 (2004).
- [285] M. Thomas, J.-J. Greffet, R. Carminati, and J. Arias-Gonzalez, *Appl. Phys. Lett.* **85**, 3863 (2004).
- [286] C. Girard, O. J. Martin, G. Lévêque, G. C. Des Francs, and A. Dereux, *Chem. Phys. Lett.* **404**, 44 (2005).
- [287] A. Akimov, A. Mukherjee, C. Yu, D. Chang, A. Zibrov, P. Hemmer, H. Park, and M. Lukin, *Nature* **450**, 402 (2007).
- [288] S. Schietinger, M. Barth, T. Aichele, and O. Benson, *Nano Lett.* **9**, 1694 (2009).
- [289] A. Kinkhabwala, Z. Yu, S. Fan, Y. Avlasevich, K. Müllen, and W. Moerner, *Nat. Phot.* **3**, 654 (2009).
- [290] J. T. Choy, B. J. Hausmann, T. M. Babinec, I. Bulu, M. Khan, P. Maletinsky, A. Yacoby, and M. Lončar, *Nat. Phot.* **5**, 738 (2011).
- [291] L. Allen and J. H. Eberly, *Optical Resonance and Two-Level Atoms* (Courier Dover Publications, 2012).
- [292] B. Dabbousi, M. Bawendi, O. Onitsuka, and M. Rubner, *Appl. Phys. Lett.* **66**, 1316 (1995).
- [293] A. Weiner, *Ultrafast optics*, vol. 72 (John Wiley & Sons, 2011).
- [294] I. Magnúsdóttir, A. V. Uskov, S. Bischoff, B. Tromborg, and J. Mørk, *J. Appl. Phys.* **92**, 5982 (2002).
- [295] T. W. Berg, J. Mørk, and J. M. Hvam, *New J. Phys.* **6**, 178 (2004).

- [296] K. E. Knowles, E. A. McArthur, and E. A. Weiss, *ACS Nano* **5**, 2026 (2011).
- [297] C. Gerry and P. Knight, *Introductory quantum optics* (Cambridge university press, 2005).
- [298] A. Auffèves, D. Gerace, J.-M. Gérard, M. F. Santos, L. Andreani, and J.-P. Poizat, *Phys. Rev. B* **81**, 245419 (2010).
- [299] W. Qin, H. Liu, and P. Guyot-Sionnest, *ACS nano* (2013).
- [300] H. T. Dung, L. Knöll, and D.-G. Welsch, *Phys. Rev. A* **64**, 013804 (2001).
- [301] V. Klimov, M. Ducloy, and V. Letokhov, *Europ. Phys. Journ. D* **20**, 133 (2002).
- [302] P. G. Eliseev, H. Li, A. Stintz, G. T. Liu, T. C. Newell, K. J. Malloy, and L. F. Lester, *Appl. Phys. Lett.* **77**, 262 (2000).
- [303] T. Okamoto, in *Near-field optics and surface plasmon polaritons* (Springer, 2001), pp. 97–123.
- [304] S. M. Tan, *J. Opt. B: Quantum Semiclass. Opt.* **1**, 424 (1999).
- [305] M. J. Holmes, K. Choi, S. Kako, M. Arita, and Y. Arakawa, *Nano Lett.* (2014).
- [306] Y.-S. Park, W. K. Bae, L. Padilha, J. M. Pietryga, and V. I. Klimov, *Nano Lett.* (2014).
- [307] E. Del Valle and F. Laussy, *Phys. Rev. A* **84**, 043816 (2011).
- [308] W. Zhang, Z. Yu, Y. Liu, and Y. Peng, *Phys. Rev. A* **89**, 043832 (2014).
- [309] I. Staude, V. K. Sreenivasan, I. Shishkin, K. Samusev, M. Decker, D. N. Neshev, A. V. Zvyagin, and Y. S. Kivshar, *Phys. Stat. Sol. RRL* **9999** (2014).
- [310] T. Yoshie, A. Scherer, J. Hendrickson, G. Khitrova, H. Gibbs, G. Rupper, C. Ell, O. Shchekin, and D. Deppe, *Nature* **432**, 200 (2004).
- [311] T. Aoki, B. Dayan, E. Wilcut, W. P. Bowen, A. S. Parkins, T. Kippenberg, K. Vahala, and H. Kimble, *Nature* **443**, 671 (2006).
- [312] A. Wallraff, D. I. Schuster, A. Blais, L. Frunzio, R.-S. Huang, J. Majer, S. Kumar, S. M. Girvin, and R. J. Schoelkopf, *Nature* **431**, 162 (2004).
- [313] S. Savasta, R. Saija, A. Ridolfo, O. Di Stefano, P. Denti, and F. Borghese, *ACS Nano* **4**, 6369 (2010).
- [314] A. González-Tudela, P. Huidobro, L. Martín-Moreno, C. Tejedor, and F. García-Vidal, *Phys. Rev. Lett.* **110**, 126801 (2013).
- [315] A. Väkeväinen, R. J. Moerland, H. T. Rekola, A.-P. Eskelinen, J.-P. Martikainen, D.-H. Kim, and P. Törmä, *Nano Lett.* **14**, 1721 (2013).
- [316] M. Sukharev, T. Seideman, R. J. Gordon, A. Salomon, and Y. Prior, *ACS Nano* **8**, 807 (2013).
- [317] A. Delga, J. Feist, J. Bravo-Abad, and F. Garcia-Vidal, *Phys. Rev. Lett.* **112**, 253601 (2014).
- [318] P. Törmä and W. Barnes, *arXiv:1405.1661* (2014).
- [319] L. C. Andreani, G. Panzarini, and J.-M. Gérard, *Phys. Rev. B* **60**, 13276 (1999).
- [320] D. Mortazavi, A. Z. Kouzani, and M. Kalani, *Opt. Expr.* **22**, 18889 (2014).
- [321] R.-C. Ge, C. Van Vlack, P. Yao, J. F. Young, and S. Hughes, *Phys. Rev. B* **87**, 205425 (2013).
- [322] Y. Mu and C. Savage, *Phys. Rev. A* **46**, 5944 (1992).
- [323] A. Gonzalez-Tudela, D. Martin-Cano, E. Moreno, L. Martin-Moreno, C. Tejedor, and F. J. Garcia-Vidal, *Phys. Rev. Lett.* **106**, 020501 (2011).
- [324] D. Martín-Cano, A. González-Tudela, L. Martín-Moreno, F. J. García-Vidal, C. Tejedor, and E. Moreno, *Phys. Rev. B* **84**, 235306 (2011).

- [325] V. Sidorkin, E. van Veldhoven, E. van der Drift, P. Alkemade, H. Salemink, and D. Maas, *Journ. Vac. Sci. & Tech. B* **27**, L18 (2009).
- [326] J. Bleuse, J. Claudon, M. Creasey, N. S. Malik, J.-M. Gérard, I. Maksymov, J.-P. Hugonin, and P. Lalanne, *Phys. Rev. Lett.* **106**, 103601 (2011).
- [327] I.-H. Chen, K.-H. Chen, W.-T. Lai, and P.-W. Li, *Electron. Dev., IEEE Trans. on* **59**, 3224 (2012).
- [328] R. Alaee, C. Menzel, U. Huebner, E. Pshenay-Severin, S. Bin Hasan, T. Pertsch, C. Rockstuhl, and F. Lederer, *Nano Lett.* **13**, 3482 (2013).
- [329] C. Hood, M. Chapman, T. Lynn, and H. Kimble, *Phys. Rev. Lett.* **80**, 4157 (1998).
- [330] R. Miller, T. Northup, K. Birnbaum, A. Boca, A. Boozer, and H. Kimble, *Journ. Phys. B* **38**, S551 (2005).
- [331] L. M. Liz-Marzán, C. J. Murphy, and J. Wang, *Chem. Soc. Rev.* **43**, 3820 (2014).
- [332] F. De Angelis, C. Liberale, M. Coluccio, G. Cojoc, and E. Di Fabrizio, *Nanoscale* **3**, 2689 (2011).
- [333] D. E. Chang, A. S. Sørensen, E. A. Demler, and M. D. Lukin, *Nat. Phys.* **3**, 807 (2007).
- [334] N. Liu, L. Langguth, T. Weiss, J. Kästel, M. Fleischhauer, T. Pfau, and H. Giessen, *Nat. Mat.* **8**, 758 (2009).
- [335] K. Ray, R. Badugu, and J. R. Lakowicz, *Journ. Am. Chem. Soc.* **128**, 8998 (2006).
- [336] S. Fischer, F. Hallermann, T. Eichelkraut, G. von Plessen, K. W. Krämer, D. Biner, H. Steinkemper, M. Hermle, and J. C. Goldschmidt, *Opt. Expr.* **20**, 271 (2012).
- [337] D. Dregely, K. Lindfors, M. Lippitz, N. Engheta, M. Totzeck, and H. Giessen, *Nat. Comm:* **5** (2014).
- [338] S. B. Hasan, F. Lederer, and C. Rockstuhl, *Mat. Today* (2014).
- [339] N. I. Zheludev, *Science* **328**, 582 (2010).
- [340] J. Hao, J. Wang, X. Liu, W. J. Padilla, L. Zhou, and M. Qiu, *Appl. Phys. Lett.* **96**, 251104 (2010).
- [341] S. G. Romanov, A. V. Korovin, A. Regensburger, and U. Peschel, *Adv. Mat.* **23**, 2515 (2011).
- [342] S. Haroche and D. Kleppner, *Phys. Today* **42**, 24 (1989).
- [343] H. Kimble, in *Cavity quantum electrodynamics* (1994).
- [344] R. K. Chang and A. J. Campillo, *Optical processes in microcavities* (World scientific, 1996).
- [345] J.-J. Greffet, R. Carminati, K. Joulain, J.-P. Mulet, S. Mainguy, and Y. Chen, *Nature* **416**, 61 (2002).
- [346] B. Luk'yanchuk, N. I. Zheludev, S. A. Maier, N. J. Halas, P. Nordlander, H. Giessen, and C. T. Chong, *Nat. Mat.* **9**, 707 (2010).
- [347] K. Wu, W. E. Rodríguez-Córdoba, Y. Yang, and T. Lian, *Nano letters* **13**, 5255 (2013).
- [348] S. Scheel and D.-G. Welsch, *Phys. Rev. Lett.* **96**, 073601 (2006).
- [349] F. Lederer, "Theoretische Elektrodynamik", Lecture Notes, Institute of Condensed Matter Theory and Solid State Optics, Friedrich-Schiller-Universität Jena (2007).
- [350] S. Wolfram and Wolfram Research, Inc, *Mathematica*, Wolfram Research, Inc., 100 Trade Center Drive, Champaign, IL 61820-7237, USA, 7th ed.
- [351] C. Moreira, A. Lima, H. Neff, and C. Thirstrup, *Sens. Actuators B: Chem.* **134**, 854 (2008).
- [352] U. Kreibitz, *J. Phys. F: Metal Phys.* **4**, 999 (1974).

- [353] W. Lawrence, Phys. Rev. B **13**, 5316 (1976).
- [354] H.-P. Chiang, Y.-C. Wang, P. Leung, and W.-S. Tse, Opt. Comm. **188**, 283 (2001).
- [355] J. F. Cochran and D. Mapother, Phys. Rev. **111**, 132 (1958).
- [356] V. Singh, A. Kulkarni, and T. Rama Mohan, Journ. Appl. Polymer Science **90**, 3602 (2003).
- [357] R. L. Olmon, B. Slovick, T. W. Johnson, D. Shelton, S.-H. Oh, G. D. Boreman, and M. B. Raschke, Phys. Rev. B **86**, 235147 (2012).
- [358] U. Kreibig and C. v. Fragstein, Z. Phys. **224**, 307 (1969).
- [359] R. Averitt, D. Sarkar, and N. Halas, Phys. Rev. Lett. **78**, 4217 (1997).
- [360] U. Kreibig and M. Vollmer (1995).
- [361] C. G. Parthey, A. Matveev, J. Alnis, B. Bernhardt, A. Beyer, R. Holzwarth, A. Maistrou, R. Pohl, K. Predehl, T. Udem *et al.*, Phys. Rev. Lett. **107**, 203001 (2011).
- [362] M. Planck, Ann. Phys. **309**, 553 (1901).
- [363] A. Einstein, Annal. d. Phys. **322**, 132 (1905).
- [364] R. P. Feynman, *The Character of Physical Law*, vol. 66 (MIT press, 1967).
- [365] J. Sakurai and S. F. Tuan, *Modern Quantum Mechanics* (Addison-Wesley, 1994).
- [366] C. Cohen-Tannoudji, *Quantum Mechanics Volume 1 with Mass Heat Transfer Set* (2002).
- [367] R. W. Boyd, *Nonlinear optics* (Academic press, 2003).
- [368] M. Fewell, Opt. Comm. **253**, 125 (2005).
- [369] R. J. Glauber, Phys. Rev. **130**, 2529 (1963).
- [370] L. Mandel and E. Wolf, Rev. Mod. Phys. **37**, 231 (1965).
- [371] A. Öttl, S. Ritter, M. Köhl, and T. Esslinger, Phys. Rev. Lett. **95**, 090404 (2005).
- [372] D. F. Walls, Nature **306**, 141 (1983).
- [373] V. Giovannetti, S. Lloyd, and L. Maccone, Nat. Phot. **5**, 222 (2011).
- [374] J. Aasi, J. Abadie, B. Abbott, R. Abbott, T. Abbott, M. Abernathy, C. Adams, T. Adams, P. Addesso, R. Adhikari *et al.*, Nat. Phot. **7**, 613 (2013).
- [375] Y. Yamamoto and H. Haus, Rev. Mod. Phys. **58**, 1001 (1986).
- [376] S. L. Braunstein and P. Van Loock, Rev. Mod. Phys. **77**, 513 (2005).
- [377] L.-A. Wu, H. J. Kimble, J. L. Hall, and H. Wu, Phys. Rev. Lett. **57**, 2520 (1986).
- [378] P. Meystre and M. Zubairy, Phys. Lett. A **89**, 390 (1982).
- [379] M. Collett, D. Walls, and P. Zoller, Opt. Comm. **52**, 145 (1984).
- [380] W. Vogel, Phys. Rev. Lett. **67**, 2450 (1991).
- [381] H. P. Yuen and J. H. Shapiro, Opt. Lett. **4**, 334 (1979).
- [382] V. P. Drachev, A. K. Buin, H. Nakotte, and V. M. Shalaev, Nano Lett. **4**, 1535 (2004).
- [383] J. P. Karr, A. Baas, R. Houdré, and E. Giacobino, Phys. Rev. A **69**, 031802 (2004).
- [384] S. Hill and W. K. Wootters, Phys. Rev. Lett. **78**, 5022 (1997).
- [385] R. Dicke, Phys. Rev. **93**, 99 (1954).
- [386] A. Einstein, B. Podolsky, and N. Rosen, Phys. Rev. **47**, 777 (1935).
- [387] E. Schrödinger, Naturwiss. **23**, 823 (1935).

- [388] N. Bohr, Phys. Rev. **48**, 696 (1935).
- [389] J. Bell, Physics **1**, 195 (1964).
- [390] O. Gühne and G. Tóth, Phys. Rep. **474**, 1 (2009).
- [391] M. Wilde, *Quantum Information Theory* (Cambridge University Press, 2013).
- [392] A. Aspect, P. Grangier, and G. Roger, Phys. Rev. Lett. **47**, 460 (1981).
- [393] R. J. Young, R. M. Stevenson, P. Atkinson, K. Cooper, D. A. Ritchie, and A. J. Shields, New Journ. Phys. **8**, 29 (2006).
- [394] N. Akopian, N. Lindner, E. Poem, Y. Berlatzky, J. Avron, D. Gershoni, B. Gerardot, and P. Petroff, Phys. Rev. Lett. **96**, 130501 (2006).
- [395] M. Müller, S. Bounouar, K. D. Jöns, M. Glässl, and P. Michler, Nat. Phot. **8**, 224 (2014).
- [396] H. Oka, Appl. Phys. Lett. **103**, 174108 (2013).
- [397] E. Del Valle, F. Laussy, F. Troiani, and C. Tejedor, Phys. Rev. B **76**, 235317 (2007).
- [398] R. Johne, N. Gippius, G. Pavlovic, D. Solnyshkov, I. Shelykh, and G. Malpuech, Phys. Rev. Lett. **100**, 240404 (2008).
- [399] C. Wang, Y. Zhang, and G.-s. Jin, Phys. Rev. A **84**, 032307 (2011).
- [400] J. Cirac, Phys. Rev. A **46**, 4354 (1992).

# Notation

## Mathematical Conventions

### Classical

imaginar unit  $i^2 = -1$

scalar function  $f(\mathbf{r})$

complex numbers  $z = z' + iz''$

complex conjugate (c.c.)  $z^* = z' - iz''$

coordinate vectors  $\mathbf{e}_i$ , *i.e.*  $\mathbf{e}_x$

vector function  $\mathbf{F}(\mathbf{r}) = \sum_i F_i(\mathbf{r}) \mathbf{e}_i$

vector product  $\mathbf{A} \times \mathbf{B} \in \mathbb{C}^3$

inner product  $\mathbf{A} \cdot \mathbf{B} = \sum_i A_i B_i \mathbf{e}_i \cdot \mathbf{e}_i$

total derivative  $\frac{df(x)}{dx}$

partial derivative  $\frac{\partial f(x)}{\partial x} \equiv \partial_x f(x)$

nabla operator  $\nabla = \sum_i \mathbf{e}_i \partial_i$

### Quantum

Dirac's notation  $|n\rangle$  (bra) and  $\langle n|$  (ket)

Hermitian conjugate (H.c.)  $|n\rangle^\dagger = \langle n|$

inner product  $\langle \phi | \psi \rangle = \int \phi^*(x) \psi(x) dx \in \mathbb{C}$

outer product  $|\phi\rangle \langle \psi|$

commutator  $[A, B] = AB - BA$

expectation value  $\langle A \rangle_\psi = \langle \psi | A | \psi \rangle$

composite Hilbert space  $|\phi\rangle \otimes |\psi\rangle \equiv |\phi, \psi\rangle$

Please note that there is no visual distinction between classical and quantum variables. It should be always clear from the context what kind of variable is present.

## Physical Quantities

See index on the last page.

## Fourier Transformation

The convention for the Fourier transformation  $\mathcal{F}$  used throughout this thesis is

$$f(k, \omega) = \frac{1}{(2\pi)^2} \int_{-\infty}^{\infty} f(x, t) e^{-i(kx - \omega t)} dx dt \text{ and } f(x, t) = \int_{-\infty}^{\infty} f(k, \omega) e^{i(kx - \omega t)} dk d\omega .$$

As a consequence,

$$\mathcal{F}[f(t) = e^{-i\omega_0 t}] (\omega) = \int_{-\infty}^{\infty} e^{i(\omega - \omega_0)t} dt = 2\pi \delta(\omega - \omega_0) .$$

In quantum optics, positive-frequency-Fourier transformations are often used. Here,  $f(t) = \mathcal{F}[f(\omega)](t) = \int_0^\infty [f(\omega) e^{-i\omega t} + f^*(\omega) e^{i\omega t}] dt$ . This definition is equivalent to the first one since for real-valued  $f(t)$   $f^*(\omega) = f(-\omega)$  holds.

Please note that we do not emphasize a Fourier transform by some additional notation. This is not only appealing from an aesthetic point of view but also fundamentally motivated: Any variable of a certain vector space can be represented in a different basis. Inspired by Dirac's notation  $\psi(x) = \langle x | \psi \rangle$ , it is evident that also  $\psi(k) = \langle k | \psi \rangle = \int \langle k | x \rangle \langle x | \psi \rangle dx \equiv \int \langle k | x \rangle \psi(x) dx$  is valid.



# Index

- adiabatic elimination, 102
- Ampère's law, 7
  
- Bohr radius  $a_0$ , 35
- BST (beam splitter transformation), 51
  
- circular NAs, 18
- closure equation, 81
- coupling strength  $\kappa$ , 32
- cQED (cavity quantum electrodynamics), 22
- CRL (cold reservoir limit), 51, 101
  
- dissipation, 9
  
- efficiency  $\eta$ , 8
- electric permittivity  $\varepsilon(\mathbf{r}, \omega)$ , 7
- excitation
  - incoherent pump, 52, 101
  - plane-wave illumination, 36, 39, 59
  
- Fabry-Perot model, 15
- Faraday's law, 7
- Fermi's Golden Rule, 20, 89
- forbidden transitions, 35
  - multipole coupling, 37
- Fröhlich condition, 13
  
- Gauss's law
  - electric, 7
  - magnetic, 7
- Green's function  $G(\mathbf{r}, \mathbf{r}', \omega)$ , 8
  
- harmonic oscillator
  - annihilation operator  $a$ , 23
  - Fock states, 24
  - Hamiltonian, 23
- Heisenberg's uncertainty principle, 106
  
- interaction picture, 87
  - modified, 99
  - perturbation theory, 88
  
- Jaynes-Cummings model, 33
  
- Lindblad operators, 31
- Lorentzian spectral density, 30
  
- magnetic permeability  $\mu(\mathbf{r}, \omega)$ , 7
- Maxwell's equations, 7
- minimal coupling, 20
- mode volume, 23
  
- NA (nanoantenna), 2
- nonclassical light
  - entangled, 107
  - single photons, 48
  - squeezed, 106
  
- Ohm's law, 7
  
- partial trace, 96
- Poynting's Theorem, 9, 72
  
- QD (quantum dot), 2
- QNMs (quasinormal modes), 28
  - determination, 30
- QS (quantum system), 1
- quadrature operators, 106
- quantization
  - cavity, 23
  - dissipative media, 24
  - NA (meaning), 22
  - QNMs, 29
- quantum efficiency  $\eta_{\text{qs}}$ , 85
  
- reflection coefficient, 15
  - calculation, 72
- RWA (rotating wave approximation), 25, 100
  
- Schrödinger's equation, 87
- second-order correlation  $g^2(\tau)$ , 55, 103
  - coherent radiation, 105
  - Fock states, 105
  - thermal radiation, 104
- speed of light  $c$ , 7
- spontaneous emission, 25, 94
  - emission rate  $\gamma_{\text{wc}}$ , 26, 51, 103
  - LDOS (local density of states)  $\rho(\omega)$ , 98
  - Purcell factor  $F(\omega)$ , 27
  - spectral density  $J(\omega)$ , 27
- SPP (surface plasmon polariton), 1
- strong coupling, 59, 97
  - condition, 60
  
- Tomonaga-Schwinger equation, 88
- two-level system, 25
  - annihilation operator  $\sigma_-$ , 25
  - coupled, Dicke basis, 108
  
- weak coupling, 26